Max-Planck-Institut für Polymerforschung

Max Planck Institute for Polymer Research

Ruthenium-thioether Coordination Bonds for Photoresponsive Polymer Gels

Dissertation

Zur Erlangung des Grades

„Doktor der Naturwissenschaften“

im Promotionsfach Chemie

Eingereicht am

Fachbereich Chemie, Pharmazie und Geowissenschaften

der Johannes Gutenberg-Universität Mainz

Von

Jiahui Liu

Mainz, 2021

Die vorliegende Arbeit wurde im Zeitraum von Okt 2017 bis Aug 2021 am Max-Planck-Institut für Polymerforschung in Mainz im Arbeitskreis von Prof. Dr. Hans-Jürgen Butt and Prof. Dr. Si Wu angefertigt.

Dekan:

Prodekan:

Gutachter 1:

Gutachter 2:

Date of oral examination:

Table of Contents

Abstract

Smart materials are materials that can be manipulated to respond in a controlled fashion to external stimuli such as pH, temperature, light, moisture, stress, magnetic or electric fields. These materials are expected to play a significant role in the future because they are capable of introducing new functions and increasing the value of the materials. Photoresponsive materials are of particular interest. Light is a non-invasive and clean stimulus, it can be switch on and off spatiotemporally and remotely. In addition, the irradiation parameters can be easily tuned, thereby, allowing the precise manipulation of the photoreactions. Photoresponsive polymer gels have emerged as promising materials for diverse applications. In this thesis novel photoresponsive gel systems were prepared based on ruthenium(Ru)-thioether coordination bonds.

In Chapter 2, we prepare a photo-controlled metallopolymer adhesive based on Ru-thioether coordination bonds for dynamic hydrogel assembly. Photoresponsive Ru-thioether coordination bonds as reversible crosslinks can control the adhesion between hydrogels. The adhesive is spread on the surfaces of hydrogels and is triggered to form a Ru-thioether coordination crosslinked polymer network entangled with the intrinsic polymer networks of hydrogels upon heating, inducing the formation of hydrogel assembly. Upon light irradiation, the Ru-thioether coordination crosslinked polymer network dissociates, resulting in photodetachment of the assembly. This adhesion approach allows for integrating various stimuli-responsive hydrogel building blocks into one assembly which shows several shape deformations under different stimuli. Furthermore, the hydrogel building blocks can be photodetached and reconfigured to generate other assemblies using the adhesive. In addition, combining a magnetical responsive hydrogel with other stimuli-responsive hydrogel assembly using adhesive endows the hydrogel assembly with mobility under a magnetic field.

In Chapter 3, we describe a method to synthesize photoresponsive metallopolymer organohydrogels based on another kind of Ru-thioether coordination bond. Photoresponsive Ru-thioether coordination bonds in the polymer networks act as reversible crosslinks to control gel properties. A water/glycerol mixture is used as an anti-freezing solvent which can expand the usage of gel in cold environments. At -20 °C, the Ru-thioether coordination bonds dissociate upon visible light irradiation and reform in the dark. In this way the crosslink densities in the polymer network can be regulated by light, resulting in significant changes in the network structures and properties. This process enables inducing reversible gel-to-sol transitions,

healing damaged gels, controlling the mechanical properties and volumes of the gels, and rewriting microstructures on the gels below 0 °C.

Zusammenfassung

Intelligente Materialien sind die Werkstoffe, die kontrolliert auf externe Reize wie pH-Wert, Temperatur, Licht, Feuchtigkeit, Stress, magnetische oder elektrische Felder reagieren. Von besonderem Interesse sind die fotoempfindliche Materialien. Das Licht gilt als ein nicht-invasiver und sauberer Stimulus, der sich räumlich und zeitlich ferngesteuert ein- und ausschalten lässt. Darüber hinaus lassen sich die Bestrahlungsparameter leicht einstellen, so dass die Fotoreaktionen präzise manipuliert werden können. Fotoempfindliche Polymergele haben sich als vielversprechende Materialien für verschiedene Anwendungen erwiesen. In dieser Arbeit wurden neuartige fotoempfindliche Gele auf der Basis von Ruthenium(Ru)-thioether-Koordinationsbindungen hergestellt.

Ein Ziel war die Herstellung eines fotokontrollierten Klebstoffs auf der Grundlage von Ru-Thioether-Koordinationsbindungen für den dynamischen Aufbau von Hydrogelen (Kapitel 2). Fotoempfindliche Ru-Thioether-Koordinationsbindungen als reversible Vernetzunger können die Adhäsion zwischen Hydrogelen steuern. Der Klebstoff wird auf die Oberflächen von Hydrogelen aufgetragen und bildet beim Erhitzen ein durch Ru-Thioether-Koordinationsbindungen vernetztes Polymernetzwerk, das sich mit den intrinsischen Polymernetzwerken der Hydrogele verschränkt und so eine Verbund bildet. Bei Lichteinstrahlung dissoziiert das vernetzte Ru-Thioether-Netzwerk. Unter Licht löst es sich daher ab. Dieser Adhäsionsansatz ermöglicht die Integration verschiedener stimulierungsempfindlicher Hydrogelbausteine in eine Baugruppe, die unter verschiedenen Stimuli verschiedene Formveränderungen zeigen. Darüber hinaus können die Hydrogel-Bausteine mit Hilfe des Klebstoffs durch Licht abgetrennt und neu konfiguriert werden, um andere Baugruppen zu erzeugen. Außerdem habe ich ein magnetisches Hydrogels mit einer anderen, auf Stimuli reagierenden Hydrogel verklebt. Dadurch ließen sich die kombinierten Hydrogele im Magnetfeld manipulieren.

Im dritten Kapitel zeige ich eine Methode zur Synthese von fotoempfindlichen Metallopolymer-Organohydrogelen, die auf einer anderen Art von Ru-Thioether-Koordinationsbindung basieren. Diese fotoempfindlichen Ru-Thioether-Koordinationsbindungen in den Polymernetzwerken als reversible Vernetzungen bis zu Temperaturen bis -20°C. Ein Wasser-Glycerin-Gemisch wird als gefriergeschütztes Lösungsmittel verwendet, das die Verwendung des Gels in kalten Umgebungen erweitern kann. Bei -20 °C dissoziieren die Ru-Thioether-Koordinationsbindungen bei Bestrahlung mit sichtbarem Licht und bilden sich im Dunkeln neu. Auf diese Weise können die

Vernetzungsdichten im Polymernetzwerk durch Licht reguliert werden, was zu erheblichen Veränderungen der Netzwerkstrukturen und -eigenschaften führt. Dieses Verfahren ermöglicht es, reversible Gel-zu-Sol-Übergänge herbeizuführen, beschädigte Gele zu heilen, die mechanischen Eigenschaften und Volumina der Gele zu kontrollieren und Mikrostrukturen auf den Gelen unter 0 °C umzuschreiben.

Motivation

Photoresponsive polymer gels have been extensively investigated and used in smart materials. To date, a wide range of photoreactions have been used to construct photoresponsive gels, including reversible reactions such as photoisomerization and photodimerization, and irreversible reactions such as photocleavage. A combination of the diversity of photoreactions and light as a stimulus makes photoresponsive gels appealed in many areas, ranging from biomaterials, medicine to soft robotics. Despite substantial effort has been made on the design and investigation of photoresponsive gels in different fields, there are still many limitations.

Photoresponsive polymer gels applied for dynamic assembly usually have tailored functional units (e.g., photoresponsive host-guest complexes) pendant on the polymeric network, to react with the interface of another functionalized gel. Nevertheless, their assembly suffers from limitations in the universality, making the assembly for non-functionalized gels impossible and lacking material versatility for gel assembly. To overcome this drawback, in the thesis, I prepared a photo-controlled adhesive for hydrogel assembly based on the mixture solution of Ru-containing polymer and thioether-containing polymer. The adhesion is dynamic, attributing to the reversible Ru-thioether coordination bond. I demonstrated that various non-functionalized hydrogels can be assembled using the adhesive. Furthermore, the assembly can be photodeched and reconfigured into different assemblies.

Another issue is reported photoresponsiveness of photoresponsive gels function at room temperature or elevated temperature. However, it is a challenge to construct photo-responsive materials that work at low temperatures because the decrease in temperature slows molecular motion, reduces reactivity, and may result in freezing. All of these temperature effects make photo-responsive materials less active or completely lose responsiveness at low temperatures. To overcome this drawback, in th thesis, I designed photoresponsive metallopolymer organohydrogels with Ru-thioether coordination bonds as photo-controlled reversible crosslinks and a water/glycerol mixture as an antifreezing solvent. Light can efficiently induce reversible photoreactions in metallopolymer organohydrogels at -20 °C. I demonstrated that the properties and functions of the metallopolymer organohydrogels can be controlled via reversible photoreactions at -20 °C.

Chapter 1: Introduction

1.1 Stimuli-responsive polymer gels

Polymer gels can be seen as cross-linked three-dimensional (3D) polymer networks that are swollen in a liquid environment.[1] The elastic 3D polymer networks hold the liquid in place to endow the gel solid-like properties. Therefore, polymer gels have properties of both liquid and solid, including high diffusion coefficients for small molecules and mechanical properties of soft solids.[1] Endowing polymer gels with stimuli-responsiveness are of great interest because they can endure reversibly gel-to-sol or shape transitions in response to external stimuli such as pH[2-4], light[5-7], temperature[8-10], electric and magnetic fields[11-14]. As early as 1978, T. Tanaka reported that the volume of polymer gels can change reversibly in response to environmental changes like temperature and solvent composition.[15] This result indicated that such a response acting on the microscopic scale can translate into a macroscopic scale conversing chemistry energy to mechanical energy. Since this discovery, stimuli-responsive polymer gels as smart materials have been developed rapidly and became one important subclass of polymer gels.

1.2 Photoresponsive polymer gels

Among these stimuli-responsive polymer gels, photoresponsive polymer gels attract much attention because light as a stimulus has many advantages. For example, light, a non-invasive stimulus, can be remotely controlled without direct contact. The irradiation parameters including wavelength, light intensity, direction, and irradiation time can be easily modulated, allowing the precise tune of the extent or rate of photoreactions. Spatial and temporal control can be achieved in both 2D and 3D by simply switching the light on and off. As a result, the response of the system can be kinetically controlled or made to occur in a stepwise fashion. The combination of physicochemical properties of polymer gels with photo responsiveness in photoresponsive hydrogels makes them ideal candidates for working in several fields, ranging from biomaterials[16-18] to intelligent materials[19-22].

1.2.1 Photoresponsive molecules

Macroscopic photoresponsiveness of polymer gels usually rises from photoresponsive groups incorporated into the polymer chains. Upon light irradiation, the photoresponsive groups absorb light of a particular wavelength and undergo photoreactions such as photoisomerization, photodimerization and photocleavage, leading to changes in physical and chemical properties. Such changes transfer to the polymer network and control its properties.

Depending on the photoreactions, the photoresponsiveness can be divided into reversible and irreversible responses. Photoinduced isomerization (e.g., azobenzene, spiropyran and diarylethene) and dimerization (e.g., coumarin and anthracene) are reversible and can be repeated several times, in which the reverse reaction occurs under light irradiation with a different wavelength or temperature. Therefore, the corresponding reversible systems can alternate material properties into two different states and be used as switches in applications such as self-healing[23], information stores[24] and artificial muscles[25].

For example, azobenzene is the most common photoresponsive molecule that undergoes reversible isomerization between trans-form to cis-form through a π-π* transition under the irradiation of ultraviolet (UV) light or visible light (Figure 1a).[26] In particular, photoisomerization of azobenzene influences the behavior of host-guest interaction with cyclodextrins (CDs). The trans azobenzenes form more stable host-guest complexes with CDs than that of the cis-form.[27]

Spiropyran is another promising photoresponsive group that can interconvert between hydrophobic ring-closed form and hydrophilic ring-opened form under UV or visible light irradiation (Figure 1b).[28] The two states of spiropyran differ in dipole moment, molecular volume and polarity. Recently, spiropyran-based hydrogel showed the abilities of phase transitions[29] and macroscopic actuation such as bending[30] and walking[31].

Dithienylethene also undergoes a reversible photo-triggered ring-opening and ring-closing reaction. Irradiating the molecule with UV light converts the opened form to the closed-form. The closed-form can be reversibly formed with the use of visible light (Figure 1c).[32, 33] The conjugation and electronic properties of two isomers are very different because the rotation is restricted and the thienyl units are conjugated in the closed-form. Moreover, the reversible process can be recycled many times without any changes.

Photodimerization is the reaction that occurs between two of the same molecules and forms covalent bonds between each other upon light irradiation. This reaction is reversible when a different wavelength of light or heating is applied. Representative photodimerization reactions are [2+2] cycloaddition of coumarins and [4+4] cycloaddition anthracenes (Figure 1d and e).[6] Both cycloadditions can be reversed with light irradiation or heating.

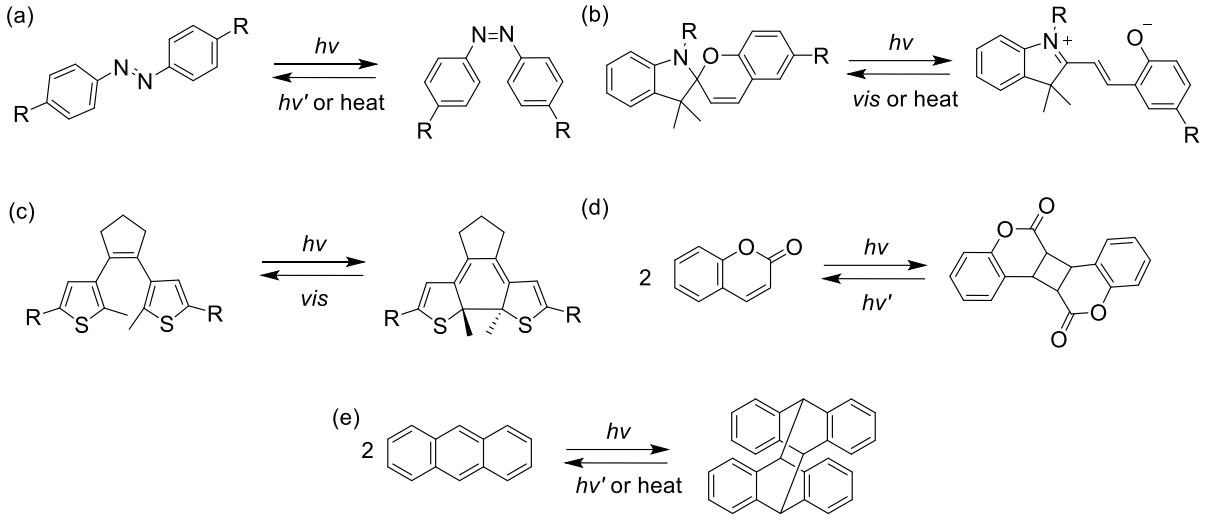

Figure 1. Representative reversible photoisomerization (a, b and c) and photodimerization (d and e).

Irreversible responses are mainly induced by photocleavage in which bonds can be permanently broken. This reaction is extensively applied in controlled drug release and dynamic cell microenvironments.[16] The most widely used photolabile groups are o-nitrobenzyl compounds which can serve as photocages or photolabile linkers in the hydrogel chemistry. [34, 35] Upon UV light irradiation, the o-nitrobenzyl group can be cleaved into o-nitroso-benzyladehyde and carboxylic acid permanently (Figure 2).

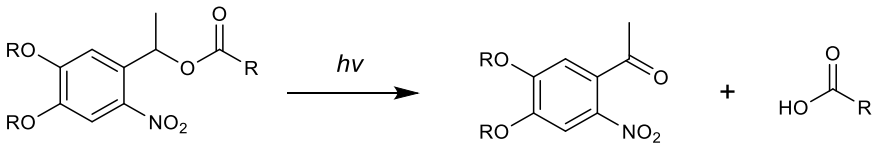

Figure 2. Representative irreversible photocleavage.

1.2.2 Applications of photoresponsive polymer gels

In this section, I will mainly introduce photoresponsive polymer gels based on reversible photoreactions used in dynamic assembly, healing materials, and soft actuators.

1.2.2.1 Dynamic assembly

Dynamic assembly of hydrogels is the process by which several hydrogel building blocks are assembled into one larger assembly, and the assembly can be easily disassembled in response to a stimulus such as pH and light.[36, 37] Photoresponsive hydrogel assembly was first reported by Harada group.[36] They developed a photo-controlled hydrogel assembly system using polyacrylamide-based hydrogel building blocks functionalized with azobenzene or aCD

moieties. Reversible adhesion and dissociation between the host gel and the guest gel were manipulated by light irradiation (Figure 3).

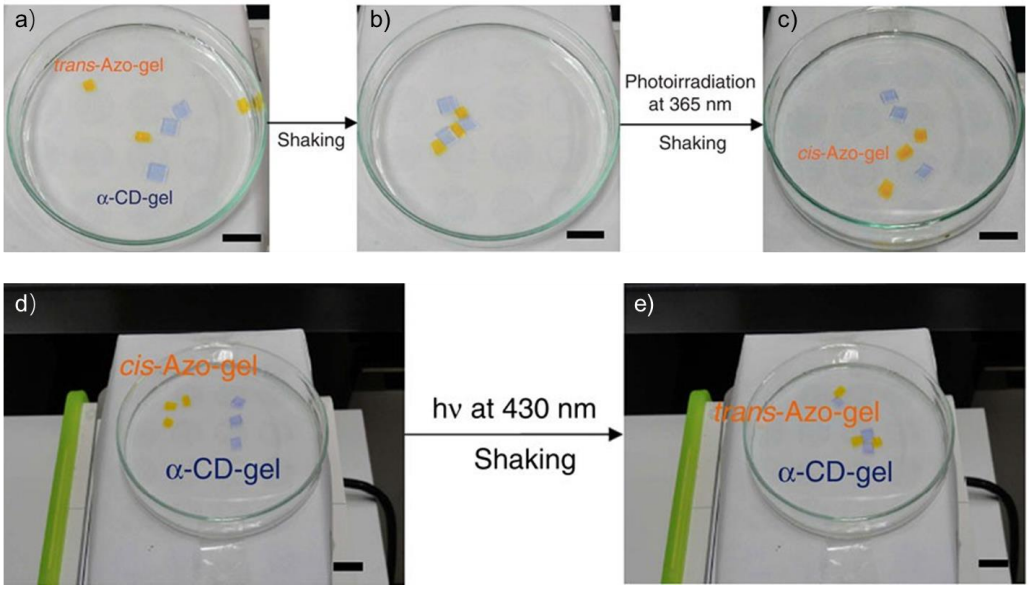

Figure 3. (a-c) Assembly and dissociation of α-CD gel with Azo-gel. (d-e) Reassembly of α-CD gel with Azo-gel. Reproduced by permission of ref. 36. Copyright 2012 Nature.

Although the dynamic assembly between hydrogels has already been proved by Harada group, a tough and dynamic interfacial adhesive between hydrogels is highly desirable. Scherman group developed a cucurbit[8]uril (CB[8])-threaded highly branched polymer which can bond with azobenzene-functionalized hydrogels via CB[8]-mediated host-guest conjugation (Figure 4).[37] The adhesion between hydrogels was controlled with light because the photoisomerization of azobenzene units promoted the reversible association and dissociation of the host-guest complexes. Furthermore, the adhesion was reversible without the extra addition of CB[8]-threaded branched polymer. They also demonstrated that CB[8]-threaded branched polymer could dynamically bond various nonporous and porous substrates.

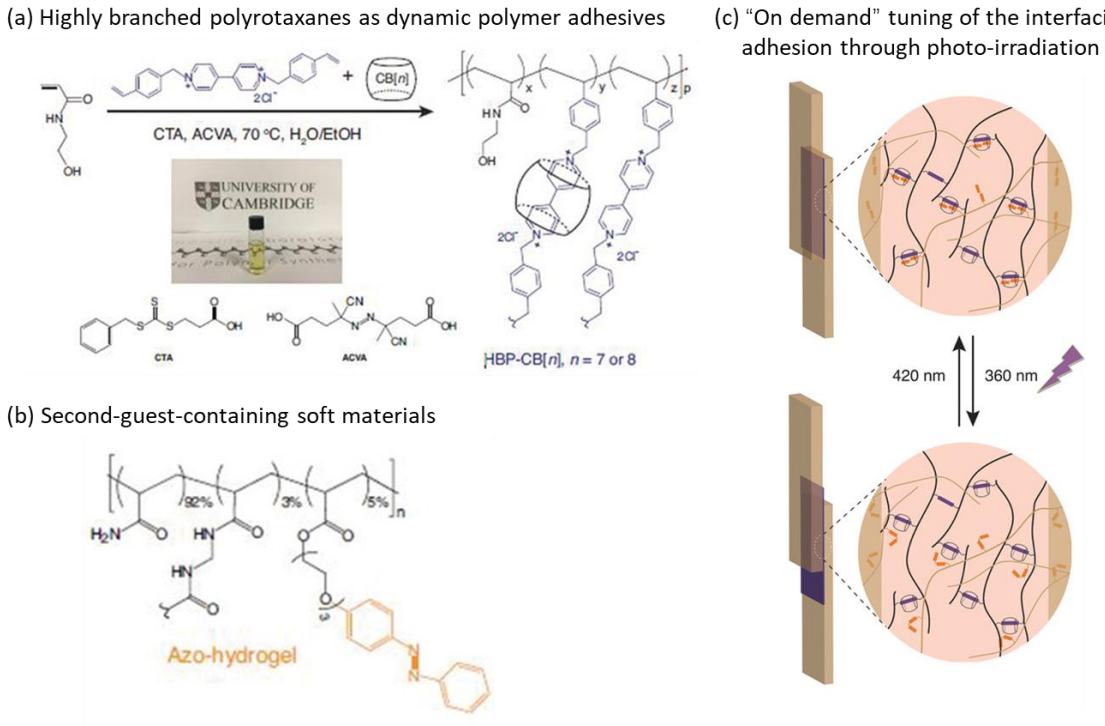

Figure 4. (a) Chemical compositions of CB[8]-threaded highly branched polymer. (b) The hydrogel networks containing azobenzene moieties as second guests. (c) Schematic of the dynamic adhesion of azo-hydrogels with CB[8]-threaded highly branched polymer as adhesive. Reproduced by permission of ref. 37. Copyright 2018 WILEY-VCH Verlag GmbH & Co. KGaA.

1.2.2.2 Healable materials

Materials have fatigue, mechanical stress or scratches when they were used for some time. These mechanical drawbacks decrease the lifetime of materials. The huge demand has forced researchers to increase the durability and expand the lifetime of materials. Healable materials capable of repairing their functionality after fatigue or damage may become valuable commodities in the future. The requirements for healable materials are: 1) they can repair themselves in a mild environment, such as in air and at room temperature, 2) they do not need additives to repair the damage, and 3) they can repair damage repeatedly. Among those, photo-induced healing polymer materials have the advantage of meeting these requirements. They can be precisely and spatiotemporally controlled and repaired on demand.

The reversible photoreactions in the polymer networks can serve as dynamic crosslinks, providing new crosslinks and repairing the damaged part upon light irradiation. Saunders and coworkers reported photo-healing microgels based on [2+2] cycloaddition reaction of coumarin (Figure 5).[23] The hydrogel was synthesized from 7-(2-methacryloyloxyethoxy)-4-

methylcoumarin, 2-(2-methoxyethoxy) ethyl methacrylate, and methacrylic acid. Microgels were photo-crosslinked under 365 nm light irradiation via [2+2] cycloaddition of coumarins, generating a photo-crosslinked gel (Figure 5b). Subsequently, the hydrogel was partly photocleaved using 254 nm light to form a photo-cleaved gel (Figure 5c). With the use of 365 nm light irradiation photo-crosslinked gel was reformed. Based on this photoreversible covalent bonding, the hydrogel showed light-assisted healing (Figure 5d). Two halves of the photocleaved gel were cross-linked with each other upon 365 nm light irradiation. Then the reunited gel showed reversible separation and healing with 254 nm or 365 nm light irradiation, respectively.

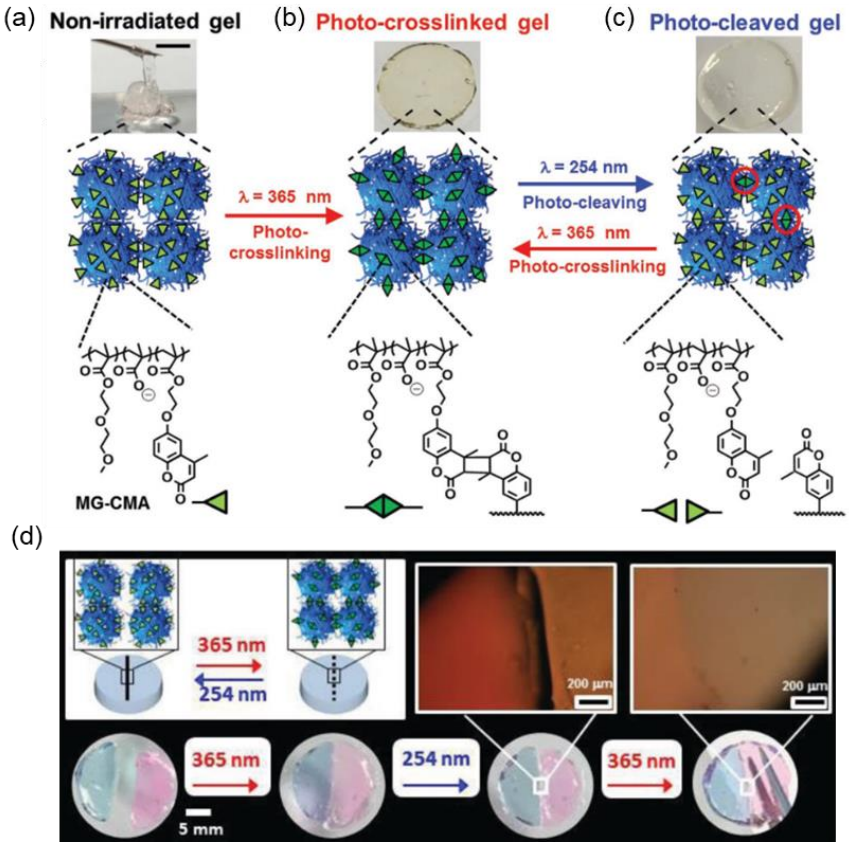

Figure 5. Photoswitching and photo-healing of hydrogels. (a) Initial non-irradiated microgel. (b) photo-crosslinked gel. (c) Photocleaved gel. (d) Reversible light-assisted healing of hydrogel. Reproduced by permission of ref. 23. Copyright 2020 WILEY-VCH Verlag GmbH & Co. KGaA .

Another approach involves the utilization of light to switch on and off the healing property of the gel network. Johnson group prepared a self-healing organogel which was cross-linked by metal-organic cages (Figure 6).[33] The gel can be photoswitched between two topological states

because the incorporation of photoresponsive diarylethene units defined the structure of the metal-organic cage which defined the polymer topology and bulk properties. The angle of the pyridine ligand of diarylethene units can be photoswitched between 62° and 138°. In the presence of Pd^{2+}, the topology network of the metal-organic cage can be reversible photoswitched between small Pd_3L_6 and large $Pd_{24}L_{48}$ junctions. These two different topological states in polymer provided distinct differences in the mechanical properties of the gel. More interestingly, the gel cross-linked by the small and flexible Pd_3L_6 exhibited self-healable behavior, while the large and rigid $Pd_{24}L_{48}$ cross-linked network could not self-heal.

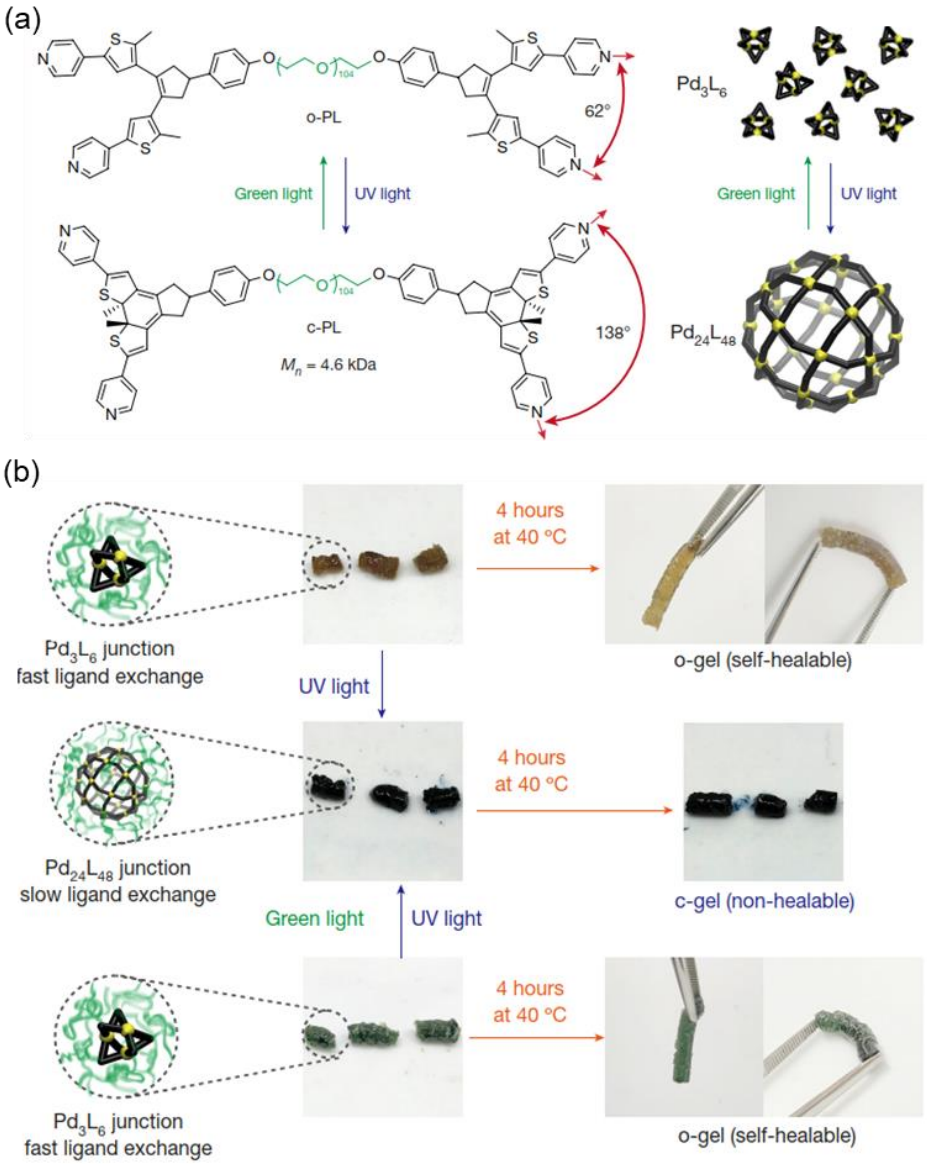

Figure 6. (a) Photoswitched polymer ligand and schematic of metal-organic cage interconversion. (b) Healing experiments of gels. Reproduced by permission of ref. 33. Copyright 2018 Nature.

1.2.2.3 Soft actuators

Photoresponsive gel actuators exhibit size (contraction-expansion) or shape changes of gel networks in response to light irradiation, in which the input of energy of light can be converted into mechanical motion. Photoresponsive actuators are attractive because they can be remotely and spatiotemporally manipulated. Incorporating photoswitchable moieties into gel networks is one of the common strategies to fabricate photo-triggered actuators.

Harada group developed a photoresponsive topologically cross-linked hydrogel actuator ([c2]AzoCD$_2$) built from α-cyclodextrin (α-CD)/azobenzene complex-based [c2]daisy chains (Figure 7).[38] The hydrogel showed extension capability attributing to sliding motions within the rotaxane-containing crosslinks. Reversibly bending and flattening behaviors of the hydrogel were found in water with alternating UV and visible light irradiation. More interestingly, the xerogel dried from hydrogel exhibited a faster response than hydrogel, which could bend toward a light source under UV light irradiation in seconds.

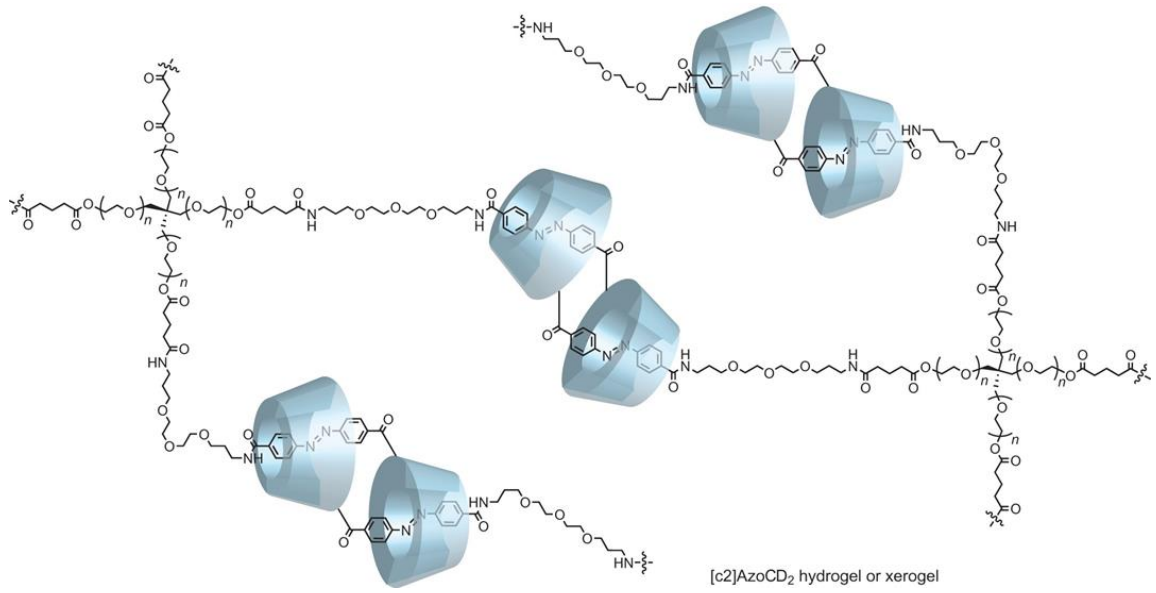

Figure 7. Chemical structure of [c2]AzoCD$_2$ hydrogel or xerogel. Reproduced by permission of ref. 38. Copyright 2016 Nature.

Florea and coworkers developed a photoresponsive hydrogel walker based on spiropyran (Figure 8).[31] The hydrogel showed reversible volume changes induced by the photoisomerization of spiropyran with light irradiation. Placing hydrogel on a rough surface expanded the volume of hydrogel because the protonation of the carboxylic acid units in water resulted in the formation of hydrophilic ring-opened spiropyran. With white light irradiation, hydrophilic ring-opened spiropyran returned to hydrophobic ring-closed form. Meanwhile, the

carboxylic acid units became protonated, causing the hydrogel to shrink. The hydrogel actuator exhibited a walking motion by the modulation of white light irradiation in water.

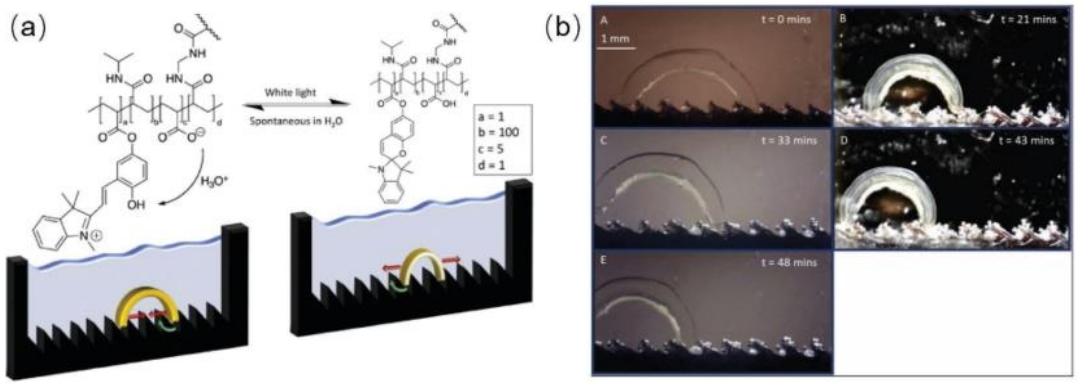

Figure 8. (a) Chemical structure of the hydrogel walkers under different conditions. (b) Photos showing that the walking behavior of the hydrogel walker. Reproduced by permission of ref. 31. Copyright 2017 ELSEVIER.

1.3 Photoresponsive ruthenium (Ru) complexes

As discussed above, photoresponsive polymer gels based on photoreactions have gained enormous attention from chemistry to materials. However, there are still many photoreactions that have not been fully explored yet. For example, Ru-ligand coordination bonds are photoresponsive.[39-41] A coordination ligand on the Ru center can be substituted by a free ligand with the use of light. This kind of photoreaction will be a powerful reaction for preparing photoresponsive polymer gels. In this section, I will introduce the photochemical properties of Ru complexes. Inspired by the fundamental knowledge of photoresponsive Ru complexes, I expect Ru complexes will be an ideal candidate to construct photoresponsive polymer gels with unique functions.

1.3.1 Ru(II) polypyridyl complexes

Ru complexes exhibit a variety of unique properties in the excited state, such as photoluminescence, photo redoxidation and photosubstitution.[42-46] Their unique photophysical and photochemical properties allow them to exploit their applications in the fields of catalysis[42], biomedicine[43], photosensitizers[44, 45] and solar energy conversion[46]. These Ru complexes have Ru^{2+} as their central cation and a coordination number of six. Generally, they can be divided into three main types based on the denticity of the coordinated ligands (Figure 9). Ru complexes containing three bidentate pyridyl ligands, for example, $[Ru(bpy)_3]^{2+}$ (bpy is 2,2′-bipyridine) are typically used as luminescent compounds and used in the photo-induced

energy and electron transfer process.[47] Ru complexes containing one or two monodentate ligands are usually photolabile. They can be photocleaved one or two monodentate ligands from the Ru center, followed by coordination of one or two ligands present in the reaction medium. These kinds of reactions can be seen as photosubstitution. $[Ru(tpy)(N\text{-}N)X]^{2+}$ (tpy is 2,2';6',2''-terpyridine) and $[Ru(bpy)_2XY]^{2+}$ are two kinds of classic photolytic Ru complexes and have been deeply studied and used as cages.

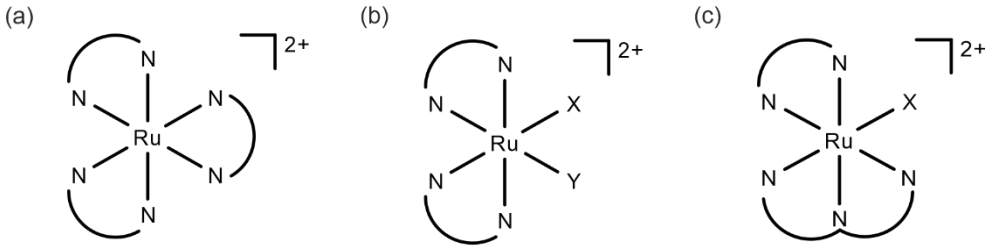

Figure 9. Schematic of Ru(II) polypyridyl complexes. (a) Ru complex containing three bidentate ligands. (b) Ru complex containing two bidentate pyridyl ligands and two monodentate ligands (X, Y can be the same or different). (c) Ru complex containing one tridentate pyridyl ligand, one bidentate pyridyl ligand and one monodentate ligand.

1.3.2 Photoresponsive Ru complexes

1.3.2.1 Photochemistry of Ru complexes

The elementary photochemistry of Ru complexes can be explained simply by the state diagram (Figure 10).[48] The maximum metal-to-ligand charge transfer band (MLCT) of these Ru complexes lies in the visible part of UV-vis spectra. Irradiation at the lowest MLCT band yields an excited single state ^{1}MLCT. Subsequently, an efficient intersystem crossing populates the triplet MLCT (^{3}MLCT) band. When the energy difference between the ^{3}MLCT and the metal-centered triplet state ^{3}MC of a Ru(II) complex is low enough, thermal promotion of the ^{3}MC state from the photochemically generated ^{3}MLCT state may lead to ligand photosubstitution.

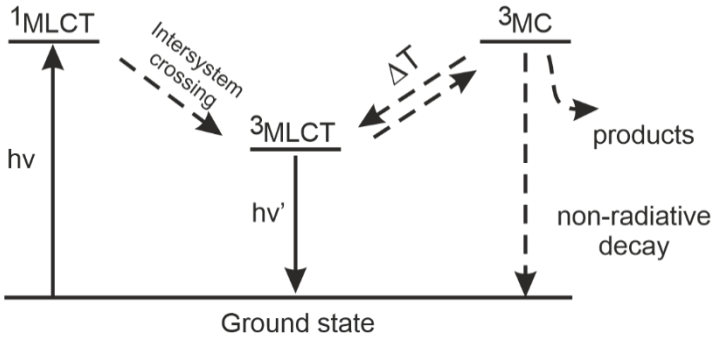

Figure 10. Photochemical pathways of Ru complexes.

1.3.2.2 Photosubstitution of Ru complexes

Photosubstitution of $[Ru(bpy)_2XY]^{2+}$ family

The monodentate ligands X and Y in the $[Ru(bpy)_2XY]^{2+}$ complexes can be efficiently photosubstituted by solvent molecules, in which X,Y are neutral monodentate ligands, typically are pyridine, amino or nitrile. In 2003, Etchenique group synthesized $[Ru(bpy)_2(4AP)_2]^{2+}$ (4AP is 4-aminopyridine) for neurochemical photodelivery.[49] The coordination bond between Ru center and the aromatic nitrogen of 4AP was stable in water under dark and was hydrolyzed upon visible light irradiation. In 2006, the same group demonstrated that $[Ru(bpy)_2XY]^{2+}$ can also act as protecting groups for amino and nitrile. For example, $[Ru(bpy)_2(tyr)_2]^{2+}$ (tyr is tyramine) was stable in water even for several days and delivered the tyramine ligand upon visible light irradiation (Figure 11a).[50] Besides, modifying the properties of monodentate ligands can promote the photodissociation of one of them and allow the other to be more photochemically stable. The classic example is $[Ru(bpy)_2(PPh_3)\ (GABA)]^{2+}$, in which PPh_3 is triphenylphosphine and GABA is 4-aminobutyric acid. PPh_3 is a stronger π-acceptor and weaker σ-donor compared with the amino group of γ-aminobutyric acid. Thus, the amine ligand can be substituted by a water molecule upon visible light irradiation, but the phosphine ligand remains coordinated even upon further irradiation (Figure 11b).[51]

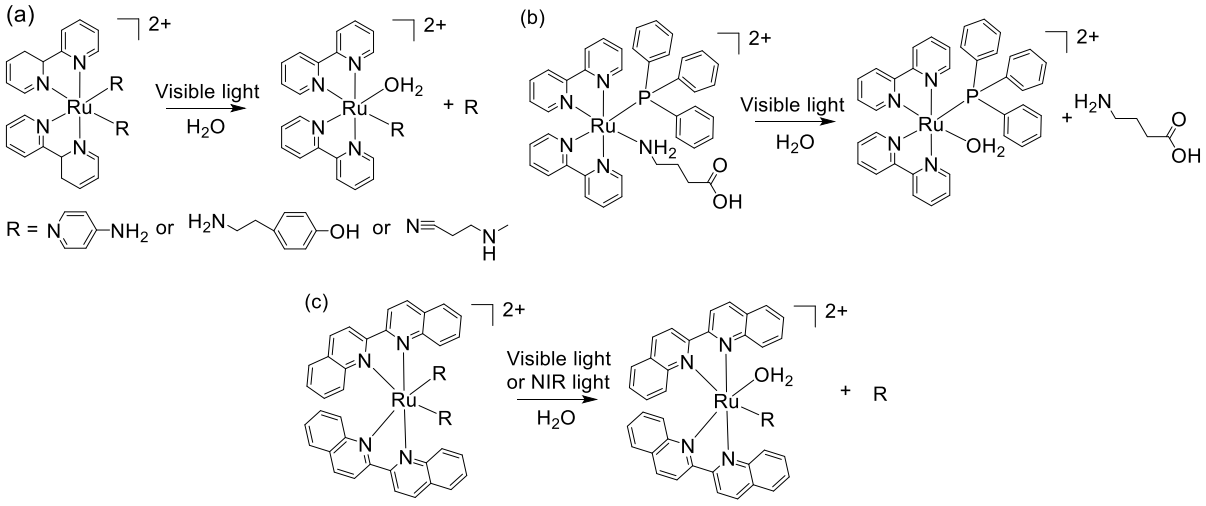

Figure 11. (a) Photosubstitution of $[Ru(bpy)_2(R)_2]^{2+}$ complex in water with visible light irradiation. (b) Photosubstitution of a monodentate ligand in the $[Ru(bpy)_2(PPh_3)(R)]^{2+}$ complex in water with visible light irradiation. (c) Photosubstitution of a monodentate ligand in the $[Ru(biq)_2(R)_2]^{2+}$ complex in water with visible or near-infrared (NIR) light irradiation.

Most of the MLCT absorption of $[Ru(bpy)_2XY]^{2+}$ family locate in the visible part. Changing the bidentate 2,2′-bipyridine by 2,2'-biquinoline (biq) in Ru complexes can redshift the MLCT absorption. Turro groups synthesized $[Ru(bip)_2(CH_3CN)_2]^{2+}$ complex, which shows an MLCT band at 500-650 nm. Therefore, acetonitrile ligands can be cleaved upon red light irradiation (Figure 11c). [52] Besides, combining Ru complexes with lanthanide-doped upconverting nanoparticles (UCNPs) can also induce the cleavage of the Ru complexes using near-infrared (NIR) light.[53-55] Our group modified the Ru complexes onto the UCNPs-based substrate. UCPNs can convert NIR light to blue light, inducing the cleavage of Ru complexes. This method was demonstrated to pattern proteins using NIR light (Figure 12). [53]

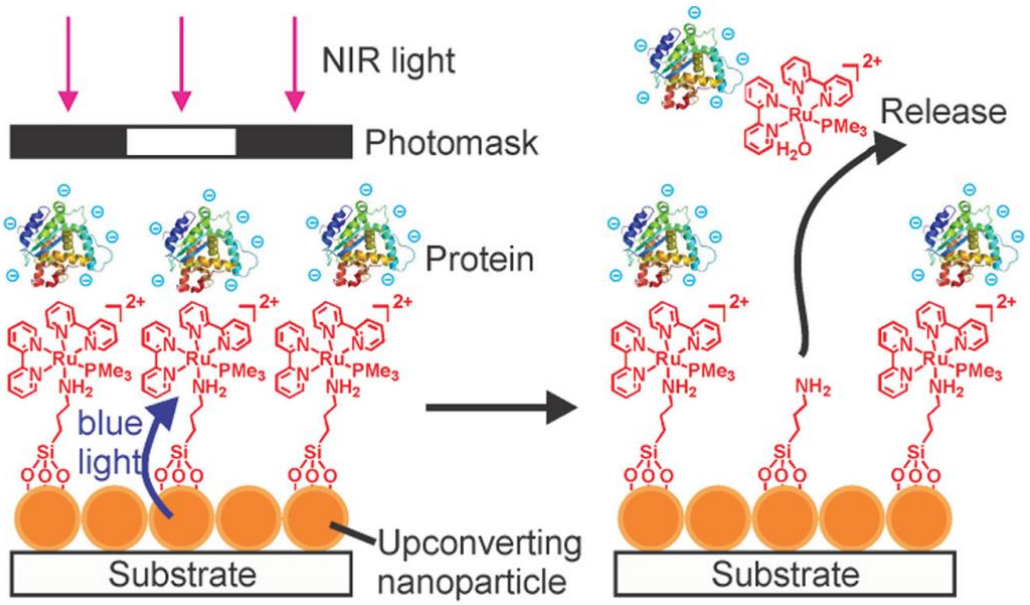

Figure 12. Schematic of photopatterning proteins via UCNP-assisted photochemistry. Reproduced by permission of ref. 53. Copyright 2015 WILEY-VCH Verlag GmbH & Co. KGaA.

Photosubstitution of $[Ru(tpy)(N\text{-}N)X]^{2+}$ family

In the $[Ru(tpy)(N\text{-}N)X]^{2+}$ family, N-N is a bidentate diamine ligand such as 2,2'-bipyridine (bpy), 2,2'-biquinoline (biq) and 1,10-phenanthroline (phen), and X can be pyridine, amino, nitrile and thioether.[56-59] In this part, I will focus on the thioether ligands that are ideal candidates for reversible coordination with Ru complexes.[60]

Bonnet group had proved that the Ru-thioether coordination bond between the $[Ru(tpy)(bpy)]^{2+}$ fragment and thioether ligands such as N-acetylmethionine or biotin was stable in the dark, and thioether ligands can be efficiently substituted by water molecules upon

visible light irradiation (Figure 13a).[61] They further demonstrated the Ru-thioether coordination bond in the Ru(tpy)(dcbpy)(Hmte)]$(PF_6)_2$ (dcbpy = 6,6'-dichloro-2,2'-bipyridine, Hmte = 2-(methylthio)ethanol)) complex is dynamic and reversible (Figure 13b).[62] In the dark, the Ru-thioether coordination bond was thermally unstable and partially hydrolyzed. Under visible light irradiation, the Ru-thioether coordination bond can be cleaved. When removing the light, the thioether ligands can spontaneously rebond to the Ru center in the dark without heating. The researcher thought this Ru-thioether coordination bond could be used as a photo-sensitive supramolecular bond in an aqueous solution. Furthermore, thioether ligand can also bond with $[Ru(tpy)(biq)(H_2O)]^{2+}$ complex spontaneously in the dark at room temperature, and this bond can be efficiently cleaved under visible light irradiation (Figure 13c).[60]

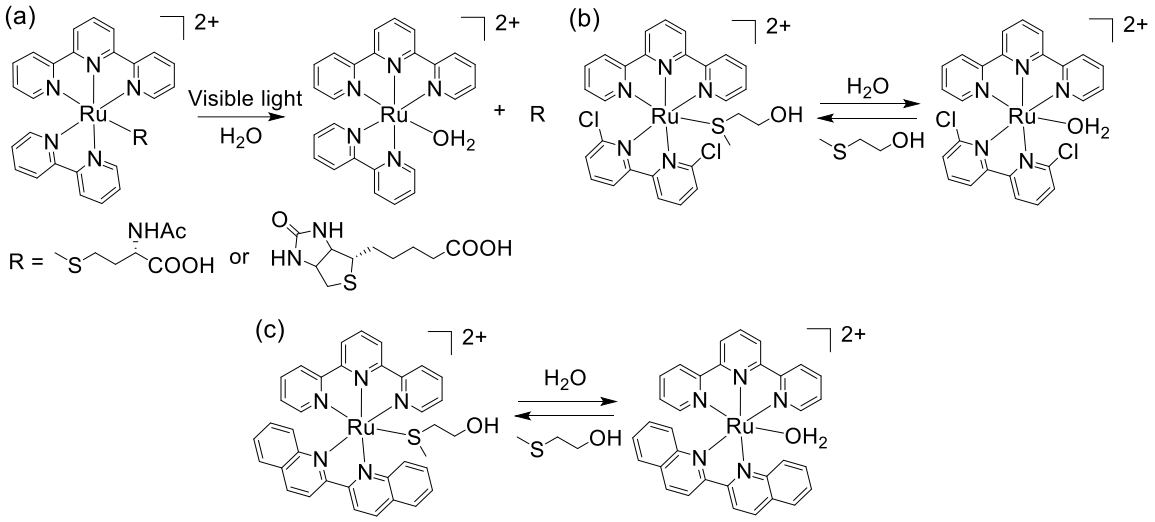

Figure 13. Photosubstitution of a monodentate ligand in the $[Ru(tpy)(bpy)(R)]^{2+}$ complex (a), $[Ru(tpy)(dcbpy)(R)]^{2+}$ complex (b) and $[Ru(tpy)(biq)(R)]^{2+}$ complex (c) in water under visible light irradiation.

Our group reported a reconfigurable surface based on Ru-thioether coordination bonds (Figure 14).[63] The Ru complex-modified surfaces were reversible and dynamic under light control. Under visible light irradiation, thioether ligands were removed from the surface. When the surface was placed in the dark, another thioether ligands were automatically attached to the surface via thermal coordination. In this way, various functions such as rewriting patterns, controlling protein absorption and surface wettability could be endowed to the reconfigurable surface based on the Ru-thioether coordination bond.

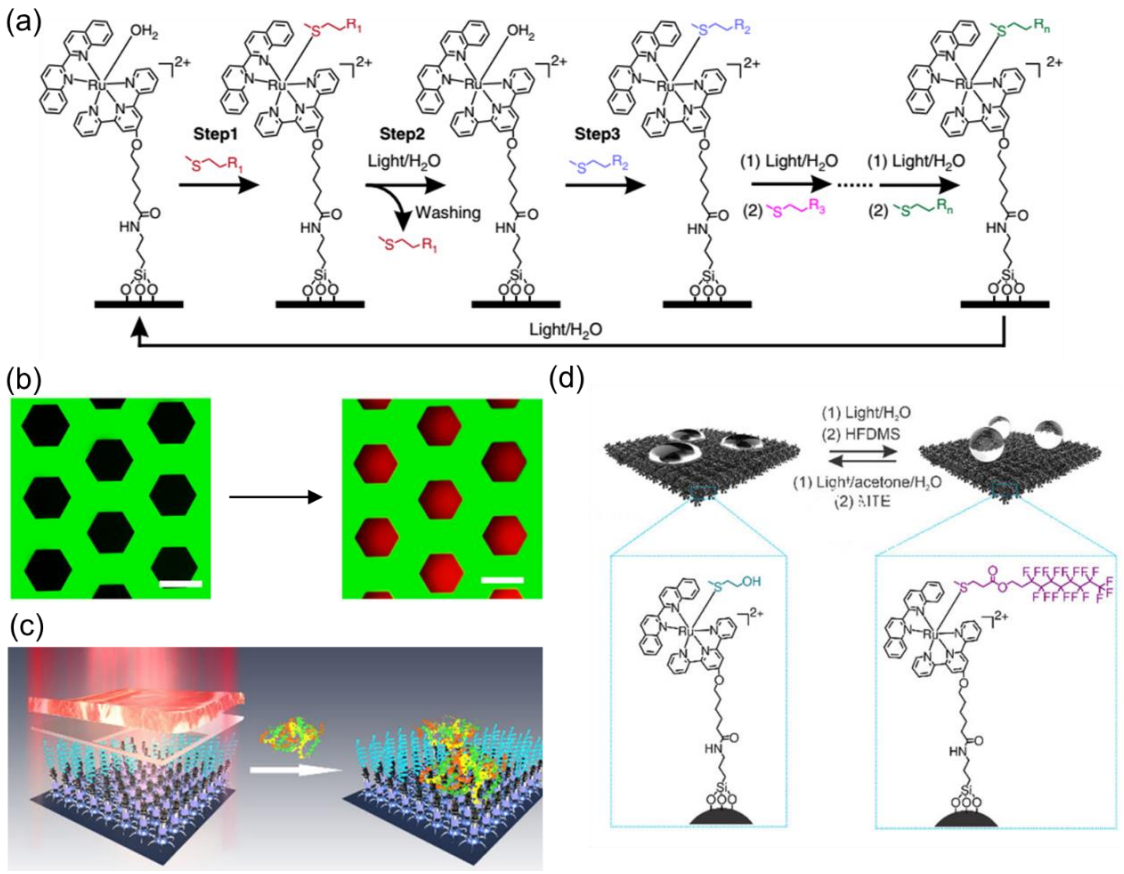

Figure 14. (a) Schematic of reconfiguring surfaces via ligand substitution. (b) Surface patterning. (c) Controllable protein absorption. (d) Reversible surface wettability. Reproduced by permission of ref. 63. Copyright 2012 Nature.

1.3.3 Photoresponsive Ru-containing polymers

As mentioned above, photolytic Ru complexes have been successfully used as cages for small molecules. The photosubstitution process exhibits radical-free cleavage of the Ru-ligand bond. Furthermore, Ru complexes can dissolve in an aqueous solution, making them amenable to use in complex polymer materials. Our group, for the first time, introduced Ru complexes into the main chain of block copolymers.[64, 65] PolyRu was a triblock copolymer consisting of photolytic Ru-containing linkers and biocompatible PEG blocks. Their potential applications in phototherapy have been demonstrated (Figure 15).[64]

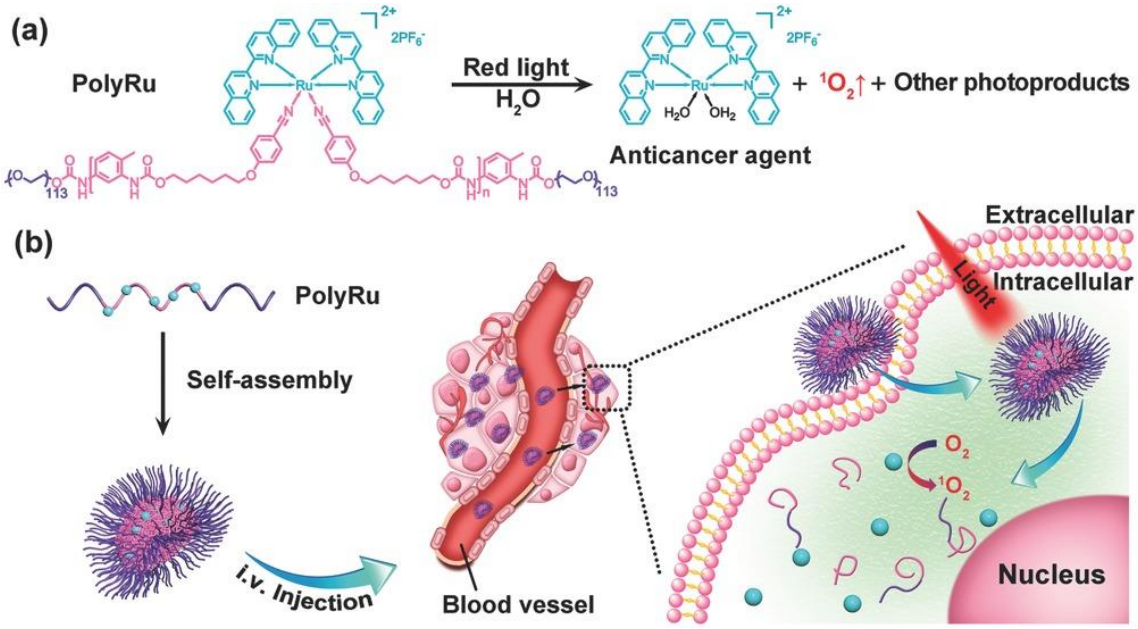

Figure 15. (a) Photosubstitution of Ru-containing block coplolymer (PolyRu) to generate the anticancer agent in water under red light irradiation. (b) Schematic of self-assembly and phototherapy using PolyRu. Reproduced by permission of ref. 64. Copyright 2016 WILEY-VCH Verlag GmbH & Co. KGaA.

The Teasdale group pioneered using photolytic Ru complexes as crosslinks for gel materials (Figure 16).[66] They synthesized an amino-functionalized Ru complexes $[Ru(bpy)_2(4AMP)_2]^{2+}(PF_6)_2$ (4AMP = 4-(aminomethyl) pyridine). Upon light irradiation in acetonitrile, pyridine ligands in the $[Ru(bpy)_2(4AMP)_2]^{2+}(PF_6)_2$ were successively substituted by acetonitrile. A photocleaved Ru-containing gel was prepared based on this photoreaction. $[Ru(bpy)_2(4AMP)_2]^{2+}(PF_6)_2$ reacted with hexamethylene diisocyanate and sequentially extended into a polymer network with ED-2003 to form a stable gel. Upon light irradiation, the gel became liquid because of the cleavage of Ru-pyridine ligands within 1 min. This photoreaction also occurred under multiphoton irradiation with NIR-laser light. 3D microscale patterns were carved into the gels upon the irradiation of a two-photon process in the NIR region. However, in this case, reversibility was not investigated.

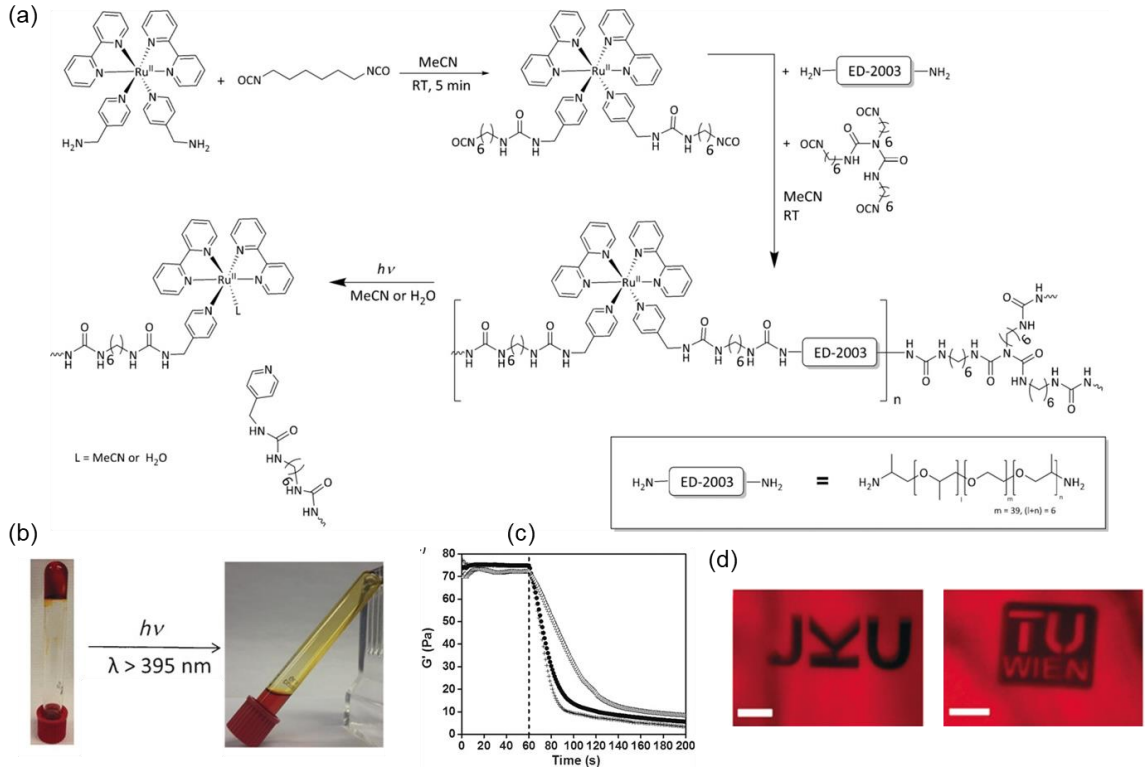

Figure 16. (a) Synthesis and photosubstitution of the Ru-containing gel. (b) Photos of the gel in acetonitrile before and after light irradiation. (c) Real-time photorheology of light-induced degelation of the hydrogel. (d) Obtained micropatterns of the hydrogel using two-photon excitation at 800 nm. Reproduced by permission of ref. 66. Copyright 2017 WILEY-VCH Verlag GmbH & Co. KGaA.

Two years later, the same group reported the use of the [Ru(bpy)$_2$] fragments as reversible crosslinks for the macromolecular ligand, poly(4-vinylpyridine) (P4VP), binding to the Ru centers, and crosslinking the polymers with heating (Figure 17).[67] Upon visible light irradiation, the Ru-pyridine bond was cleaved between the macromolecules leading to a gel-to-sol transition. Heating the sample reformed the linkage. The reversible gel-sol transition was repeated for several cycles. Both multiphoton (1028 nm) and single-photon (514 nm) lithography were used to write micropatterns on the gels. These patterns could be erased and rewritten on the same region of the gel.

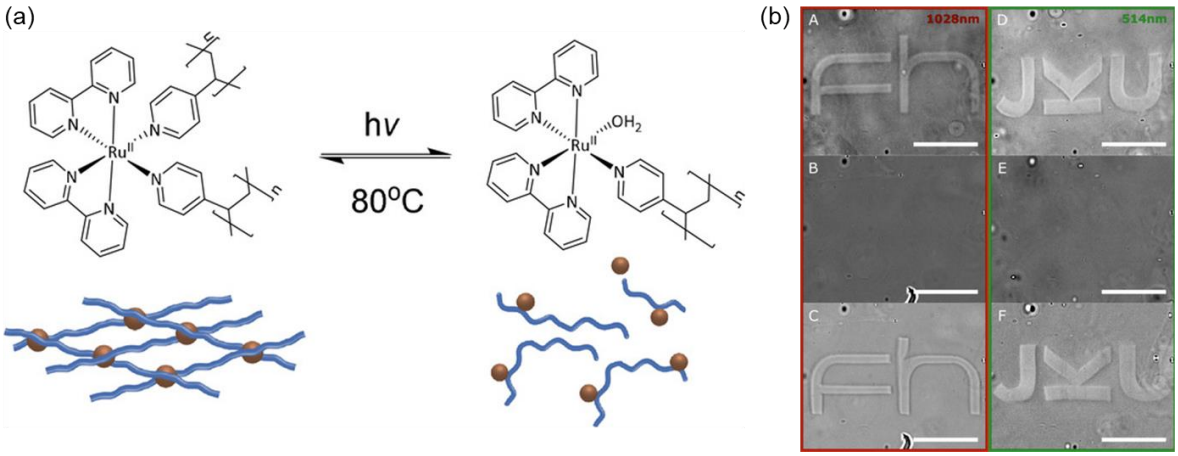

Figure 17. (a) Reversible cross-linking and cleavage of Ru-containing gels. (b) Images showing the writing, erasing and rewriting of the gels (from top to bottom). All scale bars were 50 μm. Reproduced by permission of ref. 67. Copyright 2019 WILEY-VCH Verlag GmbH & Co. KGaA.

1.3.4 Challenges of photolytic Ru complexes in photoresponsive gels

Many photolytic Ru complexes have been reported and their photochemical and physical properties have been well studied. In some cases, Ru complexes show photo-triggered ligand substitution. For example, $[Ru(biq \text{ or } bpy)_2XY]^{2+}$ and $[Ru(tpy)(N\text{-}N)X]^{2+}$ structures are developed as photocages and show an efficient cleavage of ligands upon visible light irradiation. Although some photoresponsive Ru-containing polymer gels have been reported previously, some limitations still need to be addressed. First, photoresponsive polymer gels based on the structures of $[Ru(biq)_2XY]^{2+}$ and $[Ru(bpy)_2XY]^{2+}$ using as crosslinks showed poor reversibility. Only one case showed the Ru-containing gel was reversible upon heating at 80 °C. Desirable development of photoresponsive Ru-containing gel with reversibility at room temperature and even lower temperature is appreciated. Second, the applications of photoresponsive Ru-containing gels are still limited. In this thesis, I will present my contribution to break these limitations by developing photoresponsive Ru-containing polymer gel based on photo-controlled Ru-thioether coordination bonds.

1.4 References

[1] Y. Osada, J. P. Gong, *Adv. Mater.* **1998**, *10*, 827.

[2] W. Guo, C. H. Lu, R. Orbach, F. Wang, X. J. Qi, A. Cecconello, D. Seliktar, I. Willner, *Adv. Mater.* **2015**, *27*, 73.

[3] T. S. Shim, S. H. Kim, C. J. Heo, H. C. Jeon, S. M. Yang, *Angew. Chem. Int. Ed.* **2012**, *51*, 1420.

[4] L. Dong, A. K. Agarwal, D. J. Beebe, H. Jiang, *Nature* **2006**, *442*, 551.

[5] H. Zhu, H. Yang, Y. Ma, T. J. Lu, F. Xu, G. M. Genin, M. Lin, *Adv. Funct. Mater.* **2020**, *30*, 2000639.

[6] L. Li, J. M. Scheiger, P. A. Levkin, *Adv. Mater.* **2019**, *31*, 1807333.

[7] J. Wei, Y. Yu, *Soft Matter* **2012**, *8*, 8050.

[8] C. Yu, H. Guo, K. Cui, X. Li, Y. N. Ye, T. Kurokawa, J. P. Gong, *Proc. Natl. Acad. Sci. U.S.A.* **2020**, *117*, 18962.

[9] J. Kim, S. Im, J. H. Kim, S. M. Kim, S. M. Lee, J. Lee, J. P. Im, J. Woo, S. E. Moon, *Adv. Mater.* **2020**, *32*, 1905901.

[10] L. Y. Chu, Y. Li, J. H. Zhu, W. M. Chen, *Angew. Chem. Int. Ed.* **2005**, *44*, 2124.

[11] C. Yang, Z. Liu, C. Chen, K. Shi, L. Zhang, X.-J. Ju, W. Wang, R. Xie, L.-Y. Chu, *ACS Appl. Mater. Interfaces* **2017**, *9*, 15758.

[12] D. Zhang, J. Zhang, Y. Jian, B. Wu, H. Yan, H. Lu, S. Wei, S. Wu, Q. Xue, T. Chen, *Adv. Intell. Syst.* **2020**, *3*, 2000208.

[13] J. Liao, H. Huang, *Biomacromolecules* **2020**, *21*, 2574.

[14] Y. Li, G. Huang, X. Zhang, B. Li, Y. Chen, T. Lu, T. J. Lu, F. Xu, *Adv. Funct. Mater.* **2013**, *23*, 660.

[15] T. Tanaka, *Phys. Rev. Lett.* **1978**, *40*, 820.

[16] C. Yu, J. Schimelman, P. Wang, K. L. Miller, X. Ma, S. You, J. Guan, B. Sun, W. Zhu, S. Chen, *Chem. Rev.* **2020**, *120*, 10695.

[17] E. R. Ruskowitz, C. A. DeForest, *Nat. Rev. Mater.* **2018**, *3*, 17087.

[18] C. Li, G. C. Lau, H. Yuan, A. Aggarwal, V. L. Dominguez, S. Liu, H. Sai, L. C. Palmer, N. A. Sather, T. J. Pearson, *Science Robotics* **2020**, *5*, 9822

[19] X. Zhang, L. Chen, K. H. Lim, S. Gonuguntla, K. W. Lim, D. Pranantyo, W. P. Yong, W. J. T. Yam, Z. Low, W. J. Teo, H. P. Nien, Q. W. Loh, S. Soh, *Adv. Mater.* **2019**, *31*, 1804540.

[20] C. Li, A. Iscen, L. C. Palmer, G. C. Schatz, S. I. Stupp, *J. Am. Chem. Soc.* **2020,** 142, 8447.

[21] C. Li, G. C. Lau, H. Yuan, A. Aggarwal, V. L. Dominguez, S. Liu, H. Sai, L. C. Palmer, N. A. Sather, T. J. Pearson, *Science Robotics* **2020**, *5*, 9822

[22]D. Lu, M. Zhu, S. Wu, Q. Lian, W. Wang, D. Adlam, J. A. Hoyland, B. R. Saunders, *Adv. Funct. Mater.* **2020**, *30*, 1909359.

[23] Z. Li, X. Liu, G. Wang, B. Li, H. Chen, H. Li, Y. Zhao, *Nat. Commun.* **2021**, *12*, 1363.

[24] S. Ikejiri, Y. Takashima, M. Osaki, H. Yamaguchi, A. Harada, *J. Am. Chem. Soc.* **2018**, *140*, 17308.

[25] W. C. Xu, S. Sun, S. Wu, *Angew. Chem. Int. Ed.* **2019**, *58*, 9712.

[26] G. Sinawang, M. Osaki, Y. Takashima, H. Yamaguchi, A. Harada, *Polym. J.* **2020**, *52*, 839.

[27] R. Klajn, *Chem. Soc. Rev.* **2014**, *43*, 148.

[28] T. Satoh, K. Sumaru, T. Takagi, T. Kanamori, *Soft Matter* **2011**, *7*, 8030.

[29] C. Li, A. Iscen, L. C. Palmer, G. C. Schatz, S. I. Stupp, *J. Am. Chem. Soc.* **2020**, *142*, 8447.

[30] W. Francis, A. Dunne, C. Delaney, L. Florea, D. Diamond, *Sens. Actuators B Chem*. **2017**, *250*, 608.

[31] S. Panja, D. J. Adams, *Chem. Soc. Rev.* **2021**, *50*, 5165.

[32] Y. Gu, E. A. Alt, H. Wang, X. Li, A. P. Willard, J. A. Johnson, *Nature* **2018**, *560*, 65.

[33] E. R. Ruskowitz, C. A. DeForest, *Nat. Rev. Mater.* **2018**, *3*, 17087.

[34] J. A. Shadish, G. M. Benuska, C. A. DeForest, *Nat. Mater.* **2019**, *18*, 1005.

[35] C. A. DeForest, K. S. Anseth, *Nat. Chem.* **2011**, *3*, 925.

[36] H. Yamaguchi, Y. Kobayashi, R. Kobayashi, Y. Takashima, A. Hashidzume, A. Harada, *Nat. Commun*. **2012**, *3*, 1270.

[37] J. Liu, C. S. Y. Tan, O. A. Scherman, *Angew. Chem. Int. Ed.* **2018**, *57*, 8854.

[38] K. Iwaso, Y. Takashima, A. Harada, *Nat. Chem.* **2016**, *8*, 625.

[39] S. Bonnet, J. P. Collin, *Chem. Soc. Rev.* **2008**, *37*, 1207.

[40] L. Zayat, O. Filevich, L. M. Baraldo, R. Etchenique, *Philos. trans., Math. phys. eng. sci.* **2013**, *371*, 20120330.

[41] A. Notaro, G. Gasser, *Chem. Soc. Rev.* **2017**, *46*, 7317.

[42] D. Wang, S. L. Marquard, L. Troian-Gautier, M. V. Sheridan, B. D. Sherman, Y. Wang, M. S. Eberhart, B. H. Farnum, C. J. Dares, T. J. Meyer, *J. Am. Chem. Soc.* **2018**, *140*, 719.

[43] C. Liu, R. Zhang, W. Zhang, J. Liu, Y. L. Wang, Z. Du, B. Song, Z. P. Xu, J. Yuan, *J. Am. Chem. Soc.* **2019**, *141*, 8462.

[44] Z. Lv, H. Wei, Q. Li, X. Su, S. Liu, K. Y. Zhang, W. Lv, Q. Zhao, X. Li, W. Huang, *Chem. Sci.* **2018**, *9*, 502.

[45] Y. Tsuji, K. Yamamoto, K. Yamauchi, K. Sakai, *Angew. Chem. Int. Ed.* **2017**, 57, 208.

[46] C.-C. P. Chiang, C.-Y. Hung, S.-W. Chou, J.-J. Shyue, K.-Y. Cheng, P.-J. Chang, Y.-Y. Yang, C.-Y. Lin, T.-K. Chang, Y. Chi, H.-L. Chou, P.-T. Chou, *Adv. Funct. Mater.* **2017**, *28* 1703282.

[47] G. Carrone, F. Gantov, L. D. Slep, R. Etchenique, *J. Phys. Chem. A.* **2014**, *118*, 10416.

[48] O. Filevich, L. Zayat, L. M. Baraldo, R. Etchenique, in *Luminescent and Photoactive Transition Metal Complexes as Biomolecular Probes and Cellular Reagents*, Springer, **2014**, 47.

[49] L. Zayat, C. Calero, P. Alborés, L. Baraldo, R. Etchenique, *J. Am. Chem. Soc.* **2003**, *125*, 882.

[50] L. Zayat, M. Salierno, R. Etchenique, *Inorg. Chem.* **2006**, *45*, 1728.

[51] L. Zayat, M. G. Noval, J. Campi, C. I. Calero, D. J. Calvo, R. Etchenique, *Chembiochem.* **2007**, *8*, 2035.

[52] B. A. Albani, C. B. Durr, C. Turro, *J. Phys. Chem. A* **2013**, *117*, 13885.

[53] Z. Chen, S. He, H. J. Butt, S. Wu, *Adv. Mater.* **2015**, 27, 2203.

[54] Z. Chen, R. Thiramanas, M. Schwendy, C. Xie, S. H. Parekh, V. Mailänder, S. Wu, *Small* **2017.** 1700997.

[55] S. He, K. Krippes, H. J. Butt, S. Wu. *Chem. Commun.* **2015,** 51, 431.

[56] V. H. van Rixel, A. Busemann, A. J. Gottle, S. Bonnet, *J. Inorg. Biochem.* **2015**, *150*, 174.

[57] T. N. Rohrabaugh, A. M. Rohrabaugh, J. J. Kodanko, J. K. White, C. Turro, *Chem. Commun.* **2018**, *54*, 5193.

[58] B. Siewert, M. Langerman, Y. Hontani, J. T. M. Kennis, V. H. S. van Rixel, B. Limburg, M. A. Siegler, V. Talens Saez, R. E. Kieltyka, S. Bonnet, *Chem. Commun.* **2017**, *53*, 11126.

[59] W. Sun, R. Thiramanas, L. D. Slep, X. Zeng, V. Mailander, S. Wu, *Chem. Eur. J.* **2017**, *23*, 10832.

[60] A. Bahreman, B. Limburg, M. A. Siegler, E. Bouwman, S. Bonnet, *Inorg. Chem.* **2013**, *52*, 9456.

[61] R. E. Goldbach, I. Rodriguez-Garcia, J. H. van Lenthe, M. A. Siegler, S. Bonnet, *Chem. Eur. J.* **2011**, *17*, 9924.

[62] A. Bahreman, B. Limburg, M. A. Siegler, R. Koning, A. J. Koster, S. Bonnet, *Chem. Eur. J.* **2012**, *18*, 10271.

[63] C. Xie, W. Sun, H. Lu, A. Kretzschmann, J. Liu, M. Wagner, H. J. Butt, X. Deng, S. Wu, *Nat. Commun.* **2018,** *9*, 3842.

[64] W. Sun, S. Li, B. Haupler, J. Liu, S. Jin, W. Steffen, U. S. Schubert, H. J. Butt, X. J. Liang, S. Wu, *Adv. Mater.* **2017**, *29*, 1603702.

[65] X. Zeng, Y. Wang, J. Han, W. Sun, H. J. Butt, X. J. Liang, S. Wu, *Adv. Mater.* **2020,** *32*, 2004766.

[66] S. Theis, A. Iturmendi, C. Gorsche, M. Orthofer, M. Lunzer, S. Baudis, A. Ovsianikov, R. Liska, U. Monkowius, I. Teasdale, *Angew. Chem. Int. Ed.* **2017**, *56*, 15857.

[67] I. Teasdale, S. Theis, A. Iturmendi, M. Strobel, S. Hild, J. Jacak, P. Mayrhofer, U. Monkowius, *Chem. Eur. J.* **2019**, *25*, 9851.

Chapter 2. Metallopolymer adhesive with photo-controlled coordination bonds for dynamic hydrogel assembly

2.1 Introduction

Science fictions have inspired the development of intelligent materials that can change shapes, reconfigure structures and reprogram functions in response to external stimuli. Intelligent materials are applicable to soft robots[1-3], four-dimensional (4D) printing[4-7], biomedical devices[8, 9], sensors[10, 11], and energy harvesters[12, 13]. Responsive hydrogels are a type of intelligent materials that are investigated extensively.[2, 7, 14-16] They are active and dynamic networks swollen by water, which exhibit volume changes via swelling or shrinkage when changing pH[15, 17], temperature[18, 19], light[2, 20-22], etc[23, 24]. Responsive hydrogels with homogeneous structures only show simple expansion/contraction, which limits their applications.[20, 21] To endow them with advanced shape-changing abilities, responsive hydrogels with complex and heterogeneous structures have been fabricated using photolithography[25, 26], three-dimensional (3D) printing[4, 7, 27] and other techniques[14, 28]. Such responsive hydrogels displayed various motions such as bending, winding, rotation, folding and walking. To develop intelligent materials using responsive hydrogels, the next challenge is to endow responsive hydrogels with reconfigurable structures and reprogrammable functions. However, the complex and heterogeneous structures in responsive hydrogels are usually linked by covalent bonds, which hinder reconfiguring their structures and reprogramming their functions.

A promising approach to address this challenge involves reversibly gluing complex and heterogeneous structures of responsive hydrogels using switchable adhesives. Although some mussel-inspired adhesives and supramolecular adhesives can reversibly glue wet surfaces of hydrogels, the use of reversible adhesives to construct reconfigurable hydrogel assemblies still poses a challenge.[29-33] The reversible adhesive must have strong adhesion to wet surfaces of hydrogels, be adaptable to the shape changes of hydrogels, be tolerant to the stimuli for the actuation of hydrogels.

In this section, reconfigurable hydrogel assemblies with reprogrammable functions were fabricated by reversibly gluing hydrogel units with a metallopolymer adhesive (Figure 1a-b). The metallopolymer adhesive is a mixture of a Ru-containing polymer and a thioether-containing polymer in water. Such polymers were deigned because some Ru complexes and (thioether) ligands coordinate and dissociate reversibly via thermal and photochemical

reactions, respectively.[34] Different from the reported reversible adhesives using mussel-inspired chemistry and supramolecular interactions, the reversible adhesives using photo-controlled Ru-ligand coordination have not been investigated. In this work, the metallopolymer adhesive contained Ru-S coordination bonds as reversible crosslinks. It was used to reversibly glue hydrogel units upon heating and light irradiation (Figure 1a-b). To reconfigure the glued gel assembly, light irradiation induces disadhesion; the hydrogel units are then separated, which can be reused to construct new hydrogel assemblies. A key for designing such hydrogel assemblies is the entanglement among the metallopolymer and the hydrogel.[35] In addition, the metallopolymer adhesive also needs to be a hydrogel that can adapt to actuation and shape changes of the assembly. This work demonstrates a new way to fabricate intelligent materials with complex, heterogeneous and reconfigurable structures and reprogrammable functions.

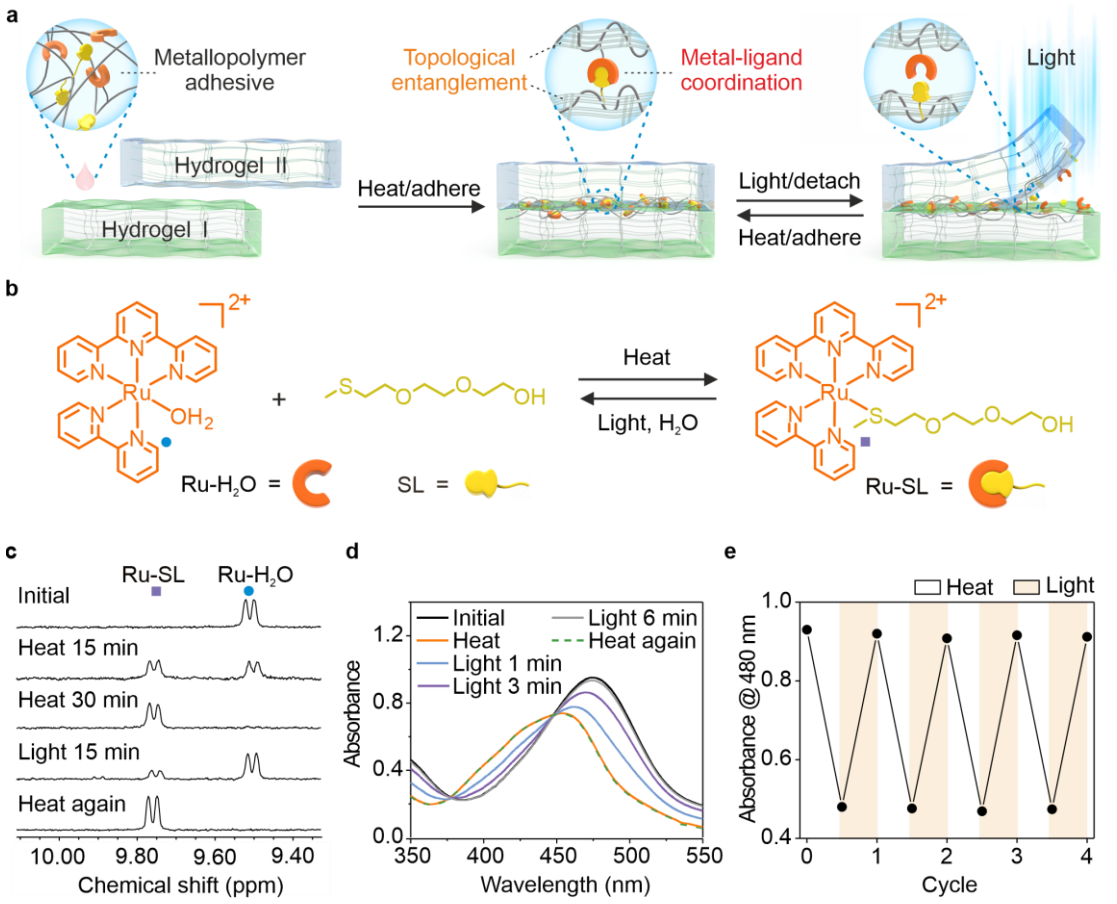

Figure 1. (a) Schematic illustration of using the photo-controlled metallopolymer adhesive to reversibly glue the hydrogels I and II. **b,** Reversible coordination of the Ru complex (Ru-H_2O) and the thioether ligand (SL) upon heating and light irradiation. The counterion of Ru-H_2O is PF_6^-. **c,** ^1H NMR spectra of Ru-H_2O (4.36 mM) and SL (43.6 mM) in D_2O before heating, after heating for 15 and 30 min at 70 °C, after light irradiation for 15 min (470 nm, 60 mW/cm^2), and

after heating again for 30 min at 70 ℃. **d,** UV-vis absorption spectra of Ru-H_2O (0.1 mM) and SL (1.0 mM) in water before and after heating for 2 h at 70 ℃, after light irradiation for 6 min (470 nm, 60 mW/cm^2), and after heating again for 2 h at 70 ℃. **e,** Absorption changes of the mixture of Ru-H_2O and SL in water under alternating heat/light irradiation cycles.

2.2 Results and discussion

2.2.1 Reversible Ru-thioether coordination

To demonstrate the reversible Ru-S coordination, the Ru complexes (Ru-H_2O and Ru-SL) and the thioether ligand (SL) as model compounds were synthesized (Figure 1b and S1-19). The reversible Ru-S coordination was studied using ^{1}H NMR spectroscopy (Figure 1c). When the mixture of Ru-H_2O (4.36 mM) and SL (43.6 mM) in D_2O was heated to 70 ℃ for 30 min, the signal from Ru-H_2O at 9.50 ppm disappeared and a new signal from Ru-SL at 9.76 ppm appeared. This result suggests that SL coordinated with the Ru center. Then, the Ru-SL solution was irradiated with blue light (470 nm, 60 mW/cm^2) for 15 min. The signal at 9.76 ppm increased significantly and the signal at 9.50 ppm largely decreased, which indicated that most Ru-SL was hydrolyzed to form Ru-H_2O upon light irradiation. The ^{1}H NMR data showed that Ru-SL reformed when the sample was heated to 70 ℃ for 30 min. Thus, the Ru-S coordination was reversible upon heating and light irradiation.

The Ru-S coordination was also studied using UV-vis absorption spectroscopy (Figure 1d). Initially, the absorption maximum of the mixture of Ru-H_2O and SL was at 476 nm. It was attributed to the metal-to-ligand charge transfer (MLCT) band of Ru-H_2O (Figure S10). When the mixture was heated to 70 ℃ for 2 h, the absorption maximum shifted to 452 nm, which was the same as that of pure Ru-SL (Fig S19). These results showed that SL coordinated with the Ru center upon heating. Then, the sample was irradiated with blue light (470 nm, 60 mW/cm^2) for 6 min. The absorption band reverted to that of the initial state, which suggested Ru-SL was hydrolyzed to form Ru-H_2O upon light irradiation. Subsequently, the sample was heated again at 70 ℃ for 2 h and its absorption maximum shifted to 452 nm again. The formation and dissociation of the Ru-S coordination bond was cycled for 4 times (Figure 1e), which revealed that the Ru-S coordination was reversible.

2.2.2 Reversible adhesives for hydrogels

To prepare reversible adhesives based on Ru-S coordination, the Ru-containing polymer (P-Ru) and the thioether-containing polymer (P-S) were synthesized (Figure 2a and Figure S20-40). P-Ru and P-S were water-soluble and gelation occurred when the mixture of P-Ru (1 wt%) and

P-S (1 wt%) in water was heated to 70 ℃ (Figure 2b and Figure S41). ^{1}H NMR spectroscopy showed that the gelation was attributed to crosslinking via the Ru-S coordination (Figure S42). Irradiating the P-Ru/P-S gel with blue light induced gel-to-sol transition (Figure 2b), which was due to light-induced dissociation of the Ru-S bonds (Figure S42). The sol-gel transitions upon heating and light irradiation were reversible.

To demonstrate that the mixture of P-Ru/P-S can be used as a reversible adhesive, two P1 gels (crosslinked N-hydroxyethyl acrylamide) as model were glued together (Figure 2c). To glue the P1 gels, P-Ru/P-S sol (6 wt%) was placed between the gels and heated to 70 ℃. Heating induced the sol-to-gel transition (Figure 2d). To separate the glued P1 gels, light irradiation induced gel-to-sol transition. The separated P1 gels were re-adhered by adding P-Ru/P-S sol and heating. The control experiments showed that P1 gels could not be glued using P-Ru or P-S only (Figure S43), which demonstrated that the sol-gel transition of P-Ru/P-S is essential for the adhesion.

The adhesion of the P-Ru/P-S adhesives for P1 gels was quantified via Lap shear tests (Figure 2e and Figure S44). The adhesion strength of P1 gels glued by P-Ru/P-S (6 wt%) was 1.18 kPa. Light irradiation induced a gel-to-sol transition and the adhesion strength decreased to almost zero. Thus, P1 gels could be separated after light irradiation. Subsequently, the separated P1 gels were re-adhered using P-Ru/P-S upon heating. The re-adhered sample had almost the same adhesion strength as the initial one.

To understand why the P-Ru/P-S adhesive exhibited strong yet reversible adhesion to P1 gels, the morphologies at the junction of two P1 gels were studied using scanning electron microscopy (SEM). For the adhered and re-adhered samples, the network of P-Ru/P-S adhesive interpenetrated with the network of P1 (Figure 2f and 2h). The polymer chains of P-Ru/P-S entangled with those of P1. In addition to the Ru-S coordination, the topological entanglements of polymer chains contributed to adhesion. For the sample after light irradiation, the network of P-Ru/P-S disappeared (Figure 2g), which resulted in disadhesion.

Importantly, the P-Ru/P-S adhesive is tolerant to temperature and pH, both of which are frequently used stimuli to actuate hydrogels. After the glued P1 gels were treated by different temperatures (25 and 70 ℃) and pH (4, 7 and 10) for 24 h, the adhesion strength did not change (Figure S45). This environment-tolerant property enabled the fabrication of responsive hydrogel actuators using the P-Ru/P-S adhesive, which are presented below.

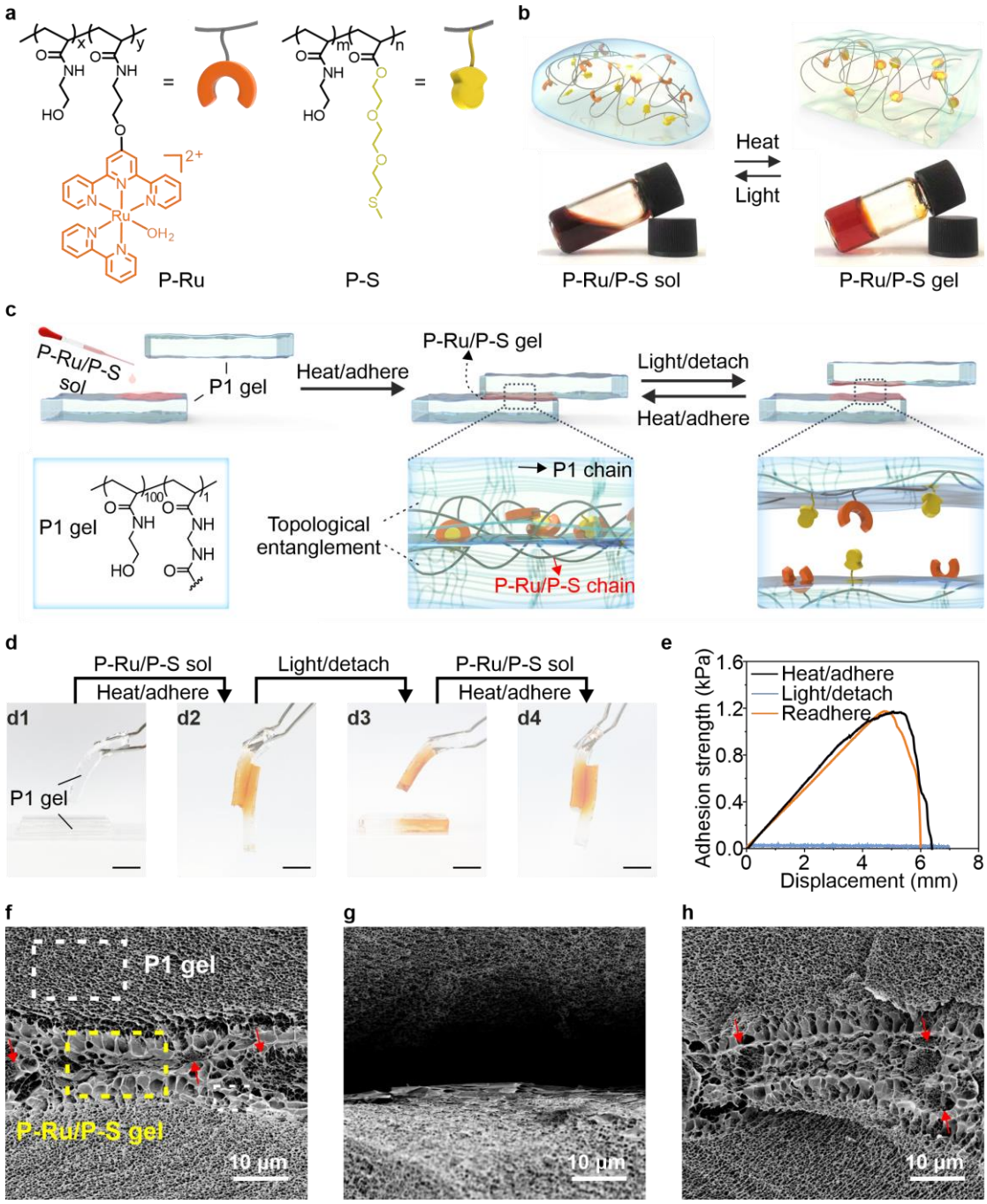

Figure 2. Reversible adhesion of P1 gels based on reversible sol-gel transitions of the P-Ru/P-S adhesive. (a) Chemical structures of P-Ru (x/y = 4.7/95.3, number-average molecular weight M_n = 16.4 kg/mol, polydispersity index PDI = 2.91) and P-S (m/n = 79/21, M_n = 14.9 kg/mol, PDI = 1.35). The counterion of P-Ru is Cl^-. (b) Schematic and photos of reversible sol-gel transitions of P-Ru/P-S upon heating and light irradiation. (c) Schematic illustration of reversible adhering two P1 gels using the P-Ru/P-S adhesive. (d) Photos showing reversible adhesion of two P1 gels using the P-Ru/P-S adhesive. Scale bars: 10 mm. (e) The adhesion strength of adhered P1 gels before irradiation, after light irradiation, and after subsequent re-

adhesion. (f-h) SEM images at the junctions of two adhered P1 gels before irradiation (f), after light irradiation (g), and after re-adhesion (h). The P1-rich network P-Ru/P-S-rich network are indicated by dashed frames in (f) and the interpenetrating networks are indicated using the red arrows in (f) and (h).

2.2.3 Responsive hydrogel actuators assembled by the reversible metallopolymer adhesive

To prepare responsive hydrogel actuators, we used P1 gel, thermo-responsive P2 gel, and pH-responsive P3 gel as units (Figure 3a). P1/P2 gel assemblies and P1/P3 gel assemblies were fabricated by gluing corresponding gels using the P-Ru/P-S adhesive. P1 gel was inert to temperature or pH change. P2 gel swelled and shrank upon heating to 70 ℃ and cooling to 25 ℃ because of the hydration and dehydration of the zwitterionic moiety (Figure S46). Therefore, the P1/P2 gel assembly bent and unbent reversibly upon cooling and heating (Figure 3b). A butterfly-shaped P1/P2 assembly was prepared, which beat the wings via temperature actuation (Figure 3d).

pH-actuated P1/P3 gel assemblies were also prepared (Figure 3c and 3e). P3 gel swelled at pH 10 and shrank at pH 4 because of the deprotonation and protonation of the acrylic acid moiety (Figure S47). Thus, pH changes induced bending/unbending of a rectangular P1/P3 gel assembly and triggered open/close of a hand-shaped P1/P3 gel assembly (Figure 3c and 3e). Bending and unbending was fully reversible for at least 10 times (Figure 3c). This observations demonstrates that the P-Ru/P-S adhesive glues responsive hydrogel assemblies firmly together, even under large shape changes. Shear measurements showed that the adhesion strength of P1/P2 gel assemblies and P1/P3 gel assemblies were still verg high even though after 10 times of bending and unbending (Figure S48-49). The strong adhesion is caused by Ru-S coordination strengthened by polymer chain entanglement (Figure 2). The adhesion of P-Ru/P-S is independent to pH and temperature (Figure S45). The P-Ru/P-S adhesive is a hydrogel that can change shape and maintain its integrated network structure during swelling and shrinkage (Figure S50). Thus, the P-Ru/P-S adhesive can adapt to the shape changes of the gel assemblies.

To verify that the P-Ru/P-S adhesive is strong yet reversible, a five-arm P1/P3 gel assembly were prepared using the adhesive (Figure 3f). The gel assembly showed reversible shape changes when varying the pH (Figure 3, f1 and f4). To illustrate the advantage of light andits high spatial resolution, some of the adhered arms were selectively detached via light irradiation (Figure 3, f2 and f3) and the gel assembly changed to different shapes via pH activation. The detached arms could be re-adhered to form the initial five-arm structure (Figure 3, f4).

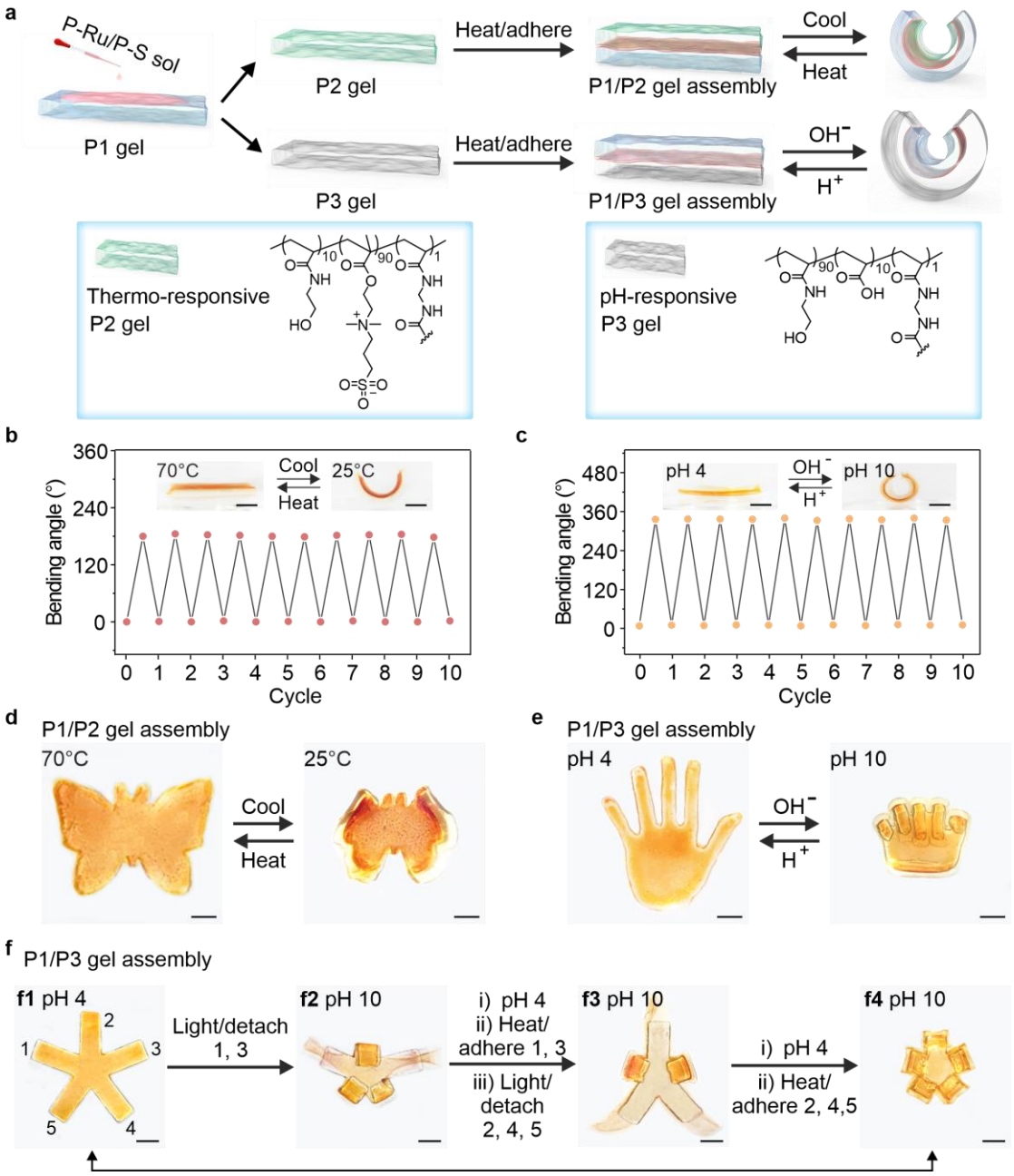

Figure 3. Preparation and actuation of responsive bilayer hydrogel assemblies. (a) Schematic of preparing responsive hydrogel assemblies using P-Ru/P-S as the adhesive and shape changes of the hydrogel assemblies actuated by temperature or pH. (b-c) Reversible bending of (b) a P1/P2 gel assembly at different temperatures and (c) a P1/P3 gel assembly at different pH. (d) Photos of a butterfly-shaped P1/P2 gel assembly at different temperatures. (e) Photos of a hand-shaped P1/P3 gel assembly at different pH. (f) Reversible detachment and adhesion of some arms of a five-arm P1/P3 gel assembly and shape changes of the gel assembly at different pH. Scale bars: 5 mm.

2.2.4 Reconfigurable hydrogel assemblies with reprogrammable shape changes

The reversible P-Ru/P-S adhesive enables the fabrication of reconfigurable hydrogel assemblies with reprogrammable shape changes. Assembly 1 with complex and heterogeneous structures was prepared by gluing a P1 gel, two P2 gels and two P3 gels together (Figure 4a). Assembly 1 changed to four shapes at different temperatures and pH (Figure 4b, first column). Moreover, the structure of Assembly 1 could be reconfigured by light-induced detachment and re-adhering using the P-Ru/P-S adhesive. So, Assemblies 2, 3 and 4 via reconfiguration were prepared using the same hydrogel units. Each gel assembly changed into four shapes upon the stimulation of pH and temperature (Figure 4b). Such hydrogel assemblies are intelligent multi-shape transformers. These results showed that the use of the reversible metallopolymer adhesive is a novel strategy for the preparation of complex, heterogeneous and reconfigurable hydrogel assemblies with reprogrammable actuation functions.

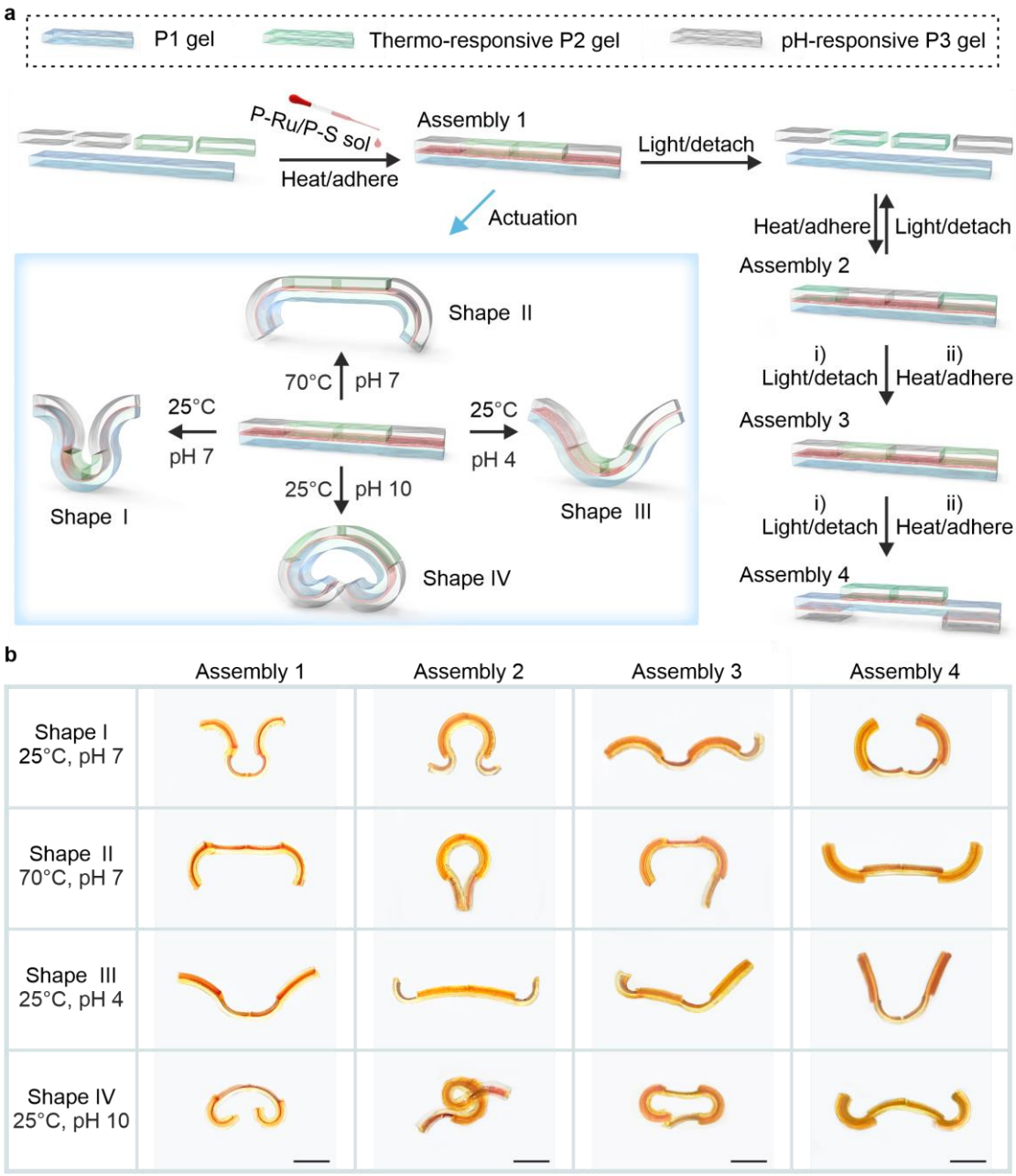

Figure 4. Reconfiguring the structures of responsive hydrogel assemblies for reprogrammable actuation. (a) Schematic of fabricating and reconfiguring hydrogel assemblies with complex and heterogeneous structures and shape changes at different temperatures and pH. (b) Photos of the hydrogel assemblies at different temperatures and pH. Scale bars:10 mm.

2.2.5 A soft robot based on hydrogel assemblies for maze navigation guided by external stimuli

A soft robot was fabricated with complex and heterogeneous structures by gluing a non-responsive P1 gel, a pH-responsive P3 gel, and a magnetically responsive P4 gel using the P-Ru/P-S adhesive (Figure 5a). P4 gel contained magnetic Ni particles so that it can move under a magnetic field. The P1/P3/P4 robot was glued firmly using the P-Ru/P-S adhesive. Thus, the P1 and P3 units followed the movement of P4 units in a magnetic field.

The P1/P3/P4 robot could go through a maze under the stimulation of pH and a magnetic field. At pH 10, the robot was too high to pass Gate 1 (Figure 5, b2 and c1). When the pH was adjusted to 4, the robot became flat and passed Gate 1 under the guide of a magnetic field (Figure 5, b2 and c2). However, the flattened robot could not pass Gate 2 (Figure 5, b1). Therefore, the robot was reshaped by changing pH to 10 and it passed Gate 2 under the guide of a magnetic field (Figure 5, b1 and c3). In similar ways, the robot went through the maze that had a few more gates and a tortuous path (Figure 5, c4 and c5).

To demonstrate that the robot is reconfigurable, the P1/P3 gels and P4 gel were separated via light irradiation (Figure 5d). The P1/P3 gels were reused as an actuator demonstrated in Figure 3f. The P4 gel was reused by gluing it with a five-armed P1/P2 assembly and a P1/P2/P4 robot was prepared (Figure 51a). Because P2 was thermo-responsive and P4 was magnetically responsive, the P1/P2/P4 robot passed a maze under the control of temperature and a magnetic field (Figure S51b).

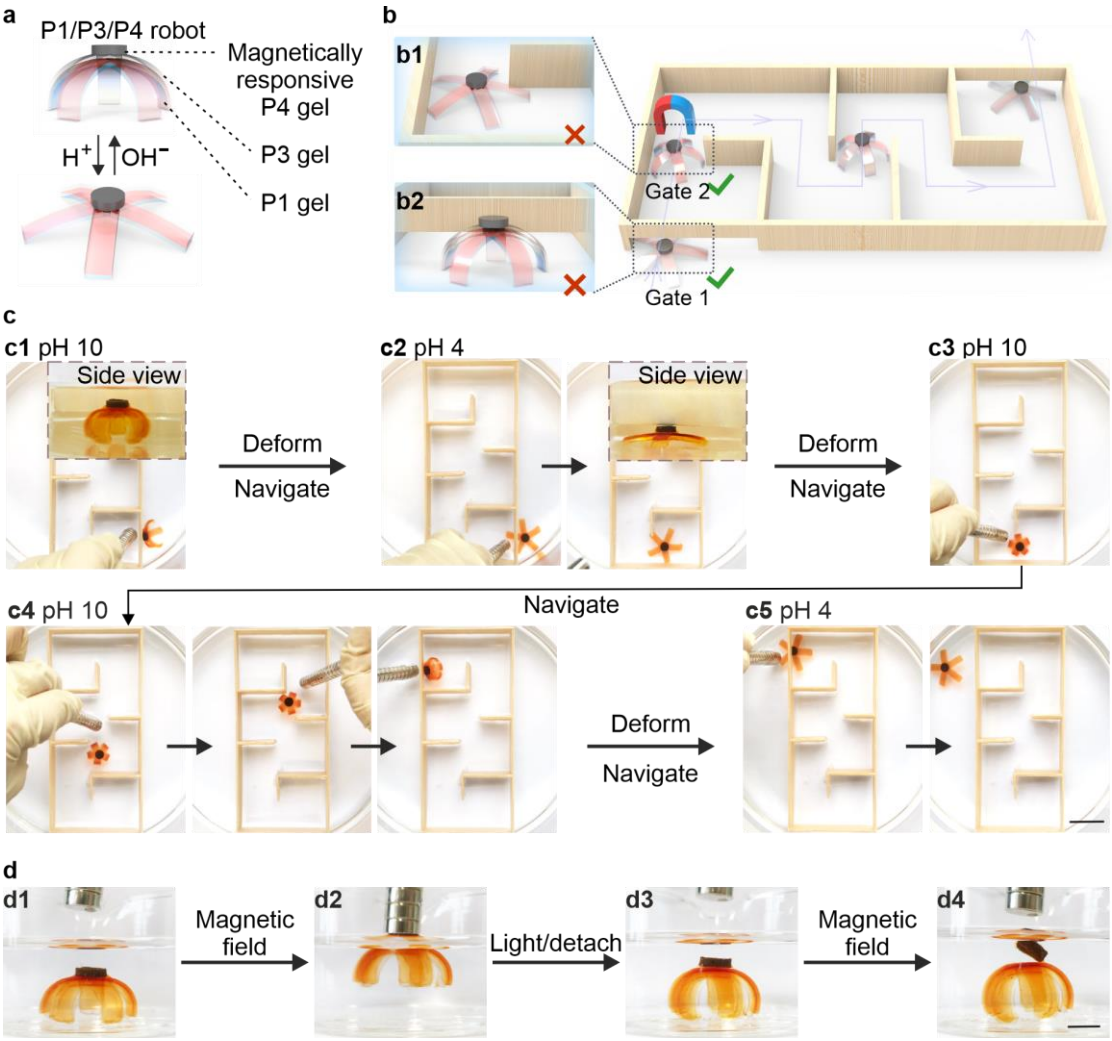

Figure 5. A soft robot based on a dual-responsive gel assembly for maze navigation. (a) Schematic of a P1/P3/P4 robot prepared by gluing the gel units using the P-Ru/P-S adhesive. (b) Schematic illustration and (c) photos of the P1/P3/P4 robot passing through a maze under the control of pH and a magnetic field. The inset of c1 showed that the robot was too high to pass through the gate. The inset of c2 showed that the flattened robot passed the gate. Scale bar: 20 mm. (d) The P1/P3/P4 robot under the attraction of a magnetic field (d1 and d2); After light irradiation, P1/P3 gels and P4 gel were separated (d3 and d4). Scale bar: 5 mm.

2.3 Conclusions

In conclusion, this work have demonstrated the fabrication of complex, heterogeneous, multi-responsive hydrogel assemblies with reconfigurable structures and reprogrammable functions by reversibly gluing hydrogel units using a metallopolymer adhesive. The newly designed metallopolymer adhesive adheres to wet surfaces of hydrogels firmly and reversibly and it adapts to actuation and shape changes of hydrogels. Different from the mussel-inspired

chemistry and supramolecular chemistry for adhesives reported in literature, the combination of photo-controlled Ru-S coordination and polymer chain entanglement represents a new strategy for designing strong yet reversible adhesives. The actuators and soft robots reported here, other intelligent materials with multi components, reconfigurability, programmability and customizable functions can be fabricated by reversibly gluing intelligent building blocks. This study opens up an avenue for the design of responsive materials, 4D printing materials, biomaterials and soft robots.

2.4 Experimental section

2.4.1 Materials

$RuCl_3 \bullet xH_2O$ (99.9%) was purchased from Fisher Scientific. Acryloyl chloride (97.0%), 3-amino-1-propanol (99%), N,N'-methylenebisacrylamide (Bis) (>99.5%), magnesium sulfate (>98%), sodium chloride (>99%), sodium thiomethoxide (95%) and Irgacure 2959 (98%) were purchased from Sigma-Aldrich. 2,2'-Bipyridine (bpy) (>99%), silver hexafluorophosphate (>98%), potassium hexafluorophosphate (>98%), 2-[2-(2-chloroethoxy)ethoxyl] ethanol (>96%), N-(2-hydroxyethyl)acrylamide (HEA) (>98%), 2,2'-azobis[2-(2-imidazolin-2-yl) propane] dihydrochloride (VA-044) (>98%), acrylic acid (AAc) (>99%) and 3-dimethyl (methacryloyloxyethyl) ammonium propane sulfonate (DMAPS) (95%) were purchased from TCI. 2,2':6',2''-Terpyridine (tpy) (97%) was purchased from Alfa Aesar. 4'-Chloro-2,2',6',2''-terpyridine (>98%) was purchased from AEchem Scientific Corporation. MagneHis^{TM} Ni-Particle was purchased from Promega. All solvents (HPLC grade) were purchased from Sigma-Aldrich or Fisher Scientific.

2.4.2 Instruments and Characterization

^{1}H nuclear magnetic resonance (^{1}H NMR) and ^{13}C nuclear magnetic resonance (^{13}C NMR) spectra were recorded on a 300-MHz Bruker Spectrospin NMR spectrometer. The molecular weights were determined using mass spectrometry (Bruker Time-of-flight MS Reflex III and Expression L Compact Mass Spectrometer). UV-vis absorption spectra were measured using a Lambda 900 spectrometer (Perkin Elmer). The molecular weights and polydispersity indeces of the polymers were determined using a PSS-WinGPC (pump: SECcurity) equipped with UV and RI detectors running in dimethylformamide (DMF) with 1g/L LiBr at 60 °C calibrated against polystyrene standards. The morphologies of the gels were observed using scanning electron microscopy (SEM, LEO Gemini 1530). Lap-shear tests were performed using a

Zwick/Roell system with a deformation rate of 20 mm min^{-1}. To fix the gel assemblies between the clamps of the tensile machine, a polyester film (thickness: 0.35 mm) was used as a back layer glued on the gels using a commercial superglue.

2.4.3 Synthesis and preparation

Synthesis of Ru(tpy)(bpy)(H_2O)] (PF_6)$_2$ (Ru-H_2O)

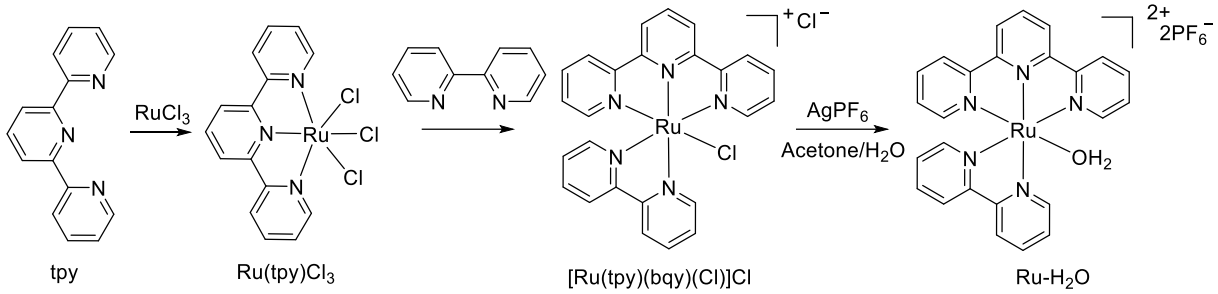

Figure S1. Synthetic route for Ru-H_2O.

Synthesis of Ru(tpy)Cl_3: $RuCl_3 \cdot xH_2O$ (262 mg, 1.0 mmol) and 2,2':6',2''-terpyridine (tpy, 233.3 mg, 1.0 mmol) were dissolved in ethanol (50 mL). The mixture was heated at reflux for 4 h with magnetic stirring. Then, the mixture was cooled to room temperature. Brown powders were obtained and filtered from the reddish-yellow solution. The brown powders were washed with ethanol and diethyl ether, and dried to obtain the compound Ru(tpy)Cl_3 as a brown solid. Yield: 363 mg (82%).

Synthesis of [Ru(tpy)(bpy)(Cl)]Cl: Ru(tpy)Cl_3 (171 mg, 0.39 mmol) and 2,2'- bipyridine (bpy, 61 mg, 0.39 mmol) were mixed in a 2/1 (v/v) ethanol/H_2O mixture (30 mL). The solution was degassed for 5 min and filled with argon before refluxing at 85 ℃ for 24 h under an argon atmosphere. After that, the mixture was filtered hot and the filtrate was evaporated under reduced pressure to obtain the crude product. The product was purified by column chromatography with silica gel (eluent: methanol/dichloromethane (v/v) = 1/8 to 1/4). The solvent was evaporated and the product was obtained as violet powers. Yield: 180 mg (77.6%).

^{1}H NMR of [Ru(tpy)(bpy)(Cl)]Cl (300 MHz, CD_3OD, 25℃) δ (ppm): 10.21 (d, J = 4.7 Hz, 1H, H-A1), 8.79 (d, J = 8.8 Hz, 1H, H-A4), 8.67 (d, J = 8.8 Hz, 2H, H-T2'), 8.56-8.51 (dd, J = 7.8 Hz, 3H, H-T4, B4), 8.34 (t, J = 8.4 Hz, 1H, H-A3), 8.17 (t, J = 8.8 Hz, 1H, H-T3'), 8.02 (t, J = 7.8 Hz, 1H, H-A2), 7.95 (t, J = 7.8 Hz, 2H, H-T3), 7.77-7.70 (m, 3H, H-B3, 2H-T1), 7.40-7.32 (m, 2H-T2, H-B1), 7.05 (t, J = 7.4 HZ, 1H, H-B2).

^{13}C NMR of [Ru(tpy)(bpy)(Cl)]Cl (75 MHz, CD_3OD, 25 °C) δ (ppm): 158. 96 (T1', T5), 158.17 (B5), 156.25 (A5), 152.18 (B1), 151.98 (T1), 151.38 (A1), 137.21 (T3), 136.52 (T3'), 135.57 (B3), 134.16 (A3), 127.18 (T2), 126.73 (B2), 126.08 (A2), 123.37 (T4), 123.07 (B4), 125.98 (A4) and 122.24 (T2').

MALDI-TOF of [Ru(tpy)(bpy)(Cl)]Cl: *m/z* calculated for $C_{25}H_{19}N_5Cl_2Ru$ ($[M\text{-}Cl]^+$): 526.04; found 525.03.

UV-vis of [Ru(tpy)(bpy)(Cl)]Cl: The absorption maximum in acetone is at 507 nm, which is attributed to the metal-to-ligand charge transfer (MLCT) band of [Ru(tpy)(bpy)(Cl)]Cl.

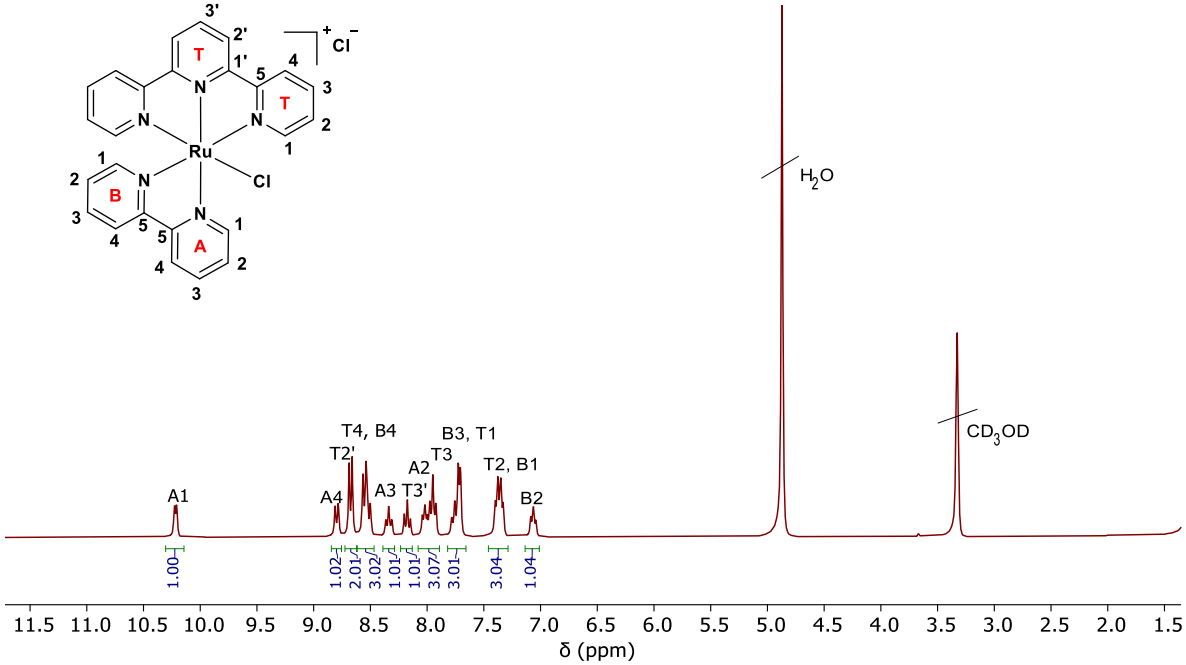

Figure S2. ^{1}H NMR spectrum of [Ru(tpy)(bpy)(Cl)]Cl (300MHz, CD_3OD, 25°C).

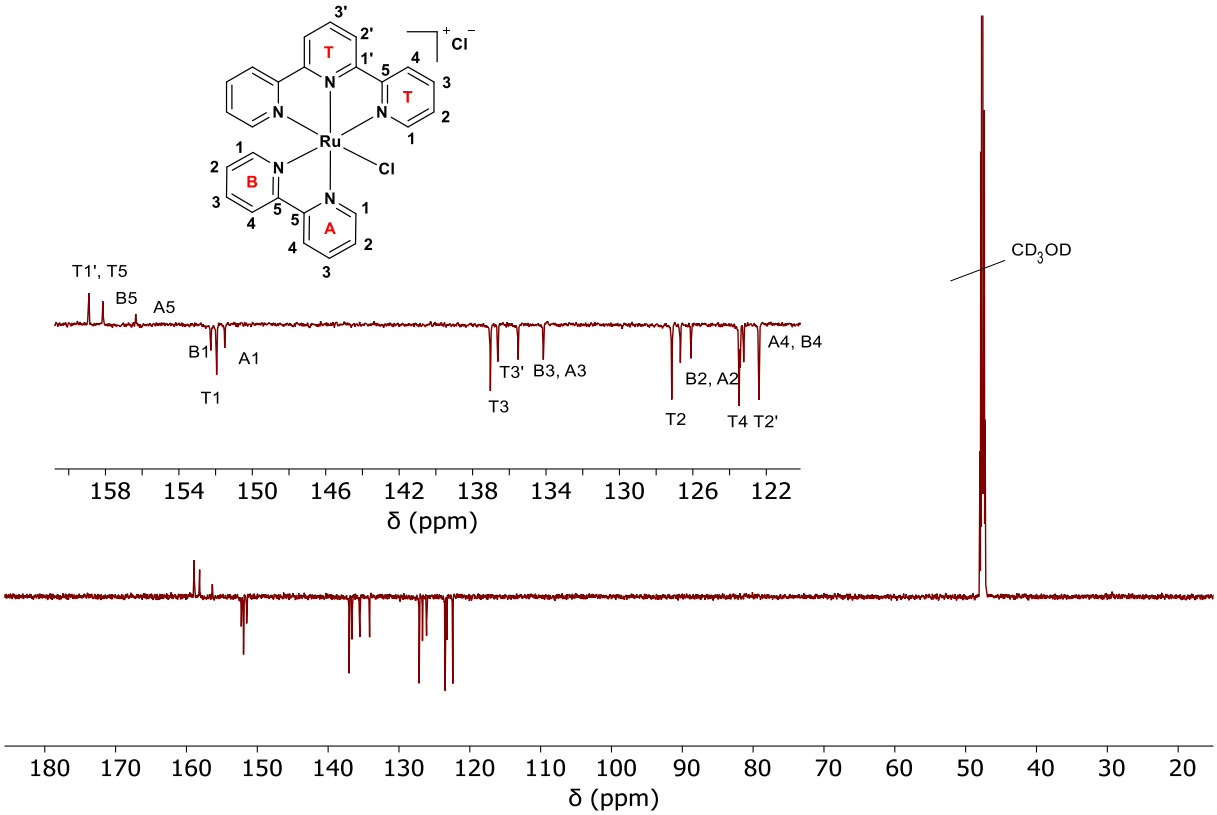

Figure S3. ^{13}C NMR spectrum of [Ru(tpy)(bqy)(Cl)]Cl (75MHz, CD_3OD, 25°C).

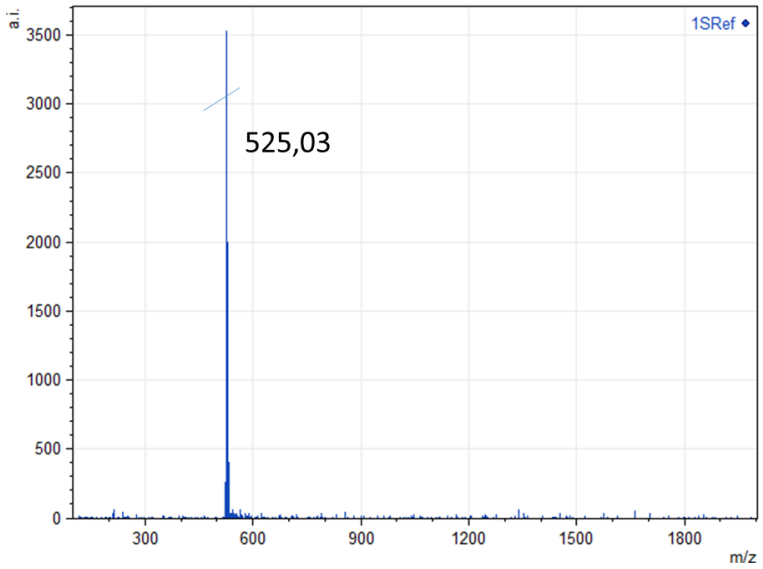

Figure S4. MALDI-TOF-MS spectrum of [Ru(tpy)(bpy)(Cl)]Cl.

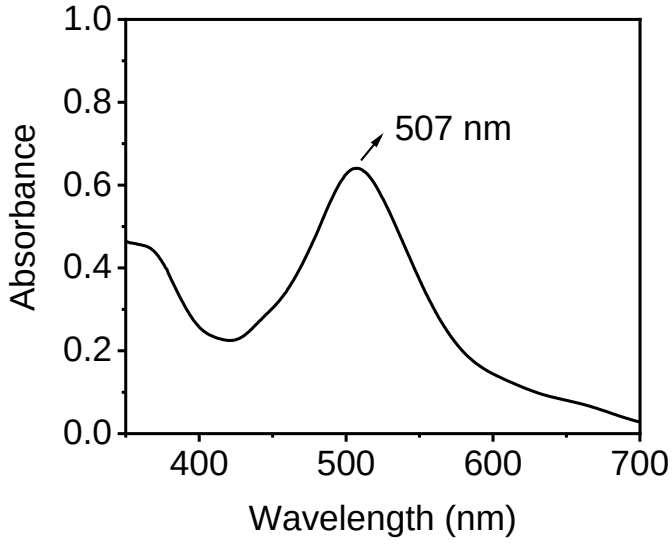

Figure S5. UV-vis absorption spectrum of [Ru(tpy)(bpy)(Cl)]Cl in acetone.

Synthesis of Ru-H_2O: [Ru(tpy)(bpy)(Cl)]Cl (28 mg, 0.049 mmol) and $AgPF_6$ (28 mg, 0.11 mmol) were mixed in a 3/1 (v/v) H_2O/acetone mixture (8 mL). The solution was degassed for 5 min and filled with argon before refluxing at 85 ℃ for 24 h under an argon atmosphere. After that, the mixture was filtered over Celite and concentrated to 1 mL under reduced pressure. The dark red solid was precipitated from a saturated KPF_6 aqueous solution (26 mg, 0.032 mmol, 66.4%).

^{1}H NMR of Ru-H_2O (300 MHz, D_2O, 25℃) δ (ppm): 9.51 (d, J = 5.3 Hz, 1H, H-A1), 8.58 (d, J = 5.5 Hz, 1H, H-A4), 8.67 (d, J = 4.6 Hz, 2H, H-T2'), 8.36 (d, J = 4.5 Hz, 2H, H-T4), 8.27-8.22 (m, 2H, H-B4, H-T3'), 8.13 (t, J = 7.3 Hz, 1H, H-A3), 7.96-7.85 (m, 3H, H-A2, 2H-T3), 7.71 (d, J = 5.5 Hz, 2H, H-T1), 7.58 (t, J = 7.6 Hz, 1H, H-B3), 7.23 (m, 3H, 2H-T2, H-B1), 6.84 (t, J = 7.7 Hz, 1H, H-B2).

^{13}C NMR of Ru-H_2O (75 MHz, CD_3OD, 25 °C) δ (ppm): 159.24 (B5), 159.07 (T1'), 158.66 (T5), 156.03 (A5), 152.88 (T1), 152.34 (B1), 150.22 (A1), 138.46 (T3), 137.51 (T3'), 136.29 (B3), 136.08 (A3), 128.10 (T2), 127.52 (B2), 126.39 (A2), 124.21 (T4), 124.00 (B4), 123.38 (A4) and 123.30 (T2').

MALDI-TOF of Ru-H_2O: *m/z* calculated for $C_{25}H_{21}N_5ORuP_2F_{12}$ ($[M-2PF_6-H]^+$): 508.55; found 508.09.

UV-vis of Ru-H_2O: The absorption maximum in water is at 476 nm, which is attributed to the metal-to-ligand charge transfer (MLCT) band of Ru-H_2O.

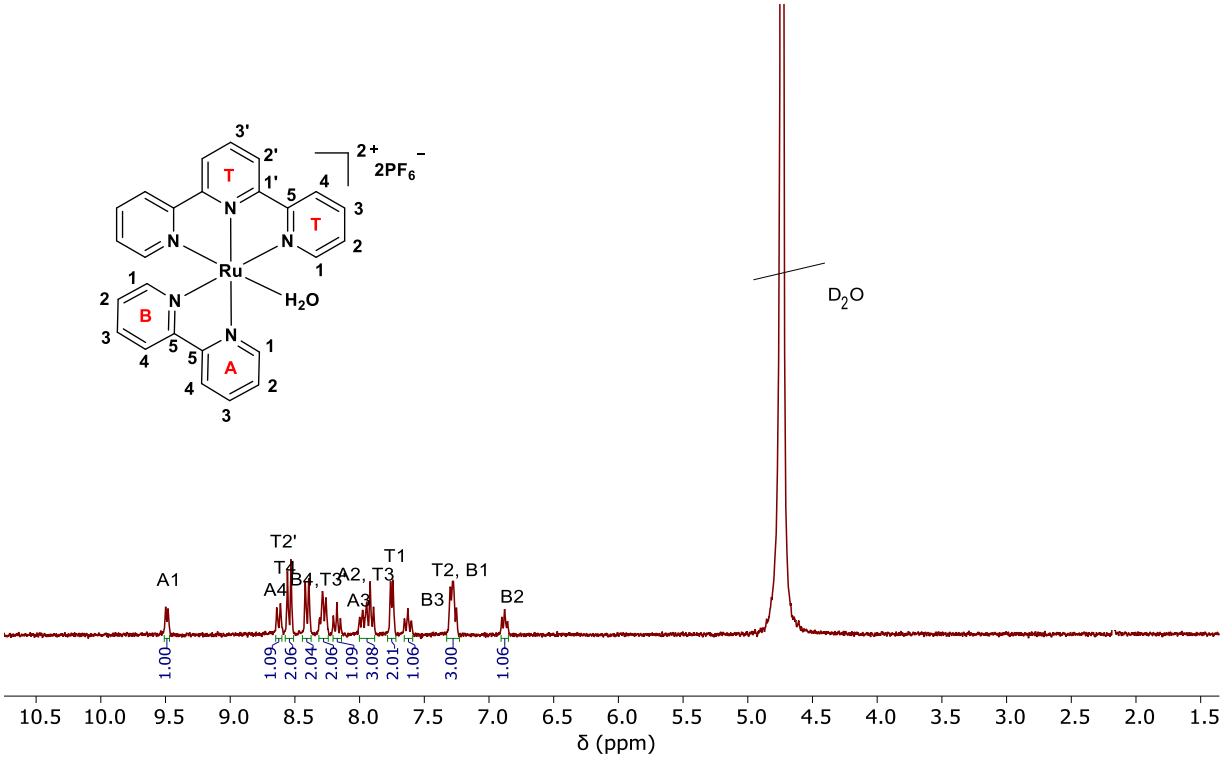

Figure S6. ^{1}H NMR spectrum of Ru-H_2O (300MHz, D_2O, 25°C).

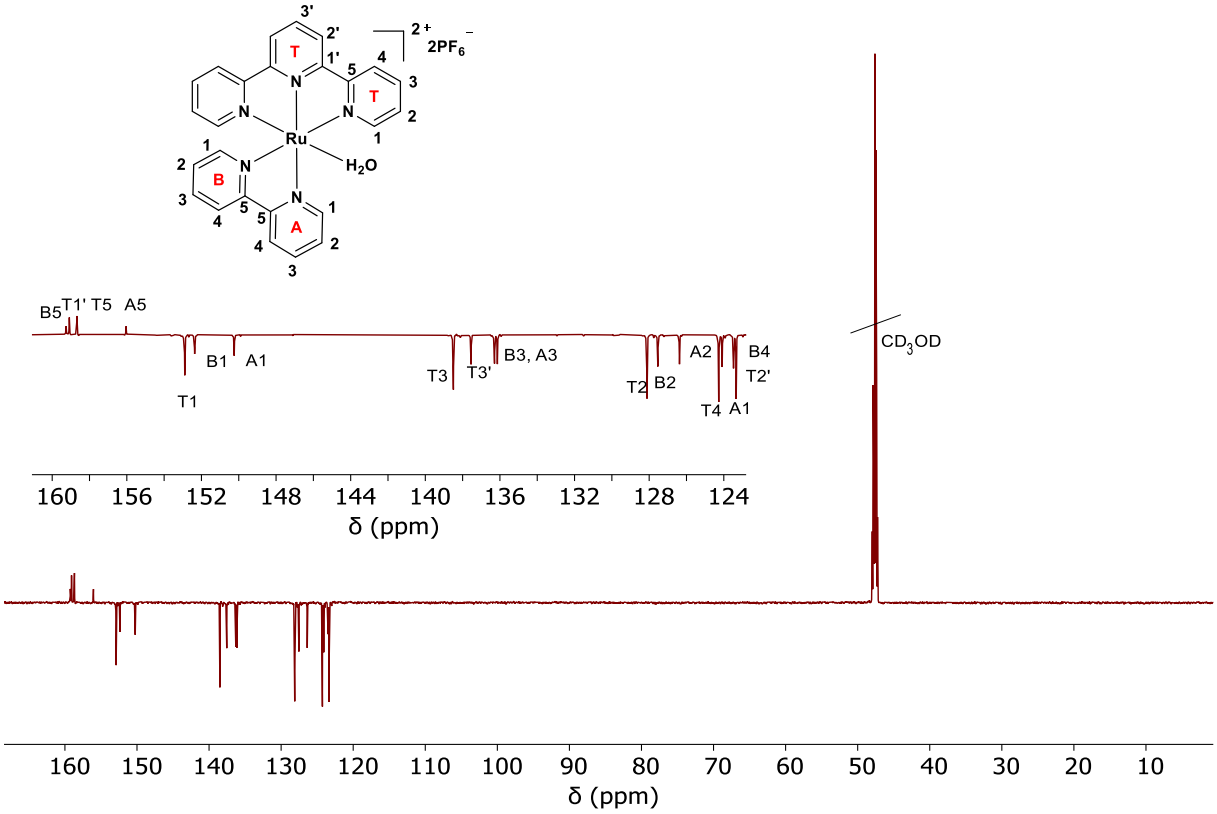

Figure S7. ^{13}C NMR spectrum of Ru-H_2O (75 MHz, CD_3OD, 25°C).

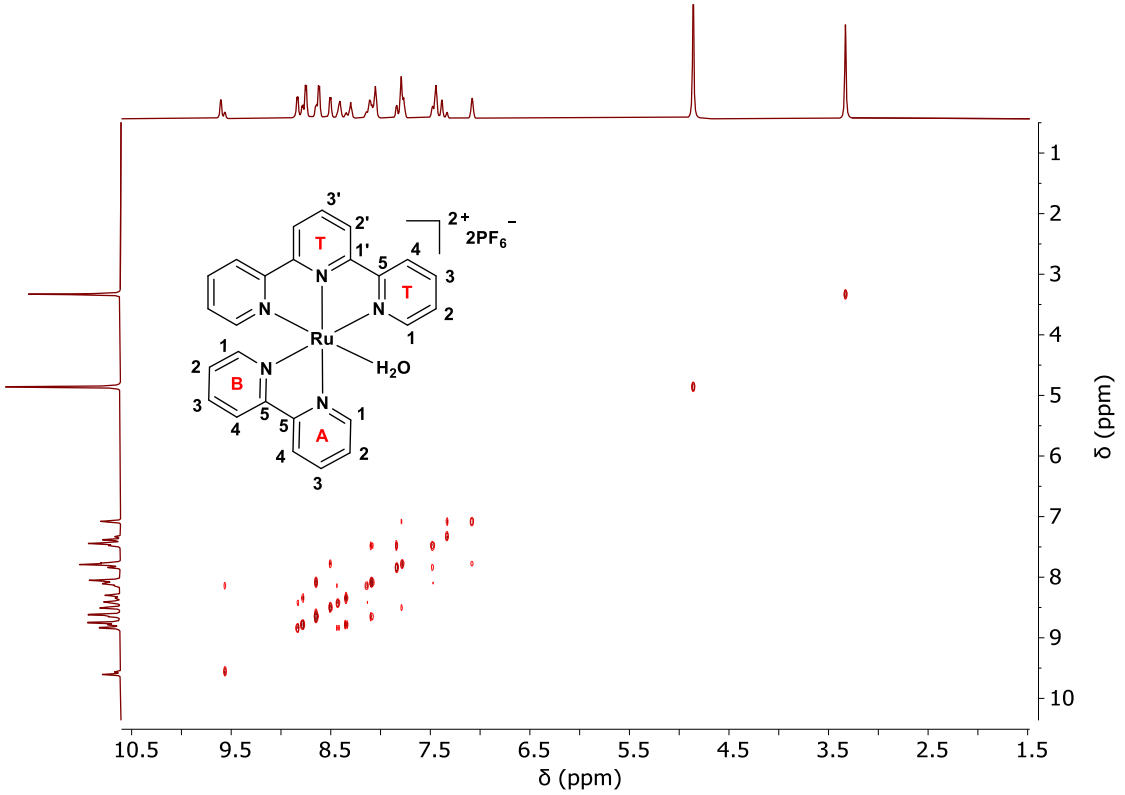

Figure S8. H-H COSY spectrum of Ru-H_2O (300 MHz, CD_3OD, 25°C).

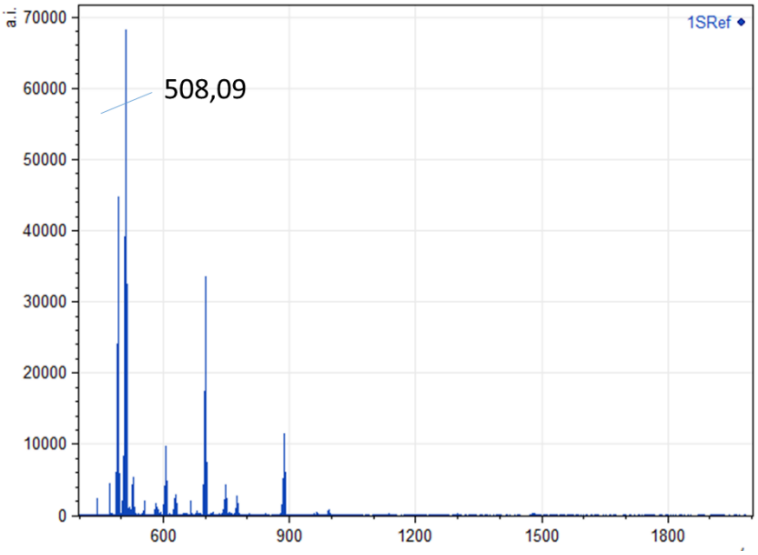

Figure S9. MALDI-TOF-MS spectrum of Ru-H_2O.

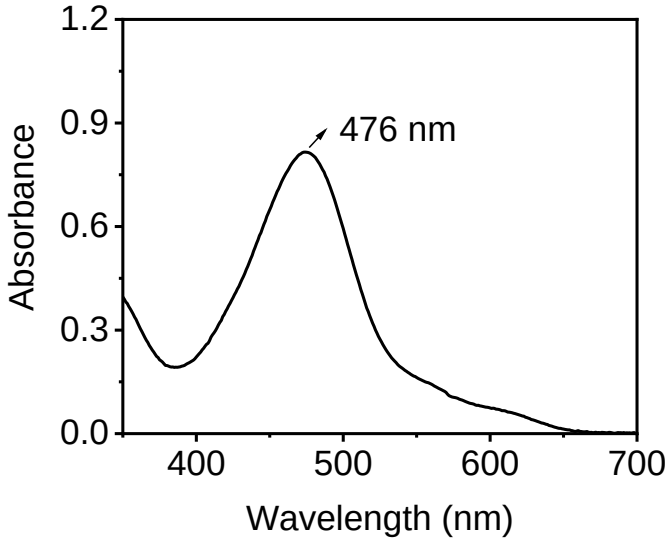

Figure S10. UV-vis absorption spectrum of Ru-H_2O in water.

Synthesis of 2-(2-(2-(methylthio)ethoxy)ethoxy)ethan-1-ol (SL)

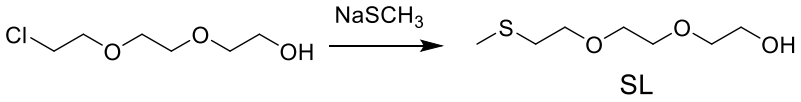

Figure S11. Synthetic route for compound SL.

Synthesis of 2-(2-(2-(methylthio)ethoxy)ethoxy)ethan-1-ol (SL): Sodium thiomethoxide (2 g, 28 mmol) was added to 30 mL deionized water and stirred for 10 min. 2-[2-(2-chloroethoxy)ethoxyl] ethanol (2.36 g, 14 mmol) was added to the flask and the mixture was stirred for 2 days at room temperature. After the reaction, sodium chloride was added to the mixture until saturation. Then, the mixture was extracted with dichloromethane. The organic layer was dried with magnesium sulfate and concentrated under reduced pressure. The product was a colorless oil. Yield: 1.84 g (65%).

^{1}H NMR of SL (300 MHz, D_2O, 25°C) δ (ppm): 3.65 (m, 10H, 2H-3, 2H-4, 2H-5, 2H-6, 2H-7), 2.71 (t, J = 6.4 Hz, 2H, H-2), 2.11 (S, 3H, H-1).

^{13}C NMR of SL (75 MHz, D_2O, 25 °C) δ (ppm): 71.78 (7), 69.52 (6), 69.50 (5), 69.47 (4), 69.12 (3), 32.61 (2) and 14.49 (1).

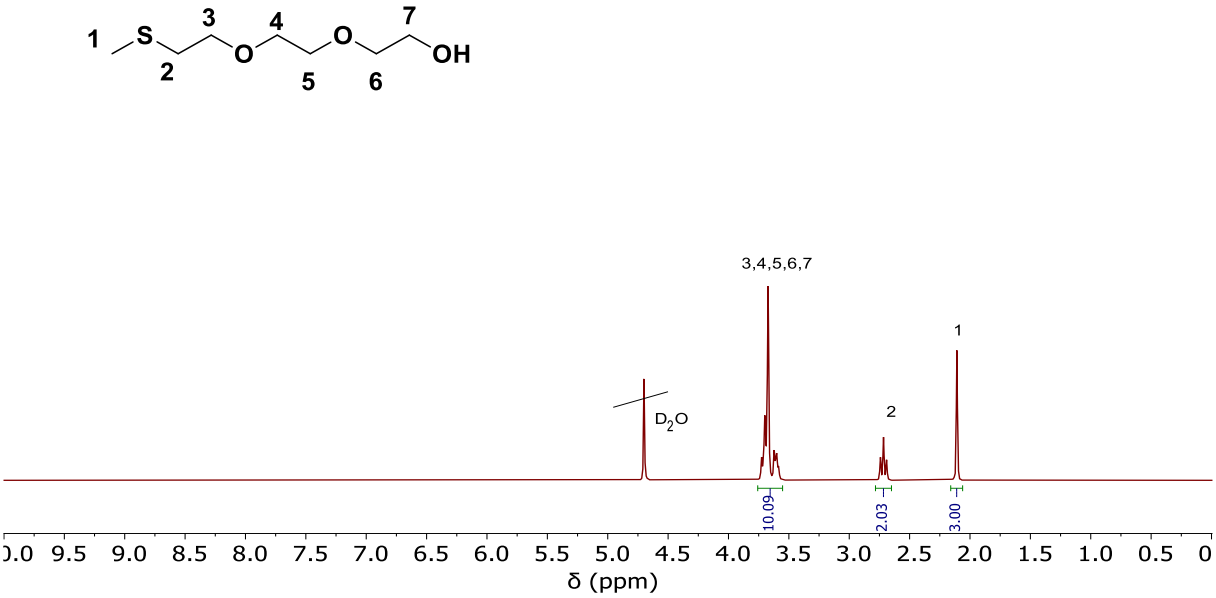

Figure S12. ^{1}H NMR spectrum of SL (300MHz, D_2O, 25°C).

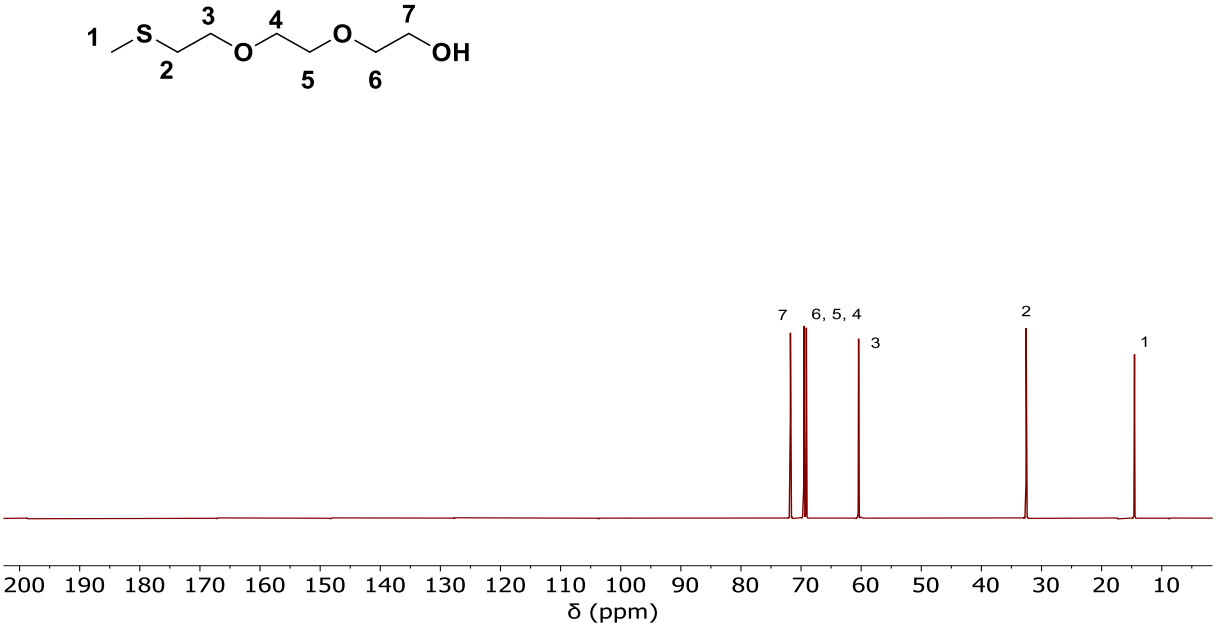

Figure S13. ^{13}C NMR spectrum of SL (75MHz, D_2O, 25°C).

Synthesis of Ru-SL

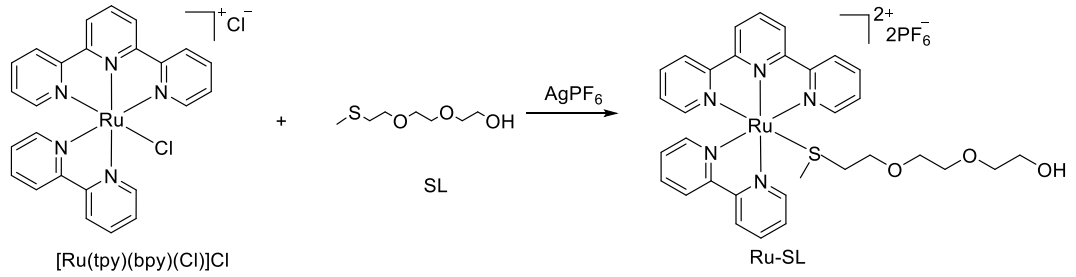

Figure S14. Synthetic route for Ru-SL.

Synthesis of Ru-SL: [Ru(tpy)(bpy)(Cl)]Cl (28 mg, 0.049 mmol) and $AgPF_6$ (28 mg, 0.11 mmol) were dissolved in a 3/5 (v/v) acetone/H_2O mixture (8 mL). SL (90 mg, 0.5 mmol) was added to the mixture solution. The mixture was refluxed at 85 °C under argon for 12 h. After that, it was filtered hot over Celite and concentrated to 1 mL under reduced pressure. The red organic solid was precipitated from a saturated KPF_6 solution. Yield: 23 mg, 0.023 mmol (46.9 %)

^{1}H NMR of Ru-SL (300 MHz, D_2O, 25°C) δ (ppm): 9.76 (d, J = 4.1 Hz, 1H, H-A1), 8.60-8.54 (m, 3H, H-A4, 2H-T2'), 8.40-8.21 (m, 5H, 2H, H-T4, H-B4, H-A3, H-T3'), 7.96-7.87 (m, 3H, H-A2, 2H-T3), 7.79-7.70 (m, 3H, H-B3, 2H-T1), 7.25 (t, J = 5.2 Hz, 2H, H-T2) 7.16 (d, J = 3.5 Hz, 1H, H-B1), 6.99 (t, J = 7.0 Hz, 1H, H-B2), 3.59-3.25 (m, 10H, 2H-c, 2H-d, 2H-e, 2H-f, 2H-g), 1.78 (t, J = 7.6, 2H, H-b), 1.28 (s, 3H, H-a).

^{13}C NMR of Ru-SL (75 MHz, Acetone-d_6, 25 °C) δ (ppm): 158.06 + 157.56 (T1', T5), 156.88 + 156.78(B5, A5), 153.60 (T1), 152.37 (B1), 150.12 (A1), 139.98 (T2), 138.29 + 138.16 (B3, A3), 137.03 (T3'), 128.61 (T3), 127.99 + 127.28 (B2, A2), 125.07 (T4), 124.74 (A4), 124.39 (T2'),123.90 (B4), 72.52 (g), 70.05 + 69.84 (e, f), 67.22 (d), 60.92 (c), 34.45 (b), 14.44 (a).
ESI-Mass of Ru-SL: *m/z* calculated for $C_{32}H_{37}N_5O_3RuSP_2F_{12}$ ($[M\text{-}2PF_6\text{-}H]^+$): 817.17; found 816.4.

UV-vis absorption spectrum of Ru-SL: The absorption maximum in water is at 452 nm, which is attributed to the metal-to-ligand charge transfer (MLCT) band of Ru-SL.

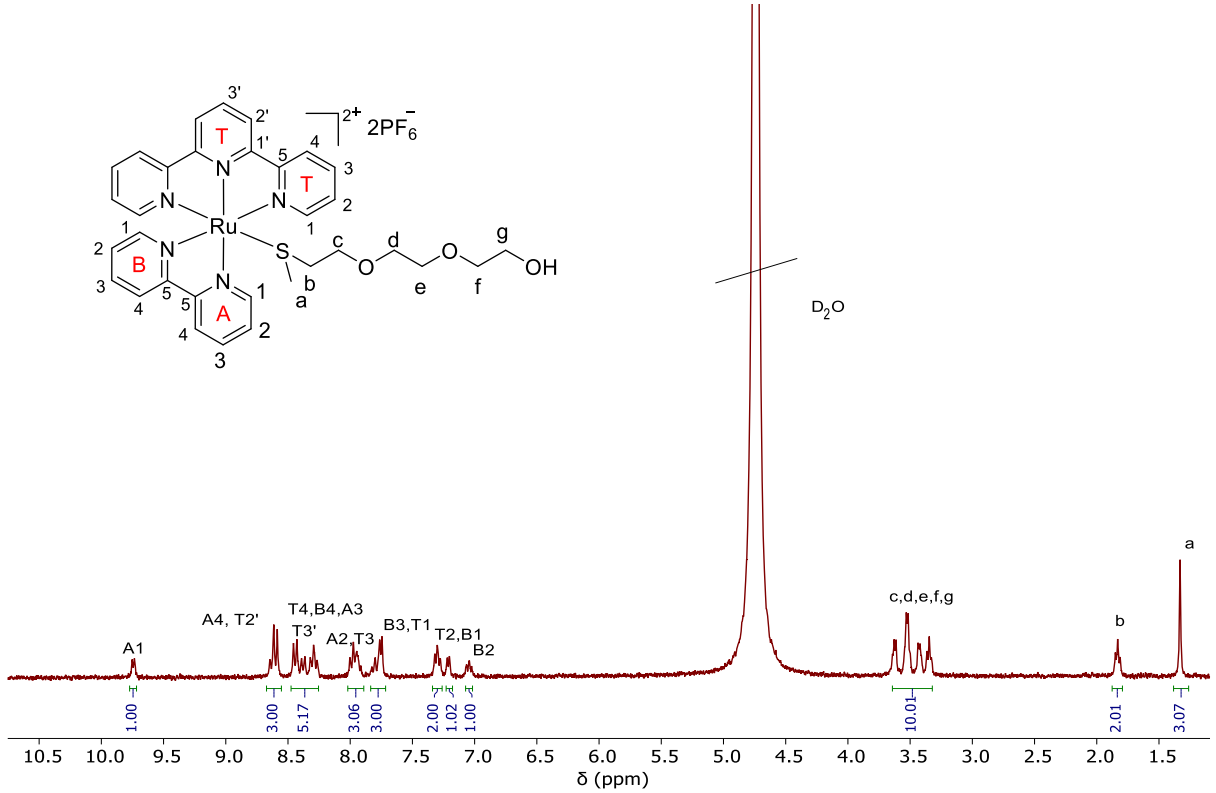

Figure S15. ^{1}H NMR spectrum of Ru-SL (300MHz, D_2O, 25°C)

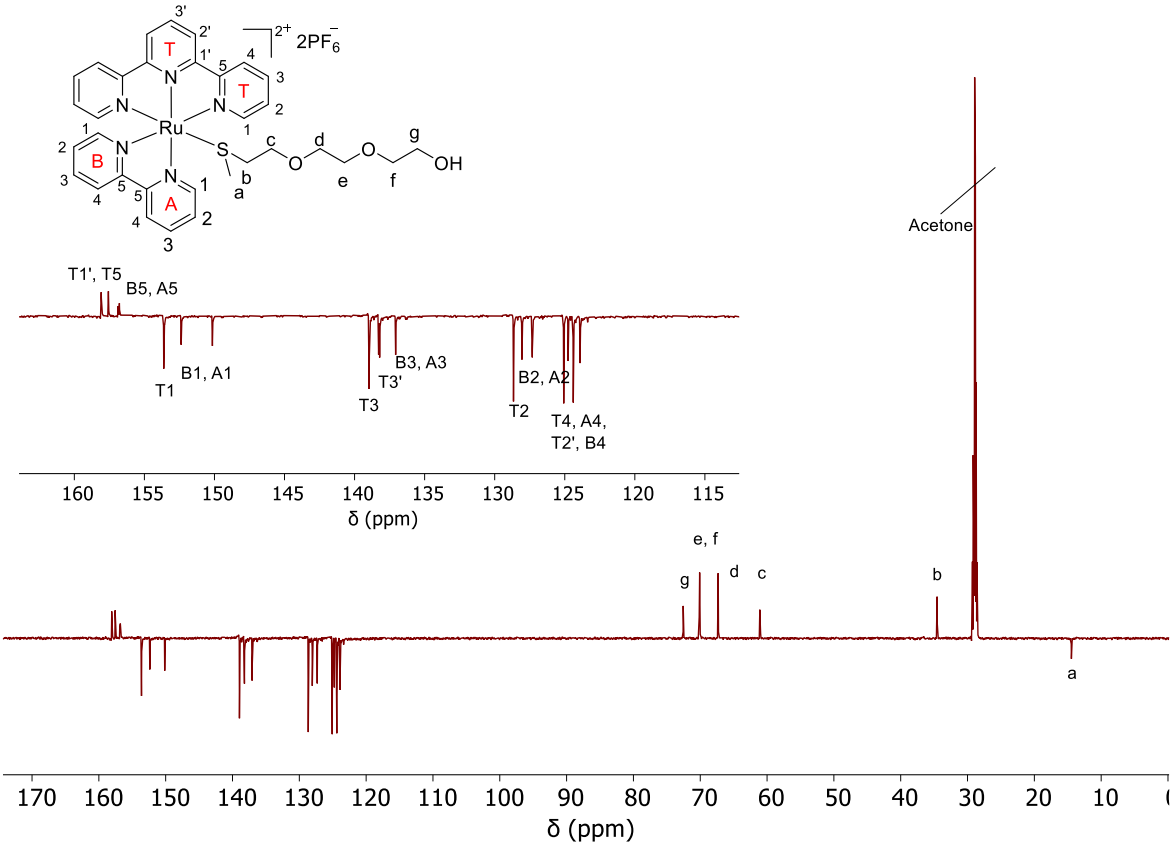

Figure S16. ^{13}C NMR spectrum of Ru-SL (75 MHz, Acetone-d_6, 25°C).

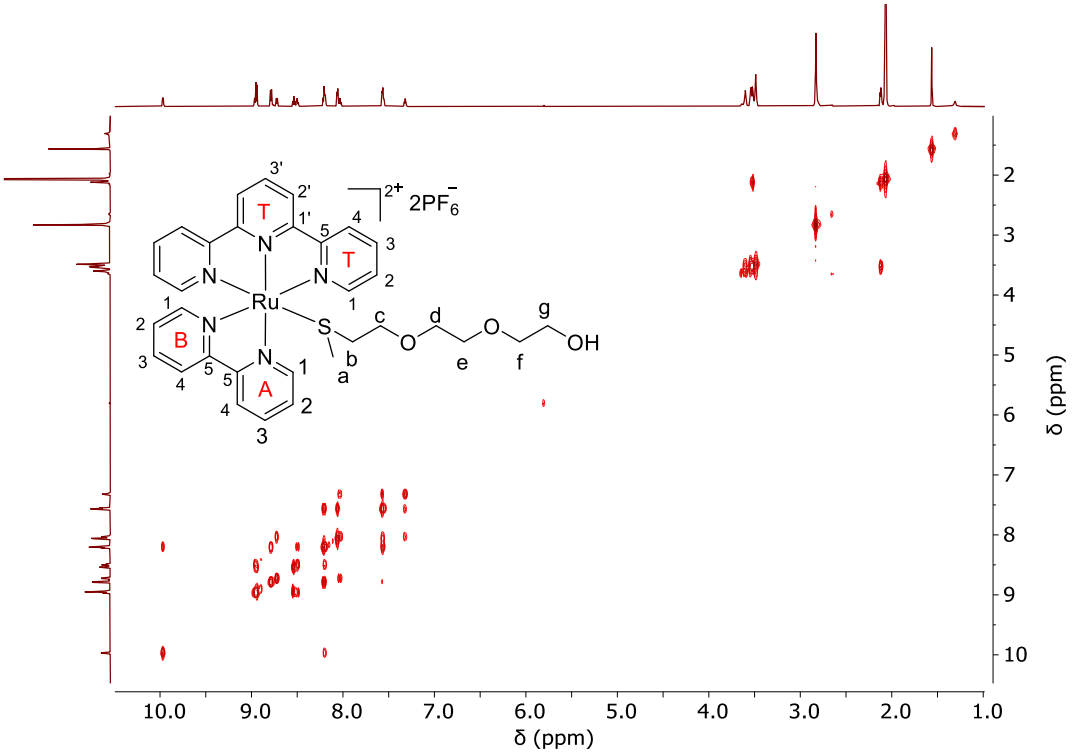

Figure S17. H-H COSY spectrum of Ru-SL (300 MHz, Acetone-d_6, 25°C).

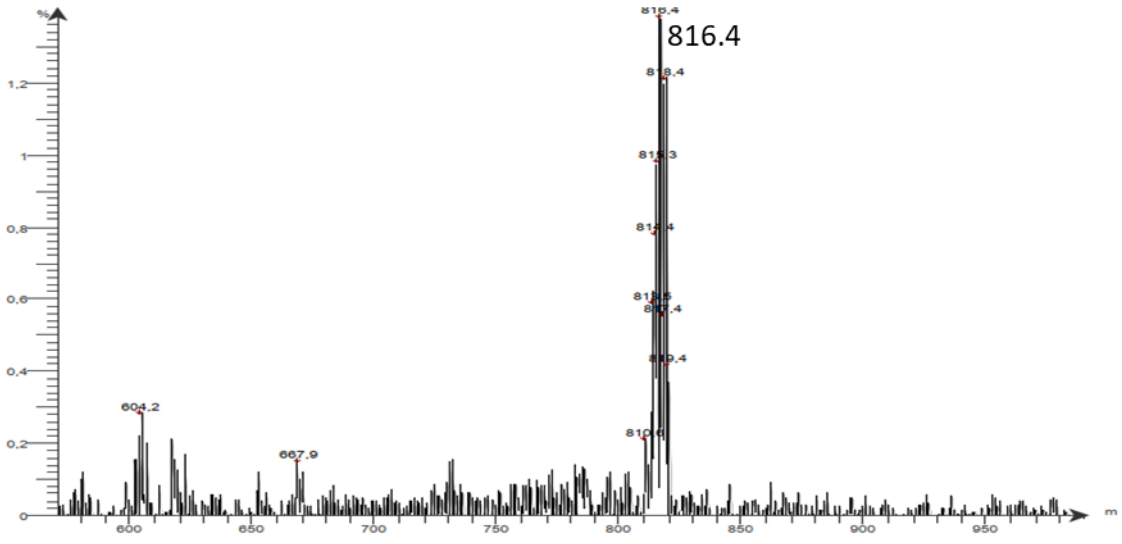

Figure S18. ESI-Mass spectrum of Ru-SL.

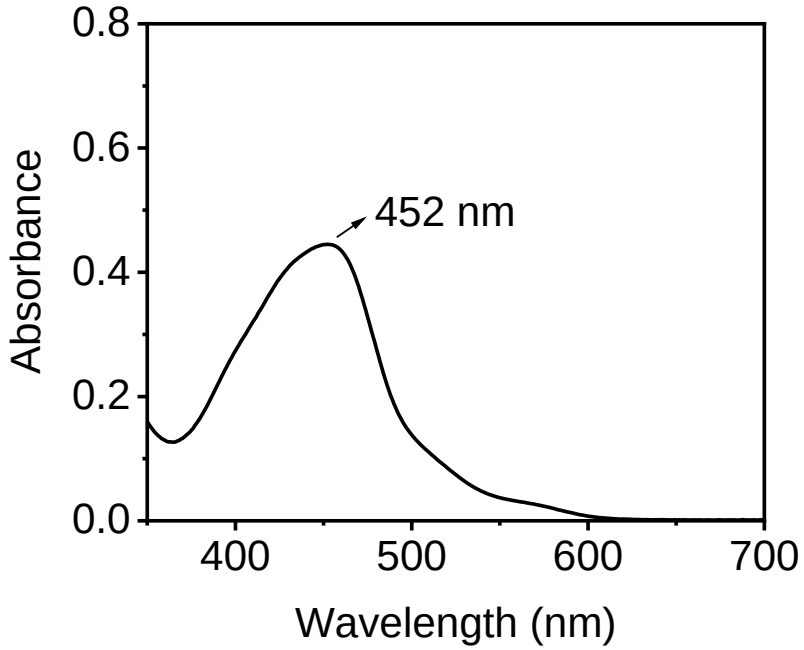

Figure S19. UV-vis absorption spectrum of Ru-SL in water.

Synthesis of [Ru(AAm-tpy)(bpy)Cl]Cl

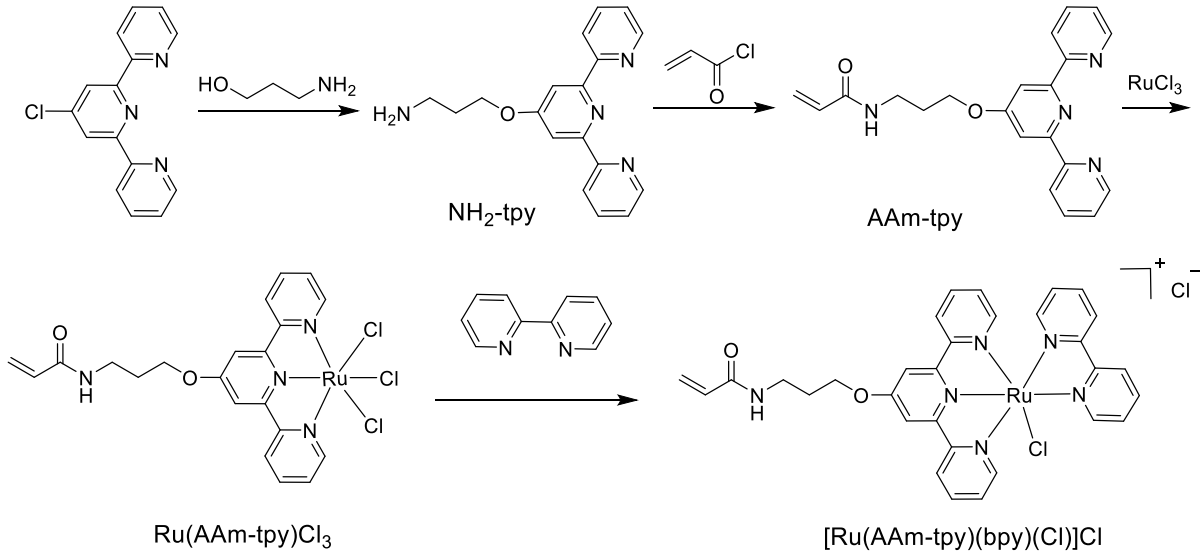

Figure S20. Synthetic route for [Ru(AAm-tpy)(bpy)Cl]Cl.

Synthesis of 3-([2, 2': 6',2''-terpyridin]-4'-yloxy)propan-1-amine (NH_2-tpy): Potassium hydroxide (392 mg, 7 mmol) was added to dimethylsulfoxide (20 mL) and heated to 65 °C under stirring. 3-Amino-1-propanol (555 mg, 7.4 mmol) was added dropwise into the solution. After 30 min, 4'-chloro-2,2',6',2"-terpyridine (1000 mg, 3.7 mmol) was added into the solution.

After stirring for 2 days at 65 °C, the reaction solution was cooled to room temperature and poured into 200 mL deionized water. The crude product was extracted with dichloromethane and dried with magnesium sulfate. After filtration and removal of the solvent in vacuum, the crude product was recrystallized from ethyl acetate to obtain light-yellow solids. Yield: 1900 mg (84%).

^{1}H NMR of NH_2-tpy (300 MHz, CD_2Cl_2, 25°C) δ (ppm): 8.70 (d, J = 5.4 Hz, 2H, H-2), 8.65 (d, J = 7.0 Hz, 2H, H-5), 8.06 (s, 2H, H-3'), 7.90 (t, J = 7.7 Hz, 2H, H-4), 7.37 (t, J = 7.7 Hz, 2H, H-3), 4.35 (t, J = 5.7 Hz, 2H, H-7), 2.95 (t, J = 8.0 Hz, 2H, H-9), 2.02 (m, 2H, H-8).

^{13}C NMR of NH_2-tpy (75 MHz, CD_3OD, 25°C) δ (ppm): 168.49 (4'), 158.32 (2'), 157.00 (6), 150.60 (2), 138.57 (4), 125.41 (3), 122.96 (5), 108.48 (3'), 67. 62 (7), 39.38 (9) and 32.44 (8).
MALDI-TOF-MS of NH_2-tpy: *m/z* calculated for $C_{18}H_{18}N_4O$ ($[M]^+$): 306.37; found 306.96.

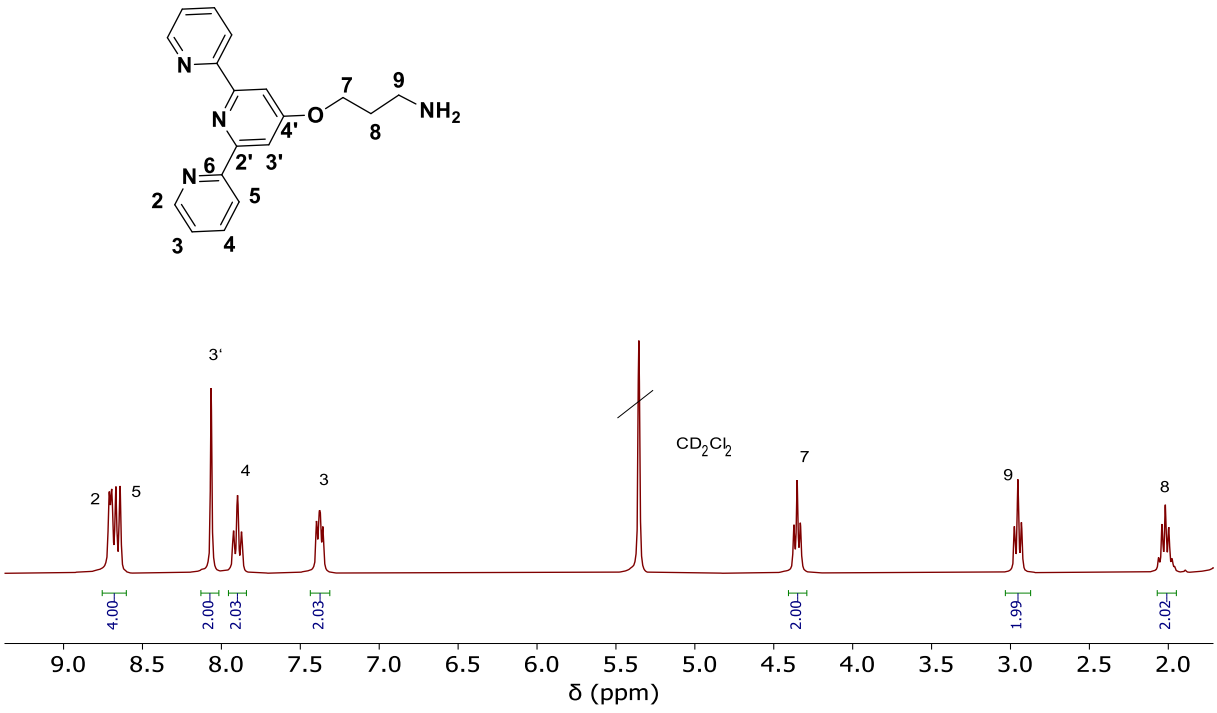

Figure S21. ^{1}H NMR spectrum of NH_2-tpy (300 MHz, CD_2Cl_2, 25°C).

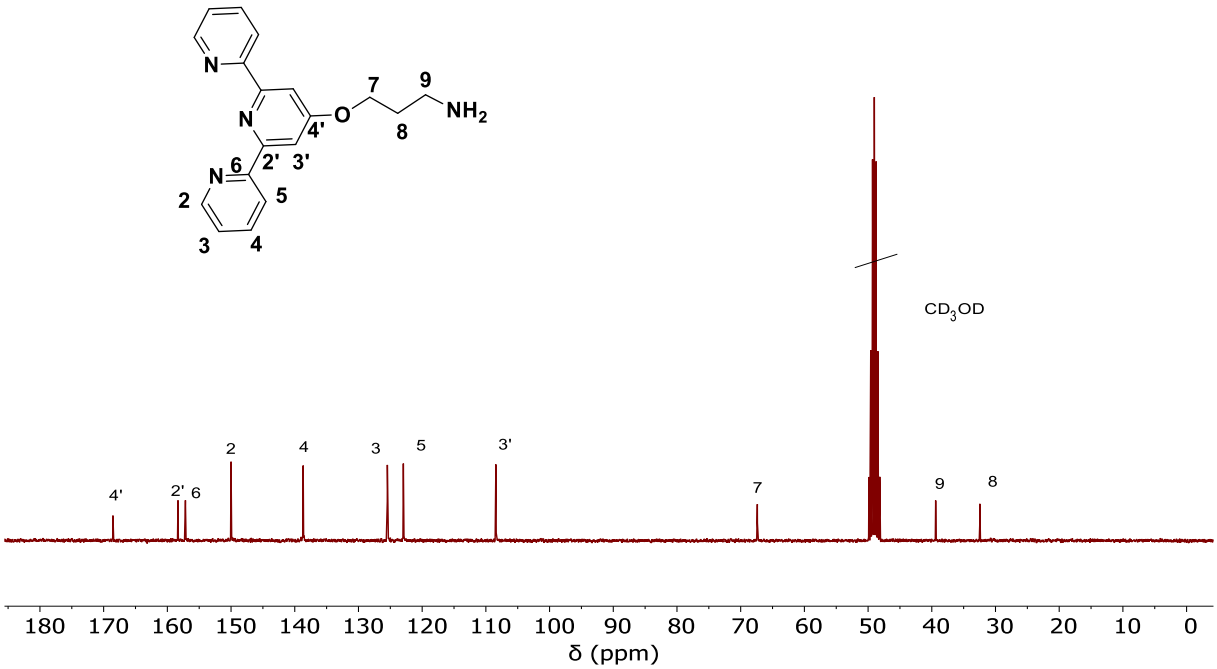

Figure S22. ^{13}C NMR spectrum of NH_2-tpy (75 MHz, CD_3OD, 25°C).

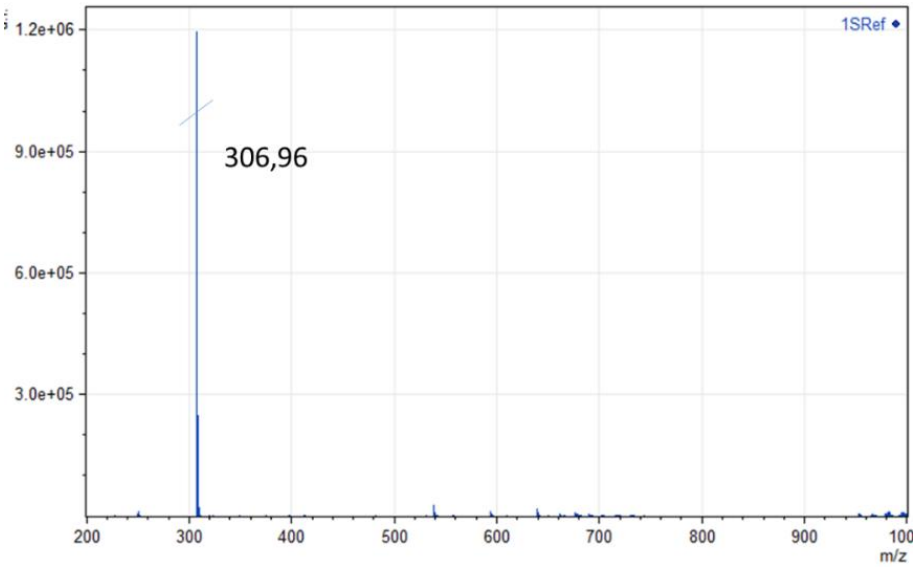

Figure S23. MALDI-TOF-MS spectrum of NH_2-tpy ($[M]^+$: found 306.96).

Synthesis of N-(3-([2,2':6',2''-terpyridin]-4'-yloxy)propyl)acrylamide (AAm-tpy) : NH_2-tpy (1360 mg, 4.7 mmol) was added to 40 mL tetrahydrofuran. Triethylamine (1.8 mL) was added into the solution. Then, acryloyl chloride (607 mg, 6.71 mmol) was slowly added under

argon at 0 ℃ after the mixture was stirred for 30 min. The reaction solution was stirred for 2 h at 0 °C and stirred for another 21 h at room temperature. After that, the solvent was removed in vacuum and the residue was dissolved in dichloromethane and washed with water and saturated brine. The organic solution was dried with magnesium sulfate, filtered, and reduced in vacuum to give crude solids. The crude solids were purified by column chromatography (Al_2O_3) using methanol/dichloromethane (v/v 1/40) as the eluent. The solvent was evaporated and the product was obtained as light-yellow solids. Yield: 1293 mg (77%).

^{1}H NMR of AAm-tpy (300 MHz, CD_2Cl_2, 25°C) δ (ppm): 8.70 (d, J = 4.7Hz, 2H, H-2), 8.61 (d, J = 8.0 Hz, 2H, H-5), 8.02 (s, 2H, H-3'), 7.85 (t, J = 6.0Hz, 2H, H-4), 7.34 (t, J = 6.0Hz, 2H, H-3), 6.25 (m, 2H, H-11, H-12), 5.64 (dd, J = 11.5 Hz, 1H, H-12), 4.34 (t, J = 6.0 Hz, 2H, H-7), 3.05 (t, J = 6.75 Hz, 2H, H-9), 2.09 (m, 2H, H-8).

^{13}C NMR of AAm-tpy (75 MHz, CD_2Cl_2, 25°C) δ (ppm): 168.49 (4'), 167 (10), 158.32 (2'), 157.00 (6), 150.60 (2), 138.57 (4), 132 (11) , 127 (12), 125.41 (3), 122.96 (5), 108.48 (3'), 67 (7), 39.38 (9) and 32.44 (8).

MALDI-TOF-MS of AAm-tpy: *m/z* calculated for $C_{21}H_{20}N_4O_2$ ($[M]^+$): 360.42; found 360.83.

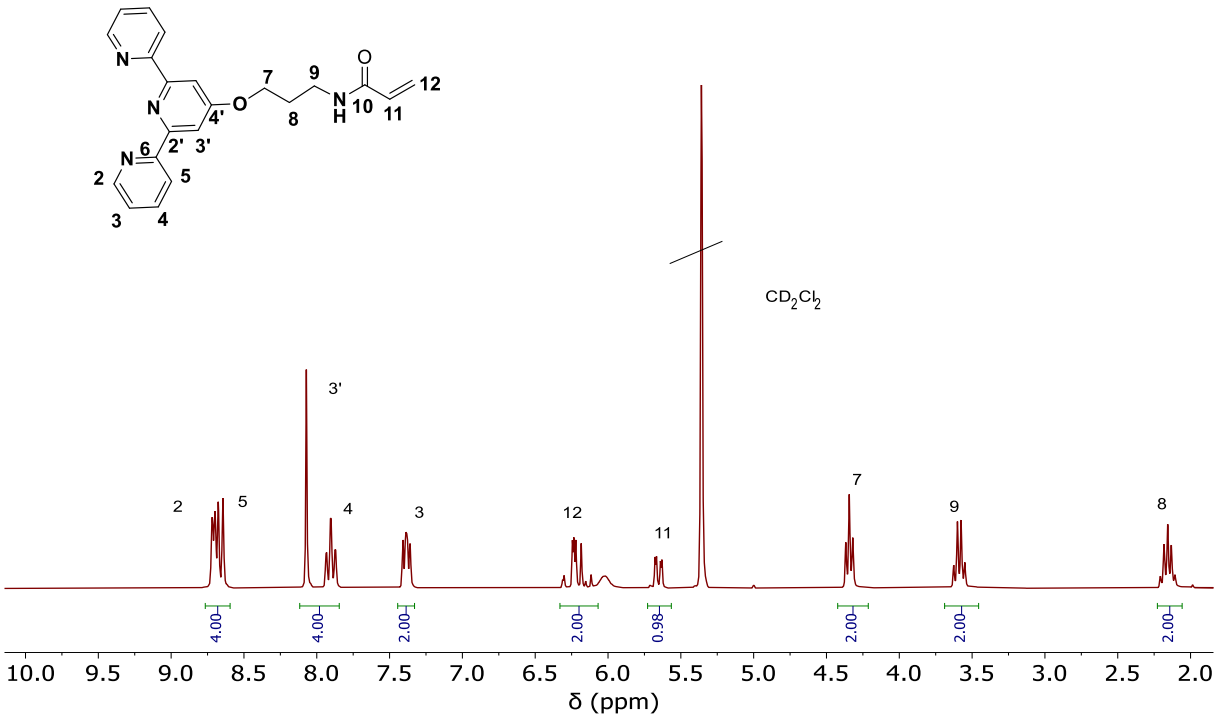

Figure S24. ^{1}H NMR spectrum of AAm-tpy (300 MHz, CD_2Cl_2, 25°C).

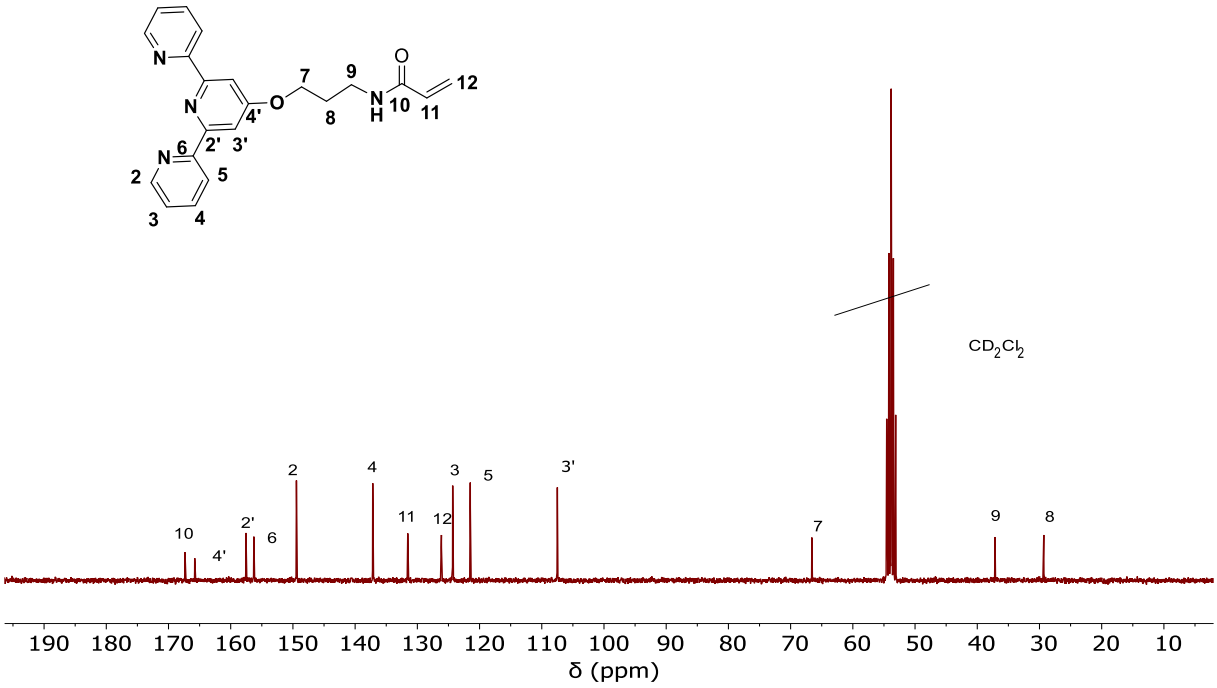

Figure S25. ^{13}C NMR spectrum of AAm-tpy (75 MHz, CD_2Cl_2, 25°C).

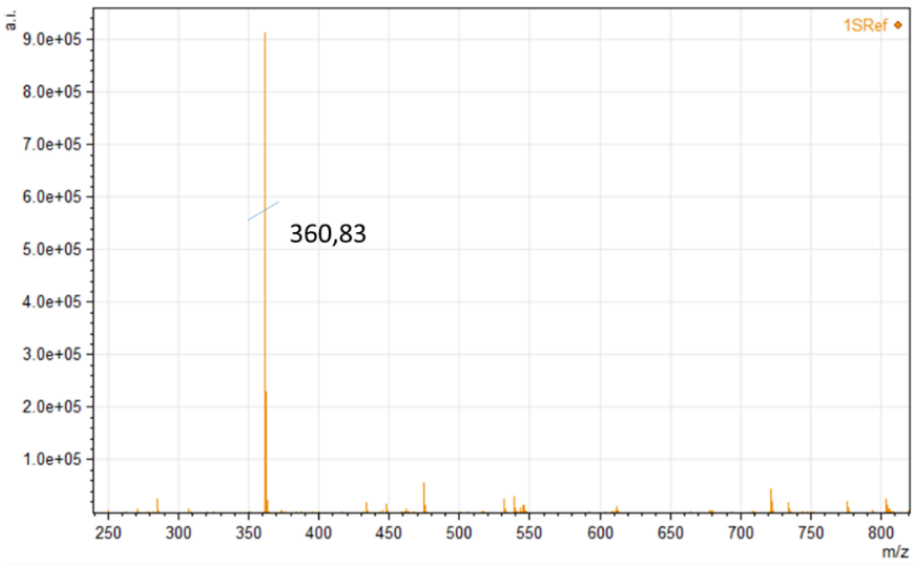

Figure S26. MALDI-TOF-MS spectrum of AAm-tpy ($[M]^+$: found 360.83).

Synthesis of Ru(AAm-tpy)Cl$_3$: $RuCl_3$•xH_2O (262 mg, 1 mmol) and AAm-tpy (359.4 mg, 1 mmol) were mixed in ethanol (60 mL). The mixture was heated at reflux for 4 h. After cooling

to room temperature, the mixture was filtered. The filtered brown powder was washed with ethanol and diethyl ether sequentially to obtain the product. Yield: 462 mg (94%).

Synthesis of [Ru(AAm-tpy)(bpy)(Cl)]Cl: Ru(AAm-tpy)Cl_3 (221 mg, 0.39 mmol) and 2,2'-bipyridine (bpy, 61 mg, 0.39 mmol) were mixed in a 3/1 (v/v) ethanol/H_2O mixture (30 mL). The solution was degassed for 5 min and filled with argon. Then, the reaction mixture was refluxed under argon for 1 day in the dark. After that, the mixture was filtered hot. The product was collected by evaporation under reduced pressure and purified by column chromatography with silica gel (eluent: methanol/dichloromethane = 1/8 to 1/4 (v/v)). Yield: 174 mg (65%).

^{1}H NMR of [Ru(AAm-tpy)(bpy)(Cl)]Cl (300 MHz, CD_3OD, 25°C) δ (ppm): 10.19 (d, J = 5.3 Hz, 1H, H-A1), 8.75 (d, J = 10.7 Hz, H-A4), 8.55 (d, J = 11.6 Hz, 2H, H-T4), 8.48 (d, J = 8.9 Hz, 1H, H-B4), 8.33 (s, 2H, H-T2'), 8.28 (t, J = 11.6 Hz, 1H, H-A3), 8.00-7.90 (m, 1H-A2, 2H-T3), 7.77-7.70 (m, 3H, 2H-T1, 1H-B3), 7.48 (d, J = 5.4 Hz, 1H, H-B1), 7.30 (t, J = 10.72 Hz, 2H, H-T2), 7.07 (t, J = 8.9 Hz, 1H, H-B2), 6.36-6.24 (m, 2H, H-10, H-11), 5.70 (d, J = 11.61 Hz, 1H, H-11), 4.53 (t, J = 6.25 Hz, 2H, H-6), 3.62 (t, J = 6.25 Hz, 2H, H-8), 2.24 (t, J = 8.93 Hz, 2H, H-7).

^{13}C NMR of [Ru(AAm-tpy)(bpy)(Cl)]Cl (75 MHz, CD_3OD, 25°C) δ (ppm): 168.22 (9), 167.12 (T3'), 160.68 (B5), 160.34 (T1'), 159.61 (T5), 158.39 (A5), 153.82 (B1), 153.48 (T1), 153.09 (A1), 138.16 (T3), 137.62 (B3), 136.60 (A3), 132.03 (10), 128.33 (T2), 127.99 (B2), 127.26 (A2), 126.73 (11), 124.78 (B4), 124.44 (A4), 110.26 (T2'), 68.70 (6), 37.23 (8) and 29.7 (7).
MALDI-TOF-MS of [Ru(AAm-tpy)(bpy)(Cl)]Cl: *m/z* calculated for $C_{31}H_{28}Cl_2N_6O_2Ru$ ([M-Cl]$^+$): 653.13; found 652.79.

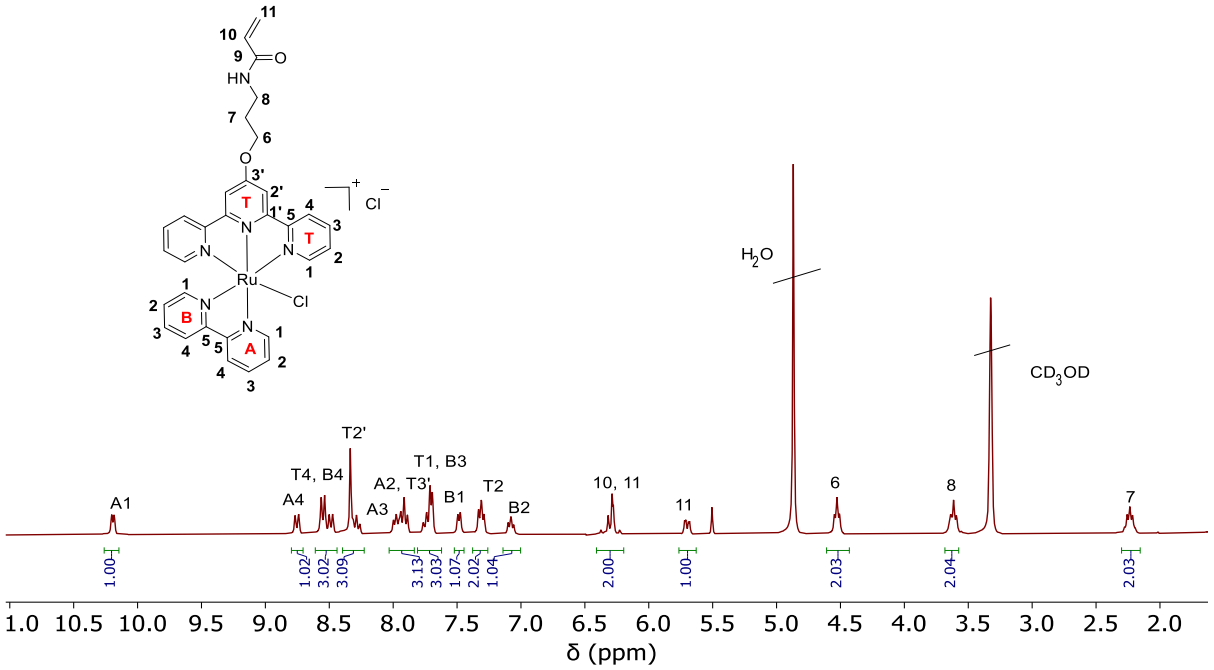

Figure S27. ^{1}H NMR spectrum of [Ru(AAm-tpy)(bpy)Cl]Cl (300MHz, CD_3OD, 25°C).

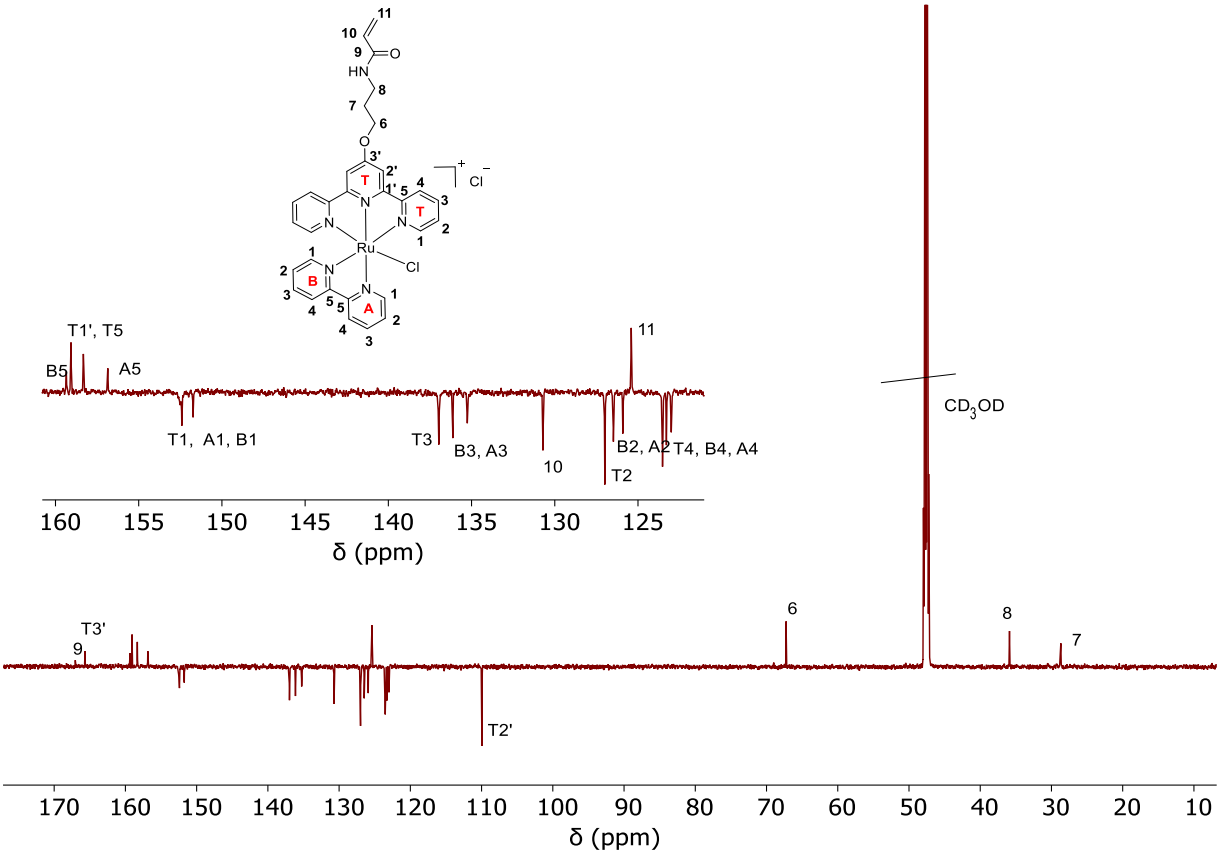

Figure S28. ^{13}C NMR spectrum of [Ru(AAm-tpy)(bpy)Cl]Cl (75MHz, CD_3OD, 25°C).

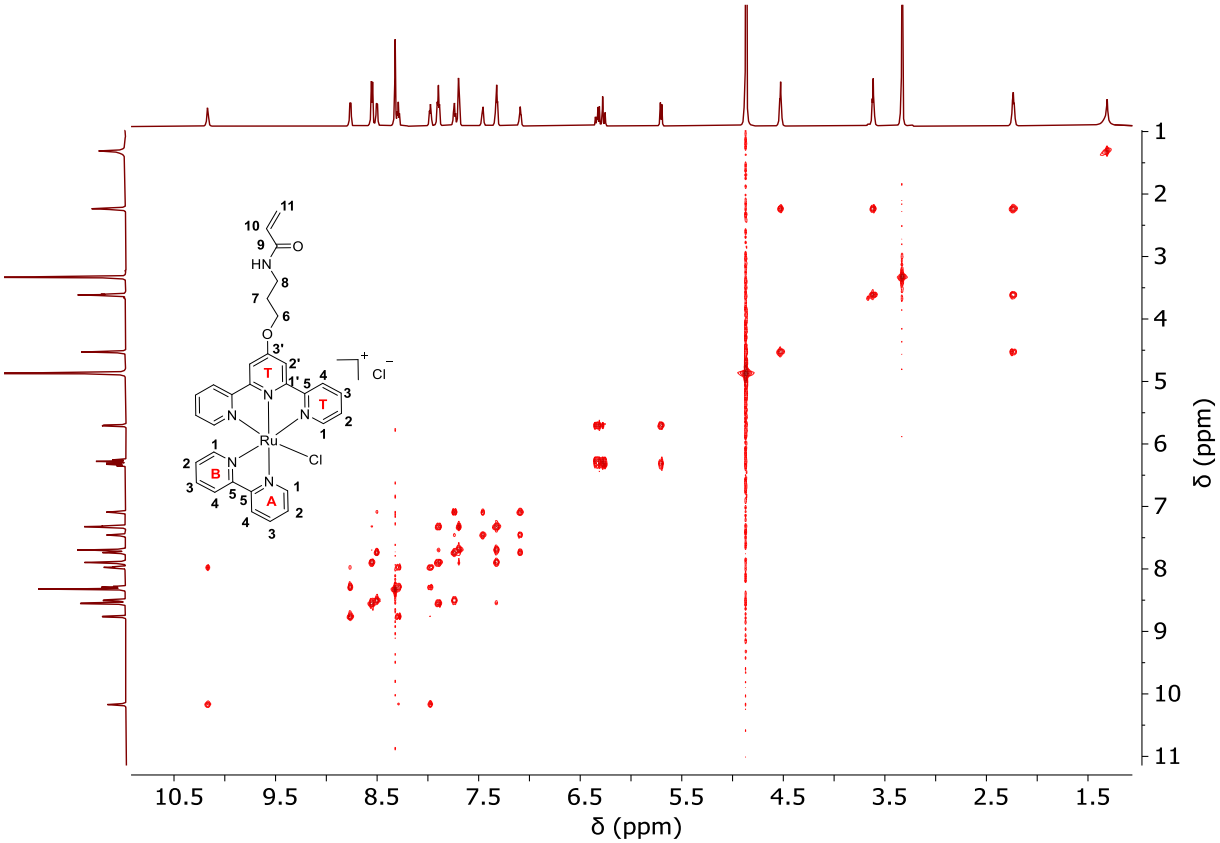

Figure S29. H-H COSY spectrum of [Ru(AAm-tpy)(bpy)(Cl)]Cl (300 MHz, CD_3OD, 25°C).

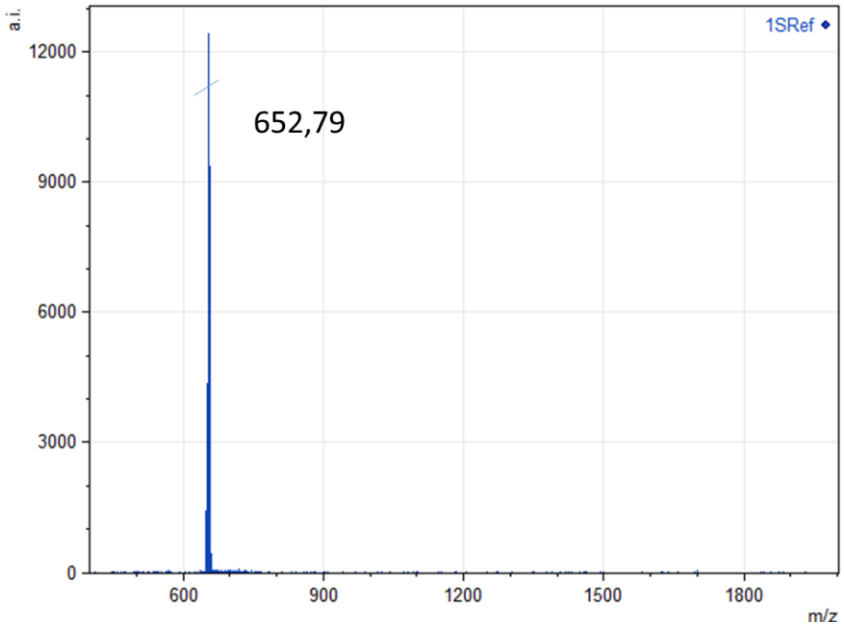

Figure S30. MALDI-TOF-MS spectrum of [Ru(AAm-tpy)(bpy)Cl]Cl.

Synthesis of 2-(2-(2-(methylthio)ethoxy)ethoxy)ethyl acrylate

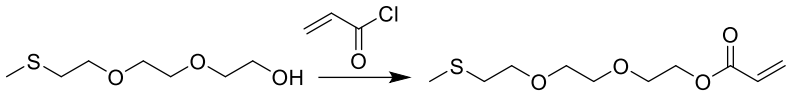

Figure S31. Synthesis route for 2-(2-(2-(methylthio)ethoxy)ethoxy)ethyl acrylate.

Synthesis of 2-(2-(2-(methylthio)ethoxy)ethoxy)ethyl acrylate: 2-(2-(2-(methylthio)ethoxy)ethoxy)ethan-1-ol (788.9 mg, 4.38 mmol) and triethylamine (531.85 mg, 5.26 mmol, 1.73 mL) were added to dichloromethane and stirred for 10 min under room temperature. Acryloyl chloride (475.6 mg, 5.26 mmol, 0.43 mL) was then added dropwise under argon at 0 ℃ for 60 min. The mixture was reacted at room temperature overnight. After that, the mixture was washed with saturated brine for three times, and then extracted with dichloromethane. The organic layer was dried with magnesium sulfate and concentrated under reduced pressure. The product was a colorless oil. Yield: 513 mg (50%).

^{1}HNMR of 2-(2-(2-(methylthio)ethoxy)ethoxy)ethyl acrylate (300 MHz, $CDCl_3$, 25°C) δ (ppm): 6.42(d, J = 16Hz, 1H, H-10), 6.10 (m, 1H, H-9), 5.76 (d, J = 12Hz, 1H, H-10), 4.25 (t, J = 5Hz, 2H, H-7), 3.63 (m, 8H, 2H-6,2H-5, 2H-4, 2H-3), 2.63 (t, J = 6.5 Hz, 2H, H-2), 2.07 (S, 3H, H-1).

^{13}C NMR of 2-(2-(2-(methylthio)ethoxy)ethoxy)ethyl acrylate (75MHz, D_2O, 25°C) δ (ppm): 168.42 (8), 132.50 (9), 127.28 (10), 69.62 (7), 69.22 (6), 69.00 (5), 68.40 (4), 63.88 (3), 32.50 (2) and 14.37 (1).

ESI of 2-(2-(2-(methylthio)ethoxy)ethoxy)ethyl acrylate: *m/z* calculated for $C_{10}H_{18}O_4SNa$ ($[M+Na]^+$): 257.31, found 257.50.

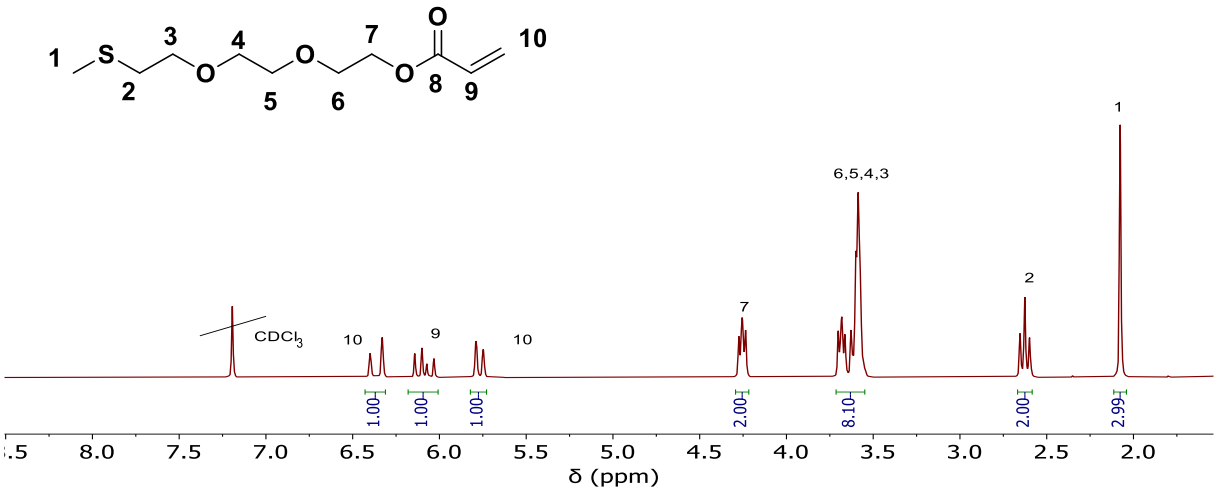

Figure S32. ^{1}H NMR spectrum of 2-(2-(2-(methylthio)ethoxy)ethoxy)ethyl acrylate (300 MHz, $CDCl_3$, 25°C).

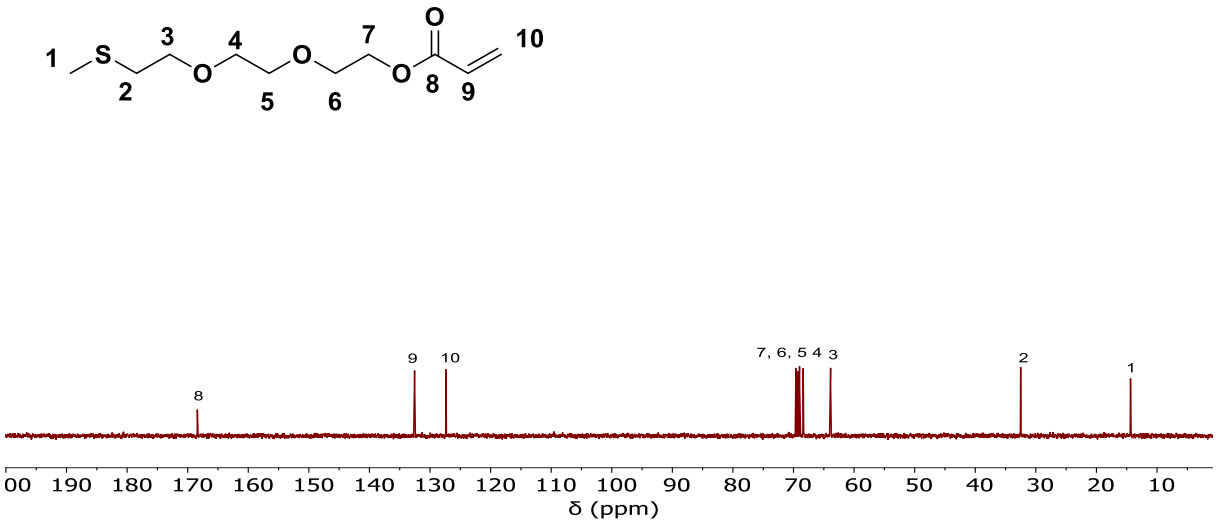

Figure S33. ^{13}C NMR spectrum of 2-(2-(2-(methylthio)ethoxy)ethoxy)ethyl acrylate (75MHz, D_2O, 25°C).

Synthesis of Ru-containing polymer (P-Ru)

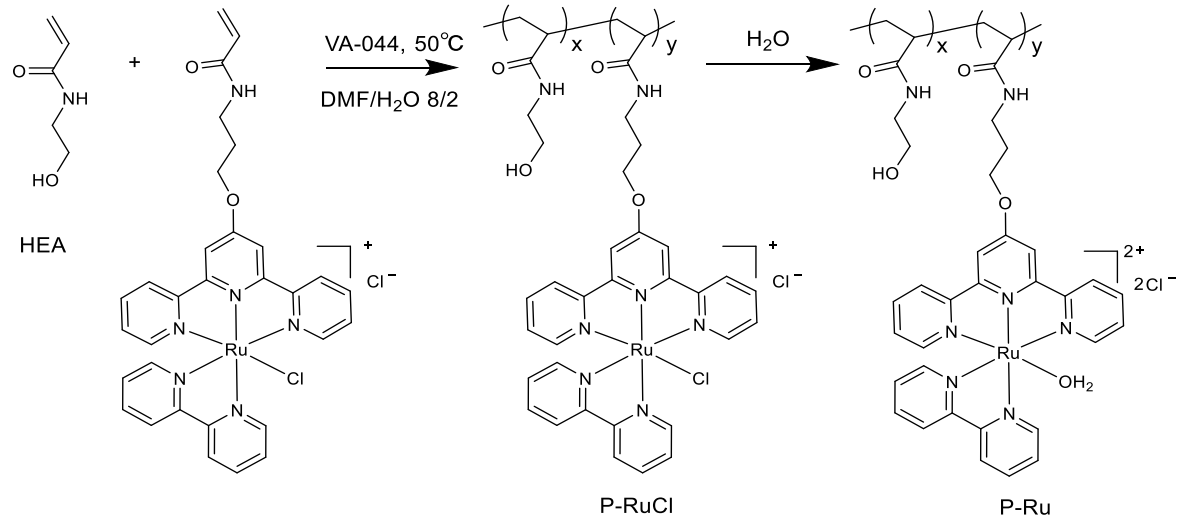

Figure S34. Synthetic route for P-Ru(x/y = 4.7/95.3).

HEA (115.13 mg, 1 mmol) and [Ru(AAm-tpy)(bpy)Cl]Cl (34.3 mg, 0.05mmol) were dissolved in a 8/2 (v/v) DMF/H_2O mixture (1 mL). Then, VA-044 (3.2 mg, 0.01 mmol) was added and the resulting mixture was degassed and filled with argon for 20 minutes at 0 ℃. The sealed flask was immersed in the oil bath at 50 ℃. The polymerization was stopped after 12 h by cooling the flask to 0 ℃. The polymer P-RuCl was isolated by precipitation in acetone and dried under reduced pressure. The ratio of HEA and Ru complex in the polymer was measured according to the integrals in the ^{1}H NMR spectrum (Figure S35). The peak at around 10.2 ppm corresponds to the signal of the proton connecting the Ru complex. The signal at around 1.0-2.5 corresponds to the signal of the proton connecting to the main chain. The ratio of HEA and Ru complex part in the polymer was 95.4: 4.7, which was in accordance with the feed ratio of the monomers. P-Ru was obtained by heating P-RuCl in water for 30 min. The resulting ^{1}H NMR showed a peak at 9.50 ppm which corresponds to the signal of the proton connecting to the Ru complex part (Figure S36). P-Ru has a number average molecular weight of Mn = 16.4 kg/mol and polydispersity index (PDI) of 2.91 (Figure S37).

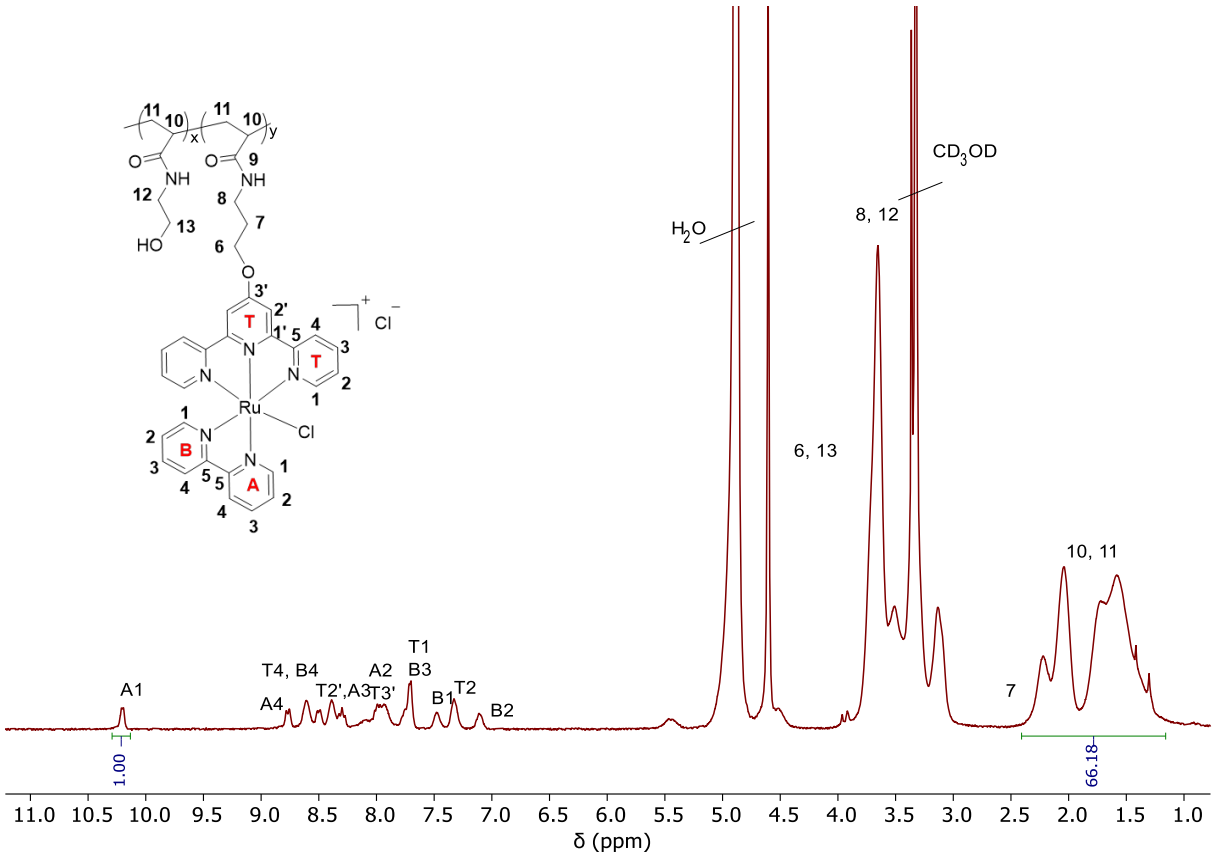

Figure S35. ^{1}H NMR spectrum of P-RuCl (300MHz, CD_3OD, 25°C) (x/y = 4.7/95.3).

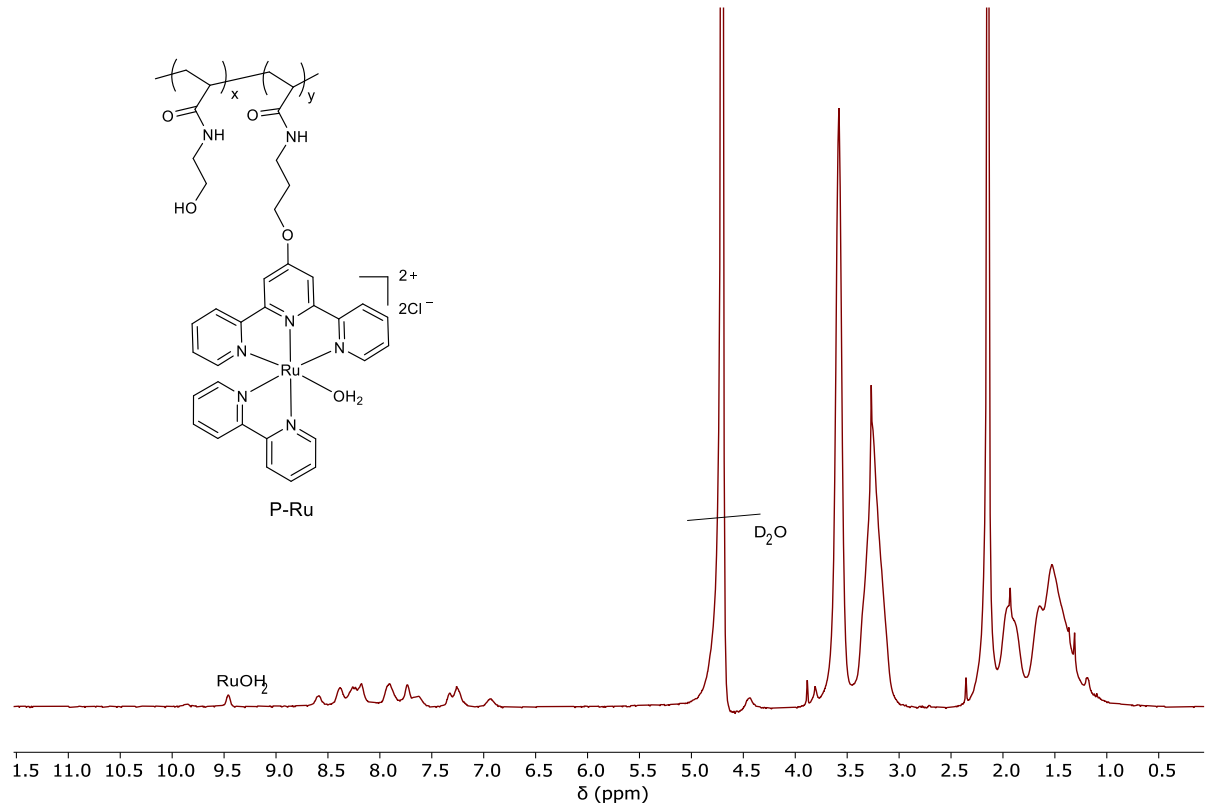

Figure S36. ^{1}H NMR spectrum of P-Ru (300MHz, D_2O, 25°C) (x/y = 4.7/95.3).

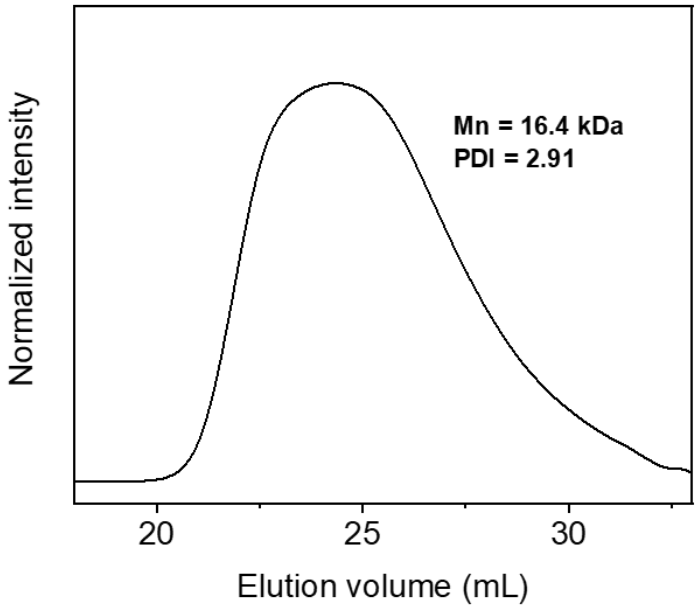

Figure S37. GPC trace of P-Ru.

Synthesis of P-S

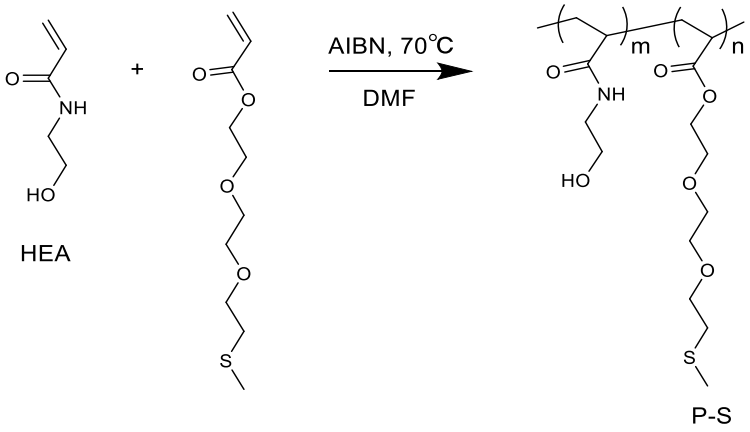

Figure S38. Synthetic route for P-S (m/n = 79/21).

P-S was synthesized by free radial copolymerization of HEA and 2-(2-(2-(methylthio)ethoxy)ethoxy)ethyl acrylate at the feed mole ratio of 80:20. HEA (184 mg, 1.60 mmol) and 2-(2-(2-(methylthio)ethoxy)ethoxy)ethyl acrylate (94 mg, 0.40 mmol) were dissolved in DMF (1 mL). Then, AIBN (3.2 mg, 0.02 mmol) was added and the resulting mixture was degassed and filled with argon for 20 minutes at 0 ℃. The sealed flask was

immersed in an oil bath at 70 °C. The polymerization was stopped after 12 h by cooling the flask to 0 °C. Then, P-S was isolated by precipitation in acetone and dried under reduced pressure. P-S was characterized using ^{1}H NMR spectroscopy (Figure S39) and GPC (Figure S40). The P-S has a M_n of 14.9 kg/mol and PDI of 1.35. The ratio of HEA and 2-(2-(2-(methylthio)ethoxy)ethoxy)ethyl acrylate in the copolymer measured using ^{1}H NMR spectroscopy was 79 : 21.

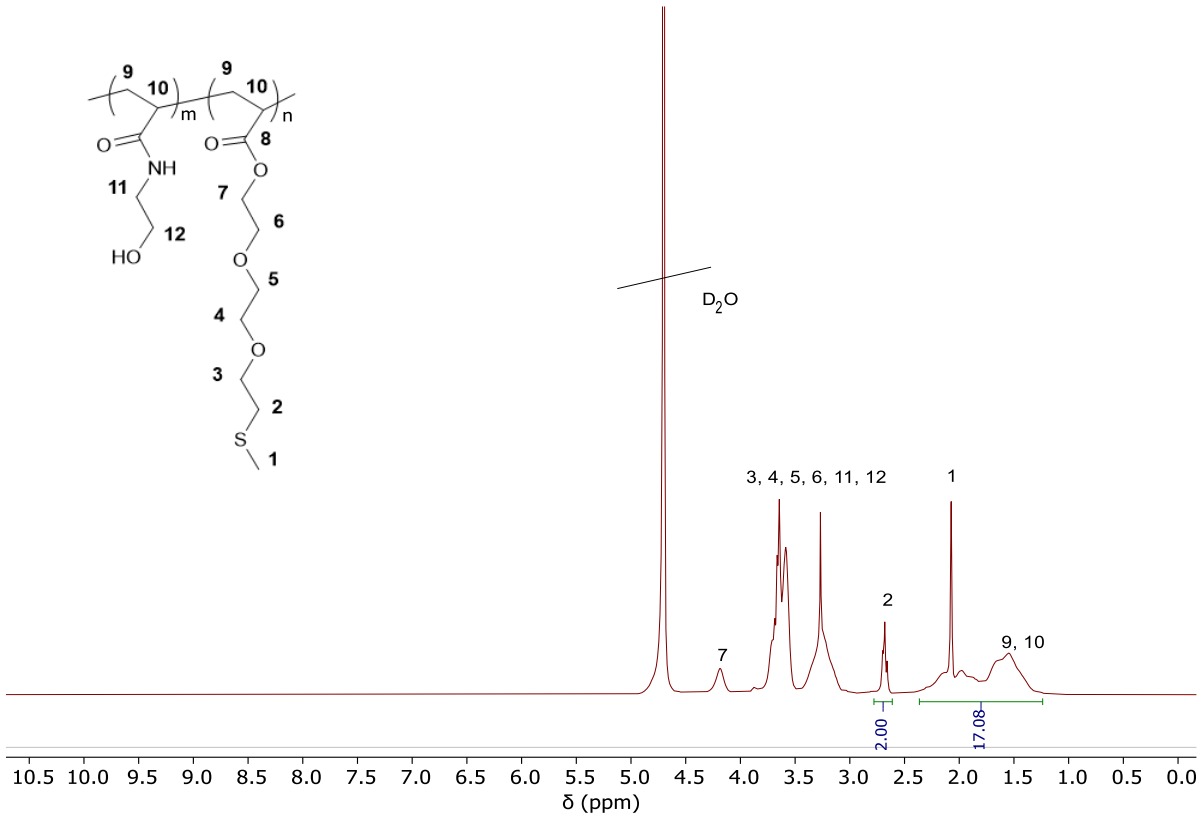

Figure S39. ^{1}H NMR spectrum of P-S (300MHz, D_2O, 25°C).

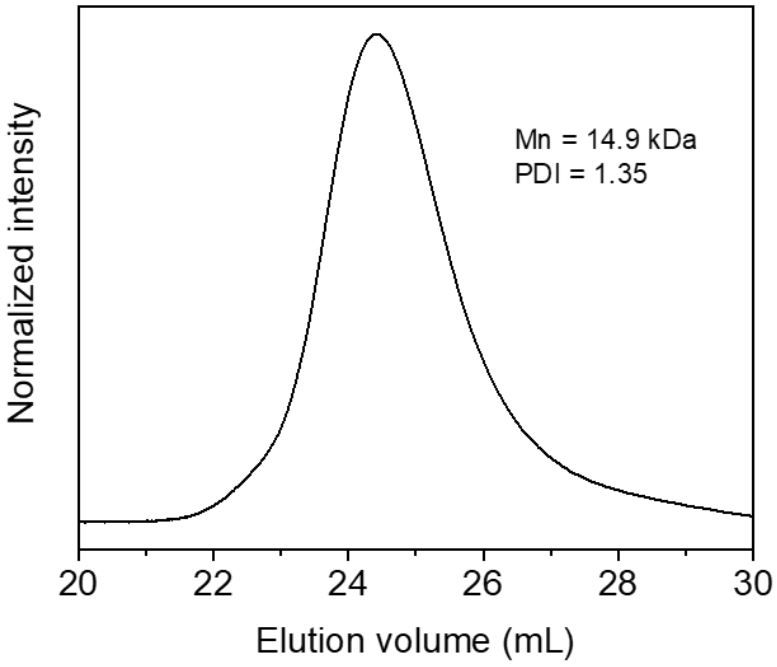

Figure S40. GPC trace of P-S.

The preparation of P-Ru/P-S hydrogels

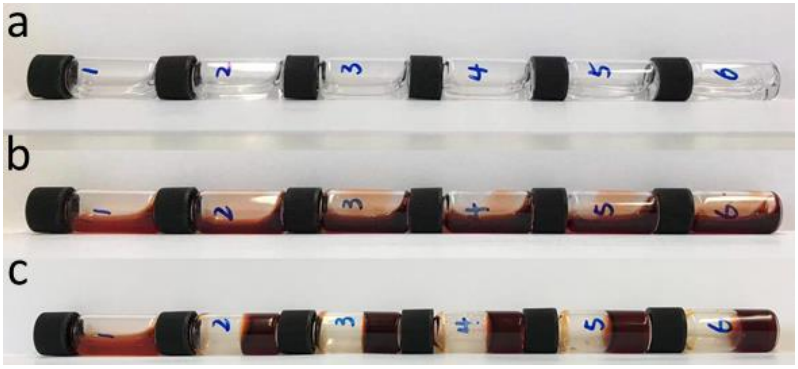

Figure S41. Photos of P-Ru, P-S, and P-Ru/P-S in water at 70 ℃. (a) P-S in water at 70 ℃ for 6 h. The weight percentages of P-S in water were from 1 wt% to 6 wt% (left to right). No gel was formed. (b) P-Ru in water at 70 ℃ for 6 h. The weight percentages of P-Ru in water were from 1 wt% to 6 wt% (left to right). No gel was formed. (c) P-Ru/P-S in water at 70 ℃ for 1 h. The weight percentages of P-Ru/P-S (1/1) were from 1wt% to 6 wt% (left to right). Gels were formed from 2 wt% to 6 wt%.

Preparation of hydrogels as adherends

Non-responsive P1 gel: N-hydroxyethyl acrylamide (HEA) (690 mg, 5.9 mmol) was dissolved in 6 mL deionized water. N,N'-methylenebisacrylamide (Bis) (9 mg, 0.058 mmol) and Irgacure 2959 (12 mg, 0.05 mmol) were added into the HEA solution. The precursor solution was degassed and filled with argon for 20 min. After that, the solution was poured into a Teflon mold and covered with a glass plate, and exposed to UV light (8 W, 366 nm curing light, CAMAG) for 2 h. Then, a gel was obtained and immersed in water to reach the swelling equilibrium.

Thermo-responsive P2 gel: 3-dimethyl (methacryloyloxyethyl) ammonium propane sulfonate (DMAPS) (1508 mg, 5.39 mmol) and HEA (69 mg, 0.60 mmol) were dissolved in 6 mL deionized water. Bis (9 mg, 0.058 mmol) and Irgacure 2959 (12 mg, 0.05 mmol) were sequentially added into the mixture. The mixture was degassed and filled with argon for 20 min. After that, the mixture was poured into a Teflon mold and covered with a glass plate, and exposed to UV light (8 W, 366 nm curing light, CAMAG) for 2 h. Then, a gel was obtained and immersed in water to reach the swelling equilibrium.

pH-responsive P3 gel: HEA (621 mg, 5.3 mmol) and acrylic acid (AAc) (39 mg, 0.54 mmol) were dissolved in 6 mL deionized water. Bis (9 mg, 0.058 mmol) and Irgacure 2959 (24 mg, 0.10 mmol) were added to the mixture. The mixture was degassed and filled with argon for 20 min. After that the mixture was poured into a Teflon mold and covered with a glass plate, and exposed to UV light (8 W, 366 nm curing light, CAMAG) for 2 h. Then, a gel was obtained and immersed in water to reach the swelling equilibrium.

Magnetically responsive P4 gel: HEA (230.26 mg, 2 mmol) was dissolved in 1 mL deionized water. Bis (0.33 mg, 0.0002 mmol), MagneHis^{TM} Ni-Particle suspension (0.1 mL) and VA-044 (5 mg, 0.015 mmol) were added into the HEA solution. The solution was degassed and filled with argon for 20 min. After that, the solution was poured into a Teflon mold and sealed with a glass plate, and put in the oven at 50 ℃ for 12 h. Then, a gel was obtained and immersed in water to reach the swelling equilibrium.

Preparation of hydrogel assemblies using P-Ru/P-S as an adhesive

An aqueous solution of P-Ru/P-S (6 wt%, 5 μL/cm^2) was spread on the surfaces of hydrogels. Then, one hydrogel was pressed on top of another gel. The hydrogels were sealed and put in a container at 70 ℃ for 6 h. After that, a gel assembly was obtained and the hydrogel assmbly was immersed in water before further investigation.

2.4.4 Additional data

Photo-controlled reversible coordination of P-Ru and P-S

The reversible coordination of P-Ru and P-S in water was studied using ^{1}H NMR spectroscopy (Figure S42). A mixture of P-Ru (10 mg) and P-S (10 mg) was prepared in 0.55 mL D_2O. Then, the mixture was measured using ^{1}H NMR spectroscopy immediately (the initial state in Figure S42). In the initial state, there was a doublet at 9.50 ppm that corresponds to the signal of P-Ru. When the sample was heated to 70 ℃, a new doublet at 9.71 ppm appeared. Its signal increased with time, while the signal of the doublet at 9.50 ppm decreased. This result indicated that Ru-thioether coordination bond was formed upon heating. After heating for 6 h, the Ru-S coordination was complete. Then, the sample was irradiated with light (470 nm, 60 mW/cm^2, 20 min) to induce photosubstitution. After light irradiation, the signals of P-Ru almost returned to the initial state. These results indicated that the Ru-S bond was cleaved by light irradiation. Heating the sample at 70 ℃ for another 6 h, the Ru-S bond was formed. Thus, P-S can coordinate with P-Ru reversibly in the heat/light cycles.

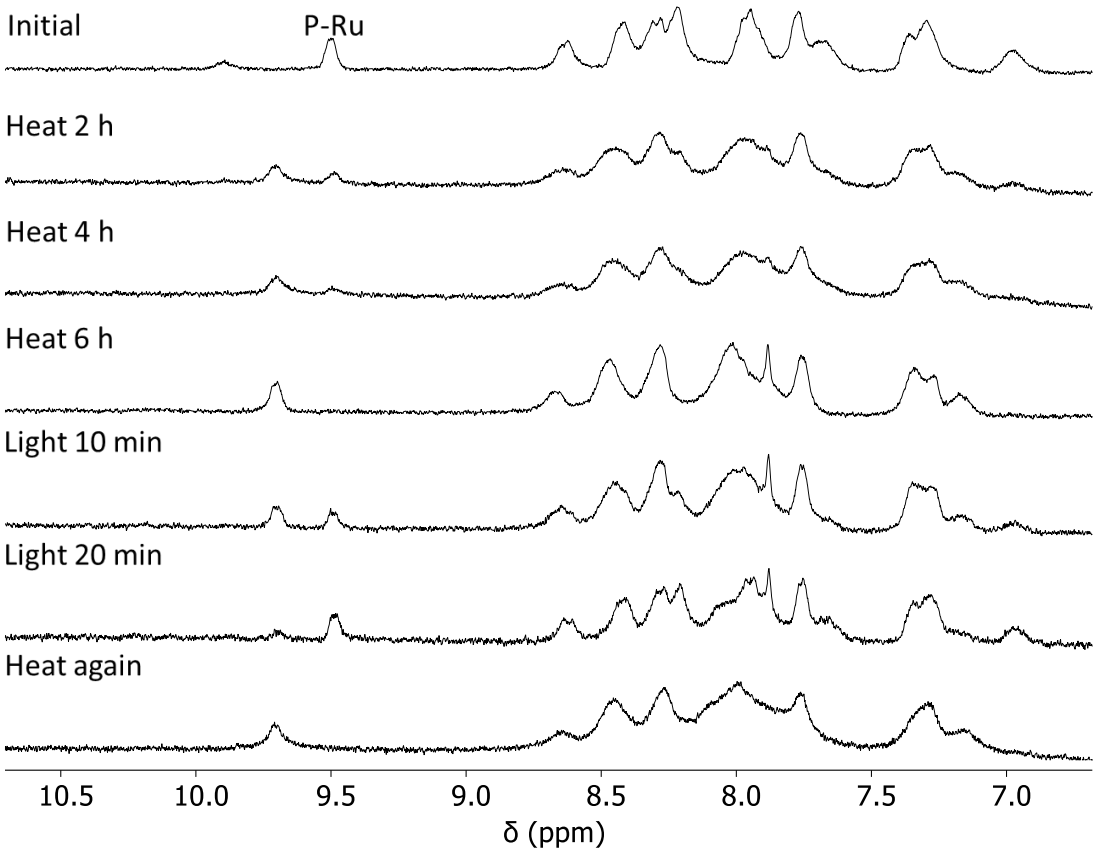

Figure S42. ^{1}H NMR showing the reversible Ru-S coordination in the mixture of P-Ru and P-S in D_2O in the heat/light irradiation cycles.

Control experiments for the adhesion of hydrogels

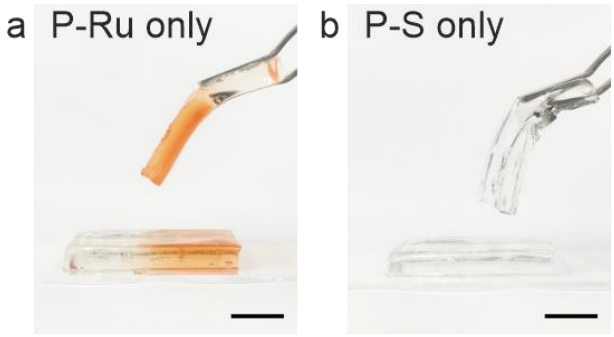

Figure S43. P1 gels could not be glued by applying P-Ru solution only (a) or P-S solution only (b) to P1 gels. Scale bars: 10 mm.

Measurements of adhesion strength of glued P1 gels

A P-Ru/P-S sol (6 wt%, 5 μL/cm^2) was spread on the surfaces of two P1 gels (length: 3 cm; width: 1.5 cm; thickness: 0.2 mm) Then, a piece of P1 gel was pressed on top of the other P1 gel (overlap area 2 cm^2). The gels were put in a sealed container at 70 ℃ for 6 h. The lap-shear adhesion tests for the glued P1 gels were performed using the tensile testing machine (Zwick/Roell) after immersing the glued P1 gels in water for 24 h.

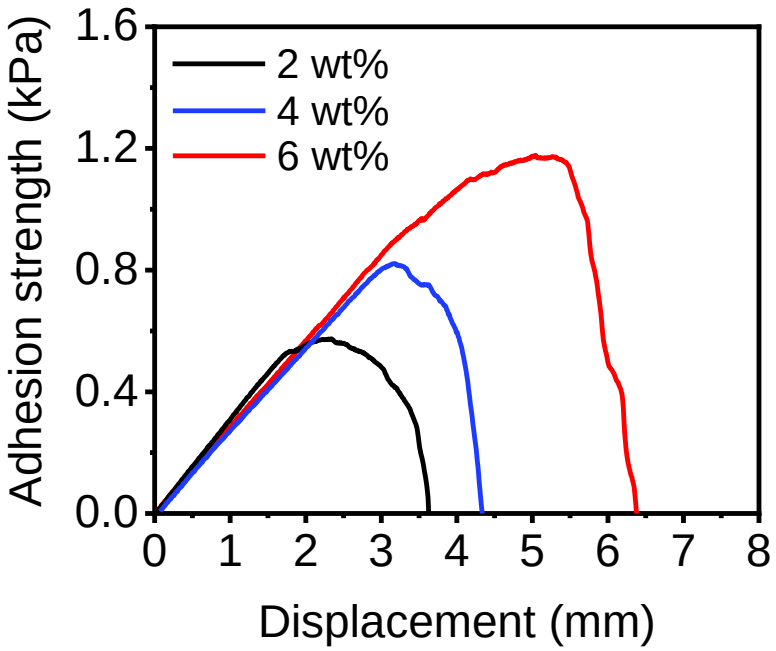

Figure S44. Adhesion strengths of the glued P1 gels with different concentrations of P-Ru/P-S as adhesives (2 wt%, 4 wt% and 6 wt%). The adhesion strength was adjustable using P-Ru/P-S adhesives with different concentrations.

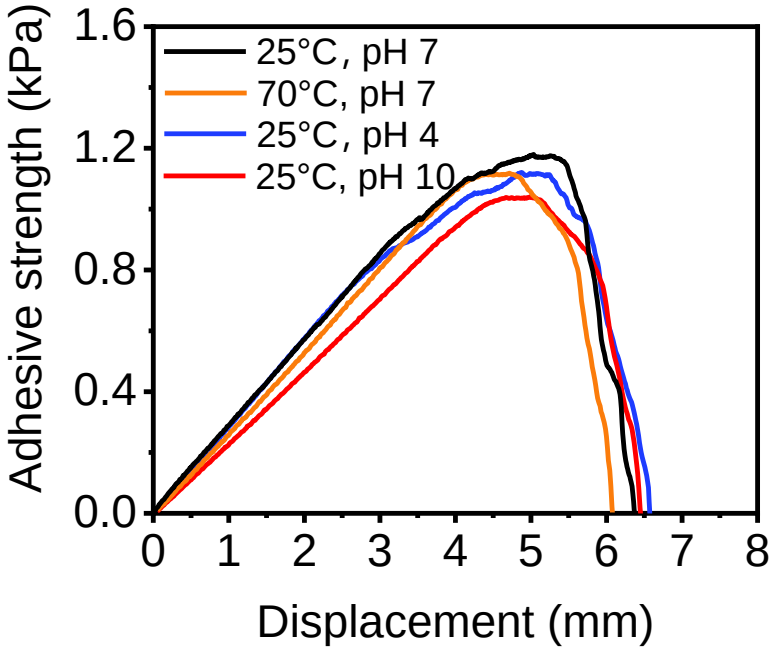

Figure S45. The adhesion strengths of glued P1 gels after different treatments for 24 h.

Volume changes of P2 and P3 gels under different stimuli

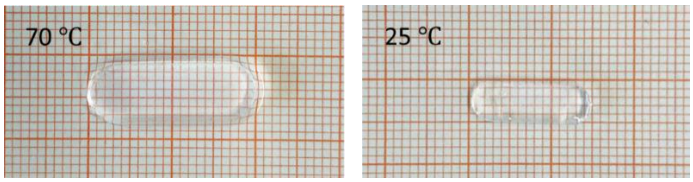

Figure S46. Photos of P2 gel in water at 70 ℃ (left) and 25℃ (right).

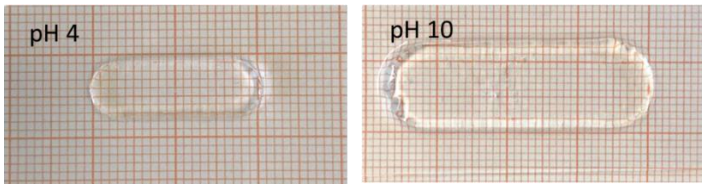

Figure S47. Photos of P3 gel at pH 4 (left) and pH 10 (right).

Measurements of adhesion strength of P1/P2 and P1/P3 gel assemblies

A P2 gel was in water at 70 ℃ to reach the swelling equilibrium before the adhesion experiment. Then, a P-Ru/P-S sol (6 wt%, 5 μL/cm^2) was spread on the surfaces of a P1 gel and a P2 gel. The length, width and thickness of each piece of gel were 3.0 cm, 1.5 cm and 0.2 mm, respectively. A P1 gel was pressed on top of a P2 gel (overlap area 2 cm^2). The gels were put in a sealed container at 70 ℃ for 6 h. Then, a gel assembly was obtained and the hydrogel assembly was immersed in water before further investigation. The lap-shear adhesion tests for the glued P1/P2 gel assembly were performed using the tensile testing machine (Zwick/Roell) after immersing the glued P1/P2 gel assembly at 70 ℃ in water for 24 h (the initial one) and after the glued P1/P2 gel assembly was bent and unbent for 10 times in response to temperature changes.

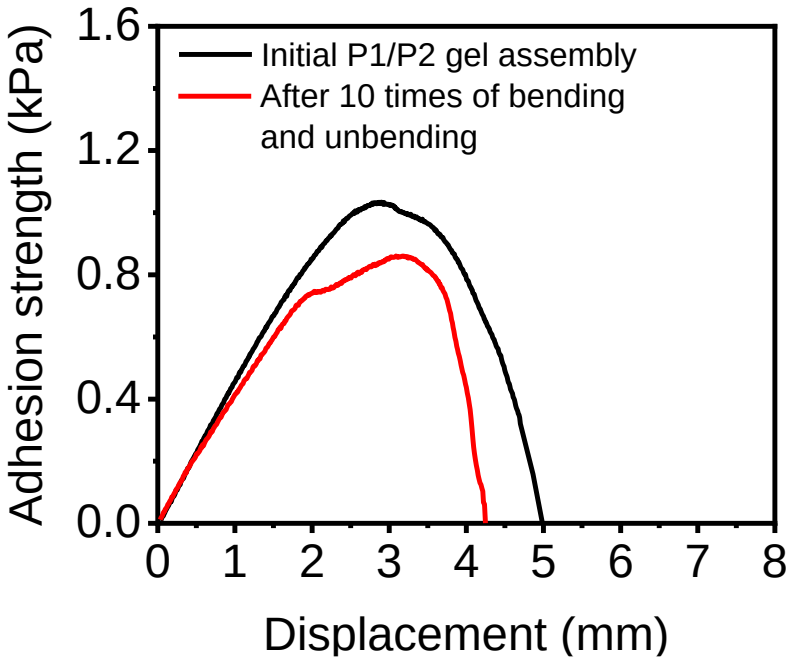

Figure S48. The adhesion strengths of a P1/P2 gel assembly before and after actuation in response to temperature changes for 10 times.

A P3 gel was in water at pH 4 to reach the swelling equilibrium before the adhesion experiment. Then, a P-Ru/P-S sol (6 wt%, 5 μL/cm^2) was spread on the surfaces of a P1 gel and a P3 gel. The length, width and thickness of each piece of gel were 3.0 cm, 1.5 cm and 0.2 mm, respectively. A P1 gel was pressed on top of a P3 gel (overlap area 2 cm^2). The gels were put in a sealed container at 70 ℃ for 6 h. Then, a gel assembly was obtained and the hydrogel assembly was immersed in water before further investigation. The lap-shear adhesion tests for the glued P1/P3 gel assembly were performed using the tensile testing machine (Zwick/Roell)

after immersing the glued P1/P3 gel assembly at pH 4 in water for 24 h (the initial one) and after the glued P1/P3 gel assembly was bent and unbent for 10 times in response to pH changes.

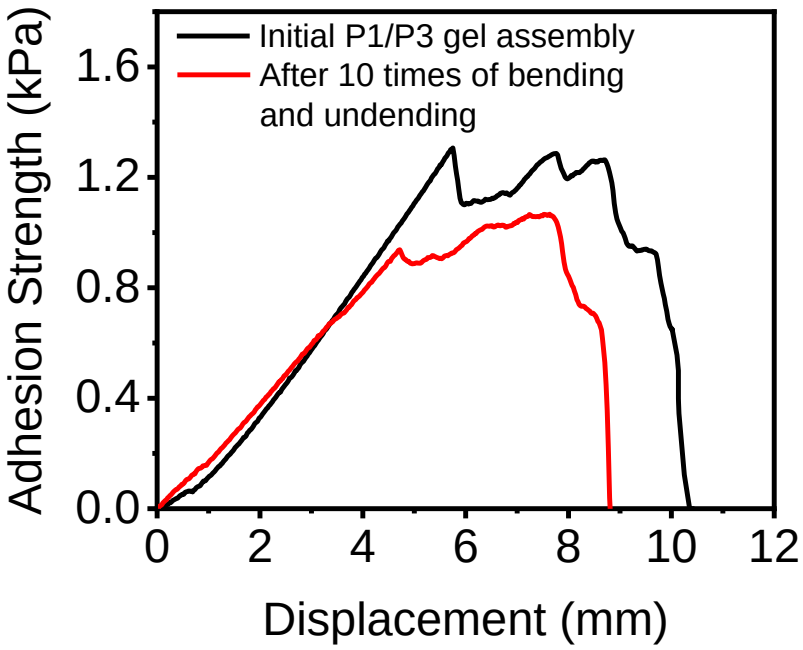

Figure S49. The adhesion strengths of a glued P1/P3 gel assembly before and after actuation in response to pH changes for 10 times.

Shape changes of a P-Ru/P-S gel and swelling of a P-Ru/P-S gel in water

The mixture of P-Ru (1 wt%) and P-S (1 wt%) in water was heated at 70 ℃ for 6 h to form a R-Ru/P-S gel. The P-Ru/P-S gel was flexible and changed its shape by pressing (Figure S50a). A P-Ru/P-S gel was put in water for 24 h. The gel maintained its integrated network structure during swelling (Figure S50b).

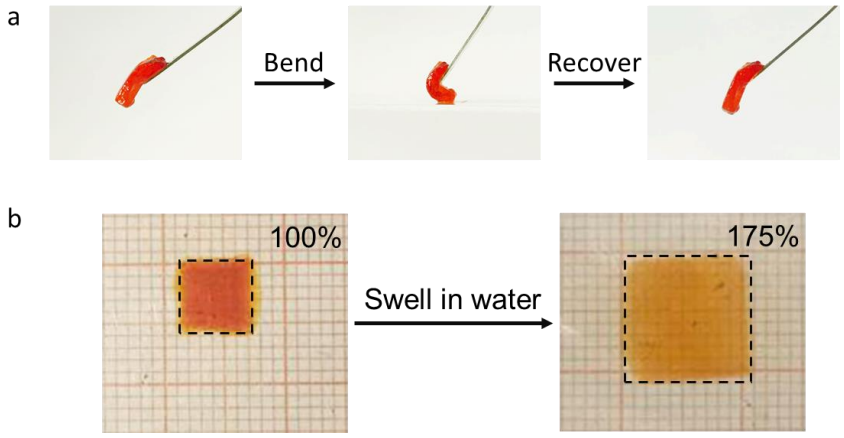

Figure S50. (a) Bending and shape recovery of a P-Ru/P-S gel. (b) Swelling of P-Ru/P-S gel in water.

A soft robot based on a dual-responsive hydrogel assembly for maze navigation

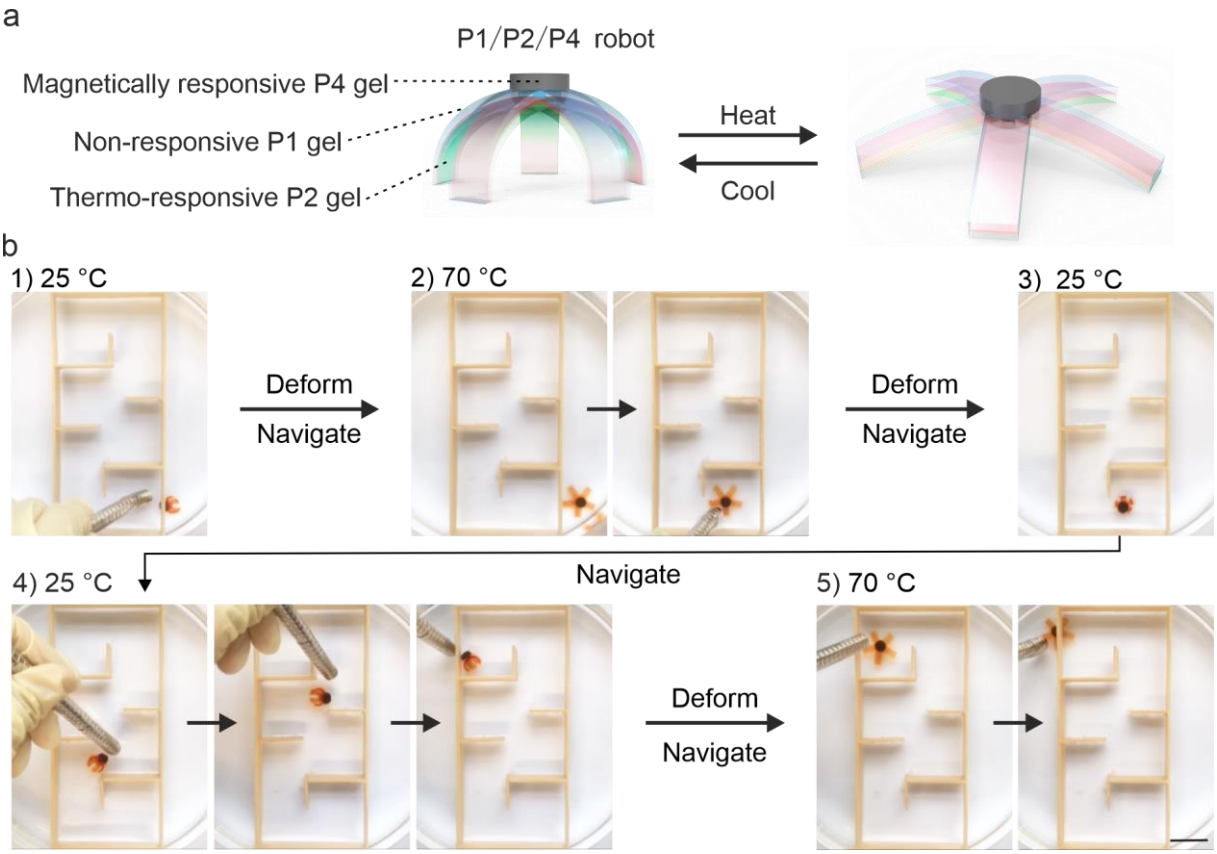

Figure S51. A soft robot based on a thermally and magnetically dual-responsive hydrogel assembly for maze navigation. (a) Schematic of a P1/P2/P4 robot prepared by gluing the gel units using the P-Ru/P-S adhesive. (b) Photos of the P1/P2/P4 robot passing through a maze under the control of temperature and a magnetic field. Scale bar: 20 mm.

Thermodynamic and Kinetic study for thermal coordination and photosubstitution

We quantified the formation and dissociation of the Ru-thioether bond using UV-vis absorption spectroscopy. The second-order rate constant k_1 for the thermal coordination was 4.2×10^{-2} $M^{-1} \cdot s^{-1}$ and the first-order constant k_{-1} for the thermal hydrolysis was 1.1×10^{-5} s^{-1} at 70 °C. The activation energy E_a of the thermal coordination is 73.3 kJ·mol^{-1}. The quantum yield φ for the photosubstitution was 0.03 (Table S1).

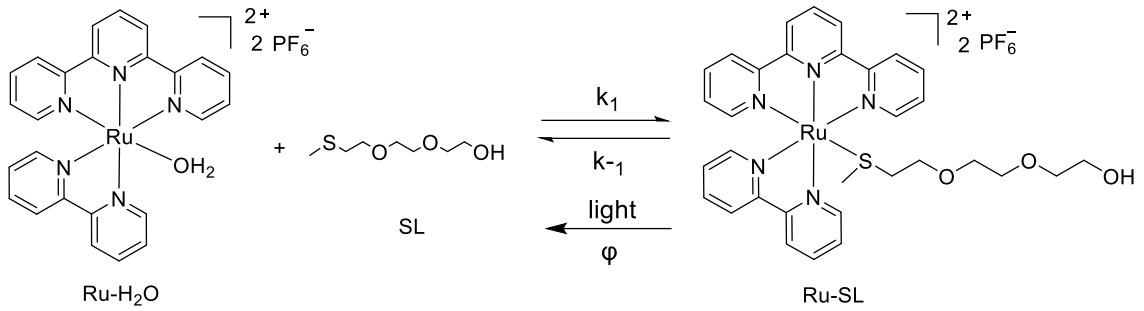

Figure S51. The reversible formation and dissociation of the Ru-S coordination bond. k_1: second-order rate constant for thermal coordination. k_{-1}: first-order rate constant for thermal hydrolysis. φ: Quantum yield for photosubstitution.

Table S1. Thermodynamic and kinetic data for thermal coordination and photosubstitution

k_1	k_{-1}	E_a	φ
$4.2 \times 10^{-2}\ M^{-1} \cdot s^{-1}$	$1.1 \times 10^{-5}\ s^{-1}$	$73.3\ kJ \cdot mol^{-1}$	0.03

(1) Rate constants of thermal substitution of H_2O ligand by ligand SL on Ru-H_2O

The rate constant was calculated according to the following two steps. First, the extinction coefficients of Ru-H_2O and Ru-SL were determined using UV-vis absorption spectroscopy. Ru-H_2O and Ru-SL are nonlabile at room temperature. The extinction coefficients were measured following the traditional procedure. Different concentrations of Ru-H_2O and Ru-SL were prepared in H_2O (1.25×10^{-5} M, 2.05×10^{-5} M, 3.08×10^{-5} M, 4.1×10^{-5} M, 5.13×10^{-5} M and 6.15×10^{-5} M, respectively). Each sample was measured by UV-vis absorption spectroscopy. The extinction coefficient of Ru-H_2O or Ru-SL was obtained from the slope of the plot of absorbance *vs.* concentration of Ru complexes at each wavelength. The extinction coefficients of Ru-H_2O at 452 nm and 476 nm were found to be 6859 $L \cdot mol^{-1} \cdot cm^{-1}$ and 8510 $L \cdot mol^{-1} \cdot cm^{-1,}$ respectively. The extinction coefficients of Ru-SL at 452 nm and 476 nm were found to be 7256 $L \cdot mol^{-1} \cdot cm^{-1}$ and 5154 $L \cdot mol^{-1} \cdot cm^{-1}$, respectively.

Then, the rate constants of thermal substitution of H_2O ligand by thioether ligand on Ru-H_2O complexes were calculated according to the following results from UV-vis absorption spectroscopy. A solution of Ru-H_2O (6.15×10^{-5} M) was prepared at a certain temperature. After adding SL (6.15×10^{-2} M), we measured the UV-vis absorption of the mixture solution at the certain temperature. The UV-vis spectrum was taken at a fixed time interval. The

concentrations of Ru-H2O and Ru-SL in the mixture solution were calculated using a two-wavelength method for each measurement. As the reactions are thermodynamic, the absorbance at two wavelengths can be expressed as Eq.1a and 1b. [$RuOH_2$], [S] and [RuS] represent the concentration of Ru-H_2O, SL and Ru-SL, respectively:

$$A_{\lambda_1} = \varepsilon_{\lambda_1}^{RuOH_2} \cdot l \cdot [RuOH_2] + \varepsilon_{\lambda_1}^{RuS} \cdot l \cdot [RuS] \quad (1a)$$

$$A_{\lambda_2} = \varepsilon_{\lambda_2}^{RuOH_2} \cdot l \cdot [RuOH_2] + \varepsilon_{\lambda_2}^{RuS} \cdot l \cdot [RuS] \quad (1b)$$

According to Eq. (1b), [$RuOH_2$] can be expressed to Eq. (2):

$$[RuOH_2] = \frac{A_{\lambda_2} - \varepsilon_{\lambda_2}^{RuS} \cdot l \cdot [RuS]}{\varepsilon_{\lambda_2}^{RuOH_2} \cdot l} \quad (2)$$

After introducing Eq. (2) to Eq. (1a), the [RuS] can be expressed as (l = 1 cm):

$$[RuS] = \frac{A_{\lambda_1} \cdot \varepsilon_{\lambda_2}^{RuOH_2} - A_{\lambda_2} \cdot \varepsilon_{\lambda_1}^{RuOH_2}}{\varepsilon_{\lambda_2}^{RuOH_2} \cdot \varepsilon_{\lambda_1}^{RuS} - \varepsilon_{\lambda_1}^{RuOH_2} \cdot \varepsilon_{\lambda_2}^{RuS}} \quad (3)$$

The rate law of coordination reaction in water can be expressed as:

$$\frac{d[RuS]}{dt} = -\frac{d[RuOH_2]}{dt} = k_1 \cdot [S] \cdot [RuOH_2] - k_{-1} \cdot [RuS] \quad (4)$$

where, k_1 is the second-order rate constant. As the concentration of SL is in large excess, the pseudo first-order rate constant k_1' can be defined as k_1'= k_1 · [S]. Thus, the Eq. (4) can be expressed by:

$$\frac{d[RuS]}{dt} = -\frac{d[RuOH_2]}{dt} = k_1' \cdot [RuOH_2] - k_{-1} \cdot [RuS] \quad (5)$$

Which can be simplified to Eq. (6):

$$\frac{d[RuS]}{dt} = -\frac{d[RuOH_2]}{dt} = k_1' \cdot [Ru] - (k_{-1} + k_1') \cdot [RuS] \quad (6)$$

Because the thermal back coordination (k_{-1}) is negligible and the pseudo first order rate constants k_1' were determined from the slope of the plot of ln([$RuOH_2$]/[Ru]) vs. time (Figure S52). The second order rate can be calculated by k_1 = k_1'/[S]. k_1' and k_1 at different temperatures for the thermal substitution of H_2O by SL on Ru-H_2O were summarized in Table S2.

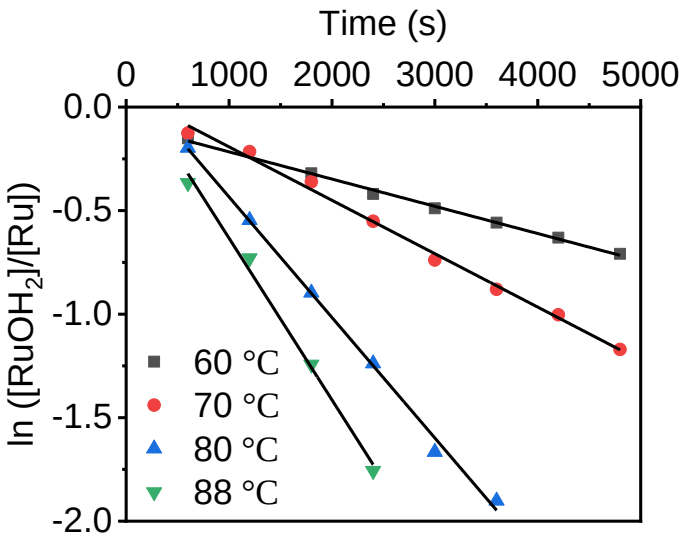

Figure S52. Polts of ln([$RuOH_2$]/[Ru]) vs time at different temperatures for the thermal coordination.

Table S2.Expermatnial pseudo first-order constant and second order rate constants at different temperatures.

Temperature (℃)	k_1'(s^{-1})	k_1 ($M^{-1} \cdot s^{-1}$)
60	1.3×10^{-4}	2.1×10^{-3}
70	2.6×10^{-4}	4.1×10^{-2}
80	5.6×10^{-4}	9.0×10^{-2}
88	7.8×10^{-4}	1.2×10^{-2}

(2) Activation energy of thermal coordination

According to Arrthenius equation (Eq. 7):

$$k = Ae^{\frac{-E_a}{RT}} \quad (7)$$

Where k is the rate constant, E_a is the activation energy, A is the pre-exponential factor, R is the gas constant (8.314 $J \cdot mol^{-1} \cdot K^{-1}$) and T is the absolute temperature. Eq.7 can be expressed as Eq. 8.

$$\ln(k) = \frac{-E_a}{R}\left(\frac{1}{T}\right) + \ln(A) \qquad (8)$$

E_a was determined from the slope of the plot of ln(*k*) vs. -1/T and ln(A) was determined from the intercept of the polt (Figure S53). E_a is 73.3 kJ·mol^{-1}.

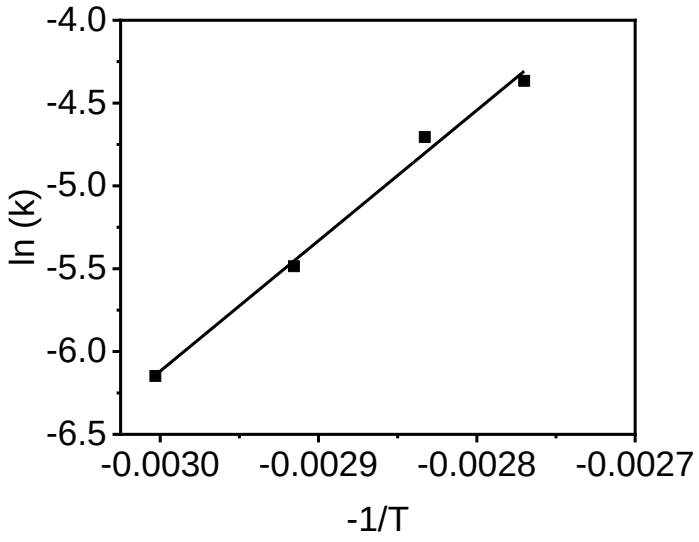

Figure S53. Polt of ln(k) vs. -1/T for the thermal substitution of H_2O by SL on Ru-H_2O.

(3) Rate constants of thermal hydrolysis of ligand SL by H_2O ligand in Ru-SL complex

A solution of Ru-SL (9.23×10^{-5} M) in water was prepared. We measured the UV-vis of the solution at a constant temperature. The UV-vis spectra were taken over time. The first-order rate constants k_{-1} were determined from the slope of the plot of ln([$RuOH_2$]/[Ru]) vs. time.

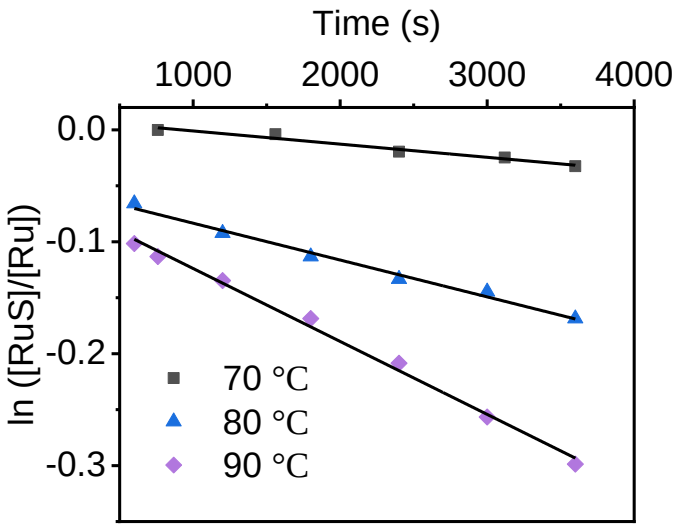

Figure S54. Polts of ln([RuS]/[Ru]) vs. time at different temperatures for the thermal hydrolysis.

Table S3.Expermatnial first-order constant of the thermal hydrolysis at different temperatures.

Temperature (°C)	k_{-1} (s^{-1})
70	1.1×10^{-5}
80	3.2×10^{-5}
90	6.5×10^{-5}

(4) Photosubstitution quantum yield for Ru-SL

The rate of the photosubstitution of SL in the Ru-SL by H_2O can be expressed by Eq. 9 and 10:

$$r_{photo} = \frac{dn_{RuS}}{dt} = -k_{\varphi} \cdot n_{RuS} \quad (9)$$

$$r_{photo} = \frac{dn_{RuS}}{dt} = -\eta_{RuS} \cdot \varphi \quad (10)$$

Where k_{φ} is the first order photosubstitution rate constant, n_{RuS} is the number of moles of Ru-SL at time t, φ is the photosubstitution quantum yield and η_{RuS} is the number of moles of photons absorbed by the RuS. η_{RuS} is calculated from Eq. 11:

$$\eta_{RuS} = \Phi \cdot (1 - 10^{-A_e}) \cdot \left(\frac{A_{RuS}}{A_{Ru}}\right) \quad (11)$$

Where A_e is the absorbance of the solution at the irradiation wavelength, $1\text{-}10^{-Ae}$ is the photon absorption probability.

Eq.10 and 11 rearrange to Eq.12:

$$r_{photo} = -\Phi \cdot (1 - 10^{-A_e}) \cdot \left(\frac{n_{RuS}}{n_{Ru}}\right) \cdot \varphi \quad (12)$$

By comparison between Eq. 9 and Eq.12, k_{φ} can be ontained from Eq. 13.

$$k_{\varphi} = \frac{\Phi \cdot \varphi \cdot (1 - 10^{-A_e})}{n_{Ru}} \quad (13)$$

To measure φ, an aqueous solution of 3mL Ru-SL (9.23×10^{-5} M) was prepared. The sample was irradiated with blue light (470 nm). After each irradiation period, a UV-vis spectrum was

measured until a total irradiation time of 30 min. The ratio of [RuS]/[$RuOH_2$] at was obtained from the UV-vis spectrum. k_φ were determined from the slope of the plot of ln([RuSL]/[Ru]) vs irradiation time. $k_\varphi = 1.3 \times 10^{-3}$. $\Phi = 1.9 \times 10^{-8}$, the photosubstitution quantum yield φ_i were calculated using Eq. 13, $\varphi = 0.026$.

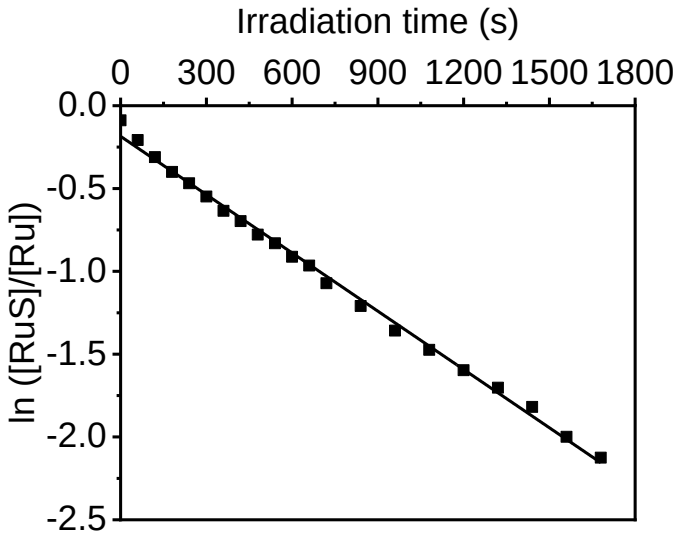

Figure S55. Plots of the ratio [RuS]/[$RuOH_2$] vs. irradiation time.

2.5 References

[1] C. Li, A. Iscen, H. Sai, K. Sato, N. A. Sather, S. M. Chin, Z. Alvarez, L. C. Palmer, G. C. Schatz, S. I. Stupp, *Nat. Mater.* **2020**, *19*, 900.

[2] J. Chen, F. K. Leung, M. C. A. Stuart, T. Kajitani, T. Fukushima, E. van der Giessen, B. L. Feringa, *Nat. Chem.* **2018**, *10*, 132.

[3] W. Hu, G. Z. Lum, M. Mastrangeli, M. Sitti, *Nature* **2018**, *554*, 81.

[4] Z. Li, P. Liu, X. Ji, J. Gong, Y. Hu, W. Wu, X. Wang, H. Q. Peng, R. T. K. Kwok, J. W. Y. Lam, J. Lu, B. Z. Tang, *Adv. Mater.* **2020**, *32*, 1906493.

[5] J. A. Shadish, G. M. Benuska, C. A. DeForest, *Nat. Mater.* **2019**, *18*, 1005.

[6] Y. Kim, H. Yuk, R. Zhao, S. A. Chester, X. Zhao, *Nature* **2018**, *558*, 274.

[7] A. S. Gladman, E. A. Matsumoto, R. G. Nuzzo, L. Mahadevan, J. A. Lewis, *Nat. Mater.* **2016**, *15*, 413.

[8] Y. S. Zhang, A. Khademhosseini, *Science* **2017**, *356*, eaaf3627.

[9] G. H. Lee, H. Moon, H. Kim, G. H. Lee, W. Kwon, S. Yoo, D. Myung, S. H. Yun, Z. Bao, S. K. Hahn, *Nat. Rev. Mater.* **2020**, *5*, 149.

[10] H. Liu, H. Zhang, W. Han, H. Lin, R. Li, J. Zhu, W. Huang, *Adv. Mater.* **2021**, *33*, 2004782.

[11] Y. Ohm, C. Pan, M. J. Ford, X. Huang, J. Liao, C. Majidi, *Nat. Electron.* **2021**, *4*, 185.

[12] V. Vallem, Y. Sargolzaeiaval, M. Ozturk, Y. C. Lai, M. D. Dickey, *Adv. Mater.* **2021**, *33*, 2004832.

[13] T. B. H. Schroeder, A. Guha, A. Lamoureux, G. VanRenterghem, D. Sept, M. Shtein, J. Yang, M. Mayer, *Nature* **2017**, *552*, 214.

[14] F. G. Downs, D. J. Lunn, M. J. Booth, J. B. Sauer, W. J. Ramsay, R. G. Klemperer, C. J. Hawker, H. Bayley, *Nat. Chem.* **2020**, *12*, 363.

[15] X. He, M. Aizenberg, O. Kuksenok, L. D. Zarzar, A. Shastri, A. C. Balazs, J. Aizenberg, *Nature* **2012**, *487*, 214.

[16] G. Weng, S. Thanneeru, J. He, *Adv. Mater.* **2018**, *30*, 1706526.

[17] T. S. Shim, S. H. Kim, C. J. Heo, H. C. Jeon, S. M. Yang, *Angew. Chem. Int. Ed.* **2012**, *51*, 1420.

[18] J. Kim, S. Im, J. H. Kim, S. M. Kim, S. M. Lee, J. Lee, J. P. Im, J. Woo, S. E. Moon, *Adv. Mater.* **2020**, *32*, 1905901.

[19] Y. S. Kim, M. Liu, Y. Ishida, Y. Ebina, M. Osada, T. Sasaki, T. Hikima, M. Takata, T. Aida, *Nat. Mater.* **2015**, *14*, 1002.

[20] K. Iwaso, Y. Takashima, A. Harada, *Nat. Chem.* **2016**, *8*, 625.

[21] Q. Li, G. Fuks, E. Moulin, M. Maaloum, M. Rawiso, I. Kulic, J. T. Foy, N. Giuseppone, *Nat. Nanotech.* **2015**, *10*, 161.

[22] Y. Gu, E. A. Alt, H. Wang, X. Li, A. P. Willard, J. A. Johnson, *Nature* **2018**, *560*, 65.

[23] H. Qin, T. Zhang, N. Li, H. P. Cong, S. H. Yu, *Nat. Commun.* **2019**, *10*, 2202.

[24] C. Yang, Z. Suo, *Nat. Rev. Mater.* **2018**, *3*, 125.

[25] J. Kim, J. A. Hanna, M. Byun, C. D. Santangelo, R. C. Hayward, *Science* **2012**, *335*, 1201.

[26] H. Therien-Aubin, Z. L. Wu, Z. Nie, E. Kumacheva, *J. Am. Chem. Soc.* **2013**, *135*, 4834.

[27] C. Li, G. C. Lau, H. Yuan, A. Aggarwal, V. L. Dominguez, S. Liu, H. Sai, L. C. Palmer, N. A. Sather, T. J. Pearson, D. E. Freedman, P. K. Amiri, M. O. de la Cruz, S. I. Stupp, *Sci. Robot.* **2020**, *5*, eabb9822.

[28] K. Liu, Y. Zhang, H. Cao, H. Liu, Y. Geng, W. Yuan, J. Zhou, Z. L. Wu, G. Shan, Y. Bao, Q. Zhao, T. Xie, P. Pan, *Adv. Mater.* **2020**, *32*, 2001693.

[29] S. H. Hong, M. Shin, E. Park, J. H. Ryu, J. A. Burdick, H. Lee, *Adv. Funct. Mate.* **2019**, *30*, 1908497.

[30] Q. Zhang, Y. Sun, C. He, F. Shi, M. Cheng, *Adv. Sci.* **2020**, *7*, 2002025.

[31] J. Liu, C. S. Y. Tan, O. A. Scherman, *Angew. Chem. Int. Ed.* **2018**, *57*, 8854.

[32] A. H. Hofman, I. A. van Hees, J. Yang, M. Kamperman, *Adv. Mater.* **2018**, *30*, 1704640.

[33] C. Heinzmann, C. Weder, L. M. de Espinosa, Chem. Soc. Rev. **2016**, *45*, 342.

[34] A. Bahreman, B. Limburg, M. A. Siegler, E. Bouwman, S. Bonnet, *Inorg. Chem.* **2013**, *52*, 9456.

[35]J. Yang, R. Bai, Z. Suo, *Adv. Mater.* **2018**, *30*, 1800671.

Chapter 3: Metallopolymer organohydrogels with photo-controlled coordination crosslinks work properly below 0 °C

Adapted with permission from my publication: J. Liu, et al. Adv. Mater. 2020, 1908324.

3.1 Introduction

A hydrogel is a jelly-like soft matter that consists of three-dimensional networks swollen by a large amount of water. Hydrogels, which are responsive to external stimuli (e.g., pH, temperature, redox, light), have many applications in science and technology, ranging from regenerative medicine to soft robotics. Photoresponsive hydrogels are a kind of stimuli-responsive hydrogels that are under intense investigation.[1-6] The photoresponsiveness of gels is mainly based on photoreactions that change the crosslinking density,[1,6] topology,[7] and other physicochemical properties of hydrogels.[8-10] Their structures and functions can be controlled with light. Compared to other stimuli, light has high spatiotemporal resolution, enables remote control of hydrogels, and can be obtained from the sun. Therefore, light has been used to fabricate three-dimensional extracellular matrices in hydrogels,[1, 3, 4] induce cargo release from hydrogels,[6,11] regulate adhesion,[12] and control the motion of actuators.[13, 14]

Although photoresponsive hydrogels function normally at room temperature, they lose photoresponsiveness below the freezing temperature of water because the frozen matrix hinders photoreactions and structural changes in the hydrogels. A binary solvent system such as water/organic solvent or water/oil can be used to prepare organohydrogels that are non-freezing at subzero temperatures.[15-17] However, simply replacing water in a photoresponsive hydrogel with a binary solvent usually does not result in a photoresponsive organohydrogel. Gelation and light-triggered structural changes are influenced by solvent-gelator interactions. Replacing water with another solvent may lead to no gelation or cause gels to lose their photo-controlled properties. Furthermore, many photoresponsive hydrogels are based on supramolecular interactions that occur only in water.[18, 19] For example, the well-known host-guest complex of cyclodextrin and azobenzene, which has frequently been used as a photoresponsive crosslink for hydrogels, does not form in organic solvents;[20] the host-guest complexes form crosslinks only upon substituting the organic solvent with water.[20] It is essential to design gelators with suitable chemical structures so that photoresponsive gels can work in antifreezing solvents below 0 °C. Previously reported gels showed photoresponsiveness only at room temperature or

elevated temperatures. The development of photoresponsive gels that function at subzero temperatures poses a challenge.

In this section, metallopolymer organohydrogels that are photoresponsive even at -20 °C were prepared. The organohydrogels consist of a water/glycerol mixture as an antifreezing solvent, poly(N-hydroxyethyl acrylamide) as a gel-forming polymer, and Ru-thioether coordination bonds as photoresponsive crosslinks (Figure 1). The photoresponsiveness is attributed to ligand photosubstitution of the Ru complex moieties. Ligand photosubstitution means that a coordinated ligand in a metal complex is replaced by another ligand upon light irradiation.[21-28] Although some Ru complexes exhibit reversible ligand photosubstitution,[21-24] their reactivity at subzero temperatures has not been explored. In our organohydrogels (Figure 1), the coordinated thioether ligands in the Ru complex moieties can be substituted by solvent molecules upon light irradiation at -20 °C; when the light is turned off, thioether moieties in the polymer network substitute for the coordinated solvent molecules spontaneously. Such reversible ligand substitution can control the crosslinking densities in the organohydrogel, resulting in significant changes in the network structures and properties. This work demonstrated that light can induce reversible gel-to-sol transitions, heal damaged organohydrogels, control the mechanical properties and volumes of organohydrogels, and fabricate dynamic microstructures on organohydrogels at -20 °C.

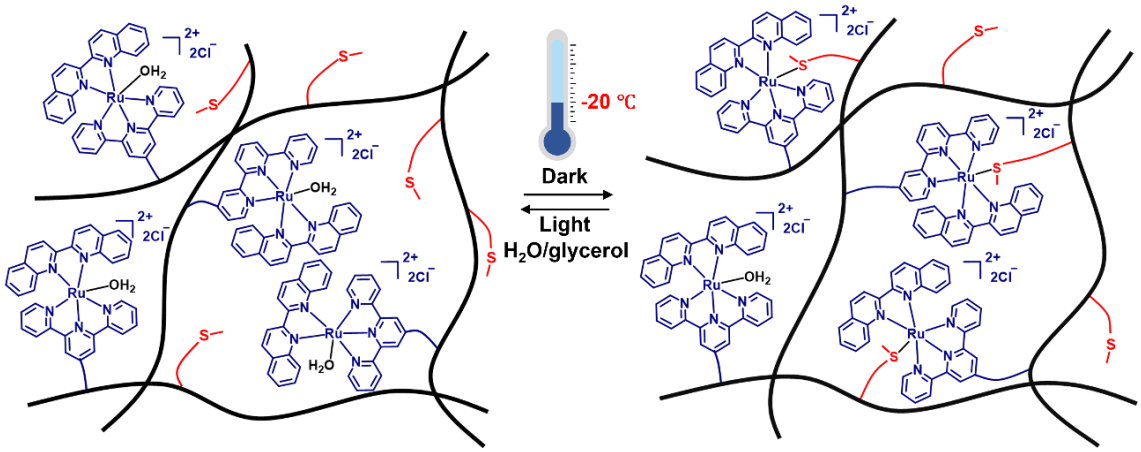

Figure 1. Schematic of a metallopolymer organohydrogel with photo-controlled Ru-thioether coordination crosslinks. The gel is called an organohydrogel because its solvent is a H_2O/glycerol (v/v, 1/1) mixture. At -20 °C, the Ru-thioether coordination bonds in the organohydrogel form automatically in the dark. Light irradiation induces cleavage of the Ru-thioether coordination bonds and aquation of the Ru complex moieties. In this way, the properties of the organohydrogel can be altered in cold environments.

3.2 Results and discussion

3.2.1 Reversible Ru-thioether coordination

Ru complex **1** and thioether ligand **2** (Figure 2a) are model compounds for the designed reversible crosslinks (Figure 1). **1** and **2** were synthesized and characterized (Figure S1-11). Their reversible coordination was studied using UV-vis absorption spectroscopy (Figure 2b). The absorption maximum of the mixture of 1 (0.68 mM) and 2 (3.4 mM) in H_2O occurred at 549 nm and is attributed to the metal-to-ligand charge transfer (MLCT) band of **1**. When the mixture was kept in the dark for 180 min, the absorption band shifted to 543 nm. The spectral change is identical to the reports in the literature regarding the formation of Ru-thioether coordination bonds,[23, 24] which suggested that thioether-coordinated Ru complex **3** was formed. Subsequently, the absorption spectrum returned to the initial state when the solution was irradiated with light (530 nm, 10 mW cm^{-2}, 5 min). This result demonstrated that the coordination was reversible (Figure 2a). The reversible Ru-thioether coordination was confirmed using ^1H NMR spectroscopy (Figure S31), which showed that **2** coordinated with the Ru centre in the dark and was substituted by a H_2O molecule upon light irradiation.

The formation and dissociation of the Ru-thioether bond was quantified using ^1H NMR and UV-vis absorption spectroscopy (Table S3). At room temperature, the equilibrium constant K for the Ru-thioether bond was 108.7 ± 4 M^{-1} (Figure S40); The second-rate constant k_1 for the thermal coordination was 1.2 × 10^{-2} M^{-1} s^{-1}; The first-order constant k_{-1} for the thermal hydrolysis was 1.1×10^{-4} s^{-1}. The quantum yield φ for the photosubstitution was 0.21 (Figure S43). The activation energy for the thermal coordination is 48.6 kJ·mol^{-1}.

The reversible coordination of **1** and **2** in H_2O at 25 °C was found with reversible colour changes (Figure 2e). However, since H_2O was frozen at -20 °C, **1**, **2**, and H_2O did not have sufficient mobility. Therefore, the reversible Ru-thioether coordination did not work at -20 °C (Figure 2f). To overcome this problem, a H_2O/glycerol (v/v, 1/1) mixture was used as the solvent, which freezes at -38 °C. The Ru-thioether coordination in the H_2O/glycerol mixture was studied using UV-vis absorption spectroscopy, which showed that a Ru-thioether coordination bond was formed by mixing **1** and **2** in the H_2O/glycerol mixture at 25 °C (Figure 2c). The Ru-thioether bond was cleaved reversibly upon light irradiation (Figure 2c). The reversible Ru-thioether coordination in the H_2O/glycerol mixture also induced reversible colour changes (Figure 2g). The formation and cleavage of the Ru-thioether bond can be cycled at least 5 times under dark/light irradiation conditions (Figure 2d). Importantly, this reversible Ru-thioether coordination functions properly in the H_2O/glycerol mixture at -20 °C (Figure 2h and

Figure S32). The second-order constant of thermal coordination at -20°C (k_1: 4.4 ×10^{-4} s^{-1} at -20°C) was calculated from the Arrhenius equation (Figure S42), which further proved that Ru-thioether coordination formed spontaneously at -20°C.

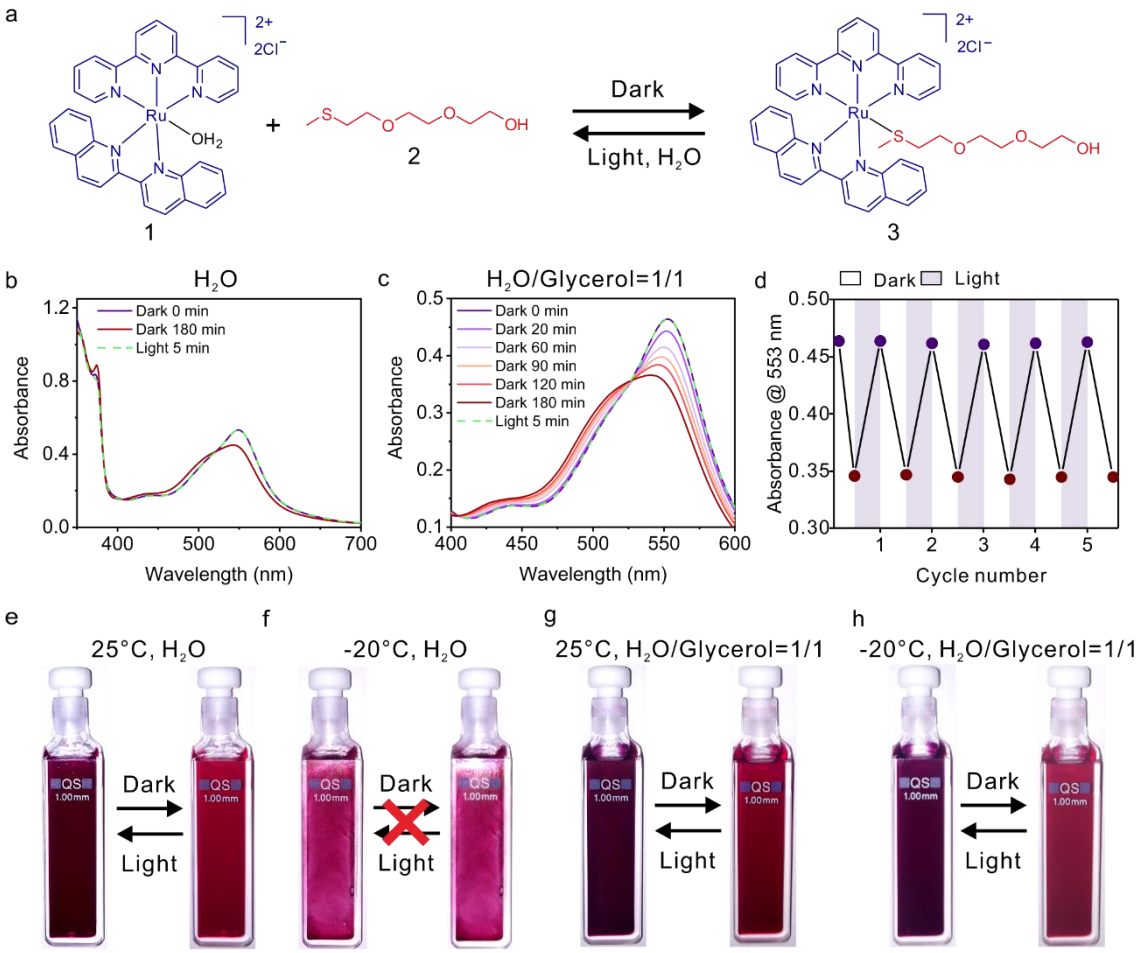

Figure 2. Photo-controlled reversible coordination of Ru complex **1** and thioether ligand **2** under different conditions. (a) Schematic of the reversible coordination in aqueous solutions. (b) UV-vis absorption spectra of **1** (0.68 mM) and **2** (3.4 mM) in H_2O just after mixing (0 min), after mixing for 180 min, and after subsequent light irradiation (530 nm, 10 mW cm^{-2}, 5 min). (c) UV-vis absorption spectra of **1** (0.68 mM) and **2** (3.4 mM) in a H_2O/glycerol mixture (v/v, 1/1) after mixing for different time and after subsequent light irradiation (530 nm, 10 mW cm^{-2}, 5 min). (d) Absorption changes of **1** (0.68 mM) and **2** (3.4 mM) in a H_2O/glycerol mixture under alternating dark/light irradiation cycles. (e-h) Photographs of **1** and **2** in H_2O at 25 °C (e) and -20 °C (f) and in a H_2O/glycerol mixture at 25 °C (g) and -20 °C (h) in the dark and after light irradiation.

3.2.2 Photoinduced reversible gel-to-sol transitions

1a and **2a** were further synthesized and characterized (Figure 3a and Figure S12-30), which are analogues of **1** and **2** with a polymerizable double bond. The gels were prepared by polymerization of **1a**, **2a**, and N-hydroxyethyl acrylamide **4** in a H_2O/glycerol (v/v, 1/1) mixture (Figure 3a, left and Figure S33). **4** constitutes the majority of the repeat units in the polymer network, so the network swells in H_2O/glycerol mixtures. Because the gels contain H_2O and glycerol as the binary solvent and Ru complex moieties as crosslinks, we call them metallopolymer organohydrogels. The Ru complex and thioether moieties spontaneously form coordination bonds in the organohydrogels, which act as photoresponsive crosslinks (Figure 3a, right). We studied the gelation of the samples with the same total monomer concentration (0.9 M) and different molar ratios of **1a**, **2a**, and **4** (Figure 3b). These samples are denoted $\mathbf{1a_x2a_y}$, where x and y are the percentages of **1a** and **2a**, respectively, and 100-x-y is the percentage of **4**. Inverted-vial tests showed that $\mathbf{1a_12a_3}$ and $\mathbf{1a_12a_5}$ formed gels, and the other samples with fewer crosslinks formed viscous solutions (Figure 3b). This result suggested that gelation needs a sufficient amount of Ru-thioether coordination bonds as crosslinks. Furthermore, we prepared samples with total monomer concentrations from 0.7 to 2 M and studied the effect of monomer concentration on gelation (Table 1). As the monomer concentration increased, the samples gelated at a relatively low amount of crosslink. Gelation can occur in samples with suitable monomer concentrations and ratios.

Irradiating the $\mathbf{1a_12a_5}$ organohydrogel with light (530 nm, 10 mW cm^{-2}, 5 min) at 25 °C induced a gel-to-sol transition (Figure 3c). Keeping the irradiated sample in the dark at 25 °C for 15 min resulted in regelation. This observation showed that the organohydrogel exhibited reversible photoinduced gel-to-sol transitions. The reversible transitions are attributed to the reversible Ru-thioether crosslinks (Figure 3a, right). Importantly, reversible photoinduced gel-to-sol transitions also occurred at -20 °C: light irradiation (530 nm, 10 mW cm^{-2}, 15 min) induced the gel-to-sol transition, and the gel reformed when the irradiated sample was kept in the dark for 30 min (Figure 3c).

The $\mathbf{1a_12a_5}$ organohydrogel is healable at both room temperature and low temperatures based on the reversible gel-to-sol transitions (Figure 3d). When the organohydrogel was damaged (Figure 3d, i and ii), the damaged part was locally irradiated with light (530 nm, 10 mW cm^{-2}, 5 min) to induce a gel-to-sol transition (Figure 3d, iii). The irradiated sample flowed across the damaged part. Healing was achieved by keeping the sample in the dark for 15 min to allow a sol-to-gel transition to occur (Figure 3d, iv). Furthermore, photoinduced healing was

studied at -20 °C (Figure 3d, v-vii). The damaged organohydrogel was healed by light irradiation (530 nm, 10 mW cm^{-2}, 15 min) and then being kept in the dark (30 min). Improved fluidity in the sol state provided sufficient polymer chain mobility for healing (Figure S34). Dissociation and re-formation of the Ru-thioether coordination bonds were involved in the healing process (Figure S35 and S36).

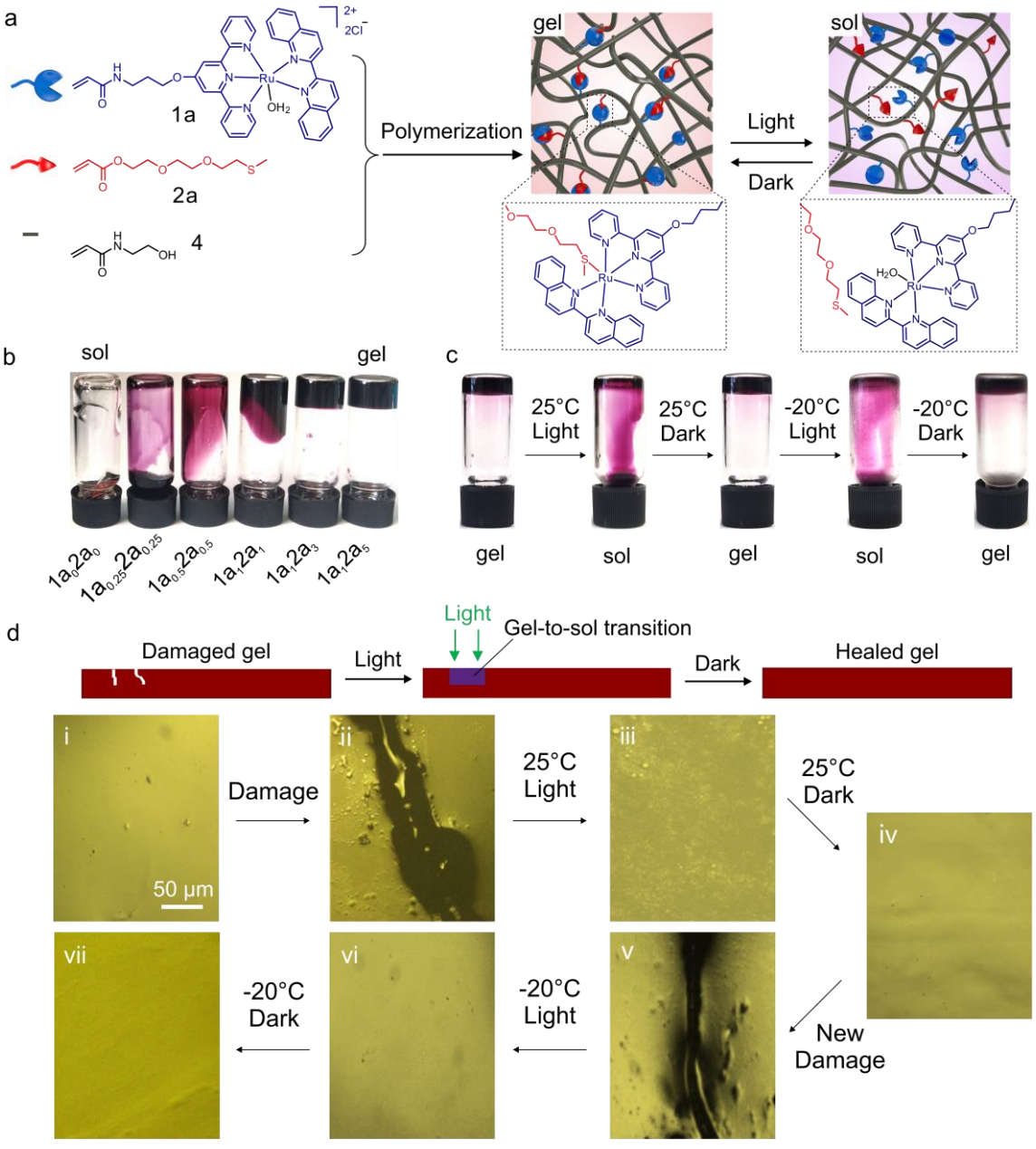

Figure 3. Preparation of photoresponsive metallopolymer organohydrogels and photoinduced reversible gel-to-sol transitions and healing at 25 °C and -20 °C. (a) Chemical structures of the monomers (**1a**, **2a**, and **4**) for the preparation of the organohydrogels and photoinduced reversible gel-to-sol transitions. (b) Photographs of the samples (monomer concentration: 0.9

M) prepared using different molar ratios of **1a** and **2a**: **1a$_0$2a$_0$** (0% **1a**, 0% **2a**, and 100% **4**), **1a$_{0.25}$2a$_{0.25}$** (0.25% **1a**, 0.25% **2a**, and 99.5% **4**), **1a$_{0.5}$2a$_{0.5}$** (0.5% **1a**, 0.5% **2a**, and 99% **4**), **1a$_1$2a$_1$** (1% **1a**, 1% **2a**, and 98% **4**), **1a$_1$2a$_3$** (1% **1a**, 3% **2a**, and 96% **4**), and **1a$_1$2a$_5$** (1% **1a**, 5% **2a**, and 94% **4**). (c) Photographs showing photoinduced reversible gel-to-sol transitions of the **1a$_1$2a$_5$** organohydrogel at 25 °C and -20 °C. (d) Optical microscopy images of photoinduced healing of the **1a$_1$2a$_5$** organohydrogel at 25 °C and -20 °C.

3.2.3 Photoswitchable mechanical properties

The reversible Ru-thioether coordination is also suitable for preparing organohydrogels with photoswitchable mechanical properties. For this purpose, organohydrogels were prepared with both coordination and covalent crosslinks by copolymerization of **1a**, **2a**, **4**, and **4a** in a H_2O/glycerol (v/v, 1/1) mixture (Figure 4a). The Ru moieties and thioether moieties spontaneously formed coordination crosslinks in the organohydrogels. **4a** is the covalent crosslinker that maintains the network structure when the Ru-thioether coordination crosslinks are cleaved upon light irradiation.

Organohydrogels with the same total monomer concentration (1 M) and different molar ratios of the monomers were studied at room temperature (Figure 4b and Table 2). These samples are denoted **1a$_x$2a$_y$4a$_1$**, where x and y are the percentages of **1a** and **2a**, respectively; the molar ratio of **4a** is always 1%; and 100-x-y-1 is the percentage of **4**. All the studied **1a$_x$2a$_y$4a$_1$** samples were gels, showing that 1% covalent crosslinks resulted in the formation of polymer networks. We studied the mechanical properties of the organohydrogels using oscillatory rheology (Figure 4b and Figure S37). Storage modulus (G') is a measure of elastic response of a material and loss modulus (G'') is a measure of viscous response of a material. Comparing G' of **1a$_0$2a$_0$4a$_1$**, **1a$_{0.5}$2a$_{2.5}$4a1** and **1a$_1$2a$_5$4a$_1$** showed that G' increased as the amount of coordination crosslinks increased. Tougher organohydrogels were obtained by increasing the crosslinking density. G'' and loss tangent (tan δ = G''/G') decreased as the amount of the coordination crosslinks increased. These data suggested that the rigidity of the organohydrogels increased as the crosslinking density increased. Comparing **1a$_0$2a$_0$4a$_1$**, **1a$_1$2a$_0$4a$_1$** and **1a$_0$2a$_5$4a$_1$** showed that adding either the Ru moiety or the thioether moiety alone into the gel network did not improve the mechanical properties. This result confirms that the improved mechanical properties of **1a$_{0.5}$2a$_{2.5}$4a$_1$** and **1a$_1$2a$_5$4a$_1$** were attributed to the Ru-thioether coordination crosslinks.

As a control sample, hydrogel **1a$_1$2a$_5$4a$_1$** was prepared by polymerization of **1a**, **2a**, **4**, and **4a** in H_2O. The hydrogel functioned properly at room temperature. However, at 0 °C, it was

frozen, lost elasticity, and became fragile under stretching (Figure 4c). In contrast, the organohydrogel **1a$_1$2a$_5$4a$_1$** did not freeze even at -20 °C (Figure 4d). It remained highly elastic and was capable of twisting, knotting, and stretching. The deformed organohydrogel also showed resilience for shape recovery.

To understand the mechanical properties of the hydrogel and the organohydrogel at different temperatures, their G' and G'' values were measured between -20 and 80 °C (Figure 4e). For the hydrogel, G' and G'' were approximately 2.8-5.2 kPa and 0.4-1.5 kPa, respectively, between 5 and 80 °C. For the organohydrogel, G' and G'' were approximately 2.5-3.0 kPa and 0.2-0.3 kPa, respectively, between 5 and 80 °C. Thus, both the hydrogel and the organohydrogel were elastic in this temperature range. However, the G' and G'' values of the hydrogel increased dramatically as the temperature decreased from 5 to -20 °C. The hydrogel lost elasticity and became fragile at approximately 0 °C because of the modulus changes induced by frozen water. In contrast, the G' and G'' values of the organohydrogel were almost constant between -20 and 80 °C. Thus, the organohydrogel had a wider working temperature than the hydrogel. Organohydrogels with different ratios of H_2O and glycerol (v/v =2/1 and 1/2) were studied, which also showed working temperatures below 0 °C (Figure S38).

The effects of light irradiation on the mechanical properties of organohydrogel **1a$_1$2a$_5$4a$_1$** were further studied at 25 and -20 °C (Figure 4f, g). At 25 °C, G' and G'' increased from 2.1 to 4.1 kPa and from 0.05 to 0.5 kPa, respectively, when the frequency increased from 0.1 to 100 rad s^{-1} (Figure 4f). These moduli are typical for elastic gels. Irradiating (530 nm, 10 mW cm^{-2}, 20 min) the organohydrogel resulted in a decrease in G' and an increase in G''. The stiffness of the organohydrogel was decreased via light irradiation. Subsequently, the moduli were recovered when the irradiated organohydrogel was kept in the dark for 6 h. The reversible changes in the moduli are in accordance with the reversible cleavage and reformation of the Ru-thioether crosslinks under light irradiation and dark storage (Figure 4a). At -20 °C, the changes in moduli showed the same trend when the organohydrogel was irradiated with light (530 nm, 10 mW cm^{-2}, 20 min) and subsequently kept in the dark (Figure 4g). These results demonstrated that the organohydrogel exhibited photoswitchable mechanical properties at both room temperature and low temperatures.

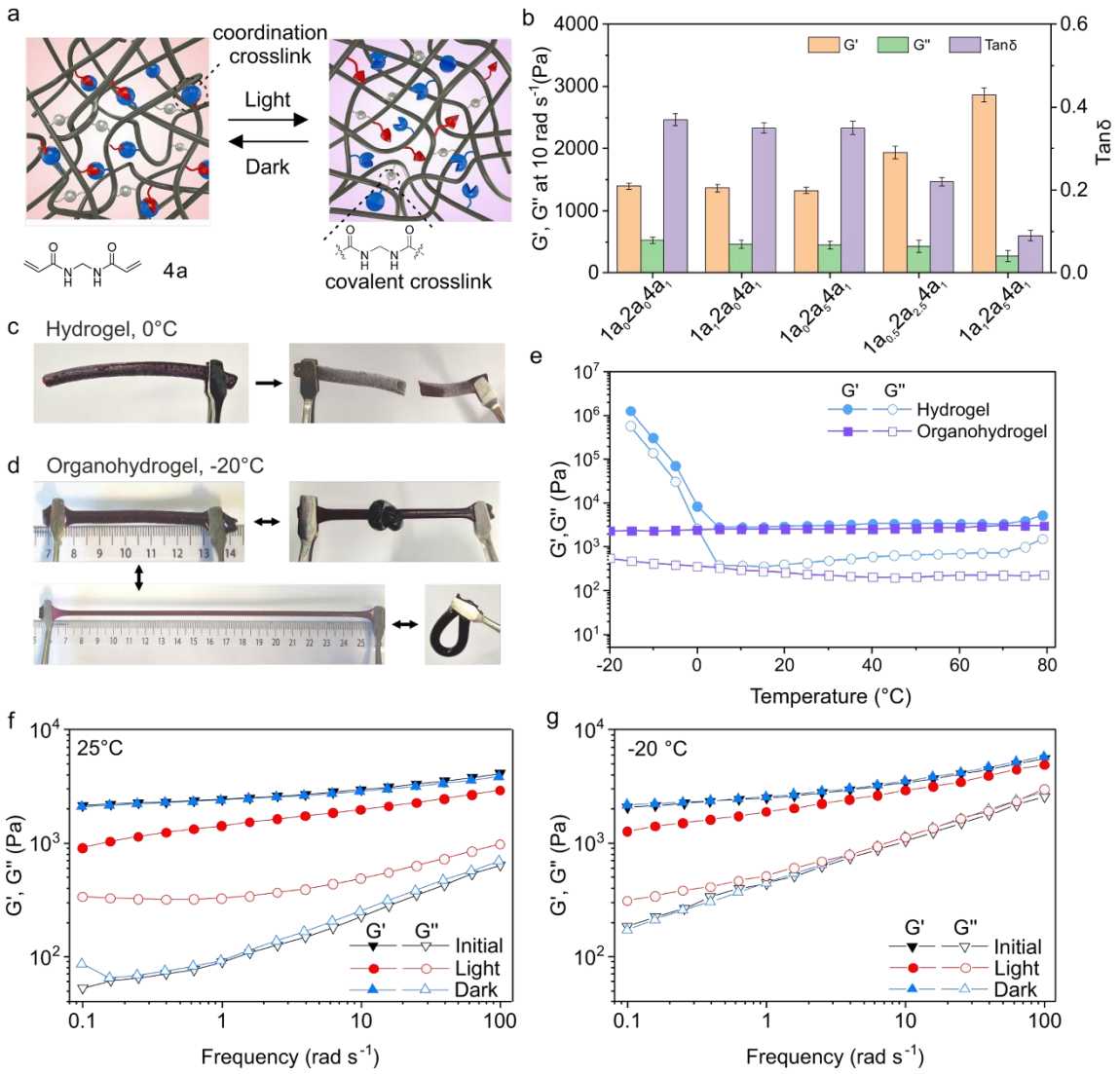

Figure 4. Organohydrogels with coordination and covalent crosslinks and their photoswitchable mechanical properties at room temperature and -20 °C. (a) Schematic illustration of organohydrogels with coordination and covalent crosslinks under light irradiation and in the dark. The chemical structure of the covalent crosslinker **4a** is shown. (b) Storage moduli (G'), loss moduli (G'') and loss tangent (tan δ = G''/G') of organohydrogels prepared using **1a**, **2a**, **4a**, and **4** with different molar ratios. (c) Photographs of hydrogel $\mathbf{1a_1 2a_5 4a_1}$ at 0 °C. (d) Photographs of organohydrogel $\mathbf{1a_1 2a_5 4a_1}$ at -20 °C. (e) Temperature dependence of G' and G'' of hydrogel $\mathbf{1a_1 2a_5 4a_1}$ and organohydrogel $\mathbf{1a_1 2a_5 4a_1}$ measured at a constant strain of 0.1% and frequency of 1 rad s^{-1}. (f) and (g) Frequency dependence of G' and G'' for organohydrogel $\mathbf{1a_1 2a_5 4a_1}$ before irradiation, after light irradiation (530 nm, 10 mW cm^{-2}, 20 min), and after being kept in the dark for 6 h at 25 °C (f) and -20 °C (g), respectively.

3.2.4 Photoinduced volume changes

Organohydrogels showed photoinduced volume changes in the H_2O/glycerol (v/v, 1/1) mixture. When disk-shaped organohydrogel **1a$_2$2a$_{10}$4a$_1$** was irradiated with light (530 nm, 10 mW cm^{-2}, 2 h) at 25 °C in the H_2O/glycerol (v/v, 1/1) mixture, its diameter increased to ~118% of the original diameter (Figure 5a). Light irradiation cleaved the Ru-thioether bonds and reduced the crosslinking density in the organohydrogel. Thus, the gel network expanded. The irradiated organohydrogel contracted to the original volume when it was kept in the dark for 6 h (Figure 5a). The volume change was reversible. Some interesting soft actuators,[20, 29, 30] which showed photoinduced volume changes at room temperature, have been reported. In contrast, our organohydrogel also showed photoinduced volume changes at -20 °C (Figure 5b). The diameter of the organohydrogel increased to ~105% of the original diameter after light irradiation (530 nm, 10 mW cm^{-2}, 3 h) and contracted to the original diameter after being kept in the dark for 6 h. The organohydrogel exhibited reversible volume changes even at -20 °C.

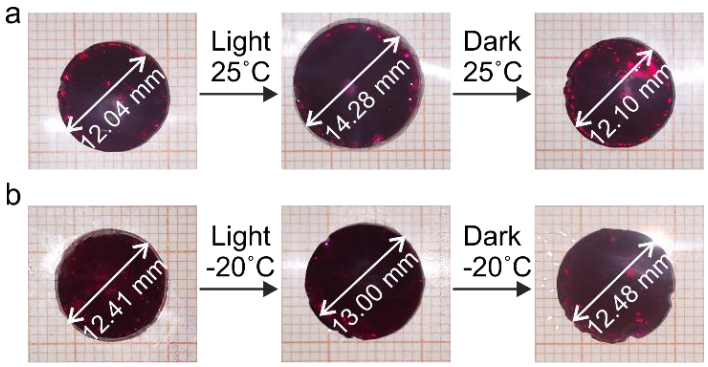

Figure 5. Photoinduced reversible volume changes of organohydrogel **1a$_2$2a$_{10}$4a$_1$**. Expansion and contraction of the organohydrogel under light irradiation and in the dark in the H_2O/glycerol (v/v, 1/1) mixture at 25 °C (a) and at -20 °C (b).

3.2.5 Rewritable and self-erasable photo-patterning

The reversible coordination of Ru-thioether not only results in changes in the crosslinking density but also results in colour changes (Figure 2g, h). Therefore, the organohydrogel is a suitable material for reversible photo-patterning (Figure 6). A piece of free-standing organohydrogel **1a$_2$2a$_{10}$4a$_1$** was prepared (Figure 6a). The organohydrogel was irradiated with light (530 nm, 10 mW cm^{-2}, 10 min) through a mask (Figure 6b, left). The colour of the exposed areas changed, and a pattern was generated (Figure 6c, d). The Ru moieties and thioether moieties coordinated spontaneously when the irradiated organohydrogel was kept in the dark.

The colour of the irradiated areas changed back, and the pattern was self- erased in the dark at room temperature (Figure 6b, right and Figure 6e).

Self-erasable gels were proposed for storing sensitive or temporary information, anti-counterfeiting, and encryption.[31, 32] The reported self-erasable gels work properly at room temperature. Self-erasable organohydrogel also worked at -20 °C. Therefore, an array was fabricated on the organohydrogel via light irradiation through Mask 2 at -20 °C (Figure 6f). The array self-erased when the organohydrogel was stored in the dark for 6 h. Different patterns were rewrote at -20 °C using different marks (Figure 6g-i). These results showed that our organohydrogel is a rewritable and self-erasable material at both room temperature and low temperatures, which expands the usage temperature of rewritable and self-erasable materials.

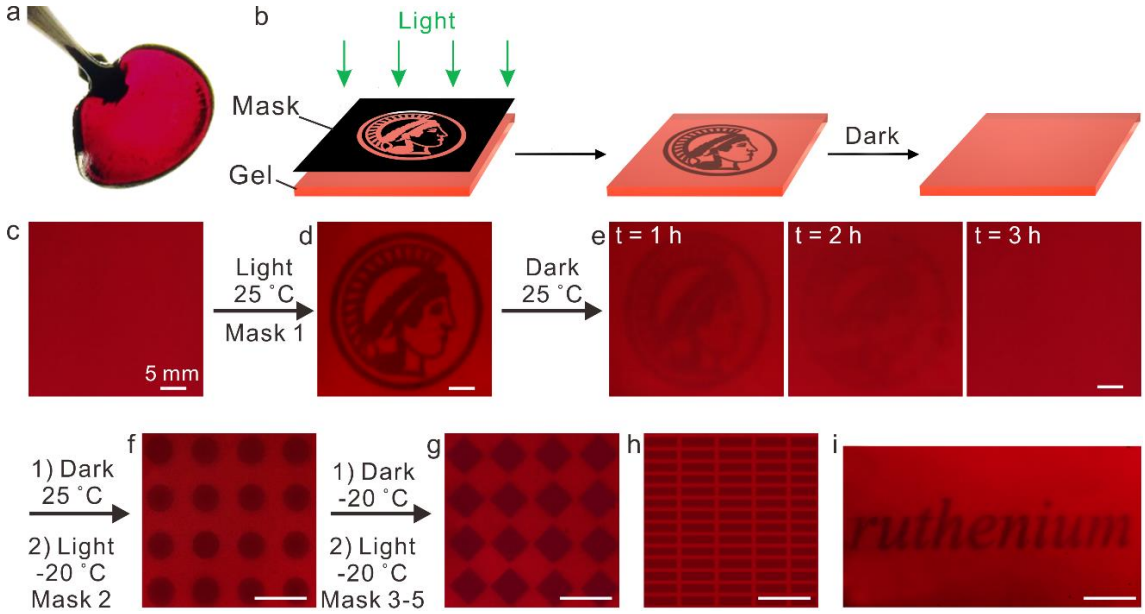

Figure 6. Preparation of self-erasing patterns on organohydrogels with light at 25 and -20 °C. (a) Photograph of freestanding organohydrogel **1a$_2$a$_{10}$4a$_1$**. (b) Schematic illustration of writing patterns on the organohydrogel and the self-erasing process in the dark. (c-i) Self-erasable and rewritable patterns fabricated on an organohydrogel using different photomasks and different temperatures.

3.3 Conclusions

In conclusion, this work have demonstrated that metallopolymer organohydrogels with photoresponsive Ru-thioether coordination crosslinks function properly even at -20 °C. The Ru-thioether coordination bond forms spontaneously in the dark and can be cleaved by light in H_2O/glycerol mixtures at -20 °C. The metallopolymer organohydrogels showed photo-triggered

reversible gel-to-sol transitions, photoinduced healing, photoswitchable mechanical properties, and photo-controlled volume changes and were applied for rewritable and self-erasable photopatterning at -20 °C. Photoresponsive metallopolymer organohydrogels are new materials with multiple functions and many potential applications in cold environments. Light can remotely and precisely control the properties of metallopolymer organohydrogels with high spatiotemporal resolution. We anticipate that the design principles can be applied to designing other materials that work in cold environments. This study opens up an avenue for remote control of soft matter below 0 °C, which is important for both the fundamentals of soft matter and their applications in cold environments.

3.4 Experimental section

3.4.1 Materials

$RuCl_3 \bullet xH_2O$ (99.9%), 2,2'-biquinoline (98%), magnesium sulfate (>98%), sodium chloride (>99%), trimethylamine (>99.5%), and sodium thiomethoxide (95%) were purchased from Fisher Scientific. 3-Amino-1-propanol (99%) and N,N'-methylenebisacrylamide (>99.5%) were purchased from Sigma-Aldrich. 2-[2-(2-Chloroethoxy) ethoxyl] ethanol (>96%), N-(2-hydroxyethyl)acrylamide (>98%), and 2,2'-azobis[2-(2-imidazolin-2-yl) propane] dihydrochloride (>98%) (VA-044) were purchased from TCI. 4'-Chloro-2,2',6',2''-terpyridine (>98%) was purchased from AEchem Scientific Corporation. 2,2':6',2''-Terpyridine (97%), acryloyl chloride (97%), and potassium hydroxide (98%) were purchased from Alfa Aesar. All solvents (HPLC grade) were purchased from Sigma-Aldrich or Fisher Scientific. N-(2-hydroxyethyl)acrylamide was purified by using basic aluminum oxide to remove 4-methoxyphenol before polymerization.

3.4.2 Instruments and characterization

^{1}H nuclear magnetic resonance (^{1}H NMR) and ^{13}C nuclear magnetic resonance (^{13}C NMR) spectra were recorded on a 300-MHz Bruker Spectrospin NMR spectrometer at 25 °C. ^{1}H COSY spectra were recorded on the same spectrometer. The molecular weights were determined using mass spectrometry (Bruker Time-of-flight MS Reflex III and Expression L Compact Mass Spectrometer). UV-vis absorption spectra were measured using a Lambda 900 spectrometer (Perkin Elmer). FTIR spectra were measured using a PerkinElmer FTIR System (Spectrum BX). Optical microscopy images were captured on an optical microscope (Zeiss) equipped with a CCD camera. Mechanical tensile test was performed using a Zwick/Roell

system with a deformation rate of 10 mm min^{-1}. Anti-freezing experiments of the solutions and gels were carried out at -20 ℃. The sample was cooled to -20 ℃ at a rate of 3 °C/min and kept at -20 ℃ for 20 min at the temperature-controlled stage (Linkam Scientific) before anti-freezing experiments. Rheological characterization was carried out on an Advanced Rheometric Expansion System (ARES, Rheometric Scientific Company) with a parallel plate (PP 20 mm) used to conduct oscillatory tests. Organohydrogels were prepared on a round plate with a diameter of 20 mm and a thickness of 2 mm. Before rheology measurements, organohydrogels were placed in the dark to reach equilibrium of the Ru-thioether crosslinks. Temperature sweep experiments were carried out by cooling the gels at a rate of 3 °C/min from 20 °C to -50 °C, and then keeping the gels at -50 °C for 10 min. After that, the gels were heated at the same rate from -50 °C to 80 °C. Meanwhile the viscoelastic moduli of both steps were monitored under small-amplitude oscillatory shear at an applied frequency of ω = 10 rad/s and strain amplitude of γ_0 = 0.1%. Frequency sweeps at -20 °C and 25 °C were carried out over a range of ω form 0.1 rad/s to 100 rad/s at the strain amplitude of γ_0 = 0.1%.

3.4.3 Synthesis and preparation

Synthesis of 1 ([Ru(tpy)(biq)(H_2O)]Cl_2)

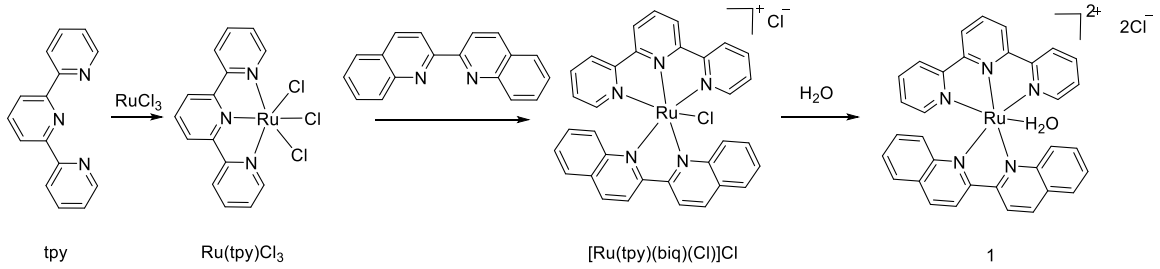

Figure S1. Synthetic route for compound **1** ([Ru(tpy)(biq)(H_2O)]Cl_2).

Synthesis of Ru(tpy)Cl_3: $RuCl_3 \cdot xH_2O$ (262 mg, 1.0 mmol) and 2,2':6',2''-terpyridine (tpy, 233.3 mg, 1.0 mmol) were dissolved in ethanol (50 mL). The mixture was heated at reflux for 4 h with magnetic stirring. Then, the mixture was cooled to room temperature. Brown powders were obtained and filtered from the reddish yellow solution. The brown powders were washed with ethanol and diethyl ether, and air-dried to obtain the compound Ru(tpy)Cl_3 as brown solid. Yield: 363 mg (82%).

Synthesis of [Ru(tpy)(biq)(Cl)]Cl: Ru(tpy)Cl_3 (171 mg, 0.39 mmol) and 2,2'-biquinoline (biq, 100 mg, 0.39 mmol) were mixed in a 3/1 ethanol/H_2O mixture (30 mL). The solution was degassed with argon for 5 min before it was heated to 85 °C under reflux for 24 h under argon. After that, the mixture was filtered hot and the filtrate was evaporated under reduced pressure to obtain the crude product. The product was purified by column chromatography with silica gel (eluent: methanol/dichloromethane = 1/15 to 1/8). The solvent was evaporated and the product was obtained as violet power. Yield: 190 mg (73.7%).

^{1}H NMR of [Ru(tpy)(biq)(Cl)]Cl (300 MHz, CD_3OD, 25 °C) δ (ppm): 9.66 (d, J = 7.7 Hz, 1H, H-B8), 8.96 (dd, J = 9.5, 8.5 Hz, 2H, H-B3,H-B4), 8.65 (m, 3H, H-B4, 2H-T3', A3), 8.49 (d, J = 8.8 Hz, 2H, H-T5), 8.22 (m, 3H, H-B5, 2H-T4', H-A4), 7.97-7.78 (m, 7H, 2H-T4, 2H-T2, H-A5, H-B6, H-B7), 7.44 (t, J = 8.5 Hz, 1H, H-A7), 7.32 (t, J = 8.5 Hz, 2H, H-T3), 7.21 (t, J = 9.0 Hz, 1H, H-A6), 6.82 (d, J = 8.7 Hz, 1H, H-A8).

^{13}C NMR of [Ru(tpy)(biq)(Cl)]Cl (75 MHz, CD_3OD, 25 °C) δ (ppm): 163.18 (B2), 160.64 (T6), 160.30 (T2'), 160.01 (A2), 153.82 (T2), 153.16+152.49 (8b, 8a), 139.78 (B4), 138.87 (T4), 137.75+136.90 (A4, T4'), 132.05 (B8), 131.85+131.80 (B6, A6), 130.79 (4b), 130.45 (A5, B7), 130.02 (B5), 129.97 (4a), 129.68 (A7), 128.40 (T3), 125+124.89 (T5, A8), 123.98 (T3') and 121.80+121.76 (A3, B3).

MALDI-TOF of [Ru(tpy)(biq)(Cl)]Cl: *m/z* calculated for $C_{32}H_{23}N_5ClRu$ ($[M\text{-}Cl]^+$): 626.07; found 626.06.

UV-vis of [Ru(tpy)(biq)(Cl)]Cl: The absorption maximum in acetone (0.2 mM) is at 585 nm, which is attributed to the metal-to-ligand charge transfer (MLCT) band of [Ru(tpy)(biq)(Cl)]Cl.

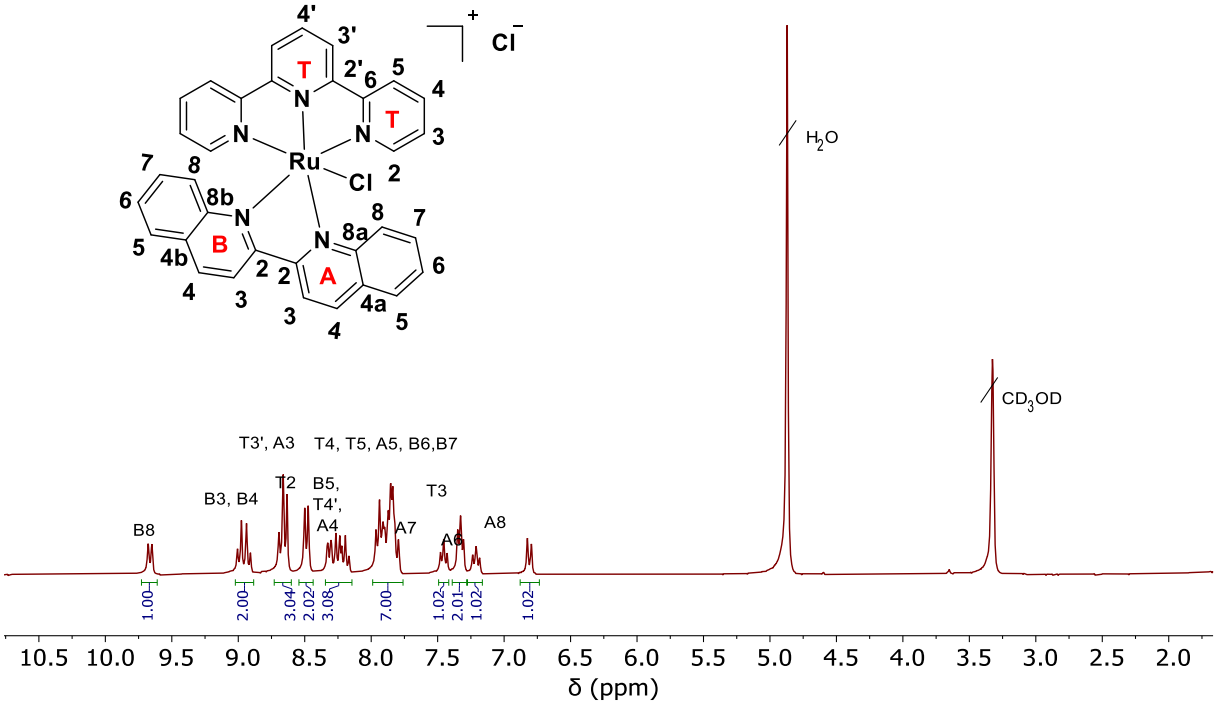

Figure S2. ^{1}H NMR spectrum of [Ru(tpy)(biq)(Cl)]Cl (300MHz, CD_3OD, 25°C).

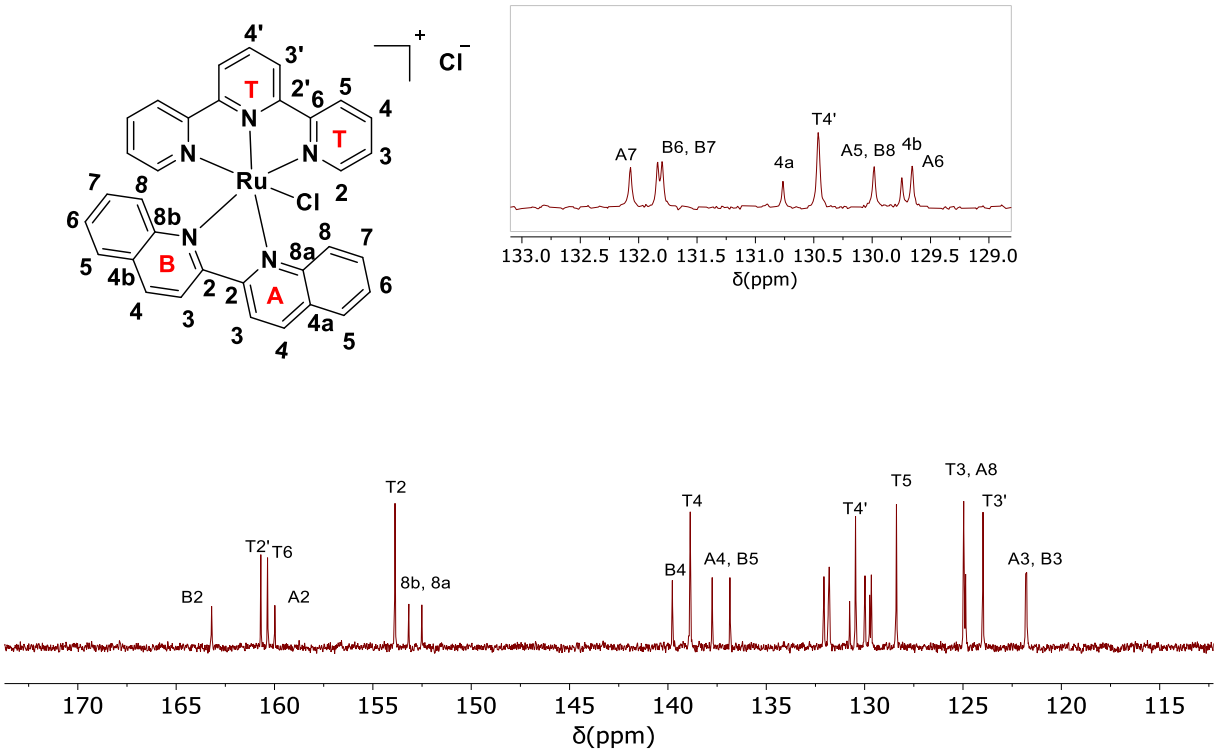

Figure S3. ^{13}C NMR spectrum of [Ru(tpy)(biq)(Cl)]Cl (75MHz, CD_3OD, 25°C). Inset shows enlarged spectrum from 129.00 ppm to 133.00 ppm.

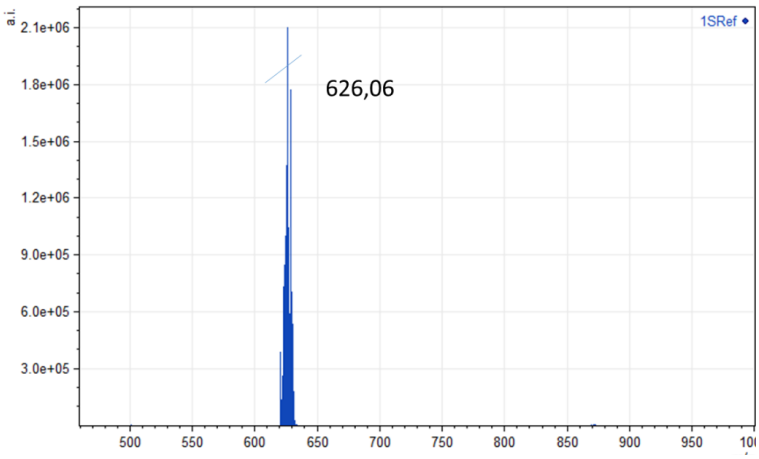

Figure S4. MALDI-TOF-MS spectrum of [Ru(tpy)(biq)(Cl)]Cl ([M-Cl]$^+$: found 626.06).

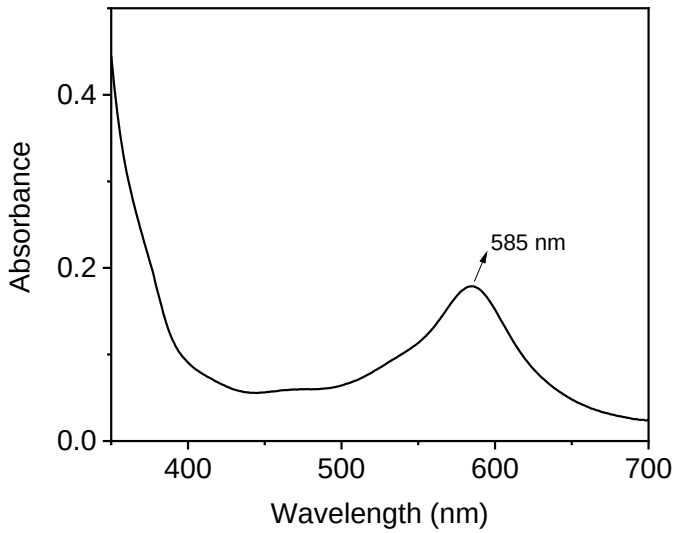

Figure S5. UV-vis absorption spectrum of [Ru(tpy)(biq)(Cl)]Cl in acetone (0.2 mM).

1 ([Ru(tpy)(biq)(H$_2$O)]Cl$_2$): 1 was prepared by hydrolysis of [Ru(tpy)(biq)(Cl)]Cl in water. The Ru-Cl coordination bond was unstable in aqueous solutions, which easily hydrolyzed into the aqua complex spontaneously and quantitatively.[33] Thus, **1** was obtained by dissolving [Ru(tpy)(biq)(Cl)]Cl in water. The Ru-Cl coordination bonds were completely hydrolyzed into the Ru-H$_2$O coordination bonds in 5 min. The obtained aqueous solution of **1** was used in the following experiments directly

^{1}H NMR of **1** (300 MHz, D$_2$O, 25 °C) δ (ppm): 8.85 (dd, J = 9.8, 9.9 Hz, 2H, H-B3, H-B4), 8.58-8.53 (m, 3H, H-B8, 2H-T3'), 8.34-8.13 (m, 5H, H-A3, H-B5, 2H-T5, H-T4'), 7.93 (d,

J=10 Hz, 1H, H-A4), 7.81 (m, 4H, 2H-T4, H-B6, H-B7), 7.50 (m, 3H, 2H-T2, H-A5), 7.18 (t, J = 8.0 Hz, 1H, H-A7),7.09 (m, 3H, 2H-T3, H-A6) 6.65 (d, J = 7.5 Hz, 1H, H-A8).

ESI of **1**: *m/z* calculated for $C_{32}H_{25}N_5ORu$ ($[M\text{-}Cl]^+$): 608.11; found 607.57.

UV-vis of **1**: The absorption maximum in water (0.68 mM) is at 549 nm, which is attributed to the metal-to-ligand charge transfer (MLCT) band of **1**.

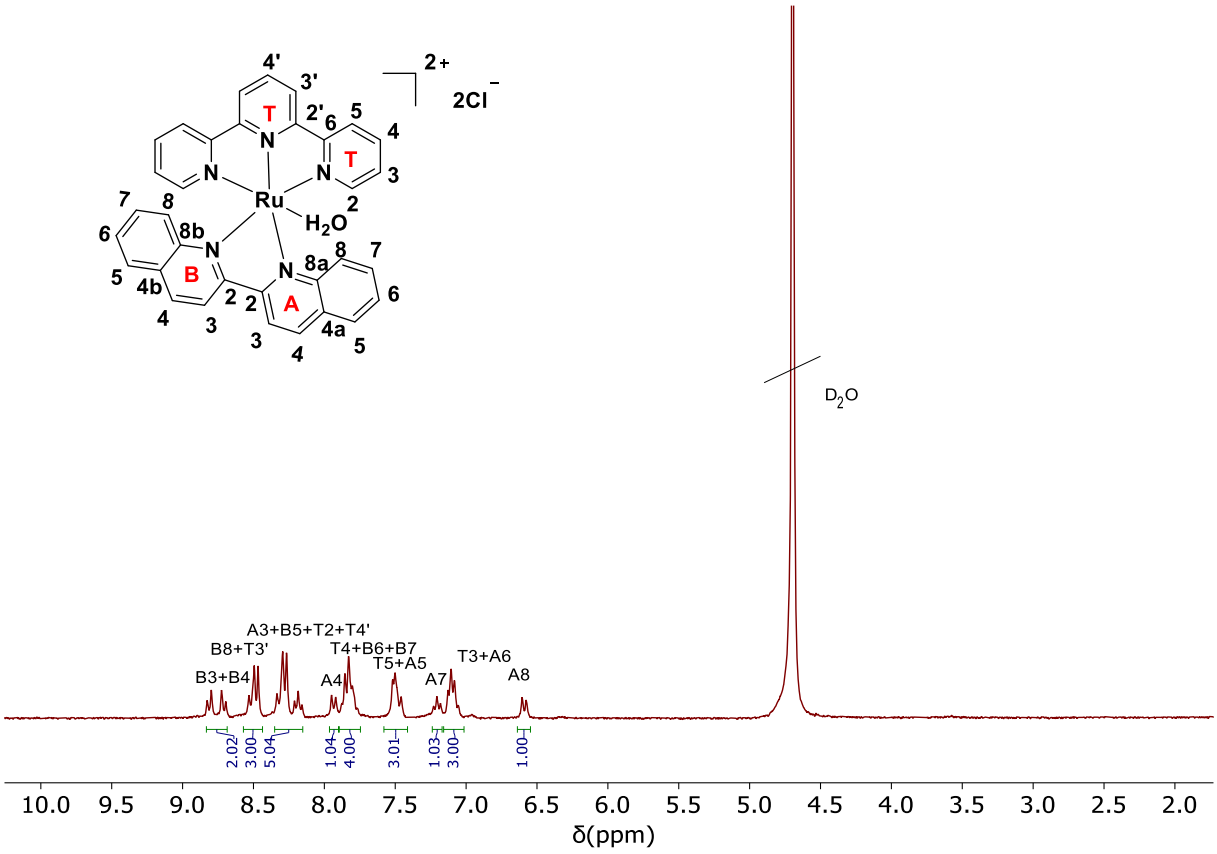

Figure S6. ^{1}H NMR spectrum of **1** (300MHz, D_2O, 25°C). [Ru(tpy)(biq)(Cl)]Cl in CD_3OD showed two characteristic peaks at 9.66 (B8) and 6.82 (A8) ppm. In pure D_2O, these two doublets totally shifted to 8.58 and 6.65 ppm respectively, which indicated that [Ru(tpy)(biq)Cl]Cl in water was completely hydrolyzed into **1**.

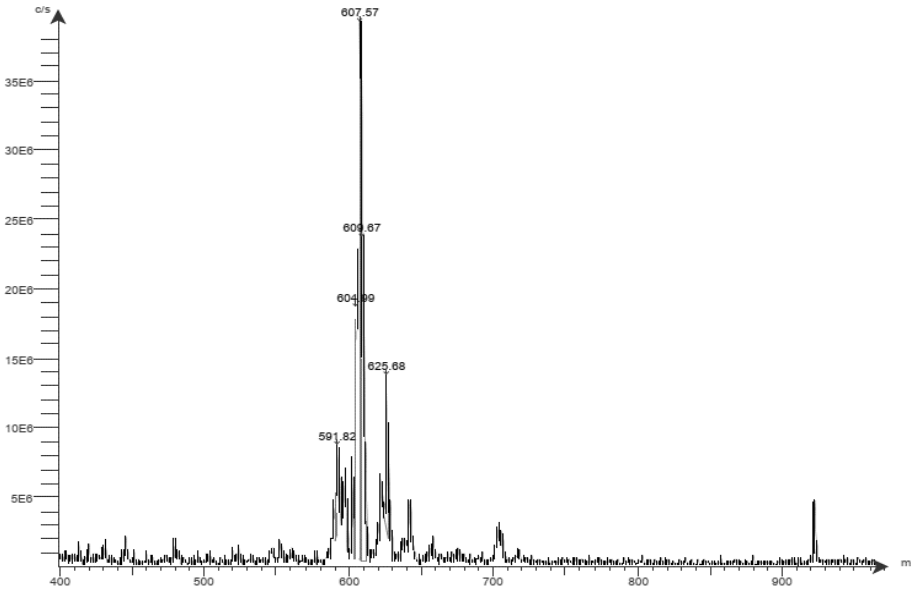

Figure S7. ESI spectrum of **1** ($[M-Cl]^+$: found 607.57).

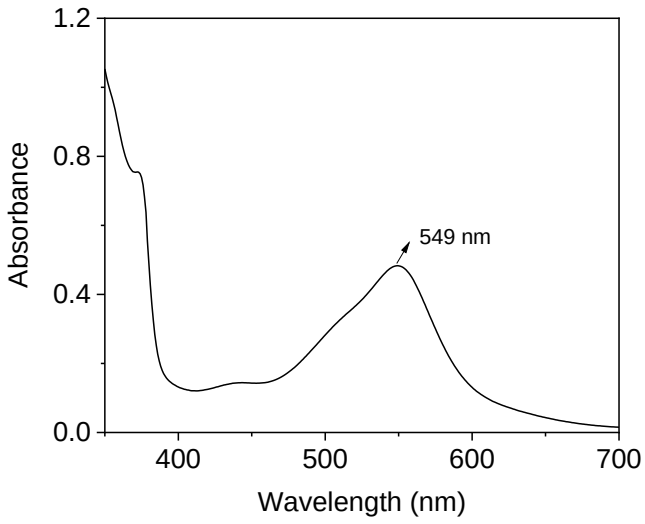

Figure S8. UV-vis absorption spectrum of **1** in water.

Synthesis of 2 (2-(2-(2-(methylthio)ethoxy)ethoxy)ethan-1-ol)

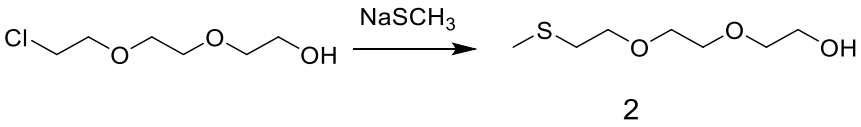

2

Figure S9. Synthetic route for compound **2**.

Synthesis of 2 (2-(2-(2-(methylthio)ethoxy)ethoxy)ethan-1-ol): Sodium thiomethoxide (2.25 g, 32 mmol) was added to 30 mL deionized water and stirred for 10 min. 2-[2-(2-chloroethoxy) ethoxyl] ethanol (3.02 g, 17.9 mmol) was added to the flask, the mixture was stirred for 2 days at room temperature. After the reaction, sodium chloride was added to the mixture of solution until saturation and then extracted with dichloromethane. The organic layer was dried with magnesium sulfate and concentrated under reduced pressure. The product was a colorless oil. Yield: 1.93 g (60%).

^{1}H NMR of **2** (300 MHz, D_2O, 25°C) δ (ppm): 3.65 (m, 10H, 2H-3, 2H-4, 2H-5, 2H-6, 2H-7), 2.71 (t, J = 6.4 Hz, 2H, H-2), 2.11 (S, 3H, H-1).

^{13}C NMR of **2** (75 MHz, D_2O, 25 °C) δ (ppm) (Figure S11): 71.78 (7), 69.52 (6), 69.50 (5), 69.47 (4), 69.12 (3), 32.61 (2) and 14.49 (1).

ESI of **2:** *m/z* calculated for $C_7H_{16}O_3SNa$ ($[M+Na]^+$): 203.08; found 203.00.

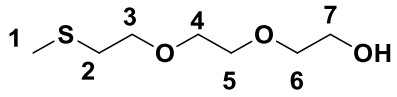

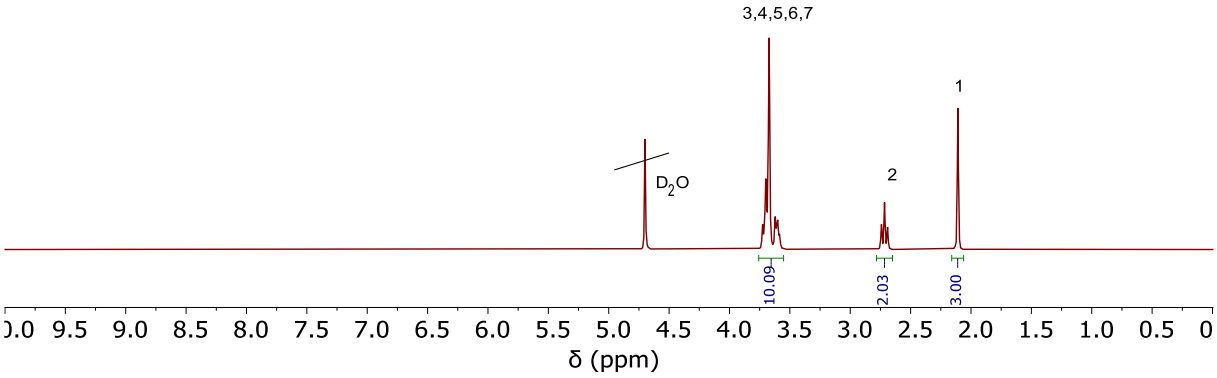

Figure S10. ^{1}H NMR spectrum of **2** (300MHz, D_2O, 25°C).

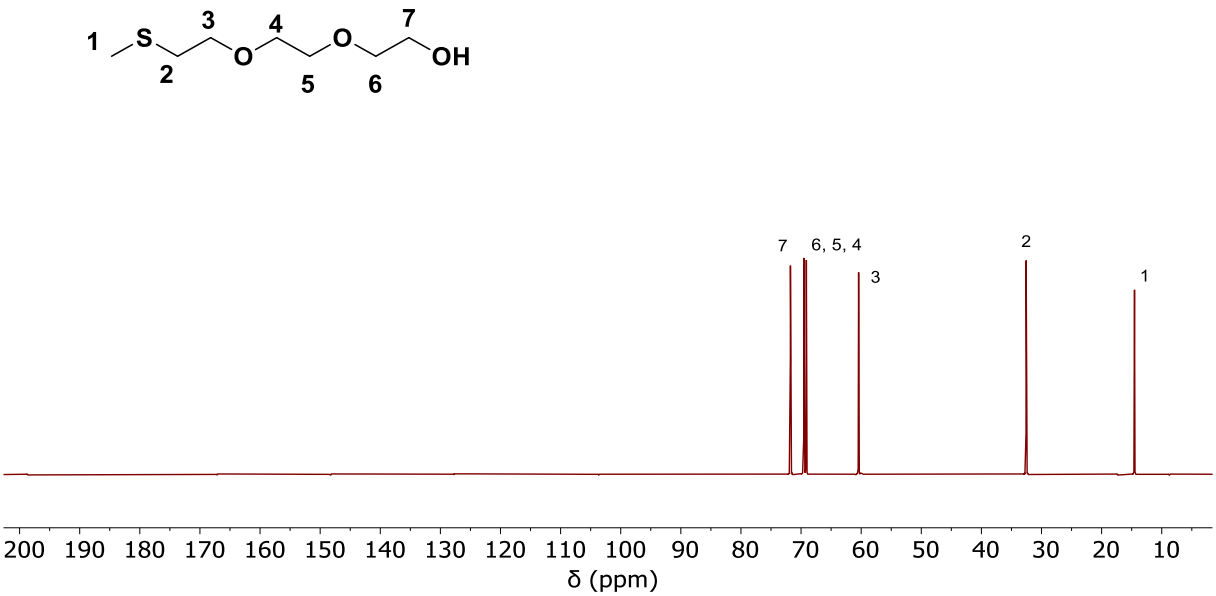

Figure S11. ^{13}C NMR spectrum of **2** (75MHz, D_2O, 25°C).

Synthesis of 1a

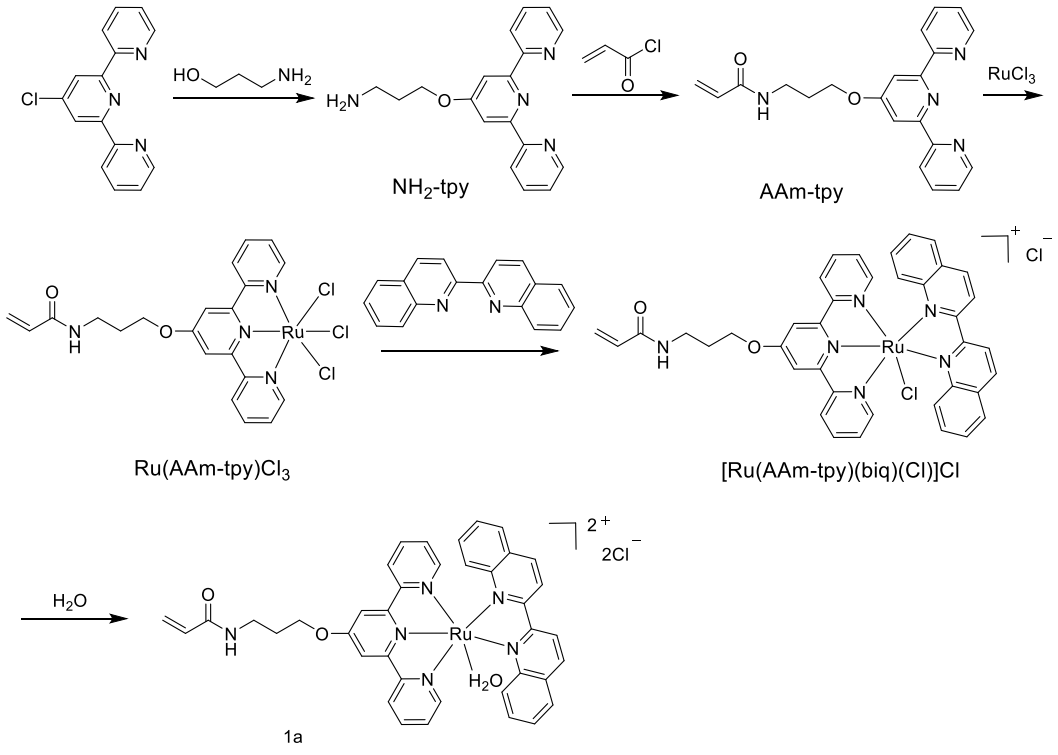

Figure S12. Synthetic route for compound **1a** ([Ru(AAm-tpy)(biq)(H_2O)]Cl_2).

Synthesis of 3-(2, 2': 6',2''-terpyridin-4'-yloxy) propylamine (NH_2-tpy): It was synthesized according to the literature.[34] Potassium hydroxide (392 mg, 7 mmol) was added to dimethylsulfoxide (20 mL) and heated to 65 °C under stirring. 3-Amino-1-propanol (555 mg, 7.4 mmol) was added dropwise into the solution. After 30 min, 4'-chloro-2,2,'6',2''-terpyridine (1000 mg, 3.7 mmol) was added into the solution. After stirring for 2 days at 65 °C, the reaction solution was cooled to room temperature and poured into 200 mL deionized water. The crude product was extracted with dichloromethane and dried with magnesium sulfate. After filtration and removal of the solvent in vacuum, the crude product was recrystallized from ethyl acetate to give the light yellow solid. Yield: 1900 mg (84%).

^{1}H NMR of NH_2-tpy (300 MHz, CD_2Cl_2, 25°C) δ (ppm): 8.70 (d, J = 5.4 Hz, 2H, H-2), 8.65 (d, J = 7.0 Hz, 2H, H-5), 8.06 (s, 2H, H-3'), 7.90 (t, J = 7.7 Hz, 2H, H-4), 7.37 (t, J = 7.7 Hz, 2H, H-3), 4.35 (t, J = 5.7 Hz, 2H, H-7), 2.95 (t, J = 8.0 Hz, 2H, H-9), 2.02 (m, 2H, H-8).

^{13}C NMR of NH_2-tpy (75 MHz, CD_3OD, 25°C) δ (ppm): 168.49 (4'), 158.32 (2'), 157.00 (6), 150.60 (2), 138.57 (4), 125.41 (3), 122.96 (5), 108.48 (3'), 67. 62 (7), 39.38 (9) and 32.44 (8).

MALDI-TOF of NH_2-tpy (Figure S15): *m/z* calculated for $C_{18}H_{18}N_4O$ ($[M]^+$): 306.37; found 306.96.

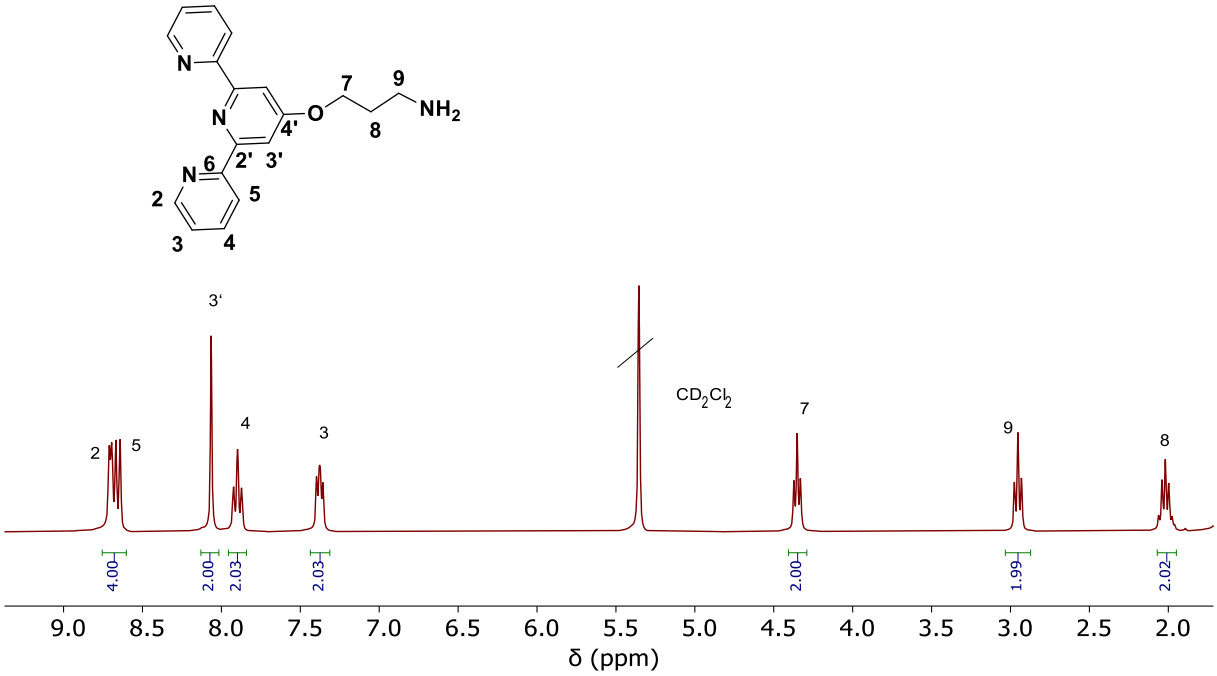

Figure S13. ^{1}H NMR spectrum of NH_2-tpy (300 MHz, CD_2Cl_2, 25°C).

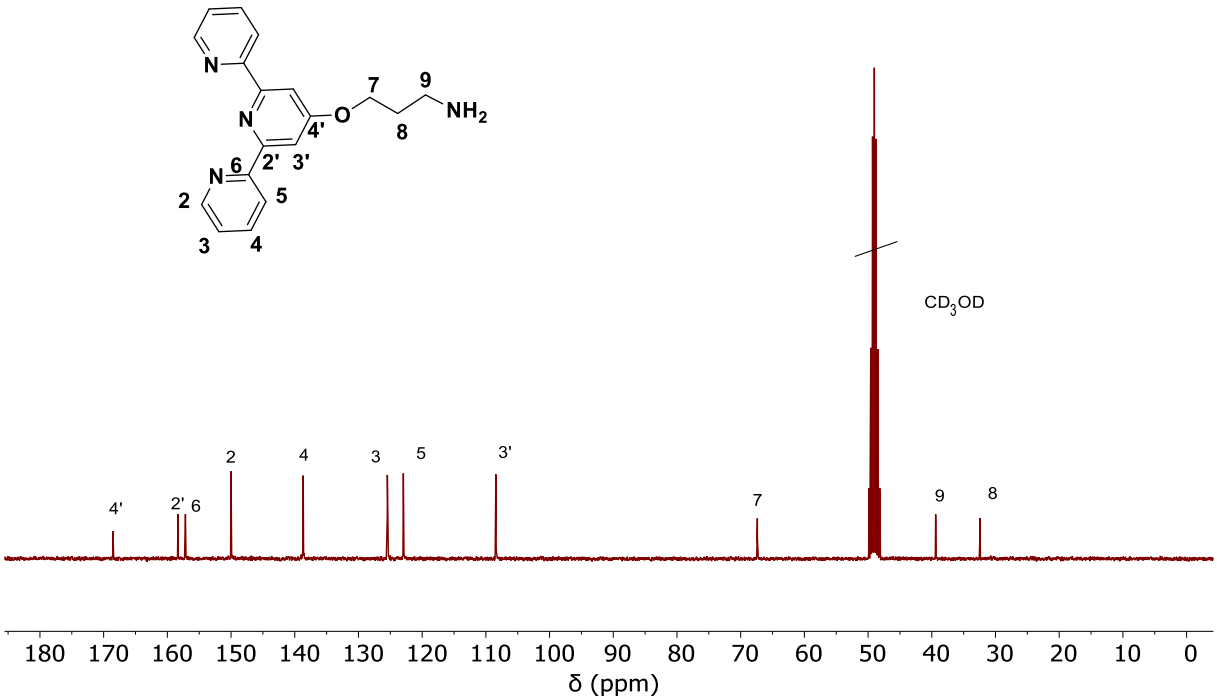

Figure S14. ^{13}C NMR spectrum of NH_2-tpy (75 MHz, CD_3OD, 25°C).

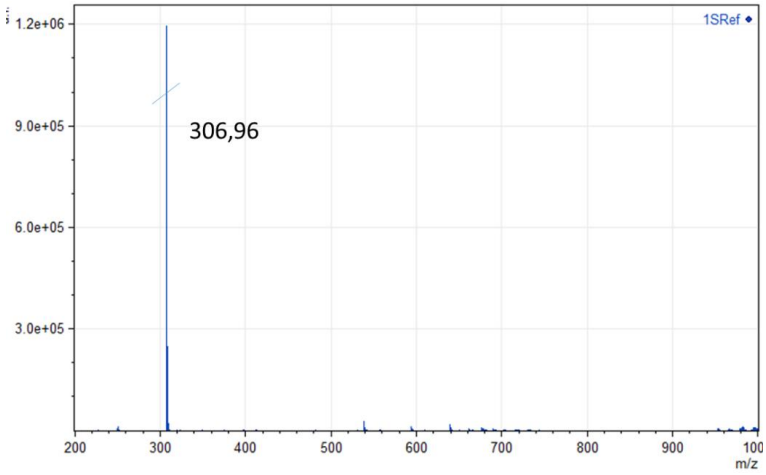

Figure S15. MALDI-TOF-MS spectrum of NH_2-tpy ($[M]^+$: found 306.96).

Synthesis of N-(3-([2,2':6',2''-terpyridin]-4'-yloxy)propyl)acrylamide (AAm-tpy) : NH_2-tpy (1360 mg, 4.7 mmol) was added to 40 mL tetrahydrofuran. Triethylamine (1.8 mL) was added into the mixture. Then, acryloyl chloride (607 mg, 6.71 mmol) was slowly added under argon at 0 ℃ after the mixture was stirred for 30 min. The reaction solution was stirred for 2 h at 0 °C and stirred for another 21 h at room temperature. After that, the solvent was removed in vacuum and the residue was dissolved in dichloromethane and washed with the water and saturated brine. The organic solution was dried with magnesium sulfate, filtered, and reduced in vacuum to give a crude solid. The crude solid was purified by column chromatography (Al_2O_3) using methanol/dichloromethane (1/40) as the eluent. The solvent was evaporated and the product was obtained as light yellow solid. Yield: 1293 mg (77%).

^{1}H NMR of AAm-tpy (300 MHz, CD_2Cl_2, 25°C) δ (ppm): 8.70 (d, J = 4.7Hz, 2H, H-2), 8.61 (d, J = 8.0 Hz, 2H, H-5), 8.02 (s, 2H, H-3'), 7.85 (t, J = 6.0Hz, 2H, H-4), 7.34 (t, J = 6.0Hz, 2H, H-3), 6.25 (m, 2H, H-11, H-12), 5.64 (dd, J = 11.5 Hz, 1H, H-12), 4.34 (t, J = 6.0 Hz, 2H, H-7), 3.05 (t, J = 6.75 Hz, 2H, H-9), 2.09 (m, 2H, H-8).

^{13}C NMR of AAm-tpy (75 MHz, CD_2Cl_2, 25°C) δ (ppm): 168.49 (4'), 167 (10), 158.32 (2'), 157.00 (6), 150.60 (2), 138.57 (4), 132 (11) , 127 (12), 125.41 (3), 122.96 (5), 108.48 (3'), 67 (7), 39.38 (9) and 32.44 (8).

MALDI-TOF of AAm-tpy: *m/z* calculated for $C_{21}H_{20}N_4O_2$ ($[M]^+$): 360.42; found 360.83.

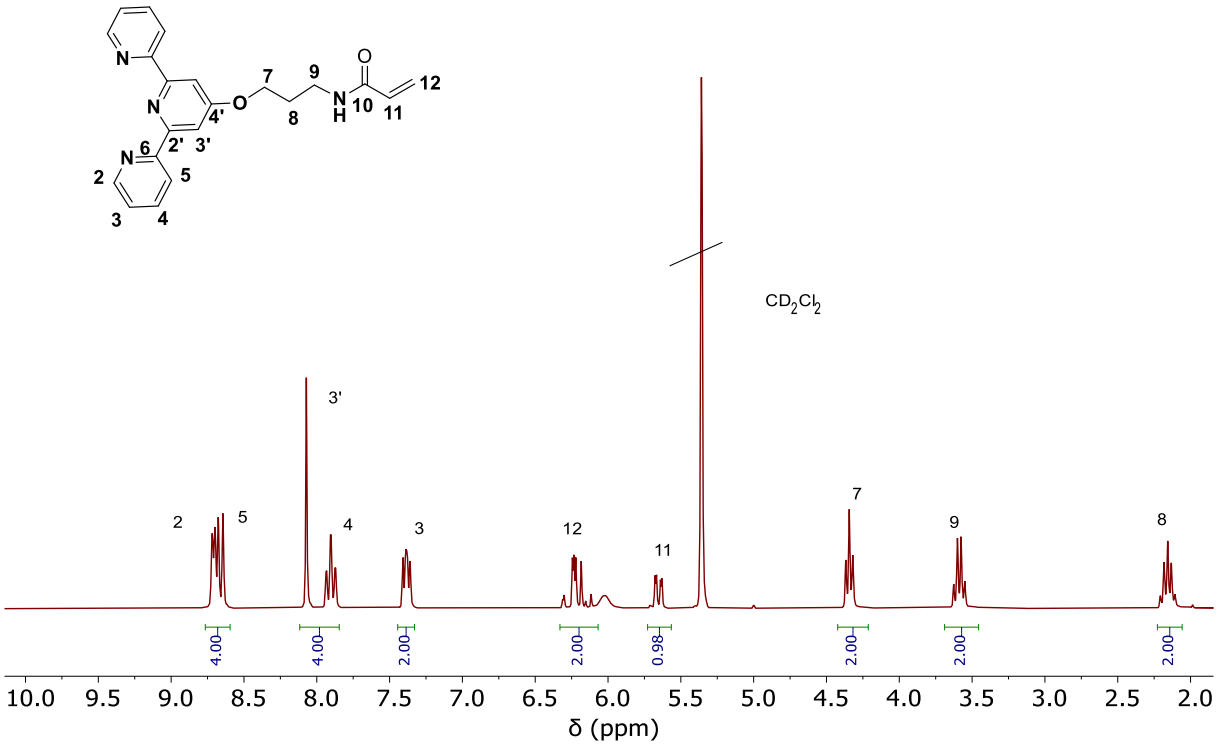

Figure S16. ^{1}H NMR spectrum of AAm-tpy (300 MHz, CD_2Cl_2, 25°C).

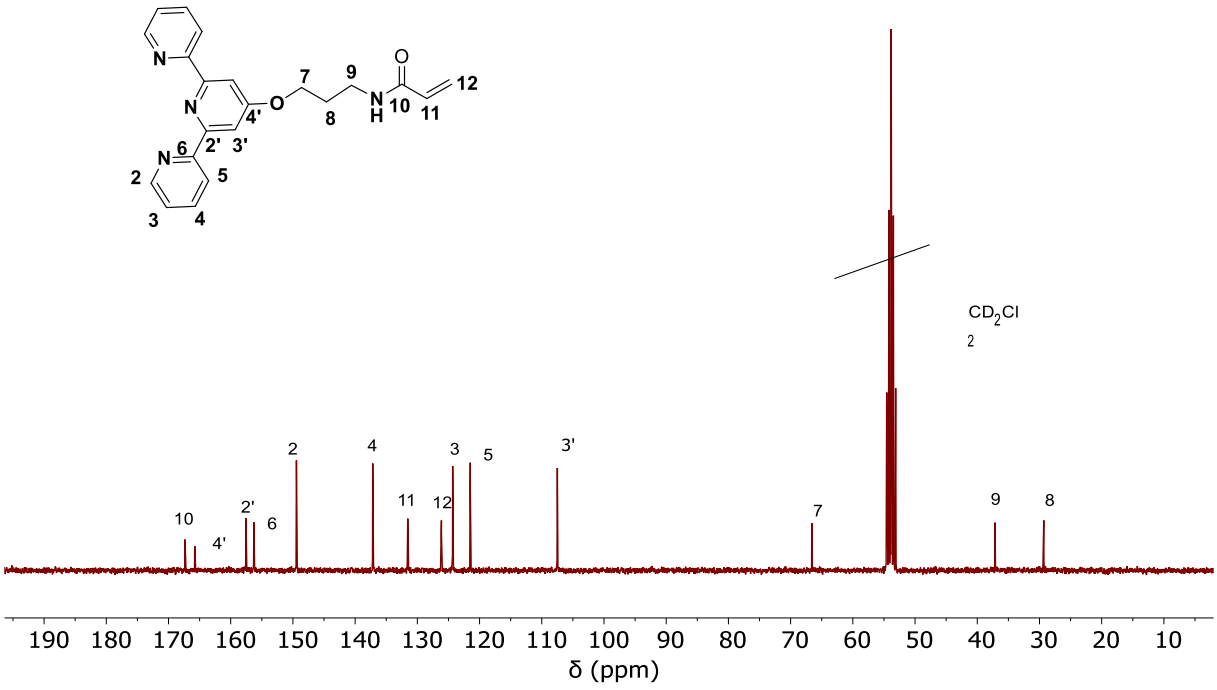

Figure S17. ^{13}C NMR spectrum of AAm-tpy (75 MHz, CD_2Cl_2, 25°C).

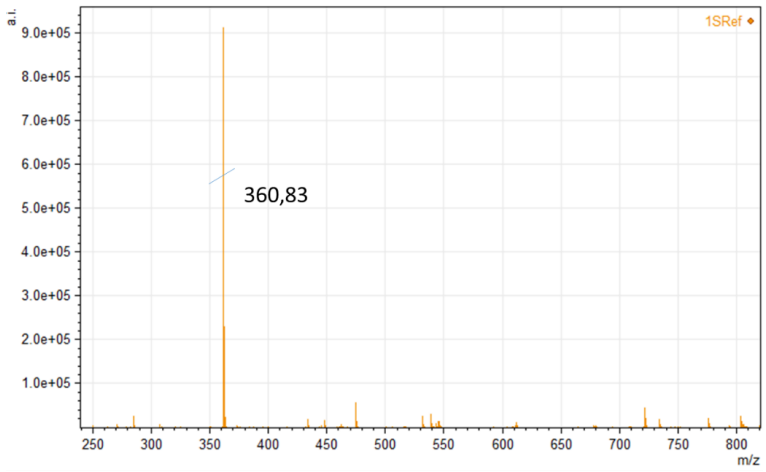

Figure S18. MALDI-TOF-MS spectrum of AAm-tpy ($[M]^+$: found 360.83).

Synthesis of Ru(AAm-tpy)Cl$_3$: $RuCl_3 \bullet xH_2O$ (262 mg, 1 mmol) and AAm-tpy (359.4 mg, 1 mmol) were mixed in ethanol (60 mL). The mixture was heated at reflux for 4 h. After cooling to room temperature, the mixture was filtered. The filtered brown powder was washed with ethanol and diethyl ether sequentially to obtain the product. Yield: 462 mg (94%).

Synthesis of [Ru(AAm-tpy)(biq)(Cl)]Cl: Ru(AAm-tpy)Cl_3 (221 mg, 0.39 mmol) and 2,2'-biquinoline (biq, 100 mg, 0.39 mmol) were mixed in a 1/1 ethanol/H_2O mixture (30 mL). The solution was degassedwith argon for 5 min and then the reaction mixture was refluxed under argon for 1 day in the dark. After that, the mixture was filtered hot. The product was collected by evaporation under reduced pressure and purified by column chromatography with silica gel (eluent: methanol/dichloromethane = 1/10 to 1/6). Yield: 180 mg (59%).

^{1}H NMR of [Ru(AAm-tpy)(biq)(Cl)]Cl (300 MHz, CD_3OD, 25°C) δ (ppm): 9.63 (d, J = 7.0 Hz, 1H, H-B8), 8.92 (dd, J = 9.0, 8.0 Hz, 2H, H-B3, H-B4), 8.66 (d, J = 9.0 Hz, 1H, H-A3), 8.49 (d, J = 9.0 Hz, 2H, H-T5), 8.31-8.23 (m, 4H, 2H-T3', H-B5, H-A4), 7.93-7.86 (m, 7H, 2H-T4, H-A5, 2H-T2, H-B7, H-B6), 7.46 (t, J = 7.0 Hz, 1H, H-A7), 7.29 (m, 3H, 2H-T3, H-A6), 6.88 (d, J = 9.0 Hz, 1H, H-A8), 6.29 (m, 2H, H-13, H-14), 5.70 (d, J = 5.0 Hz, 1H, H-14), 4.53 (t, J = 7.0 Hz, 2H, H-9), 3.61 (m, 2H, H-11), 2.24 (m, 2H, H-10).

^{13}C NMR of [Ru(AAm-tpy)(biq)(Cl)]Cl (75 MHz, CD_3OD, 25°C) δ (ppm): 168.38 (12), 167.89 (T4'), 163.43 (B2), 160.85 (T6), 160.55 (T2'), 160.27 (A2), 154.04 (T2), 153.39+152.74 (8b, 8a), 139.23 (B4), 138.71 (T4), 137.37 (A4), 132.13 (13), 132.01 (B8), 131.8+131.27 (B6, A6),

130.62 (4b), 130.43+130.37 (B7, A5), 129.96 (B5), 129.70 (4a), 129.60 (A7), 128.26 (T3), 126.85 (14), 125.12+125.10 (T5, A8), 121.78 (A3, B3), 111.56 (T3'), 68.83 (9), 37.26 (11) and 29.98 (10).

MALDI-TOF of [Ru(AAm-tpy)(biq)(Cl)]Cl: *m/z* calculated for $C_{39}H_{31}ClN_6O_2Ru$ ($[M-Cl]^+$): 753.13; found 752.84.

UV-vis of [Ru(AAm-tpy)(biq)(Cl)]Cl: The maximum absorption in acetone (0.48 mM) is at 585 nm, which is attributed to the metal-to-ligand charge transfer (MLCT) band of [Ru(AAm-tpy)(biq)(Cl)]Cl.

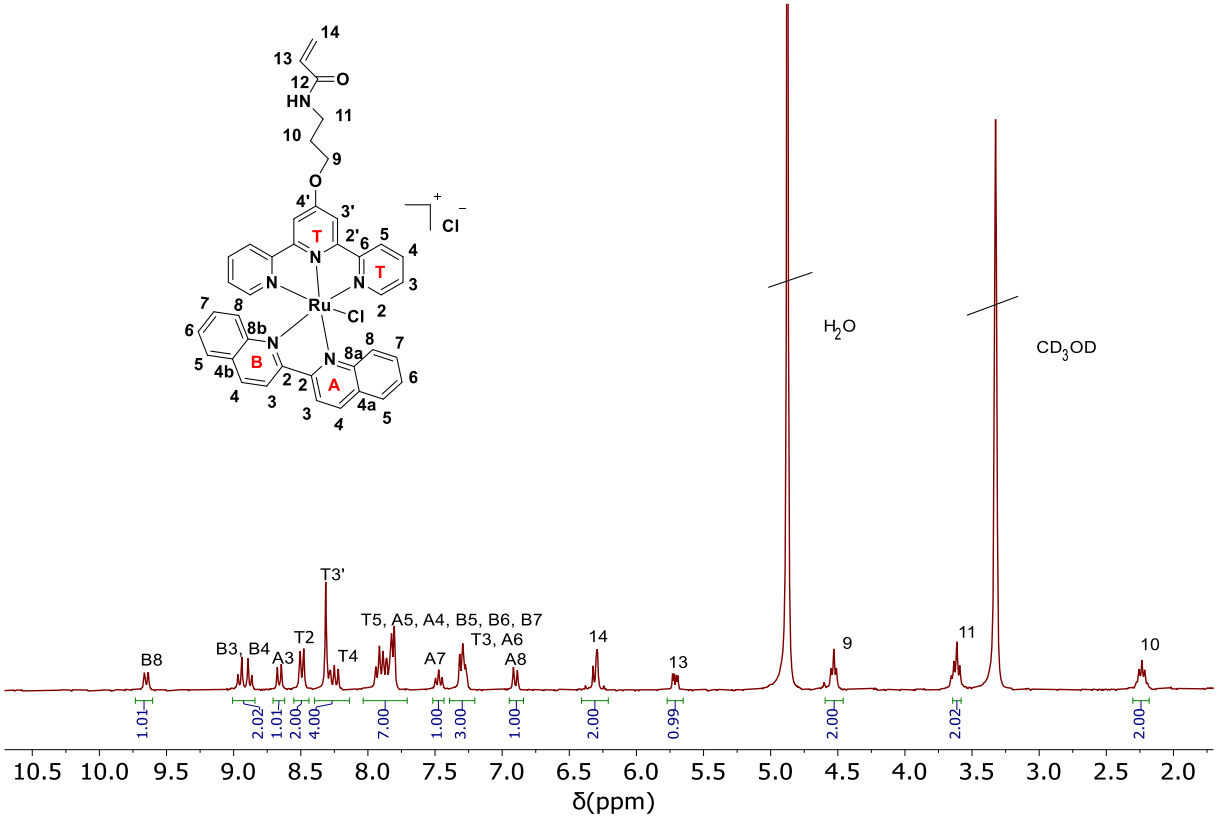

Figure S19. ^{1}H NMR spectrum of [Ru(AAm-tpy)(biq)(Cl)]Cl (300 MHz, CD_3OD, 25°C).

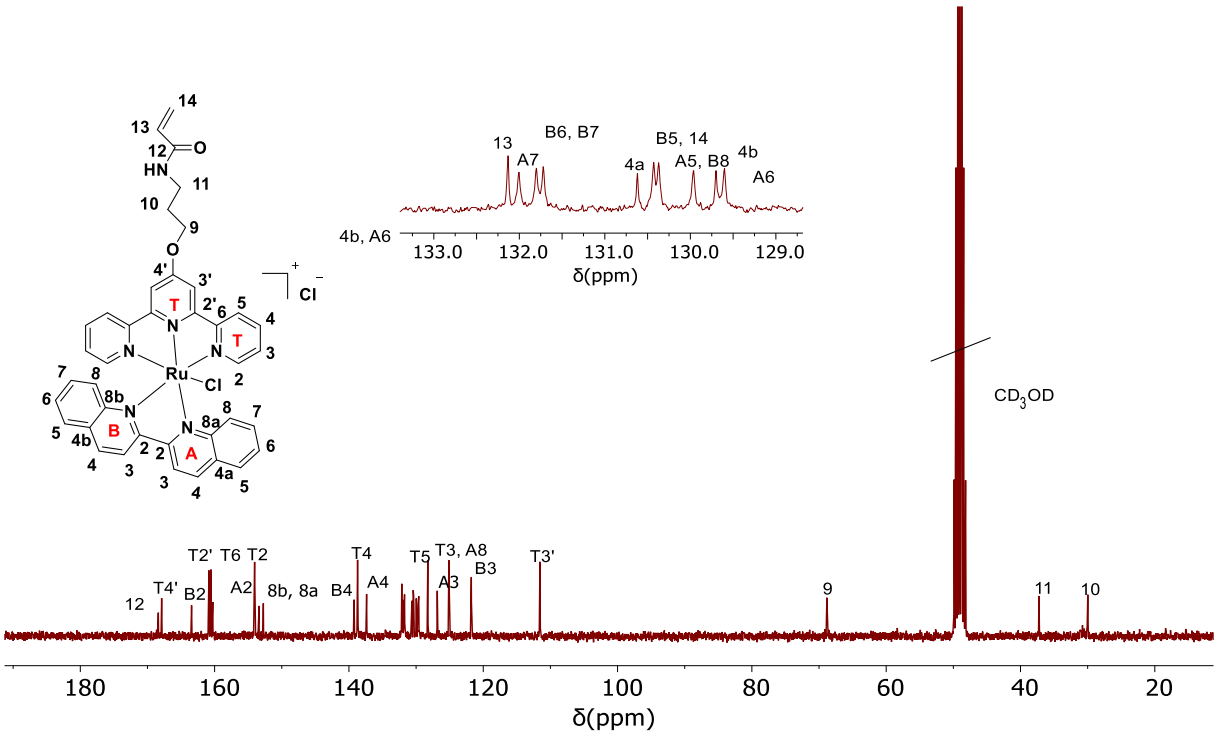

Figure S20. ^{13}C NMR spectrum of [Ru(AAm-tpy)(biq)(Cl)]Cl (75 MHz, CD_3OD, 25°C). Inset shows enlarged spectrum from 128.75 ppm to 133.25 ppm.

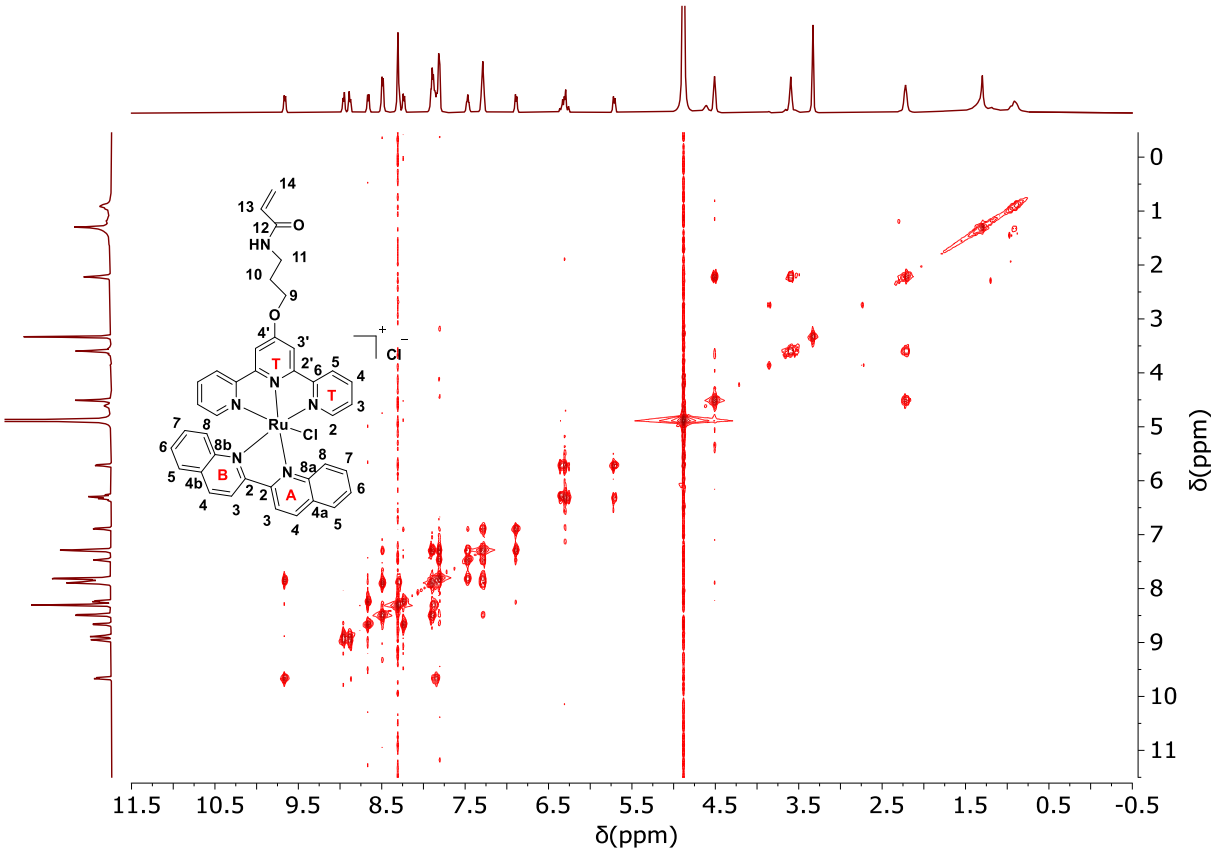

Figure S21. H-H COSY spectrum of [Ru(AAm-tpy)(biq)(Cl)]Cl (300 MHz, CD_3OD, 25°C).

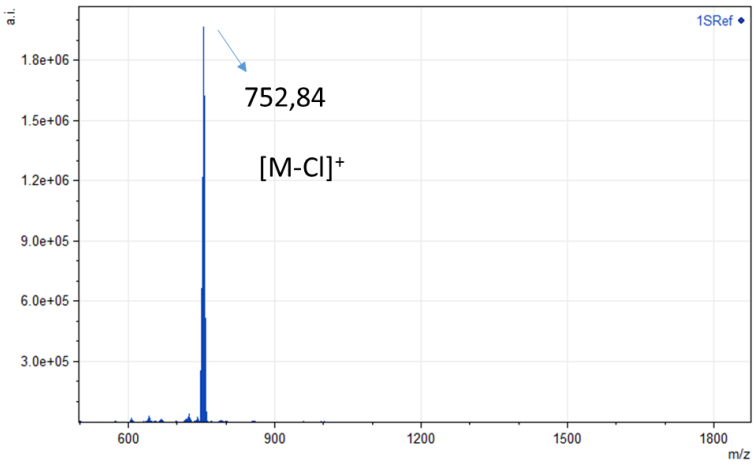

Figure S22. MALDI-TOF-MS spectrum of [Ru(AAm-tpy)(biq)(Cl)]Cl ($[M-Cl]^+$: found 752.84).

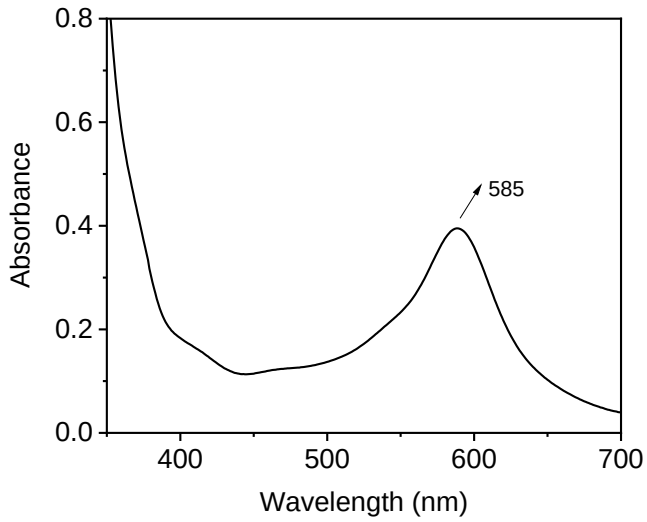

Figure S23. UV-vis absorption spectrum of [Ru(AAm-tpy)(biq)(Cl)]Cl in acetone (0.48 mM).

Synthesis of 1a: **1a** was prepared by using the same preparation method of **1**. The obtained aqueous solution of **1a** was used for polymerization directly.

^{1}H NMR of **1a** (300 MHz, CD_3OD, 25 °C) δ (ppm): 8.75 (dd, J = 6.4, 8.5 Hz, 2H, H-B3, H-B4), 8.57 (d, J = 8.5 Hz, 1H, H-B8), 8.37-8.23 (m, 4H, H-A3, 2H-T5, H-B5), 8.09 (s, 2H, H-T3'), 8.00-7.80 (m, 5H,H-A4, 2H-T4, H-B6, H-B7), 7.54 (m, 3H, 2H-T2, H-A5), 7.26 (t, J = 9.3 Hz, 1H, H-A7), 7.14 (m, 3H, 2H-T3, H-A6), 6.68 (d, J = 11.5 Hz, 1H, H-A8), 6.26 (m, 1H,

H-13), 6.06 (d, J = 15, 1H, H-14). 5.65 (d, J = 13.5 Hz, 1H, H-14), 4.50 (t, J = 8.5 Hz, 2H, H-9), 3.65 (t, J=9.0 Hz, 2H, H-11), 2.17 (m, 2H, H-10).

ESI of **1a**: *m/z* calculated for $C_{39}H_{33}N_6O_3Ru$ ($[M-Cl]^+$): 735.81; found 734.34.

UV-vis of **1a**: The maximum absorption in water (0.68 mM) is at 553 nm, which is attributed to the metal-to-ligand charge transfer (MLCT) band of **1a**.

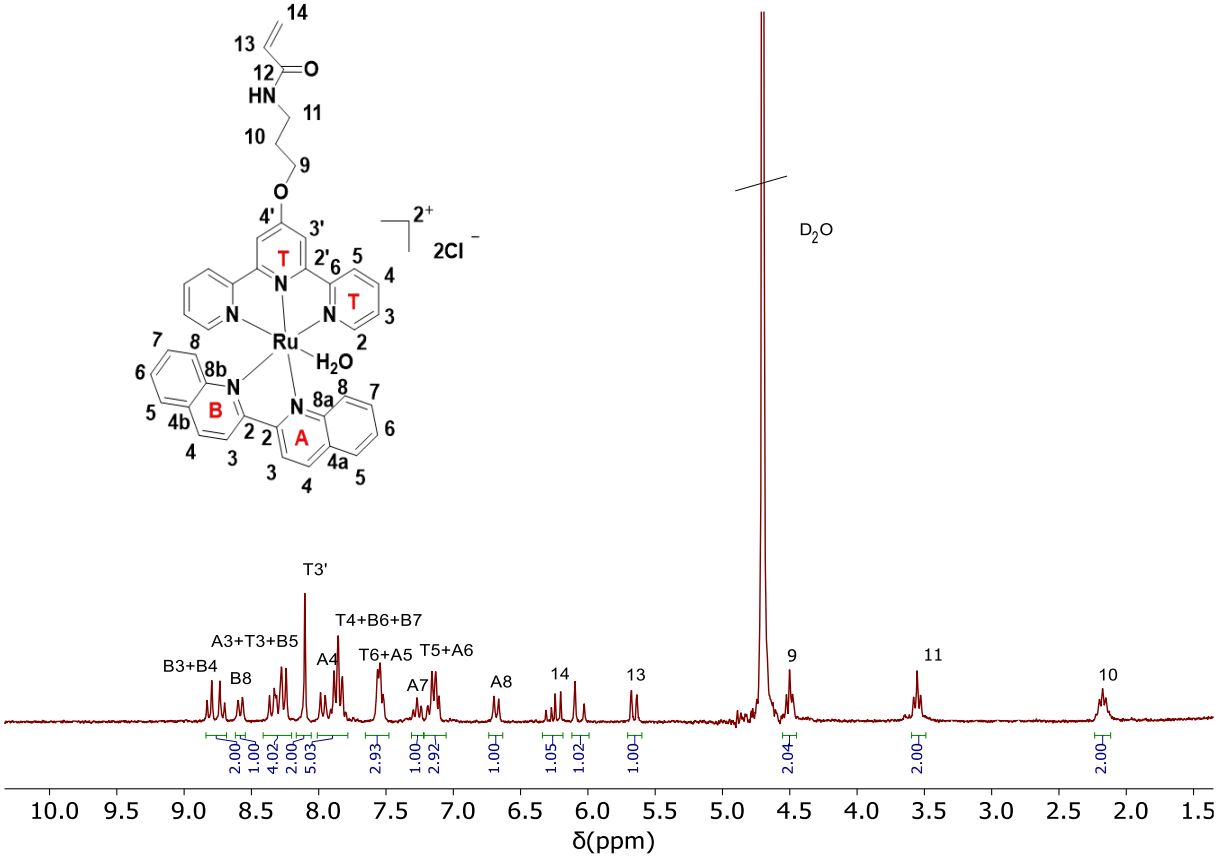

Figure S24. ^{1}H NMR spectrum of **1a** (300 MHz, D_2O, 25°C). [Ru(AAm-tpy)(biq)(Cl)]Cl in CD_3OD showed two characteristic peaks at 9.65 (B8) and 6.88 (A8) ppm (Fig. 25). In pure D_2O, these two doublets totally shifted to 8.75 and 6.68 ppm respectively, which indicated that Ru(AAm-tpy)(biq)(Cl)]Cl in water was completely hydrolyzed into **1a**.

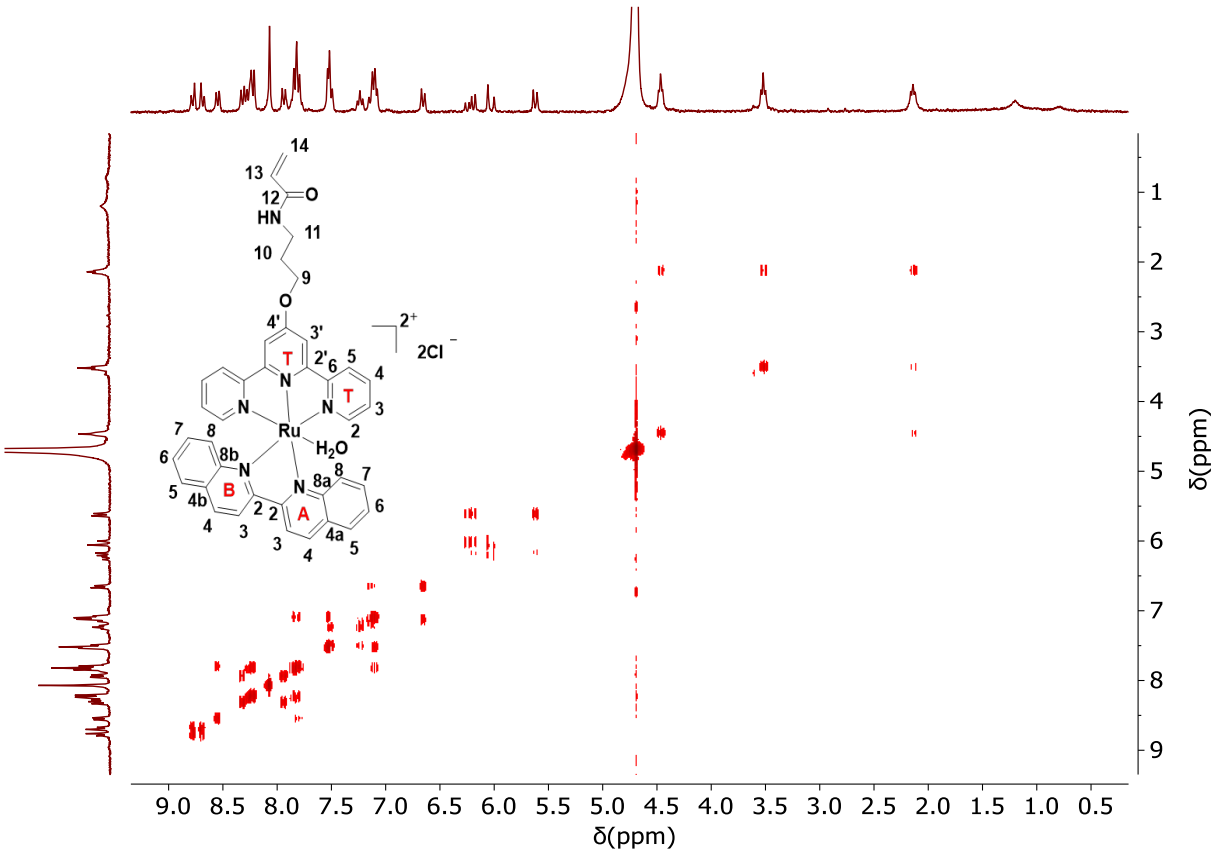

Figure S25. H-H COSY spectrum of **1a** (300 MHz, D_2O, 25°C).

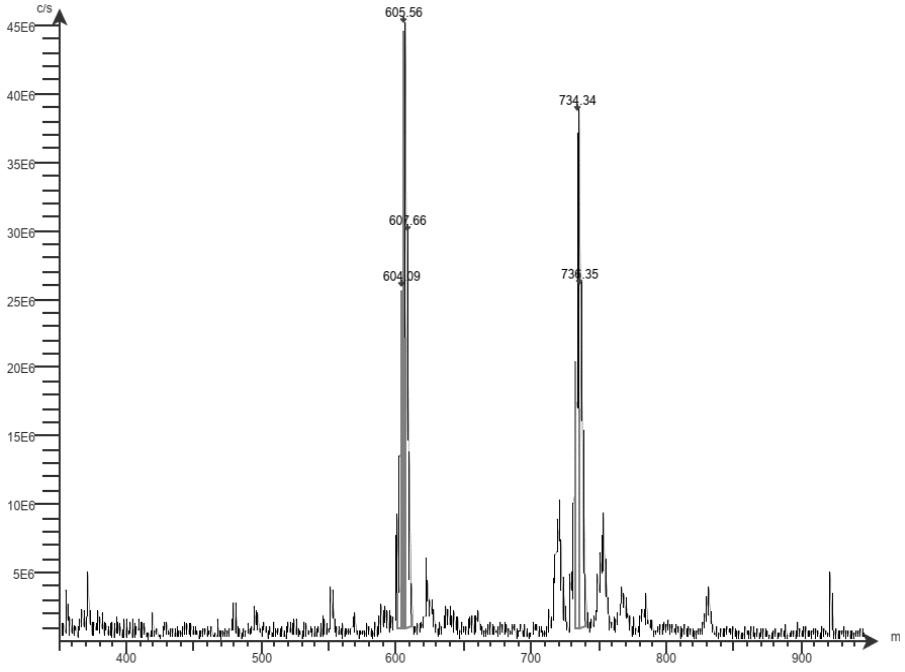

Figure S26. ESI spectrum of **1a** ($[M\text{-}Cl]^+$: found 734.34).

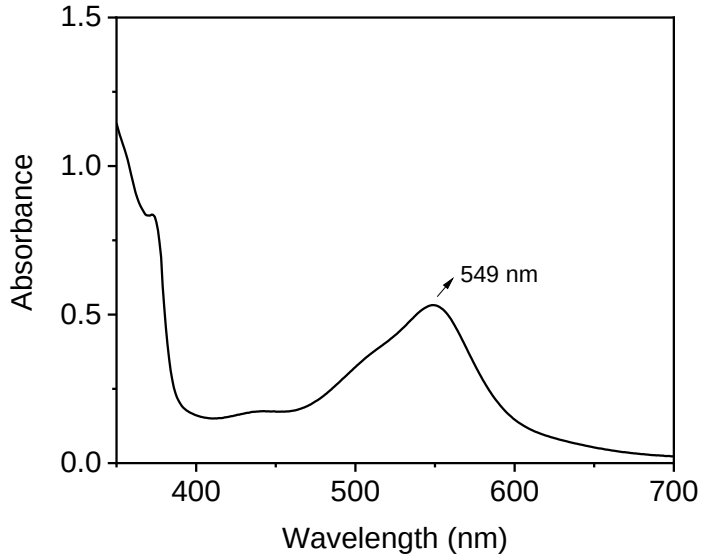

Figure S27. UV-vis spectrum of **1a** in water (0.68 mM).

Synthesis of 2a (2-(2-(2-(methylthio)ethoxy)ethoxy)ethyl acrylate)

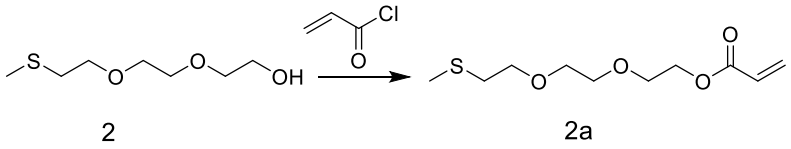

Figure S28. Synthetic route for compound **2a**.

Synthesis of 2a: 2-(2-(2-(methylthio)ethoxy)ethoxy)ethan-1-ol (788.9 mg, 4.38 mmol) and triethylamine (531.85 mg, 5.26 mmol, 1.73 mL) were added to dichloromethane and stirred for 10 min under room temperature. Acryloyl chloride (475.6 mg, 5.26 mmol, 0.43 mL) was then added dropwisely under argon at 0 ℃ for 60 min and then at room temperature overnight. After that, the mixture solvent was washed by saturated brine for three times, and then extracted with dichloromethane. The organic layer was dried with magnesium sulfate and concentrated under reduced pressure. The product was a colorless oil. Yield: 513 mg (50%).

^{1}HNMR of **2a** (300 MHz, $CDCl_3$, 25°C) δ (ppm): 6.42(d, J = 16Hz, 1H, H-10), 6.10 (m, 1H, H-9), 5.76 (d, J = 12Hz, 1H, H-10), 4.25 (t, J = 5Hz, 2H, H-7), 3.63 (m, 8H, 2H-6,2H-5, 2H-4, 2H-3), 2.63 (t, J = 6.5 Hz, 2H, H-2), 2.07 (S, 3H, H-1).

^{13}C NMR of **2a** (75MHz, D_2O, 25°C) δ (ppm): 168.42 (8), 132.50 (9), 127.28 (10), 69.62 (7), 69.22 (6), 69.00 (5), 68.40 (4), 63.88 (3), 32.50 (2) and 14.37 (1).

ESI of **2a**: *m/z* calculated for $C_{10}H_{18}O_4SNa$ ($[M+Na]^+$): 257.31, found 257.50.

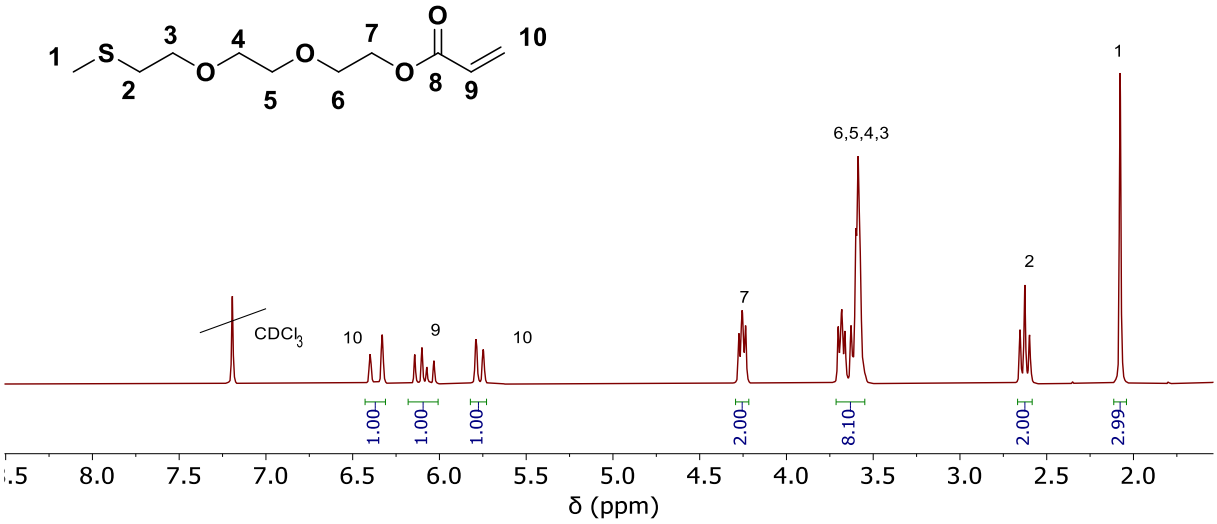

Figure S29. ^{1}H NMR spectrum of **2a** (300 MHz, $CDCl_3$, 25°C).

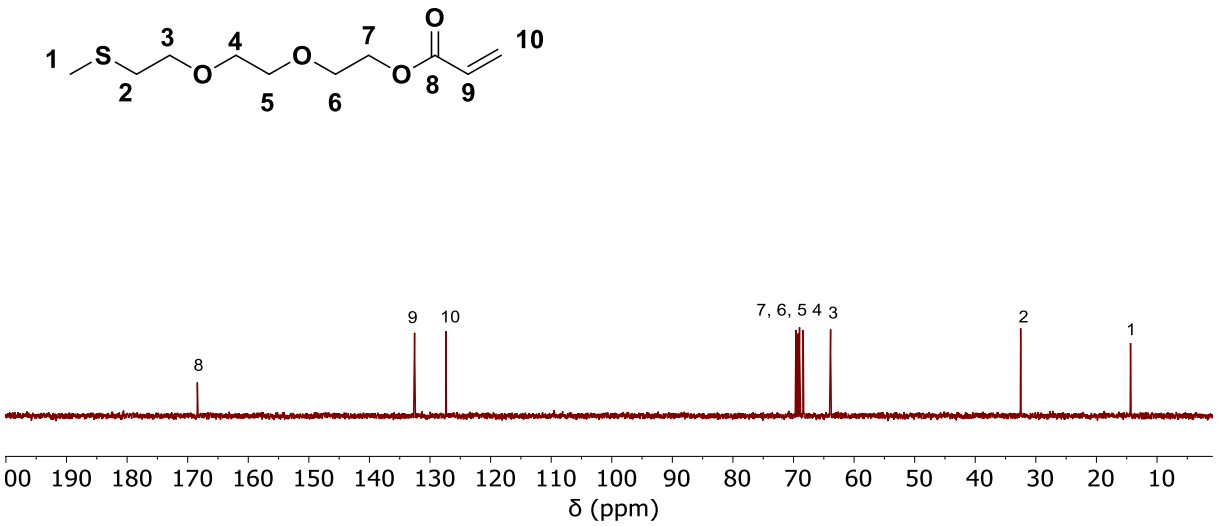

Figure S30. ^{13}C NMR spectrum of **2a** (75MHz, D_2O, 25°C).

Preparation of $1a_x2a_y$ organohydrogels

We use **$1a_1$2a_5** as an example to show the typical process. **2a** (10.5 mg, 0.045 mmol) in glycerol (0.5 mL) was mixed with **1a** (7.1 mg, 0.009 mol) in H_2O (0.5 mL). The mixture was placed in the dark overnight for the formation of Ru-thioether coordination bonds. Then, **4** (97 mg, 0.84 mmol) and 2,2'-azobis[2-(2-imidazolin-2-yl) propane] dihydrochloride (VA-044, 2.9 mg, 0.009 mmol) were added to the mixture. VA-044 was used as the initiator because of its good water solubility. The volume ratio of monomers and the solvent was 9.6 : 100. Polymerization was conducted by sealing the mixture and heating at 50 °C for 12 h after purging with nitrogen for 30 min. An organohydrogel was obtained by cooling the mixture to room temperature.

Table S1. Chemical compositions of **$1a_x2a_y$** organohydrogels. The samples were examined by an inverted-vial test.

Concentration of monomers (mol/L)	Molar ratio of compound **1a**, **2a** and **4** in gels (**1a**:**2a**:**4**)					
	$1a_02a_0$	**$1a_{0.25}2a_{0.25}$**	**$1a_{0.5}2a_{0.5}$**	**$1a_12a_1$**	**$1a_12a_3$**	**$1a_12a_5$**
	0:0:100	0.25:0.25:99.5	0.5:0.5:99	1:1:98	1:3:97	1:5:94
0.7	Sol	Sol	Sol	Sol	Sol	Gel
0.8	Sol	Sol	Sol	Sol	Gel	Gel
0.9	Sol	Sol	Sol	Sol	Gel	Gel
1.0	Sol	Sol	Gel	Gel	Gel	Gel
2.0	Sol	Gel	Gel	Gel	Gel	Gel

Preparation of organohydrogel $1a_x2a_y4a_1$

We use **$1a_1$2$a_5$4a_1** as an example to show the typical process. **1a** (7.8 mg, 0.010 mol) in H_2O (0.5 mL) was mixed with **2a** (11.7 mg, 0.050 mmol) in glycerol (0.5 mL). The mixture was placed in the dark overnight. Then, **4a** (1.5 mg, 0.01 mmol), **4** (107 mg, 0.93 mmol) and VA-044 (3.2 mg, 0.01 mmol) were added to the mixture. The volume ratio of the monomers and the solvent was 10.6 : 100. Polymerization was conducted by sealing the mixture and heating at

50 °C for 12 h after purging with nitrogen for 30 min. An organohydrogel was obtained by cooling the mixture to room temperature.

Table S2. Chemical compositions of the organohydrogel $\mathbf{1a_x2a_y4a_1}$.

Concentration of monomers (mol/L)	Molar ratio of compound **1a**, **2a**, **4a** and **4** in gels (**1**:**2a**:**4a**:**4**)					
	$\mathbf{1a_02a_04a_1}$	$\mathbf{1a_12a_04a_1}$	$\mathbf{1a_02a_54a_1}$	$\mathbf{1a_{0.5}2a_{2.5}4a_1}$	$\mathbf{1a_12a_54a_1}$	$\mathbf{1a_22a_{10}4a_1}$
1	0:0:1:100	1:0:1:98	0:5:1:99	0.5:2.5:1:96	1:5:1:93	2:10:1:87

3.4.4 Additional data

Investigation of photo-controlled reversible coordination of Ru complex 1 and thioether ligand 2

We studied the reversible coordination of **1** and **2** in water at room temperature using ^{1}H NMR spectroscopy (Figure S31). First, we prepared a solution of **1** (5.5 mM) and **2** (27.5 mM) in D_2O. Then, the sample was measured using ^{1}H NMR spectroscopy immediately (the initial state in Figure S31b). In the initial state, there was a doublet at 6.71 ppm that corresponds to the A8 signal of **1**. When the sample was stored in the dark, a new doublet at 6.35 ppm appeared. Its signal increased with time, while the signal of the doublet at 6.71 ppm decreased. This result indicated that Ru-thioether bond spontaneously formed in the dark. The reaction reached equilibrium when the sample was stored in the dark for 180 min. Ru complexes cannot coordinate with thioether completely because it is a reversible equilibrium between Ru complexes and ligands.[35] To induce photosubstitution, the sample was irradiated with light (530 nm, 10 mW cm^{-2}, 5 min). After light irradiation, the signals of A8 for **1** and **3** almost returned to the initial states. These results indicated that the Ru-thioether bond was cleaved by light irradiation. The sample was stored in the dark for 180 min again. The signal of A8 of **1** decreased and the signal of A8 of **3** increased. Thus, thioether ligand **2** can coordinate with Ru complex **1** reversibly in the dark/light cycles.

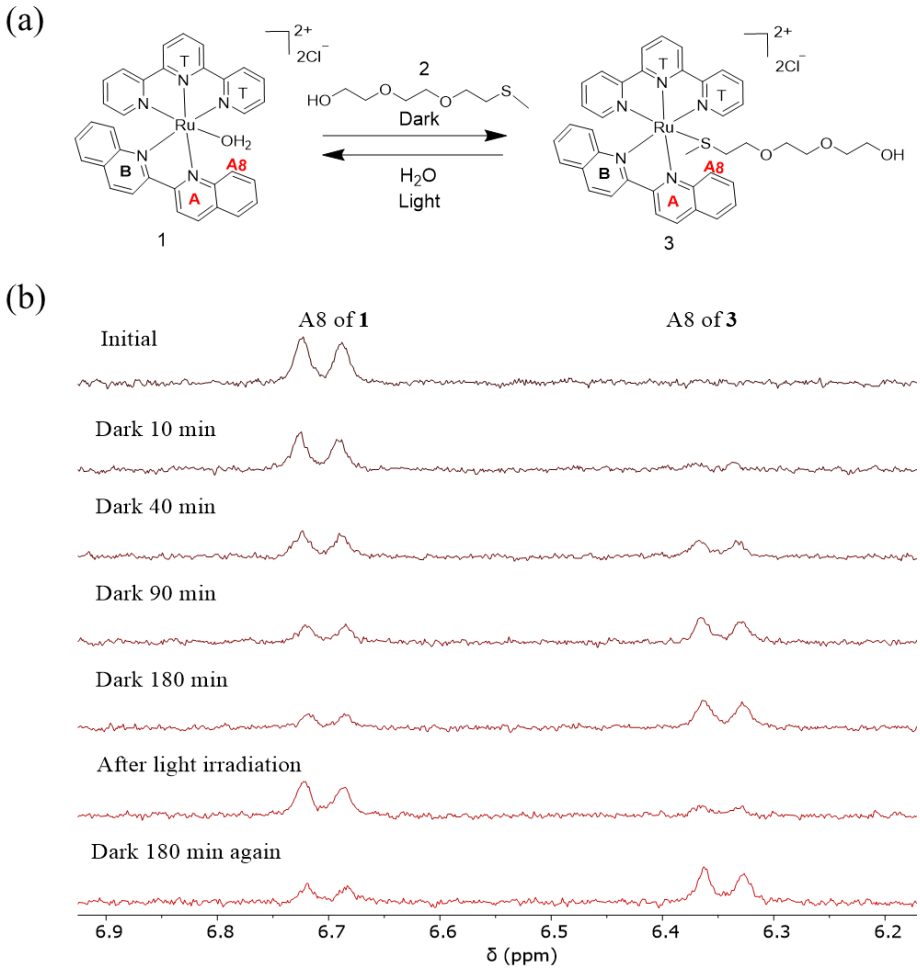

Figure S31. a) Photo-controlled reversible coordination of Ru complex **1** and thioether ligand **2**. b) ^{1}H NMR spectra (300 MHz) showing the reversible ligand substitution **1** and **2**. The mixture of **1** and **2** was kept in the dark for 10, 40, 90, and 180 min, irradiated with green light, and kept in the dark again. The concentration of **1** was 5.5 mM and the concentration of **2** was 27.5 mM.

To investigate the reversible Ru-thioether coordination at -20 °C, we prepared **1** (0.4 mM) and **2** (2 mM) in a H_2O/glycerol mixture (v/v, 1/1) at -20 °C. First, we dissolved **1** in the H_2O/glycerol mixture (v/v, 1/1, 4 mL) and cooled the mixture to -20 °C using a temperature-controlled stage. The mixture solution was kept in the dark at -20 °C all the time. Then **2** was added to the mixture, and we took 0.33 mL of the mixture to measure the UV-vis spectrum immediately (Quartz Cuvette, 1 mm light path). After that, we took 0.33 mL of the mixture and measured the UV-vis spectrum of the mixture every 2 hours. The results showed that Ru-thioether coordination bonds were formed by mixing **1** and **2** in the H_2O/glycerol mixture at -

20 °C. After subsequent light irradiation at -20 °C, Ru-thioether coordination bonds were cleaved.

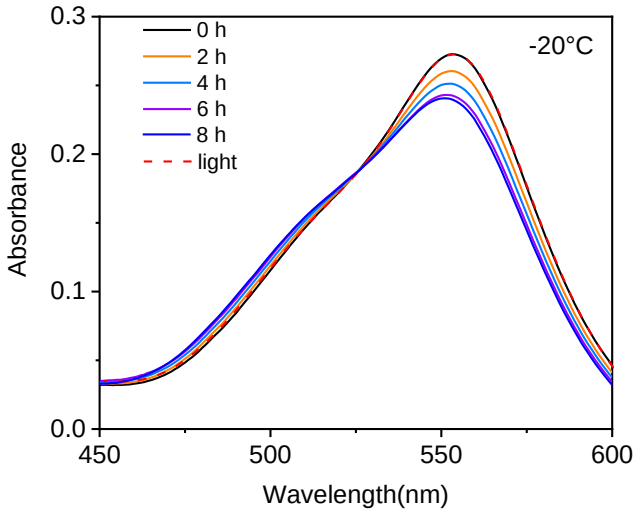

Figure S32. UV-vis absorption spectra of **1** (0.4 mM) and **2** (2 mM) in a H_2O/glycerol mixture (v/v, 1/1) at -20 °C after mixing for different time and after subsequent light irradiation (530 nm, 10 mW cm^{-2}, 5 min).

FTIR spectra of the monomer mixture before and after polymerization

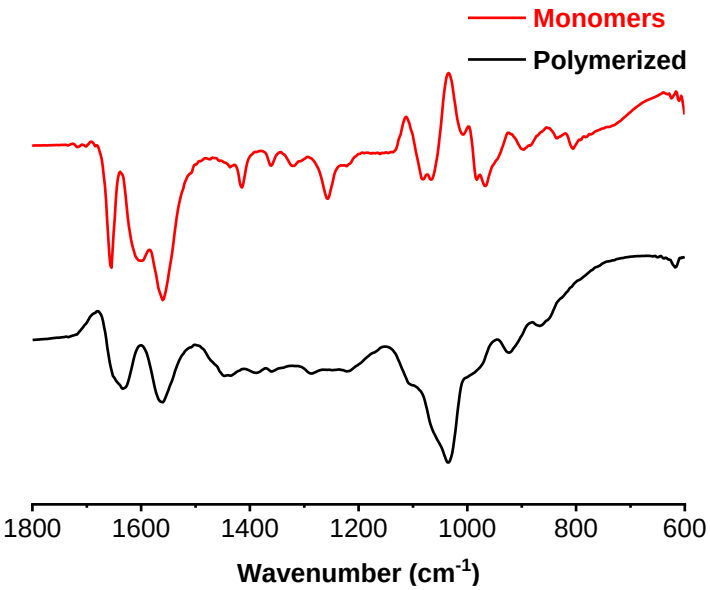

Figure S33. FTIR spectra of the monomer mixture before and after polymerization for the preparation of gel **1a$_1$2a$_5$**. After polymerization, the signals of the polymerizable acrylamide group at 985, 964 and 806 cm^{-1} disappeared, suggesting that the polymerization was efficient.[36]

Photoinduced healing of organohydrogel $\mathbf{1a_12a_5}$

To investigate the photoinduced healing of organohydrogel $\mathbf{1a_12a_5}$, we prepared a thin film of the gel. When the gel was damaged, it could not self-heal after 24 h because the fluidity of the gel was not good (Figure S34). In contract, the damaged gel showed a gel-to-sol transition after light irradiation for 5 min. The material flowed across the damaged part after keeping the sol for 15 min. Ru-thioether coordination bonds reformed when the material was kept in the dark. The reversible dissociation and re-formation of the Ru-thioether coordination bonds in the photoinduced healing process was confirmed using UV-vis spectroscopy (Figure S35). The absorption maximum of the initial $\mathbf{1a_12a_5}$ organohydrogel was at 544 nm, which was attributed to the Ru-thioether complex. After light irradiation, the absorption maximum of the sample shifted to 549 nm, which suggested that Ru-thioether coordination bonds were cleaved and thioether ligands were substituted by solvent molecules. When the sample was kept in the dark for 3 h, the absorption spectrum returned to the initial state. These results demonstrated that improved fluidity in the sol state provided sufficient polymer chain mobility for healing. healing based on the reversible gel-to-sol transitions involves the dissociation and re-formation of the Ru-thioether crosslinks under light irradiation and in the dark.

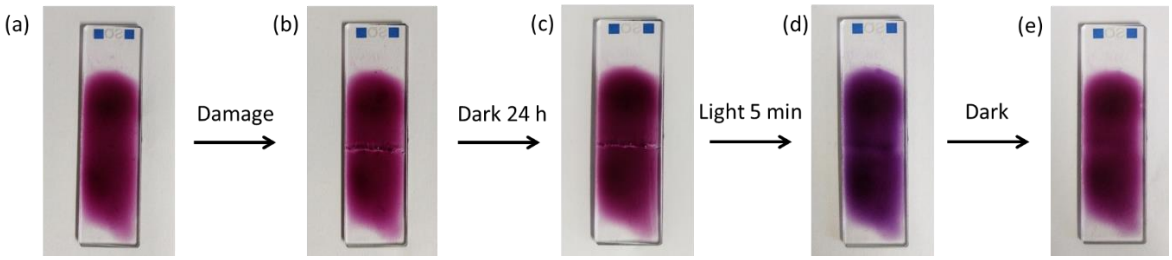

Figure S34. Photographs of $\mathbf{1a_12a_5}$ organohydrogel (a), after damage (b), after dark for 24 h (c), after light for 5 min (d), after dark (e).

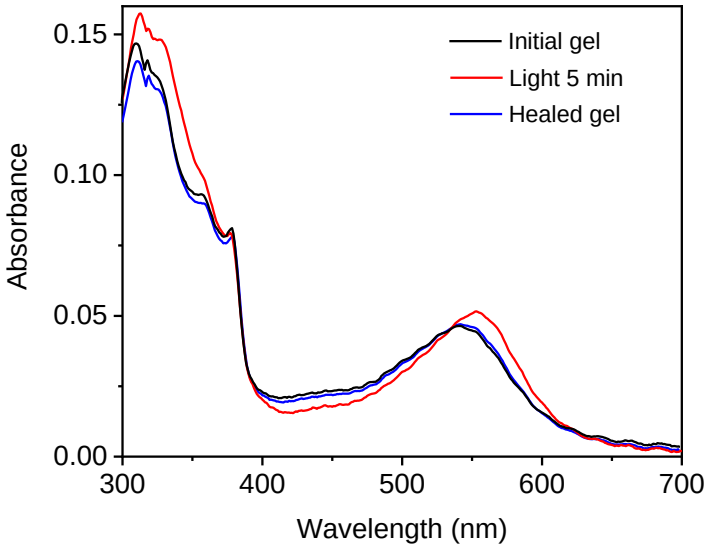

Figure S35. The UV-vis spectra of original organohydrogel **1a$_1$2a$_5$** (black line), organohydrogel after light irradiation (red line), and healed gel (blue line).

Photoinduced dynamic adhesion of organohydrogels 1a$_1$2a$_5$

To investigate the difference between photoinduced healing and mere adhesion, we prepared organohydrogels **1a$_1$2a$_5$** (1.5 M) to measure mechanical properties using mechanical tensile test system. First, we studied original organohydrogel **1a$_1$2a$_5$**. Its breaking point was at 0.38 N. Then, we cut an organohydrogel **1a$_1$2a$_5$** into halves, and the cut surfaces were irradiated with light (530 nm, 10 mW cm^{-2}) for 30 min. After that, the cut surfaces were reattached for 24 h at room temperature or -20 °C. The loading curve of the healed gel showed the breaking point was at 0.34 N and 0.30 N, respectively. It demonstrated that organohydrogel **1a$_1$2a$_5$** has a good photoinduced healing property at room temperature and at -20 °C. As a control experiment, we cut organohydrogel **1a$_1$2a$_5$** into halves, and the cut surfaces were reattached directly for 24 h without irradiation. The cut gels attached together mainly because of adhesion. The loading curve of the gel showed a breaking point was 0.10 N, which indicated that mere adhesion could not heal the gel efficiently.

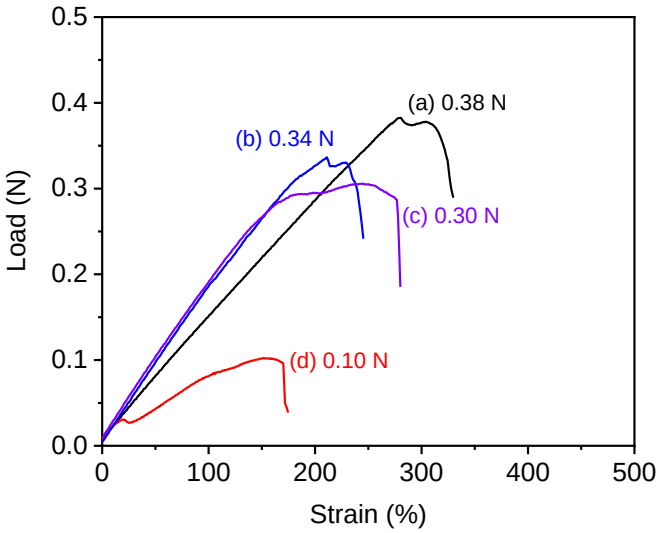

Figure S36. Photoinduced healing of organohydrogel **1a$_1$2a$_5$** (1.5 M) **s**tudied by mechanical tensile test. Test curves for organohydrogel **1a$_1$2a$_5$** was in (a). The organohydrogel was cut into halves, and the cut surfaces were irradiated with light (530 nm, 10 mW cm^{-2}, 30 min). After that, the cut surfaces were reattached for 24 h at room temperature (b) and at -20 °C (c) before measurement. (d) Organohydrogel **1a$_1$2a$_5$** was cut into halves, and the cut surfaces were reattached for 24 h without irradiation before measurement.

Rheology tests of organohydrogel 1a$_x$2a$_y$4a$_1$

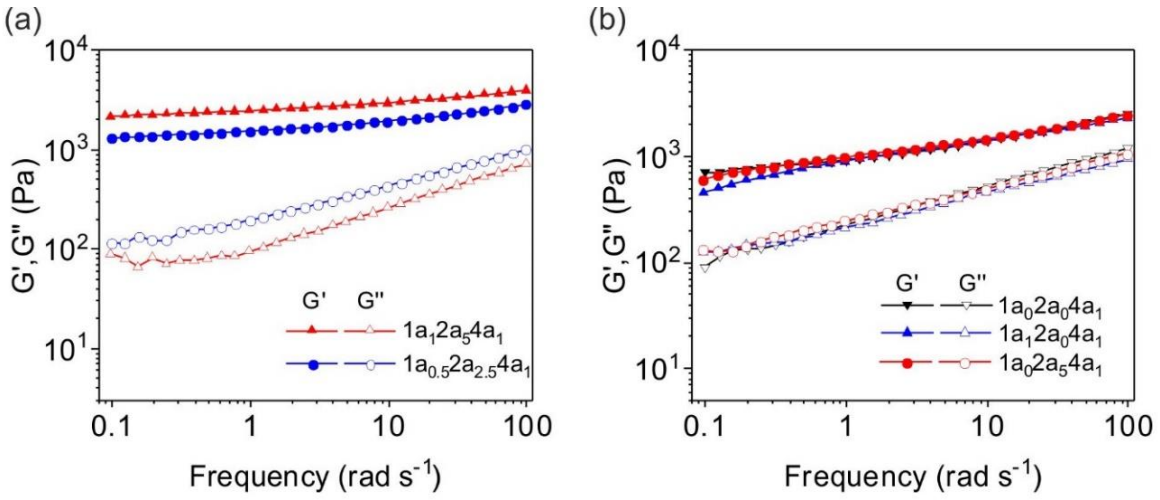

Figure S37. Rheology tests of organohydrogels at room temperature. (a) Frequency sweeps of organohydrogels (H_2O/glycerol (v/v, 1/1)) with increasing amount of **1a** and **2a** at constant strain 0.1%. (b) Frequency sweeps of organohydrogels (H_2O/glycerol (v/v, 1/1)) with or without **1a** and **2a** at constant strain 0.1%.

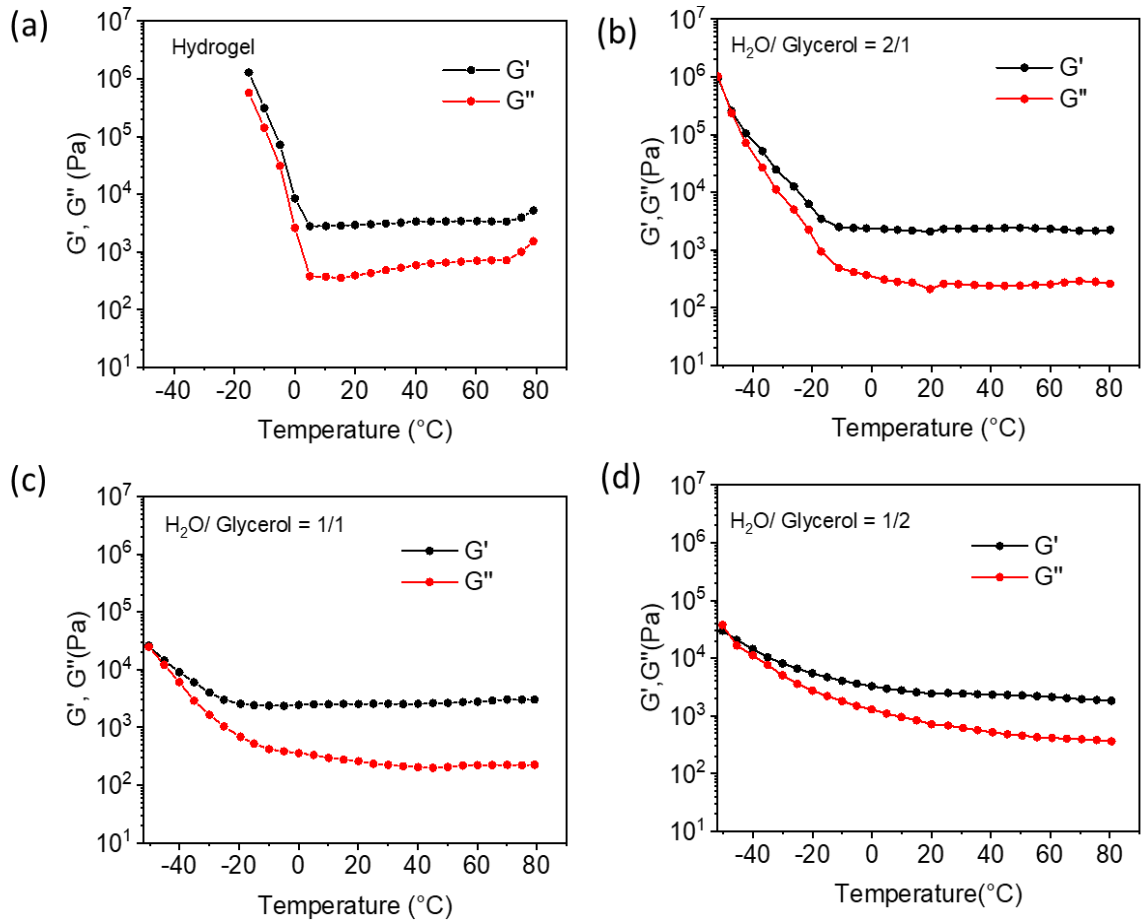

Figure S38. The rheology data of **1a$_1$2a$_5$4a$_1$** gels with different ratios of water and glycerol from -50°C to 80°C at a constant strain 1% and frequency 10 rad s^{-1}. a) G' and G'' of **1a$_1$2a$_5$4a$_1$** hydrogel with 100% H_2O as solvent. Both G' and G'' increased dramatically around 0 ℃, which indicated that the hydrogel lost its elasticity. b-d) G' and G'' of organohydrogels **1a$_1$2a$_5$4a$_1$** in the H_2O/glycerol (v/v, 2/1) (b), (v/v, 1/1) (c), and (v/v, 1/2) (d). Compared to the hydrogel, all the organohydrogels in the H_2O/glycerol can keep their elasticities at around -20 ℃. When the surrounding temperature was further cooled down to -40~50 ℃, G'' was over G', showing the organohydrogels were frozen. The joint points of G' and G'' can be considered as the theoretical lowest working temperatures for the organohydrogels.

Thermodynamic and Kinetic study for thermal coordination and photosubstitution

We quantified the formation and dissociation of the Ru-thioether bond using ^{1}H NMR and UV-vis absorption spectroscopy. The equilibrium constant *K* for the Ru-thioether bond was 108.7 ± 4 M^{-1}. The second-order rate constant k_1 for the thermal coordination was 1.2 × 10^{-2} M^{-1}·s^{-1} and the first-order constant k_{-1} for the thermal hydrolysis was 1.1 × 10^{-4} s^{-1} at room temperature.

The activation energy *Ea* of the thermal coordination is 48.6 kJ·mol^{-1}. The quantum yield φ for the photosubstitution was 0.21 (Table S3).

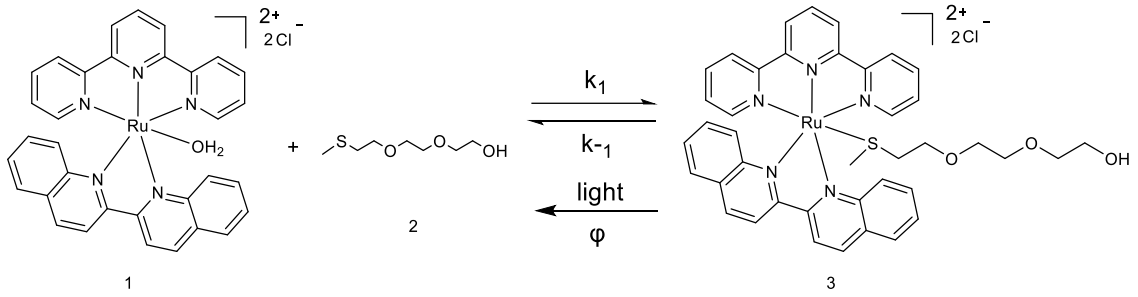

Figure S39. The reversible formation and dissociation of the Ru-S coordination bond. $k_{1:}$ second-order rate constant for thermal coordination; $k_{-1:}$ first-order rate constant for thermal hydrolysis; φ: Quantum yield for photosubstitution.

Table S3. Thermodynamic and kinetic data for thermal coordination and photosubstitution

K	k_1	k_{-1}	Ea	φ
108.7 ± 4 M^{-1}	1.2 × 10^{-2} $M^{-1} \cdot s^{-1}$	1.1 × 10^{-4} s^{-1}	48.6 kJ·mol^{-1}	0.21

(1) Measurements of the equilibrium constant

For the equilibria between **1** and **3**, the equilibrium constant *K* was determined by the following equation:

$$\frac{[RuS]}{[RuOH_2]} = K[S] \qquad (1)$$

where [$RuOH_2$] is the concentration of **1**, [RuS] is the concentration of **3**, and [S] is the equilibrium concentration of free compound **2**.

[Ru(tpy)(biq)(Cl)]Cl (5.5 mM) was mixed with different amounts of **2** in D_2O (the concentration of **2** in each sample was 1.8 mM, 3.6 mM, 5.5 mM, 8.0 mM, 16.5 mM and 27.5 mM respectively). After keeping in the dark overnight, the samples were measured by ^{1}H NMR at room temperature (Figure S40a). The ratios of [RuS] and [$RuOH_2$] were determined by integration of the peaks at 6.35 ppm and 6.71 ppm corresponding to **3** and **1**, respectively. A plot of [RuS]/[$RuOH_2$] as a function of equilibrium concentration of free compound **2** was made. The slope of this line corresponds to *K* (108.7 ± 4 M^{-1}) (Figure S40b).

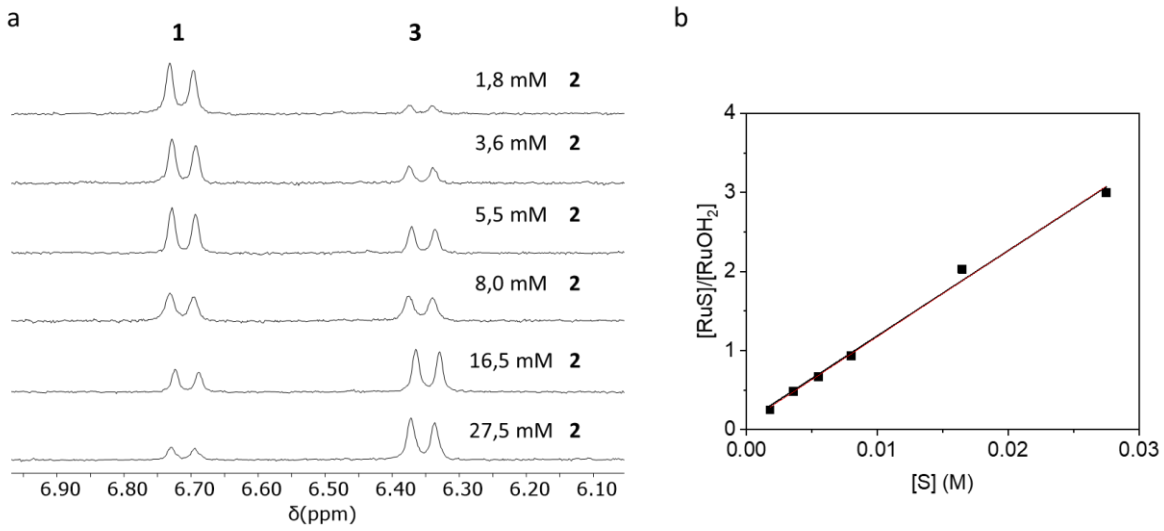

Figure S40. Equilibrium constant between **1** and **3**

(2) Rate constants of thermal substitution of H_2O ligand by ligand **2** on Ru complex **1**

The rate constant was calculated according to the following two steps. First, the extinction coefficients of **1** and **3** were determined using UV-vis absorption spectroscopy. The extinction coefficient of **1** was measured using the traditional method. Different concentrations of [Ru(tpy)(biq)(Cl)]Cl were prepared in H_2O (1.25×10^{-5} M, 2.05×10^{-5} M, 3.08×10^{-5} M, 4.1×10^{-5} M, 5.13×10^{-5} M and 6.15×10^{-5} M, respectively). Hydrolysis of [Ru(tpy)(biq)(Cl)]Cl to **1** is fast and complete in water. Therefore, each sample was measured by UV-vis absorption spectroscopy. The extinction coefficient of **1** was obtained from the slope of the plot of absorbance *vs* concentration of Ru complexes at each wavelength. The extinction coefficients of **1** at 519 nm and 549 nm were found to be 6075 $L\cdot mol^{-1}\cdot cm^{-1}$ and 8154 $L\cdot mol^{-1}\cdot cm^{-1}$ respectively.

The extinction coefficient of **3** was obtained by a different method because **3** is in thermodynamic equilibrium with **1**. We prepared four different mixture solutions of **1** and **2**. In these mixture solutions, the concentration of **2** is the same (0.16 M), the total concentration of Ru complexes was 4.3×10^{-5} M, 8.6×10^{-5} M, 1.3×10^{-4} M, and 1.7×10^{-4} M, respectively. All mixtures were measured by UV-vis absorption spectroscopy. The ratio $[RuS]/[RuOH_2]$ is a constant because the [S] is the same.

$$K' = \frac{[\mathrm{RuS}]}{RuOH_2} = K \cdot [S] \qquad (2)$$

According to the $[Ru] = [RuS] + [RuOH_2]$, the Eq. (2) can be replaced by Eq. (3):

$$r = \frac{[RuS]}{[Ru]} = \frac{K'}{K'+1} \qquad (3)$$

The value of *r* can be obtained from Eq. (3), and the extinction coefficient of $RuOH_2$ was determined above. Thus, the extinction coefficient of **3** can be calculated by Eq. (4):

$$\varepsilon_{\lambda}^{RuS} = \frac{\varepsilon_{\lambda}^{Rueq} - (1-r)\varepsilon_{\lambda}^{RuOH_2}}{r} \qquad (4)$$

The extinction coefficients of **3** at 519 nm and 549 nm were found to be 6550 $L \cdot mol^{-1} \cdot cm^{-1}$ and 4898 $L \cdot mol^{-1} \cdot cm^{-1}$, respectively.

Then, we measure the rate constant of thermal coordination by **3** on **1**. A solution of **1** (6.15×10^{-5} M) in water was prepared at a certain temperature. After adding **2** (6.15×10^{-2} M), the UV-vis absorption of the mixture solution was taken at a fixed time interval at the same temperature. The rate constants of thermal substitution of H_2O by **2** on **1** were calculated according to the same method used in Chapter 2. The pseudo first order rate constants k_1' were determined from the slope of the plot of ln([$RuOH_2$]/[Ru]) vs time (Figure S41). The second order rate can be calculated by $k_1 = k_1'/[S]$. k_1 and k_{-1} at different temperatures for the thermal substitution of H_2O by **2** on **1** were summarized in Table S4.

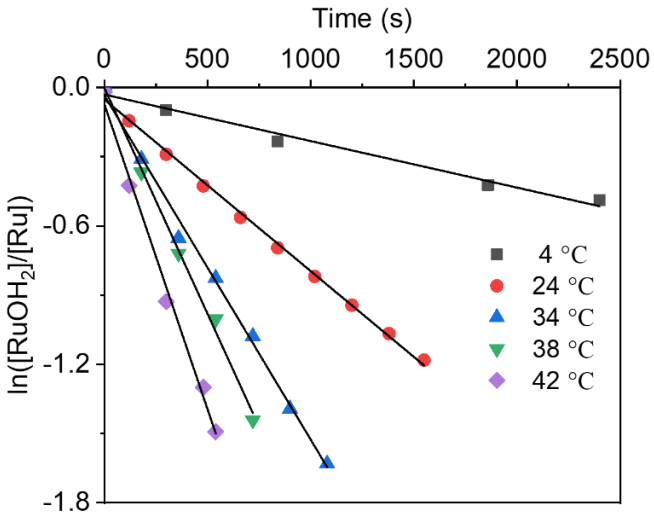

Figure S41. Polts of ln([$RuOH_2$]/[Ru]) vs time at different temperatures for the thermal coordination in the dark.

Table S4. Expermatnial pseudo first order constant and second order rate constants at different temperatures.

Temperature (°C)	k_1' (s^{-1})	k_1 ($M^{-1}\cdot s^{-1}$)
4	2.1×10^{-4}	3.4×10^{-3}
24	7.4×10^{-4}	1.2×10^{-2}
34	1.5×10^{-3}	2.5×10^{-2}
38	2.1×10^{-3}	3.4×10^{-2}
42	2.7×10^{-3}	4.3×10^{-2}

(3) Activation energy of thermal coordination

According to Arrthenius equation (Eq. 5):

$$k = \mathrm{A}e^{\frac{-E_a}{RT}} \quad (5)$$

Where k is the rate constant, E_a is the activation energy, A is the pre-exponential factor, R is the gas constant (8.314 $J\cdot mol^{-1}\cdot K^{-1}$) and T is the absolute temperature. Eq.5 can be expressed as Eq. 6. E_a was determined from the slope of the plot of ln(*k)* vs. -1/T and ln(A) was determined from the intercept of the polt. E_a is 48.6 $kJ\cdot mol^{-1}$ and k_1 at -20°C is 4.4×10^{-4}.

$$\ln(k) = \frac{-E_a}{R}\left(\frac{1}{T}\right) + \ln(A) \quad (6)$$

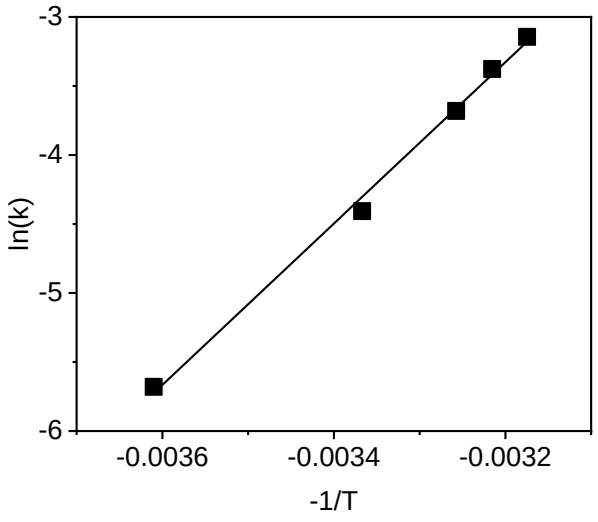

Figure S42. Polt of ln(k) vs ln(-1/T) for the thermal substitution of H_2O by **2** on **1**.

(3) Rate constants of thermal hydrolysis of ligand **2** by H_2O ligand in Ru complex **3**

Due to the thermodynamic equilibrium between **1**, **2** and **3** in water, the rate for the hydrolysis of **3** (k_{-1}) can be calculated by Eq. 7 and 8. k_{-1} =1.1 × 10^{-4}

$$k_{-1}[RuS] = k_1[S][RuOH_2] \quad (7)$$

$$k_{-1} = {}^{k_1}/_{K} \quad (8)$$

(4) Photosubstitution quantum yield for Ru complex 3

To measure φ, an aqueous solution of 3mL [Ru(tpy)(biq)Cl]Cl (6.15 × 10^{-5} M) with large excess of **2** (6.15 × 10^{-2} M) was prepared. The mixture solution was placed in the dark overnight at room temperature. After reaching the equilibrium, the UV-vis spectrum of the solution was measured. The ratio [RuS]/[$RuOH_2$] is 5.44 (Figure S43). Then the sample was exposed to visible light. The UV-vis spectra were taken every 10 seconds. During this process, three reations take place simultaneously: 1) the photochemical cleavage of the Ru- thioether bond; 2) the thermal cleavage of the Ru-thioether bond, 3) the thermal binding of **2** back to the aqua complex. In that conditions, the change of the concentration of **3** can be given by Eq. 9. When the system reached the thermal equilibrium in the dark, Eq. 9 can be changed to Eq. 9a; when the system reached the photochemical steady state, Eq. 9 can be changed to Eq. 9b:

$$\frac{d[RuS]}{dt} = k_1[RuOH_2][S] - k_{-1}[RuS] - k_{\varphi}[RuS] \qquad (9)$$

$$\frac{[RuS]_{eq}}{[RuOH_2]_{eq}} = \frac{k_1[S]}{k_{-1}} \qquad (9a)$$

$$\frac{[RuS]_{eq}}{[RuOH_2]_{eq}} = \frac{k_1[S]}{k_{-1} + k_{\varphi}} \qquad (9b)$$

The ratio of [RuS]/[$RuOH_2$] at thermal equilibrium was obtained by the UV-vis spectra and k_1 is already known, k_{-1} can be calculated from the Eq.9a (k_{-1} = 1.35×10^{-4}). Therefore, k_{φ} was obtained by Eq.9b in the photochemical steady state. Light irradiation leads to a photochemical steady state after 350 s irradiation. The steady-state was characterized by a [RuS]/[$RuOH_2$] ratio of 0.31 (Figure S43). k_{φ} = 2.2 × 10^{-3} calculated from the Eq.9b. The photosubstitution quantum yield φ were calculated using Eq. 10, Φ = 5.83 × 10^{-11}, φ = 0.21.

$$k_{\varphi} = \frac{\Phi \cdot \varphi \cdot (1 - 10^{-A_e})}{n_{Ru}} \quad (10)$$

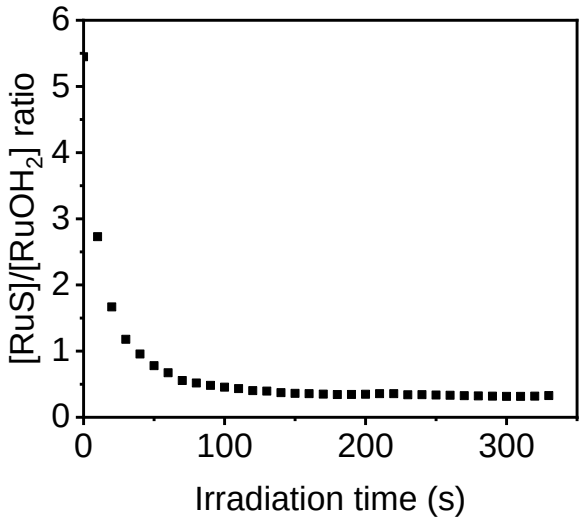

Figure S43. Plots of the ratio [RuS]/[$RuOH_2$] vs. irradiation time.

3.5 References

[1] A. M. Kloxin, A. M. Kasko, C. N. Salinas, K. S. Anseth, *Science* **2009,** *324,* 59.

[2] S. J. Jeon, A. W. Hauser, R. C. Hayward, *Acc. Chem. Res.* **2017,** *50,* 161.

[3] A. Farrukh, J. I. Paez, A. del Campo, *Adv. Funct. Mater.* **2018,** *29,* 1807734.

[4] C. A. DeForest, D. A. Tirrell, *Nat. Mater.* **2015,** *14,* 523.

[5] T. T. Lee, J. R. García, J. I. Paez, A. Singh, E. A. Phelps, S. Weis, Z. Shafiq, A. Shekaran, A. del Campo, A. J. García, *Nat. Mater.* **2015,** *14,* 352.

[6] B. Yan, J. C. Boyer, D. Habault, N. R. Branda, Y. Zhao, *J. Am. Chem. Soc.* **2012,** *134,* 16558.

[7] Y. Gu, E. A. Alt, H. Wang, X. Li, A. P. Willard, J. A. Johnson, *Nature* **2018,** *560,* 65.

[8] G. Weng, S. Thanneeru, J. He, *Adv. Mater.* **2018,** *30,* 1706526.

[9] J. T. Foy, Q. Li, A. Goujon, J.-R. Colard-Itté, G. Fuks, E. Moulin, O. Schiffmann, D. Dattler, D. P. Funeriu, N. Giuseppone, *Nat. Nanotechnol.* **2017**, 12, 540.

[10] D. J. Smith, G. A. Brat, S. H. Medina, D. Tong, Y. Huang, J. Grahammer, G. J. Furtmuller, B. C. Oh, K. J. Nagy-Smith, P. Walczak, G. Brandacher, J. P. Schneider, *Nat. Nanotechnol.* **2016**, 11, 95.

[11] X. Tong, J. Xiang, F. Shi, Y. Zhao, *Adv. Optical Mater.* **2016,** *4,* 1392.

[12] J. Liu, C. S. Y. Tan, O. A. Scherman, *Angew. Chem. Int. Ed.* **2018,** *57,* 8854.

[13] L. Zhang, H. Liang, J. Jacob, P. Naumov, *Nat. Commun.* **2015,** *6,* 7429.

[14] L. Zhang, P. Naumov, *Angew. Chem. Int. Ed.* **2015,** *54,* 8642.

[15] Q. Rong, W. Lei, L. Chen, Y. Yin, J. Zhou, M. Liu, *Angew. Chem. Int. Ed.* **2017,** *56,* 14159.

[16] L. Han, K. Liu, M. Wang, K. Wang, L. Fang, H. Chen, J. Zhou, X. Lu, *Adv. Funct. Mater.* **2018,** *28,* 1704195.

[17] F. Chen, D. Zhou, J. Wang, T. Li, X. Zhou, T. Gan, S. Handschuh-Wang, X. Zhou, *Angew. Chem. Int. Ed.* **2018,** *57,* 6568.

[18] A. Harada, Y. Takashima, M. Nakahata, *Acc. Chem. Res.* **2014,** *47,* 2128.

[19] T. Kakuta, T. A. Yamagishi, T. Ogoshi, *Acc. Chem. Res.* **2018,** *51,* 1656.

[20] Y. Takashima, S. Hatanaka, M. Otsubo, M. Nakahata, T. Kakuta, A. Hashidzume, H. Yamaguchi, A. Harada, *Nat. Commun.* **2012,** *3,* 1270.

[21] S. Bonnet, B. Limburg, J. D. Meeldijk, R. J. Gebbink, J. A. Killian, *J. Am. Chem. Soc.* **2011,** *133,* 252.

[22] E. R. Schofleld, J. P. Collin, N. Gruber, J. P. Sauvage, *Chem. Commun.* **2003,** 188.

[23] A. Bahreman, B. Limburg, M. A. Siegler, E. Bouwman, S. Bonnet, *Inorg. Chem.* **2013,** *52,* 9456.

[24] C. M. Xie, W. Sun, H. Lu, A. Kretzschmann, J. Liu, M. Wagner, H. J. Butt, X. Deng, S. Wu, *Nat. Commun.* **2018,** *9,* 3842.

[25] W. Sun, S. Li, B. Haupler, J. Liu, S. Jin, W. Steffen, U. S. Schubert, H. J. Butt, J. X. Liang, S. Wu, *Adv. Mater.* **2017,** *29,* 1603702.

[26] O. Filevich, L. Zayat, L. Baraldo, R. Etchenique, in *Luminescent and Photoactive Transition Metal Complexes as Biomolecular Probes and Cellular Reagents*, Vol. 165 (Eds: K. K. Lo), Springer International Publishing, Switzerland, **2015**, pp 47-68.

[27] J. D. Knoll, B. A. Albani, C. Turro, *Acc. Chem. Res.* **2015,** *48,* 2280.

[28] A. Li, C. Turro, J. J. Kodanko, *Acc. Chem. Res.* **2018,** *51,* 1415.

[29] Z. Shi, P, Peng, D. Strohecker, Y. Liao, *J. Am. Chem. Soc.* **2011,** *133,* 14699.

[30] Y. Liao, *Acc. Chem. Res.* **2017,** *50,* 1956.

[31] P. K. Kundu, D. Samanta, R. Leizrowice, B. Margulis, H. Zhao, M. Borner, T. Udayabhaskararao, D. Manna, R. Klajn, *Nat. Chem.* **2015,** *7,* 646.

[32] R. Klajn, P. J. Wesson, K. J. Bishop, B. A. Grzybowski, *Angew. Chem. Int. Ed.* **2009,** *48,* 7035.

[33] A. Bahreman, B. Limburg, M. A. Siegler, E. Bouwman, S. Bonnet, Inorg. Chem. 2013, 52, 9456.

[34] P. R. Andres, R. Lunkwitz, G. R. Pabst, K. Böhn, D. Wouters, S. Schmatloch, U. S. Schubert, Eur. J. Org. Chem. 2003, 3769.

[35] C. M. Xie, W. Sun, H. Lu, A. Kretzschmann, J. H. Liu, M. Wagner, H.-J. Butt, X. Deng,

S. Wu, Nat. Commun. 2018, 9, 3842.

[36] J. E. Stumpel, B. Ziółkowski, L. Florea, D. Diamond, D. J. Broer, A. P. H. J. Schenning, ACS Appl. Mater. Interfaces 2014, 6, 7268.

Chapter 4: Summary and Outlook

In this thesis, we have successfully synthesized photoresponsive Ru-containing polymer gels based on two different Ru-thioether coordination bonds, expanded the working temperature of photoresponsiveness and developed the applications in healing materials, soft actuators, photopatterning and dynamic assembly between hydrogels.

First, we developed an adhesive consisting of a Ru-containing polymer and a thioether-containing polymer for hydrogel assembly. Due to the photoresponsive Ru-thioether coordination bond, the adhesive exhibit reversible gel-to-sol transitions. Various hydrogels can adhere and can be on-demand photodetached by using this adhesive. This adhesion approach enabled integrating multiple stimuli-responsive hydrogel building blocks into one assembly which showed several shape deformations under different stimuli. Furthermore, the hydrogel building blocks can be photodetached, which allows reassembly of the building blocks. We envision that the adhesive has promising potential in macroscopic and dynamic hydrogel assembly for intelligent soft materials.

Second, we developed photoresponsive metallopolymer organohydrogels based on photoresponsive Ru-thioether coordination crosslinks, and exploited its applications at subzero temperature. The photoresponsive metallopolymer organohydrogels as new materials are expected to exhibit multiple functions and potential applications in cold environments. The metallopolymer organohydrogels were demonstrated to have the ability of photo-triggered reversible gel-to-sol transitions, photoinduced healing, photoswitchable mechanical properties, photo-controlled volume changes and rewritable and self-erasable photopatterning at -20 °C. Light can control the properties of metallopolymer organohydrogels with high spatiotemporal resolution. This work provides the guidance and principle for designing other materials that work in cold environments.

Although some efforts have been made to develop photoresponsive Ru-containing polymer to provide novel functionalities, many aspects of chemistry require further investigation. First, the formation and dissociation of the Ru-thioether bond need to be quantified in various environments. It is also important to investigate the formation and dissociation of the Ru-thioether bond on the polymer chains. These will help us further understand the relation between structure and properties of materials. Second, a new Ru complex and ligand system with a high rate constant at mild conditions need to be designed. For stimuli-responsive materials, fast response and recovery are very important in many applications such as healing materials, soft actuators and dynamic assembly. Improving the rate constant of thermal

coordination and photosubstitution of Ru complex together may provide photoresponsive materials with the ability to respond and recover rapidly.

Acknowledgments

It is time to express my deepest appreciation to all the people who helped and accompanied me during my PhD period.

First of all, I would like to thank my supervisors Prof. Dr. Hans-Jürgen Butt and Prof. Dr. Si Wu for giving me the chance to join your group as a Ph.D. student at the Max Planck Institute for Polymer Research in Mainz and for supporting these scientific ideas as well as additional activities such as academic conferences, summer schools and soft skill training. Prof. Dr. Hans-Jürgen Butt is nice, helpful and patient to all students, giving us strong support, encouragement and scientific guidance.

I would like to thank my daily supervisor Prof. Dr. Si Wu for scientific discussions, feedbacks and constructive guidance. At the first day of my PhD study, everything starts with him. Although he had backed to China, he kept the contact like before and was available to help me solve many problems. He always gave me critical suggestions for improving my research to a better level than that I cannot reach by myself.

I would like to thank all my colleagues and collaborators who support me during the past time. Dr. Kaloian Koynov helped with rheology analysis. Dr. Manfred Wagner helped with NMR analysis. Andreas Hanewald helped with rheology technical support. I also want to express my gratitude to Gunnar Kircher and Gabriele Schafer for their help with daily lab work.

I would like to thank all my group members, Annika Kretzschmann, Philipp Weis, Chaoming Xie, Xiaolong Zeng, Jianxiong Han and Yazhi Liu. I will never forget the happy time we experienced together. Thank you for bring me a lot of joy and encouraging me during the past years.

At last, I would like to thank my parents and my sister for their selfless love, encouragement, and support no matter what I do. Thank you to everyone that I have met during my PhD. I will miss all of you and remember all the good times in Mainz.

Publications

1. Jiahui Liu, Chaoming Xie, Annika Kretzschmann, Kaloian Koynov, Hans-Jürgen Butt, and Si Wu*, Metallopolymer organohydrogels with photo-controlled coordination crosslinks work properly below 0 °C. *Adv. Mater.* 2020, 1908324.

2. Jiahui Liu, Hans-Jürgen Butt* and Si Wu*, Reconfigurable surfaces based on photocontrolled dynamic bonds. *Adv. Funct. Mater.* 2019, 1907605.

3. Jiahui Liu, Hans-Jürgen Butt and Si Wu, Metallopolymer adhesive with photo-controlled coordination bonds for dynamic hydrogel assembly. *In Preparation.*